

Primary and Secondary Relaxations in Neat and Binary Glass Formers Studied by Means of Dielectric Spectroscopy

Von der Universität Bayreuth zur
Erlangung des Grades eines Doktors
der Naturwissenschaften (Dr. rer. nat.)
genehmigte Abhandlung

von
Robert Kahlau
geboren am 3. Juni 1982 in Coburg

Erster Gutachter: Prof. Dr. Ernst Rößler
Zweiter Gutachter: Prof. Dr. Roland Böhmer

Tag der Einreichung: 10. Januar 2014
Tag des Kolloquiums: 12. März 2014

Falls Gott die Welt geschaffen hat, war seine
Hauptsorge sicher nicht, sie so zu machen,
dass wir sie verstehen können.

Albert Einstein

Contents

1	Abstract	5
2	Kurzdarstellung	9
3	Extended Abstract	13
3.1	Introduction	13
3.2	Properties of Liquids, Supercooled Liquids and Glasses	15
3.3	Molecular Dynamics of a Liquid	17
3.4	Dynamic Heterogeneities	20
3.5	Dielectric Spectroscopy	21
3.5.1	Dipole Fluctuations and Macroscopic Polarization	21
3.5.2	Static Electric Fields	23
3.5.3	Dynamic Response	25
3.5.4	Measurement Setup	29
3.6	Contemporary Broadband Dielectric Spectroscopy	32
3.7	Existing Approaches to Describe Generic Relaxation Phenomena, Open Questions, and Major Results	35
4	Publications	53
4.1	Generalization of the Cole–Davidson and Kohlrausch Functions to Describe the Primary Response of Glass-Forming Systems	59
4.2	Evolution of Excess Wing and β -Process in Simple Glass Formers	67
4.3	Quinaldine: Accessing Two Crystalline Polymorphs via the Super- cooled Liquid	79
4.4	Secondary Relaxations in a Series of Organic Phosphate Glasses Revealed by Dielectric Spectroscopy	91
4.5	On the Cooperative Nature of the β -Process in Neat and Binary Glasses: A Dielectric and Nuclear Magnetic Resonance Spectroscop- y Study	101
4.6	Dynamics of Asymmetric Binary Glass Formers. I. A Dielectric and Nuclear Magnetic Resonance Spectroscopy Study	115
	Bibliography	129
	Danksagung	137

1 Abstract

The subject of this thesis is the investigation of neat and binary molecular glass formers studied with the help of dielectric spectroscopy (DS). One of two main interests followed by this thesis is to refine the generic picture of the dynamic susceptibility, including the temperature evolution of primary and secondary relaxation phenomena. The other objective is to gain insight into the microscopic origin of the β -process (a secondary relaxation observed for $T \lesssim T_g$) in neat and binary systems, as well as the primary relaxation phenomena in binary systems. The results of all investigations are collected in six partially interrelated publications.

Three classes of glass forming systems are analyzed: type-A systems showing no discernible β -process, but in most cases the so-called excess wing (EW) appearing as a power law $\varepsilon''(\nu) \propto \nu^{-\gamma}$ in the susceptibility at frequencies beyond the α -peak position ($\nu \gg \nu_{max}$); type-B systems which have a β -process clearly resolved as a susceptibility peak; and binary systems which are represented by mixtures of the type-A system polystyrene (PS, $M_w \approx 2$ kg/mol) and the type-B system tripropyl phosphate (TPP) in this thesis.

The analysis of type-A systems as presented in Papers 1 & 2 is based on the application of a specifically introduced three-parameter fit function, which interpolates continuously between Kohlrausch and Cole–Davidson spectral shapes. With the help of this function small temperature-affected spectral changes of the α -peak can be assigned fully to a variation of its low-frequency behavior. In the framework of this ansatz the method of spectral analysis, which has become usual to be applied for type-A systems by our group, can be advanced.

The investigation of the type-A glass former quinaldine (2-methyl quinoline) leads to the discovery of a family of substances which have metastable dielectrically active crystalline polymorphs. Dielectric spectra of all observed phases are presented in Paper 3. The phase transitions, occurring in the deeply supercooled state, show temperature-dependent transformation kinetics, which are tracked and quantified by performing long-term DS experiments. As a consequence of the temperature dependence of the transformation kinetics, the metastable phases (including the supercooled liquid) can be kinetically stabilized by lowering temperature. In addition to DS experiments X-ray diffraction (XRD) and differential scanning calorimetry (DSC) measurements are performed, which help to characterize the quinaldine phases and to track their phase transitions.

Further, a family of neat, chemically related type-B glass formers, i.e. symmetric phosphoric esters, are investigated in Paper 4 in order to find a possible correlation between their molecular structures and the corresponding molecular dynamics, in

particular concerning the β -processes. In two aspects a universal behavior of their β -processes is observed. Firstly, temperature-independent distributions of activation energies $g(E)$, which control the spectral evolution of the β -processes, are found for all systems for temperatures well below the glass transition temperature ($T < 0.9T_g$). Secondly, the relaxation strength $\Delta\varepsilon_\beta(T)$ is nearly constant for $T < 0.9T_g$. When T_g is approached ($T > 0.9T_g$), a distinct increase of the mean activation energy as well as a strong increase of the relaxation strength is observed. Both mentioned properties are interpreted to be sensitive to the softening of the glassy sample near T_g , pointing, in turn, towards the cooperative nature of the β -processes. Since the behavior of $\Delta\varepsilon_\beta(T)$ is known for structural as well as for orientational glasses made up by rigid molecules, and since no strong correlation between $g(E)$ and the number of internal degrees of freedom of the phosphoric esters is found, all types of β -processes appear to be mainly determined by intermolecular interactions and are not of merely local nature. Rather they may be considered as a generic feature of the glass transition.

The system TPP/PS, a so-called asymmetric binary glass former with a T_g contrast of $\Delta T_g = 201$ K, is investigated in the form of a joint study by DS and $^{31}\text{P}/^2\text{H}$ NMR, supported by depolarized light scattering (DLS) as well as DSC experiments. The results are collected in Papers 5 & 6. Tripropyl phosphate (TPP), which is also subject of the just summarized study on phosphoric esters, acts now as low- T_g component with a well-resolved β -process. The high- T_g component polystyrene (PS) has a relatively low molecular mass and shows no indication of a β -relaxation. The β -process found in neat TPP is also observed in the mixtures (Paper 5), and for high TPP concentrations (c_{TPP}) its properties are nearly concentration-independent. Selective NMR experiments prove the cooperative nature of the β -process: the β -relaxation, which is induced by the TPP molecules, is imposed on the PS monomers in the mixture. NMR experiments show that, when c_{TPP} is reduced continuously, there exist increasing fractions of TPP molecules as well as PS monomers not being involved in the β -process.

Due to the high T_g contrast of the components in TPP/PS, two primary relaxations (α_1 and α_2) and, correspondingly, two calorimetric glass transition temperatures (T_{g1} and T_{g2}) are resolved (Paper 6). Selective NMR experiments allow for a general assignment of the α_1 -relaxation to matrix dynamics and of the α_2 -relaxation to additive dynamics. On the other hand, it is shown that a fraction of TPP molecules is involved in the matrix dynamics, i.e. the molecules relax on the long time scale of the PS monomers. The analysis of the DS spectra shows that this fraction is temperature-dependent and vanishes above a temperature T_c . As a further result, the α_2 -process is found to change its appearance with varying TPP concentration: at high c_{TPP} its temperature-dependent peak shape resembles the α -peak of a liquid in confinement, while its time constants follow a non-Arrhenian temperature dependence. While, on the one hand, NMR experiments prove that the α_2 -process is also isotropic at low c_{TPP} , it develops, on the other hand, into a thermally activated process with a temperature-independent distribution of activation energies $g(E)$ when c_{TPP} is decreased. In addition, a further reduction

of c_{TPP} leads to a decrease of the mean activation energy of the α_2 -process. As a consequence, the glass transition temperature related to the α_2 -relaxation (T_{g2}) exhibits a maximum at intermediate TPP concentrations.

2 Kurzdarstellung

Gegenstand dieser Arbeit ist die Untersuchung reiner und binärer Glasbildner mit Hilfe der dielektrischen Spektroskopie (DS). Eines von zwei Hauptinteressen, die mit dieser Arbeit verfolgt werden, ist es, das generische Bild von der dynamischen Suszeptibilität einschließlich der Temperaturabhängigkeit der Primär- und Sekundärrelaxationen zu ergänzen. Das andere Ziel ist die Gewinnung neuer Erkenntnisse bezüglich des mikroskopischen Ursprungs des β -Prozesses (einer Sekundärrelaxation, die bei $T \lesssim T_g$ beobachtet wird) in reinen und binären Systemen sowie der Primärrelaxationsphänomene in binären Systemen. Die Ergebnisse aller Untersuchungen sind in sechs zum Teil miteinander verknüpften Publikationen gesammelt.

Drei Klassen von Glasbildnern werden untersucht: Typ-A-Systeme, die keinen erkennbaren β -Prozess, jedoch einen sogenannten Excess-Wing (EW) aufweisen, der als ein Potenzgesetz $\varepsilon''(\nu) \propto \nu^{-\gamma}$ in der Suszeptibilität bei Frequenzen oberhalb des α -Maximums ($\nu \gg \nu_{max}$) in Erscheinung tritt, Typ-B-Systeme, die einen β -Prozess in Form eines deutlich aufgelösten Suszeptibilitätsmaximums (Peaks) aufweisen und binäre Systeme, die in dieser Arbeit von Mischungen aus dem Typ-A-System Polystyrol (PS, $M_w \approx 2 \text{ kg/mol}$) und dem Typ-B-System Tripropylphosphat (TPP) repräsentiert werden.

Die Untersuchung der Typ-A-Systeme, wie sie in den Papers 1 & 2 vorgestellt wird, basiert auf der Anwendung einer eigens entwickelten Dreiparameter-Fitfunktion, die kontinuierlich zwischen spektraler Kohlrausch- und Cole-Davidson-Form interpoliert. Mit Hilfe dieser Funktion können kleine, temperaturbedingte Veränderungen der Linienform des α -Peaks völlig der Variation seines Niederfrequenzverhaltens zugeschrieben werden. Im Rahmen dieses Ansatzes kann die Methode der Spektralanalyse, deren Anwendung auf Typ-A-Systeme in unserer Arbeitsgruppe gang und gäbe geworden ist, verbessert werden.

Die Untersuchung des Typ-A-Systems Chinaldin (2-Methylchinolin; engl.: quinaldine) führt zur Entdeckung einer Klasse von Substanzen, die metastabile, dielektrisch aktive, kristalline Polymorphe besitzen. In Paper 3 werden dielektrische Spektren aller beobachteten Phasen vorgestellt. Die im tief unterkühlten Zustand stattfindenden Phasenumwandlungen weisen eine temperaturabhängige Umwandlungskinetik auf, die mit Hilfe von dielektrischen Langzeitexperimenten verfolgt und quantifiziert wird. Aus der Temperaturabhängigkeit der Umwandlungskinetik folgt, dass die metastabilen Phasen (einschließlich der unterkühlten Flüssigkeit) durch Absenken der Temperatur kinetisch stabilisiert werden können. Neben DS-Experimenten werden Röntgenbeugungs- (XRD) und differenzialkalorimetrische

(DSC) Messungen durchgeführt, mit deren Hilfe die Chinaldinphasen charakterisiert und ihre Phasenumwandlungen verfolgt werden.

Des Weiteren wird in Paper 4 eine Reihe reiner, chemisch verwandter Typ-B-Glasbildner (symmetrische Phosphorsäureester) untersucht, um einen etwaigen Zusammenhang zwischen ihren Molekülstrukturen und der entsprechenden Moleküldynamik, insbesondere der β -Prozesse, zu finden. In zweierlei Hinsicht wird ein universelles Verhalten ihrer β -Prozesse beobachtet. Zum einen werden temperaturunabhängige Aktivierungsenergieverteilungen $g(E)$, die die spektrale Evolution der β -Prozesse bestimmen, bei allen Systemen für Temperaturen deutlich unterhalb der Glasübergangstemperatur ($T < 0.9 T_g$) gefunden. Zum anderen erweist sich die Relaxationsstärke $\Delta\varepsilon_\beta(T)$ als nahezu konstant für $T < 0.9 T_g$. Bei der Annäherung an T_g ($T > 0.9 T_g$) wird sowohl ein deutlicher Anstieg der mittleren Aktivierungsenergie als auch ein starkes Ansteigen der Relaxationsstärke beobachtet. Beide genannten Größen werden dahingehend interpretiert, dass sie empfindlich auf das Erweichen der glasartigen Probe nahe T_g reagieren, was wiederum auf eine kooperative Eigenschaft der β -Prozesse hindeutet. Da das Verhalten von $\Delta\varepsilon_\beta(T)$ für Orientierungs- und strukturelle Gläser starrer Moleküle bekannt ist und keine starke Korrelation zwischen $g(E)$ und der Zahl interner Freiheitsgrade der Phosphorsäureester beobachtet wird, scheinen alle Arten von β -Prozessen hauptsächlich von intermolekularen Wechselwirkungen bestimmt zu sein und haben keine rein lokale Natur. Vielmehr können sie als generische Erscheinung des Glasübergangs betrachtet werden.

Das System TPP/PS, ein sogenannter asymmetrischer binärer Glasbildner mit einem T_g -Kontrast von $\Delta T_g = 201$ K, wird in Form einer gemeinsamen Studie von DS und ^{31}P -/ ^2H -NMR untersucht, unterstützt von Experimenten der depolarisierten Lichtstreuung (DLS) und der DSC. Die Ergebnisse sind in den Papers 5 & 6 gesammelt. Tripropylphosphat (TPP), welches auch Gegenstand der oben zusammengefassten Untersuchung von Phosphorsäureestern ist, dient hierbei als Nieder- T_g -Komponente mit einem gut aufgelösten β -Prozess. Die Hoch- T_g -Komponente Polystyrol (PS) hat eine relativ geringe Molekülmasse und zeigt keine Anzeichen eines β -Prozesses. Der β -Prozess des reinen TPP wird auch in den Mischungen beobachtet (Paper 5), und für hohe TPP-Konzentrationen (c_{TPP}) erweisen sich seine Eigenschaften als nahezu konzentrationsunabhängig. Selektive NMR-Experimente weisen die kooperativen Eigenschaften des β -Prozesses nach: Die β -Relaxation, die von den TPP Molekülen angeregt wird, wird in der Mischung auf die PS-Monomere übertragen. NMR-Experimente zeigen, dass unter kontinuierlicher Verringerung von c_{TPP} zunehmende Anteile sowohl der TPP-Moleküle als auch der PS-Monomere existieren, die nicht in den β -Prozess involviert sind.

Aufgrund des großen T_g -Kontrasts der Komponenten können zwei Primärrelaxationen (α_1 und α_2) und entsprechend zwei kalorimetrische Glasübergangstemperaturen (T_{g1} und T_{g2}) aufgelöst werden (Paper 6). Selektive NMR-Experimente ermöglichen es, grundsätzlich die α_1 -Relaxation der Dynamik der Matrix und die α_2 -Relaxation der Dynamik des Additivs zuzuordnen. Andererseits wird gezeigt,

dass ein Teil der TPP-Moleküle in die Dynamik der Matrix involviert ist, d.h. dass sie auf der langsamen Zeitskala der PS-Monomere relaxieren. Die Analyse der DS-Spektren zeigt, dass dieser Anteil temperaturabhängig ist und oberhalb einer Temperatur T_c verschwindet. Als weiteres Ergebnis ist zu nennen, dass sich das Erscheinungsbild des α_2 -Prozesses unter Variation der TPP-Konzentration verändert: Bei hohen c_{TPP} ähnelt seine temperaturabhängige Linienform der des α -Peaks einer Flüssigkeit in "Confinement" (also in räumlicher Einschränkung auf Nanometerskala), wobei seine Zeitkonstanten einer nichtarrhenischen Temperaturabhängigkeit folgen. Während einerseits NMR-Experimente zeigen, dass der α_2 -Prozess auch bei niedrigen c_{TPP} isotrop ist, entwickelt er sich andererseits in einen thermisch aktivierten Prozess mit einer temperaturunabhängigen Aktivierungsenergieverteilung $g(E)$, wenn c_{TPP} verringert wird. Des Weiteren führt eine weitere Reduktion von c_{TPP} zu einem Rückgang der mittleren Aktivierungsenergie des α_2 -Prozesses. Eine Konsequenz ist, dass die Glasübergangstemperatur, die mit dem α_2 -Prozess in Verbindung steht (T_{g2}), bei mittleren TPP-Konzentrationen ein Maximum aufweist.

3 Extended Abstract

3.1 Introduction

Structural glasses are amorphous solids, which we encounter in everyday life in a multitude of ways. The most important examples are, of course, windows and drinking glasses, which mainly consist of anorganic silica (SiO_2) and other oxides of metalloids and metals. Ceramics are anorganic materials which are partially amorphous. Even the properties of metallic glasses are appreciated, for example, by the medical or aerospace industry. But, also a variety of organic, polymeric materials are in fact amorphous solids. Molecular, organic active substances of many pharmaceuticals exhibit a better bioavailability in an amorphous state than in a crystalline form.

Actually, it is believed that principally every liquid can form a glass. The investigations of this thesis are restricted to molecular systems as well as mixtures of molecular and oligomeric glass formers, and dielectric spectroscopy (DS) is used as the primary experimental method.

The structure of all of these glasses mentioned above is the structure of a liquid, i.e., in contrast to crystals, no long-range order exists and no structural phase transition between liquid and glass is observed. The easiest way to produce a glass is to supercool a liquid and avoid a crystallization by, e.g., applying sufficiently high cooling rates. In a more general sense one could say that any thermodynamically meta-stable phase, which becomes kinetically stable when the mobility of the microscopic constituents is decreased, is the starting point of the glass formation (e.g. a supercooled plastic crystal [1–9] becoming an orientational glass upon continuing cooling). A further reduction of the mobility of the constituents makes then any phase transition to the stable phase more and more improbable. In fact, there are also other methods of glass preparation like, e.g., the removal of the solvent of an oversaturated solution [10].

The process of glass formation, usually referred to as *glass transition*, is accompanied by a tremendous increase of viscosity and, correspondingly, the correlation times of molecular reorientation (probed by, e.g., DS), over more than 14 orders of magnitude. The underlying mechanisms are not yet fully understood, which, on the one hand, manifests itself in the lack of a comprehensive theory being able to describe the observed phenomena over the huge dynamical range. A promising theoretical attempt to describe the physics of the glass transition is made by the mode coupling theory (MCT), which describes the process as a purely kinetic phenomenon without the need of a structural phase transition [11–13]. On

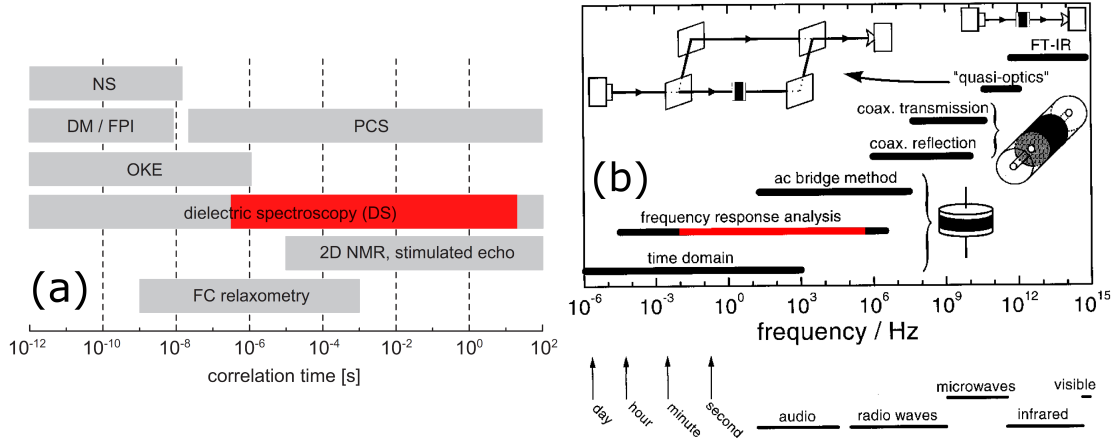


Figure 3.1: (a) Sketch of the dynamic ranges of several experimental methods; figure taken from [14]. (b) Sketch of the dynamic ranges of the dielectric methods applied by P. Lunkenheimer and co-workers in Augsburg; figure taken from [15]. Red marks indicate the dynamic range of the DS setup used for this thesis.

the other hand, covering 14 decades or more of a physical property is naturally an experimental challenge, too. Figure 3.1 (a) gives an overview of the accessible correlation time ranges of several experimental methods probing molecular dynamics of liquids [14]. Neutron scattering (NS), optical Kerr effect (OKE) and depolarized light scattering (DLS) consisting of photon correlation spectroscopy (PCS) and the application of a double monochromator in combination with a tandem Fabry–Pérot interferometer (DM/FPI) are taken into account, besides dielectric spectroscopy (DS), solid state NMR methods (2D NMR, stimulated echo) and fast field cycling (FC) relaxometry. Obviously, DS covers the widest dynamical range without any gaps, which is again demonstrated in Fig. 3.1 (b), where the frequency ranges of the dielectric methods used by A. Loidl, P. Lunkenheimer and co-workers in Augsburg are compiled [15]. The dynamical range covered in this thesis is marked red in both parts of Fig. 3.1. Dielectric spectroscopy has the further advantage of a uniquely large resolution, i.e. dielectric losses of 10^{-4} are still measured with high accuracy with up-to-date instruments. Due to this high resolution, even tiny secondary relaxation features or small variations of the main relaxation peak are discovered with the help of dielectric spectroscopy. Often it is difficult to judge if the observed phenomena are qualitatively generic features of the glass transition or rather individual properties of the analyzed substance. Consequently, the establishment of a coherent picture of the temperature evolution of the dynamic susceptibility of supercooled liquids and glasses constitutes a great challenge and is one important issue dealt with in this thesis.

Since DS is, compared to NMR methods, basically not selective to different types of molecules within the sample, NMR experiments are indispensable in this thesis for the investigation of the complex dynamics of a binary system. Also for

gaining new information on the microscopic origin of secondary (β -) relaxations the combination of DS and NMR is a successful recipe.

3.2 Properties of Liquids, Supercooled Liquids and Glasses

A liquid is a form of condensed matter, i.e. an ensemble of particles (e.g. atoms, molecules, monomeric units of polymer chains, particles of colloidal suspensions) with inter-particle distances of the order of the particle size [11]. The structure of a liquid shows short range order, but no long range order. This is demonstrated in Fig. 3.2 (taken from [16]), where the radial distribution function $g(r)$ of liquid argon is plotted, clearly showing broad periodic peaks which lose intensity at higher r . Liquids show a low compressibility and a high density, just like crystals.

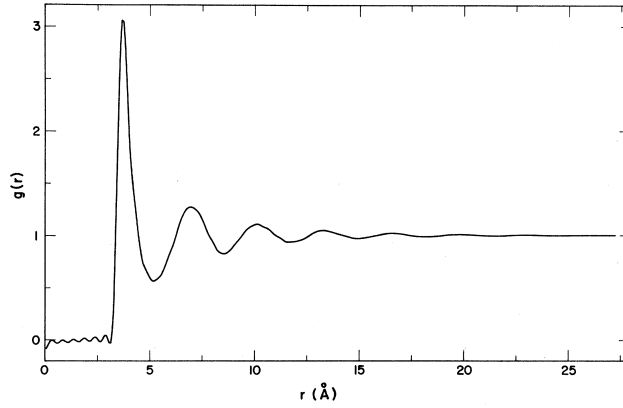


Figure 3.2: Radial distribution function $g(r)$ of liquid Argon at $T = 85$ K [16].

Unlike crystals, liquids show a finite viscosity being still higher than the viscosity of gases with much larger inter-particle distances.

The reason for the fluid character of liquids lies in the mobility of their particles, which have to rearrange permanently when the liquid flows. In this context the Stokes-Einstein equation

$$D = \frac{kT}{6\pi\eta R} \quad (3.1)$$

is usually cited, which connects the diffusion coefficient D with the viscosity η , a macroscopic property. Together with

$$\langle r^2 \rangle = 6Dt, \quad (3.2)$$

which is valid for diffusional processes in three-dimensional space on long time scales, it follows that the mean squared displacement of a particle of the liquid per unit time increases with decreasing viscosity [11, 17].

Cooling a liquid and, at the same time, avoiding any phase transitions like the crystallization below T_m , results in smooth variations of all macroscopic properties. Variables like the thermodynamic potentials, heat capacity or specific volume undergo only small changes, while the viscosity η increases over 14 decades [18]. Similar to the increase of η , the *structural relaxation time* τ of the liquid undergoes a tremendous increase until any laboratory time scale is exceeded. Then no rearrangement of the microscopic particles in the sample is possible any more. In the simplest case the sample has become a structural glass with the mechanical properties of a solid ($\eta \rightarrow \infty$) and the structure of a liquid (cf. $g(r)$ in Fig. 3.2).

Figure 3.3 shows the temperature dependence of the entropy $S(T)$ of o-terphenyl. The black line follows the thermodynamically stable behavior of the sample: at the melting point T_m the first order phase transition between liquid and crystal manifests itself as a step in $S(T)$. If a liquid sample is supercooled below T_m the entropy evolution of the liquid is continued (blue solid line). Here, although the liquid phase is not the thermodynamically stable state, the sample may be considered as being in thermal equilibrium (i.e. the equilibrium of the liquid phase) as long as any experiment is performed after waiting at least for the structural relaxation time τ ($\tau_{obs} \geq \tau$). When temperature falls further, τ exceeds laboratory time scales ($\tau_{obs} \ll \tau$). At this point, any measurement will investigate a non-ergodic sample which is structurally arrested or, respectively, a sample still approaching equilibrium (compare so-called aging experiments [19, 20]). The entropy evolution (now representative for any thermodynamic variable) bends over and runs nearly parallel to (or mimics) $S(T)$ of the crystal (red solid line in Fig. 3.3). In this temperature regime the sample is considered to be in the glassy state. The glass temperature T_g is only arbitrarily definable since no phase transition is observable between liquid and glass. Conventionally, the calorimetric T_g is defined as the onset of the “glass-step” in the DSC (differential scanning calorimetry) signal recorded at the heating rate $Q = 10$ K/min, detecting the temperature where the structural relaxation time is on the order of $\tau \approx 100$ s (see, e.g., [21]). An often preferred, more precise definition follows the rule $\tau_\alpha(T_g) = 10^2$ s, i.e. the correlation time of molecular reorientation, which is accessed amongst other methods by dielectric spectroscopy, assumes 100 s at the glass temperature. Further, independent of the applied definition, T_g depends strongly on the cooling rate [17, 22].

In Fig. 3.3 the so-called Kauzmann paradox [23] is sketched, which is not observed in real experiments but which is of theoretical relevance: if the supercooled liquid was further cooled *very* slowly in order to allow for full relaxation, the entropy evolution of the liquid is assumed to be continued uninterruptedly (dashed line in Fig. 3.3). As a consequence, $S(T)$ of the supercooled liquid would, firstly, intersect the entropy curve of the crystal at the Kauzmann temperature T_K and, secondly, finally vanish at finite temperatures. Different theoretical scenarios are possible in order to resolve this paradox, e.g. a phase transition to an ideal glassy state [24, 25]. Yet an answer cannot be found experimentally since τ increases above experimentally accessible time scales already above T_K .

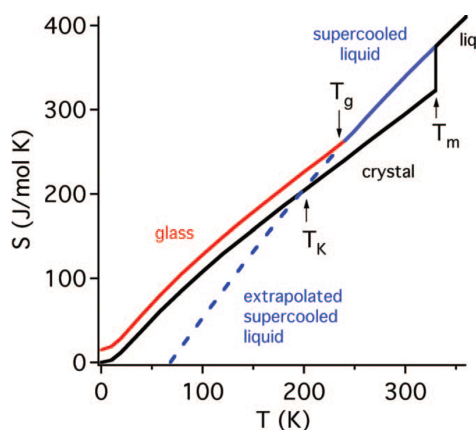


Figure 3.3: Entropy $S(T)$ of o-terphenyl, taken from [26].

The picture of the dynamic glass transition given above may be generalized to any supercoolable phase, e.g. plastic crystals and rotor phases [1–9, 27] forming orientational glasses, or colloidal suspensions [28, 29]. Further, a glass transition can be induced by partially removing the solvent of a solution [10].

3.3 Molecular Dynamics of a Liquid

In the following section a closer look on the particle dynamics of supercooled liquids shall be taken by introducing the incoherent intermediate scattering function $F_s(q, t)$, which reflects the (q -dependent) autocorrelation of the position of a tagged particle.

In Fig. 3.4 (a) $F_s(q, t)$ of a Lennard-Jones mixture, as obtained by a molecular dynamics simulation [30, 31], is shown for different simulation temperatures T and a constant $q = q_{max} = 7.25$, the latter defining the maximum position of the structure factor $S(q)$. Choosing q -values in the vicinity of q_{max} assures that dynamics on microscopic length scales (comparable to inter-particle distances) on correspondingly short time scales are probed, which further allows for a comparison with other experimental methods, e.g. probing molecular reorientation [32–35]. Correlation times (now and in the following called τ) obtained for such length scales are thus comparable with the structural relaxation time introduced above. Inspecting now Fig. 3.4 (a), a single-step correlation decay at high temperatures is observed, which approximately has the shape of a simple exponential decay. When T is decreased, the curve shifts to longer times and, simultaneously, develops into a two-step decay. Fig. 3.4 (b) displays the same data as part (a), now scaled to the correlation time τ , here defined as the point of time when $F_s(q, t)$ has reached the value e^{-1} . From this representation one can infer that the long-time parts of the two-step decays collapse to a common master curve. Additionally, they are more stretched than the single-step decays corresponding to highest temperatures. The temperature independence of the curve shapes is

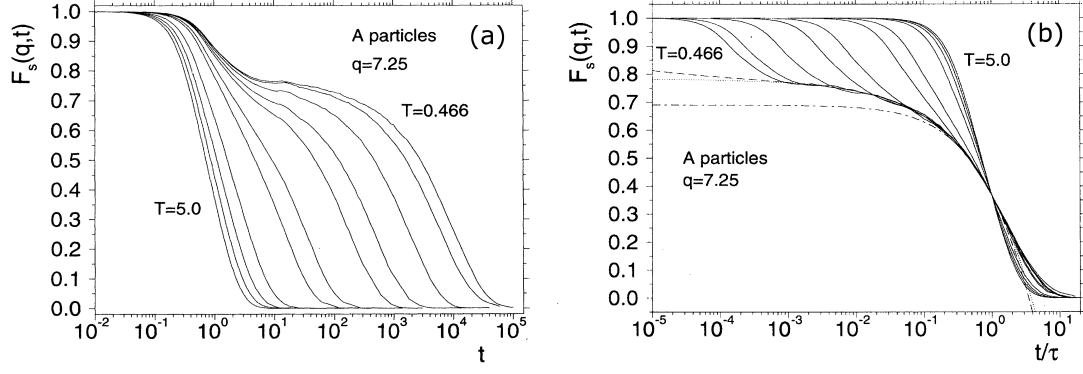


Figure 3.4: Incoherent intermediate scattering function of one component of a binary Lennard-Jones liquid (solid lines). Figures adapted from [31]. Simulation temperatures T indicated. (a) Raw simulation data. (b) Data scaled to correlation time τ . Dashed lines: guides for the eye.

a phenomenon usually referred to as time-temperature superposition (TTS) or, in frequency domain, frequency-temperature superposition (FTS). The two-step character of the correlation functions as well as the validity of TTS/FTS and the non-exponentiality (stretching) of the long time behavior are characteristic of “glassy dynamics”, i.e. the molecular dynamics of liquids appearing below the boiling point, yet well above the melting point ($T_m < T < T_b$) [36].

Figure 3.5 shows the mean squared displacement $\langle r^2(t) \rangle$ of one component of the binary Lennard-Jones liquid just discussed. Here, another typical signature of glassy dynamics is seen: looking at first to high temperature curves in Fig. 3.5 (a), a crossover from $\langle r^2(t) \rangle \propto t^2$ at short times to $\propto t^1$ at long times is observed. When T is decreased, the whole curve shifts to longer times, and the t^1 -regime becomes more and more separated from the $\langle r^2(t) \rangle \propto t^2$ -regime by a plateau ($\propto t^0$) emerging at intermediate times. The t^2 -regime is called ballistic regime. Here the

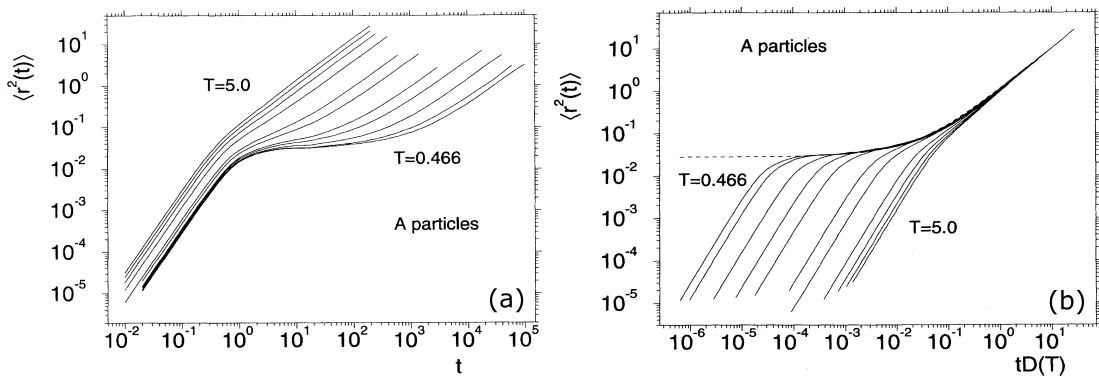


Figure 3.5: Mean squared displacement of one component of a binary Lennard-Jones liquid. Figures taken from [30]. Simulation temperatures T indicated. (a) Raw simulation data. (b) Data scaled to long time behavior (see abscissa).

particle simply moves at a constant velocity. On longer time scales the particle inevitably interacts with its neighbors. Thus, the mechanism of translation must transform into a diffusive process at long times, manifesting itself as a t^1 -law (diffusive regime). When temperature is lowered, the diffusive process is slowed down more strongly than the ballistic one, leading to a separation of both regimes. In between a plateau emerges, because at intermediate times the particle is trapped by its neighbors for a certain period. This is usually referred to as the “cage effect” [11]. At longer times the particle escapes again from its cage via the delayed diffusional process. Figure 3.5 (b) shows the same data as part (a) after scaling the abscissa with the temperature-dependent diffusion coefficient $D(T)$. Similar to the scaling behavior demonstrated for $F_s(q, t)$ in Fig. 3.4 (b) the long time parts of the $\langle r^2(t) \rangle$ collapse.

In many cases the microscopic particles of a liquid are no highly symmetric objects like the particles in the simulation just considered; the latter interact via spherically symmetric potentials. Molecular liquids, for example, consist of generally asymmetric molecules. The spatial rearrangement of the molecules, leading finally to the full decay of $F_s(q, t)$, involves also their reorientation. Probing molecular reorientations of supercooled liquids with the help of different methods, thus, constitutes a variety of experimental ways to investigate the glass transition. The experimental method of depolarized light scattering (DLS) probes collective molecular reorientations by measuring the collective reorientational autocorrelation function $C^{(2)}(t)$ of the anisotropic part of the molecular polarizability tensor [36, 37]. Figure 3.6 shows the time domain representation of DLS data of m-tricresylphosphate (m-TCP). For all temperatures a monotonic decay of $C^{(2)}(t)$ from 1 to 0 is observed. When T is decreased, the curve shifts to longer times and, above all, develops into a two-step decay. This emergence of a two-step correlation function upon cooling is comparable to the temperature evolution of the $F_s(q, t)$ -curves in Fig. 3.4 as well as the $\langle r^2(t) \rangle$ -data in Fig. 3.5, and is considered again as the signature of glassy dynamics. The terminal relaxation in Fig. 3.6 will later be attributed to the structural relaxation or α -process of the liquid. On cooling close to T_g , the terminal loss of correlation shifts to long times. The corresponding correlation times increase about twelve orders of magnitude from $\tau \approx 10^{-11}$ s to $\tau \approx 10^1$ s, which is again the manifestation of the glass transition described above. From Fig. 3.6 one also infers that TTS is fulfilled over the complete temperature range. This is demonstrated for the $T = 290$ K $\approx T_m$ curve, which matches exactly the shape of the $T = 207$ K $\approx T_g$ curve (blue dashed line). Lowering temperature below T_g would result in the terminal decay shifting out of the accessible time range. The sample would fall out of equilibrium, since the experiment takes place on a shorter time scale than the structural relaxation of the sample. Then, the sample may be considered as a glass.

As will become clear below, dielectric spectroscopy (DS) experiments reveal a multitude of dynamical processes, which appear on time scales between the short time limit and the terminal step of the correlation function. The analysis of the

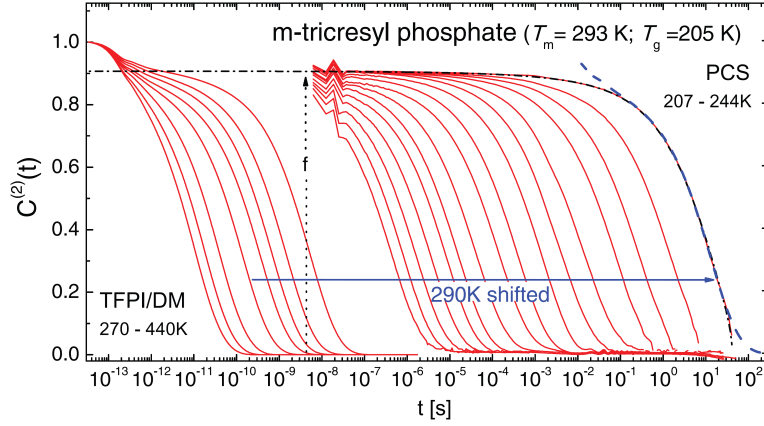


Figure 3.6: Time domain representation of DM/TFPI as well as photon correlation spectroscopy data of *m*-tricresyl phosphate (red solid lines), taken from [36]. Dashed blue line: data from $T = 290$ K shifted on top of the $T = 207$ K curve.

manifestation of these processes as spectral features in the dielectric susceptibility is the actual scope of this work.

3.4 Dynamic Heterogeneities

Although the origin of the phenomenon is not clarified, it is a commonly accepted view that supercooled liquids show dynamic heterogeneity [26,38–41]. This means that different subensembles of molecules in the liquid show different mobilities, which causes a distribution of correlation times. Figure 3.7 shows results of a molecular dynamics simulation of a binary Lennard-Jones liquid. Here, each arrow indicates the displacement of a particle after some waiting time on the order of the structural relaxation time. As can be seen clearly, spatially contiguous regions of quite different mobilities are found, demonstrating strong spatial correlations.

There are also experimental attempts to explore dynamic heterogeneities. Russel et al. detected the fluctuations of dielectric properties of a polyvinyl-acetate film on nm-scale with the help of a piezo-cantilever of an atomic force microscope [42,43]. The authors found domains of common dynamical properties on the length scale of about 10 nm, surviving on the time scale of the structural relaxation. Another experimental possibility of monitoring dynamic heterogeneities are, e.g., non-resonant dielectric hole burning experiments [39,44,45]. If a sample shows dynamic heterogeneity, this method leads to a selective heating of dynamically related subensembles of molecules, which leads to a deformation of the distribution of correlation times $G(\ln \tau)$. Blochowicz et al. [45] found particularly strong effects in binary mixtures. Binary systems analyzed within this thesis by DS and NMR show, likewise, broad distributions of correlation times, which are attributed to strong dynamic heterogeneities.

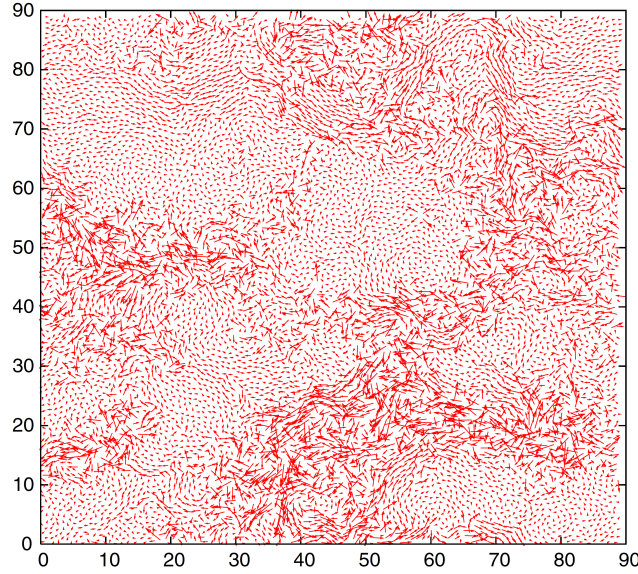


Figure 3.7: MD simulation results for a binary Lennard-Jones mixture in two dimensions. Arrows of different lengths indicate single particle displacements after a period of the order of the structural relaxation time. Figure taken from [41].

Dynamic heterogeneity is a possible explanation for the decoupling of diffusivity and viscosity close to T_g [38,46], which is subject of many experimental approaches. For example Ediger et al. [47] analyze crystallization kinetics of several organic and inorganic systems in order to find a dependence $D \propto \eta^{-\xi}$ with $\xi < 1$ (fractional Stokes-Einstein relation, compare Eq. 3.1). Mapes et al. [48] find a violation of Eq. 3.1 by performing vacuum desorption experiments with protonated/deuterated *o*-terphenyl bilayer films, and Ehlich et al. [49] use forced Rayleigh scattering at holographic gratings made of several glass formers. Important to mention are also the contributions by Stickel et al. [50,51], where the decoupling of the structural relaxation time from the ionic conductivity contribution to the dielectric loss (see below) is interpreted as a decoupling of viscosity from diffusivity.

3.5 Dielectric Spectroscopy

3.5.1 Dipole Fluctuations and Macroscopic Polarization

Reorientations of polar particles (i.e. polar molecules of molecular liquids or polar monomeric units in polymer melts) cause fluctuations of the macroscopic polarization

$$\vec{P}_{or}(t) = \frac{1}{V} \sum_i \vec{\mu}_i(t) \quad (3.3)$$

of the sample, where V is the sample volume and $\vec{\mu}_i$ are the permanent dipole moments of the molecules. Note that the time average of \vec{P}_{or} vanishes when no

external field is present. When the liquid under investigation is placed into a capacitor, these fluctuations can be measured. The actual quantity of interest, with a clear atomistic meaning, is the dipole autocorrelation function

$$C_\mu(t) = \frac{1}{\mu^2} \langle \vec{\mu}(0) \vec{\mu}(t) \rangle, \quad (3.4)$$

with $\langle \cdot \rangle$ denoting the ensemble average [44, 52, 53]. $C_\mu(t)$ is a single particle autocorrelation function and has to be connected with the (collective) autocorrelation function of the macroscopic polarization $C_P(t)$:

$$\begin{aligned} C_P(t) &= \frac{\langle \vec{P}_{or}(0) \vec{P}_{or}(t) \rangle}{\langle \vec{P}_{or}(0) \vec{P}_{or}(0) \rangle} = \frac{\sum_{i,j=1}^N \langle \vec{\mu}_i(0) \vec{\mu}_j(t) \rangle}{\sum_{i,j=1}^N \langle \vec{\mu}_i(0) \vec{\mu}_j(0) \rangle} \\ &= \frac{\sum_{i=1}^N \langle \vec{\mu}_i(0) \vec{\mu}_i(t) \rangle + \sum_{\substack{i,j=1 \\ i \neq j}}^N \langle \vec{\mu}_i(0) \vec{\mu}_j(t) \rangle}{N\mu^2 + \sum_{\substack{i,j=1 \\ i \neq j}}^N \langle \vec{\mu}_i(0) \vec{\mu}_j(0) \rangle}. \end{aligned} \quad (3.5)$$

Here the sum terms with identical indices ($i = j$) are autocorrelation contributions, while expressions with $i \neq j$ represent so-called cross-correlation contributions. If the latter vanish due to some approximation, the expression

$$C_P(t) = \frac{1}{N\mu^2} \sum_{i=1}^N \langle \vec{\mu}_i(0) \vec{\mu}_i(t) \rangle = \frac{1}{\mu^2} \langle \vec{\mu}(0) \vec{\mu}(t) \rangle = C_\mu(t) \quad (3.6)$$

follows. One could argue that this approximation never holds in polar liquids. However, it is usually assumed that the cross-correlation contributions behave similarly to the autocorrelation terms [54] and, thus, do not play a significant role. As a further approximation, the equivalence of ensemble and time average, actually only valid in ergodic systems [55], is extended to temperatures below T_g , i.e. to thermodynamic situations where the liquid has fallen out of equilibrium. Thus, the autocorrelation function of the macroscopic polarization may be generally defined as

$$C_P(t) = \langle \vec{P}_{or}(0) \vec{P}_{or}(t) \rangle = \lim_{T \rightarrow \infty} \left(\frac{1}{T} \int_0^T \vec{P}_{or}(\tau) \vec{P}_{or}(\tau + t) d\tau \right). \quad (3.7)$$

According to the Wiener-Khintchine theorem [56,57], the spectral density of dipole fluctuations can be formulated like [58]

$$S_P(\omega) = \frac{1}{2} \int_{-\infty}^{\infty} C_P(t) \exp[i\omega t] dt = \int_0^{\infty} C_P(t) \cos(\omega t) dt. \quad (3.8)$$

The last equality in Eq. 3.8 is due to the fact that $C_P(t)$ is an even function.

Dielectric spectral densities of glycerol and PVC have been measured above and below T_g by Israeloff et al. [59,60]. As will become clear below, molecular dynamics may be investigated alternatively by measuring the reaction of the sample to an external field. In order to adapt this statement to dielectric spectroscopy, the question of how electric fields interact with polar samples has to be addressed at first.

3.5.2 Static Electric Fields

If a static external electric field is present, a non-vanishing time average of the macroscopic polarization \vec{P} is found. If the external field is sufficiently low, the linear dependence

$$\vec{P} = \varepsilon_0 \underline{\chi} \vec{E} \quad (3.9)$$

with the generally tensorial susceptibility $\underline{\chi}$ is a good approximation. The macroscopic polarization consists of the orientational part \vec{P}_{or} (cf. previous section) and a contribution \vec{P}_{ind} due to a deformation of the molecular charge density distribution:

$$\vec{P} = \vec{P}_{or} + \vec{P}_{ind} \quad and \quad (3.10)$$

$$\underline{\chi} = \underline{\chi}_{or} + \underline{\chi}_{ind}. \quad (3.11)$$

When the dynamic response is discussed (see next section), this has to be kept in mind. The dielectric displacement is then calculated to

$$\begin{aligned} \vec{D} &= \varepsilon_0 \vec{E} + \vec{P} \\ &= \varepsilon_0 \left(\mathbb{1} + \underline{\chi} \right) \vec{E} \\ &= \varepsilon_0 \underline{\varepsilon} \vec{E} \end{aligned} \quad (3.12)$$

with the tensorial permittivity $\underline{\varepsilon}$. In isotropic media the tensorial quantities introduced above become scalars:

$$\begin{aligned}\vec{P} &= \varepsilon_0 \chi \vec{E} \\ \vec{D} &= \varepsilon_0 \varepsilon \vec{E} \\ \varepsilon &= \chi + 1.\end{aligned}\tag{3.13}$$

If orientational and induced contributions are separated, the equations

$$\begin{aligned}\varepsilon &= \varepsilon_{or} + \varepsilon_{ind} \\ \chi &= \chi_{or} + \chi_{ind} \\ \varepsilon_{or} &= \chi_{or} \quad (= \Delta\varepsilon) \\ \varepsilon_{ind} &= \chi_{ind} + 1 \quad (= \varepsilon_{\infty})\end{aligned}\tag{3.14}$$

hold. The expression $\Delta\varepsilon$ is called *relaxation strength* and often used in the context of the dynamic susceptibility. In the same context ε_{∞} may be used instead of ε_{ind} (next section). The scalar nature of χ and ε in isotropic media may suggest that all microscopic dipoles point along the direction of the external field. This picture is not true since thermal fluctuations act antagonistically to the external field and avoid a perfect arrangement of the molecules. Hence, it is intuitively clear that χ_{or} must decrease with increasing temperature. A quantitative assessment [61] yields

$$\chi_{or} = \Delta\varepsilon = \frac{n\mu^2}{3kT\varepsilon_0},\tag{3.15}$$

which is valid for small interaction energies ($\frac{\mu E}{kT} \ll 1$) [53, 62] and usually referred to in literature as *the Curie law*. Here, $n = N/V$ denotes the dipole density in the sample. The relaxation strength $\Delta\varepsilon$ is used equivalently to the orientational static susceptibility χ_{or} (cf. Eq. 3.14).

Equation 3.15 is actually expected to hold quantitatively only in dipolar gases. In condensed matter the interaction among the dipoles as well as the effect of local fields must be taken into account, and several theoretical attempts have been made in this regard. The Clausius-Mosotti relation, based on a local Lorentz field for each dipole, or the Onsager reaction field [62, 63], accounting for the influence of a dipole on the surrounding “continuum” by calculating a correction factor, are important examples. In the case of associating liquids, Onsager’s predictions do not hold and another correction, a correlation factor introduced by Kirkwood and Fröhlich, has to account for static dipole–dipole correlations. Contemporary papers usually forgo a quantitative discussion of any of these factors, thus the reader shall be referred to standard literature (e.g. [62]). If deviations from the Curie law (Eq. 3.15) are discussed, a single, merely empirical correction factor g is introduced, which is, nevertheless, sloppily called *Kirkwood factor*. The modified

Curie law is then given by

$$\chi_{or} = \frac{n\mu^2}{3kT\varepsilon_0} \cdot g. \quad (3.16)$$

3.5.3 Dynamic Response

In the previous section the special case of static external electric fields have been considered. After any change of the external field infinitely long waiting times were assumed in order to find a fully established thermal equilibrium. The fluctuation-dissipation-theorem (FDT) states that a thermodynamic system, which is exposed to a disturbance by a (small) external field and, thus, pushed into thermal inequilibrium, will relax to the new equilibrium state via the same microscopic mechanisms that are also responsible for the thermal fluctuations in equilibrium. Since, finally, molecular dynamics shall be accessed with the help of DS, the time dependence of the orientational polarization on finite time scales are of particular interest in this section. The subsequent paragraphs follow closely Refs. [44, 52, 53, 62]. Note that now scalar instead of vectorial quantities are discussed for the sake of clarity.

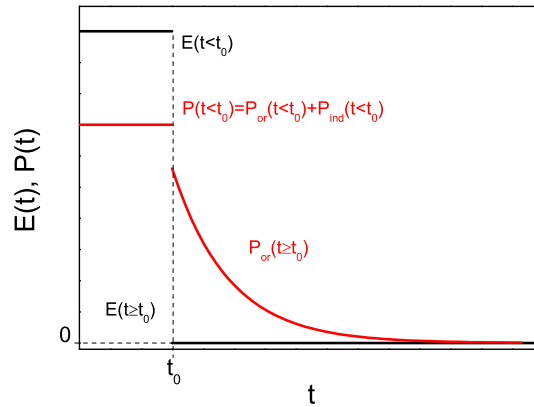


Figure 3.8: Sketched time dependence of the sample polarization (red) after switching off a static external field (black) at $t = t_0$.

Figure 3.8 shows schematically the time dependence of the sample polarization $P(t)$ as a response to the abrupt switching off of the external electric field $E(t)$ at the time $t = t_0$. The induced polarization $P_{ind}(t)$ (cf. Eq. 3.10) vanishes for $E = 0$, which manifests itself as an apparently immediate decrease of the polarization at $t = t_0$ (the equilibration of $P_{ind}(t)$ takes place on very short time scales not resolvable with conventional dielectric experiments). The orientational polarization $P_{or}(t)$ approaches its new equilibrium value (zero in Fig. 3.8) on a finite and measurable time scale.

The time dependence of the orientational polarization (for $t \geq t_0$) can be used to generally define the so-called step response function

$$\Phi_P(t) = \frac{P_{or}(t) - P_{or}(t \rightarrow \infty)}{P_{or}(0)} . \quad (3.17)$$

Note that $P_{or}(0) = P_{or}(t_0)$; for the sake of convenience $t_0 = 0$ shall be valid from this point on. Without loss of generality it shall further be assumed that $P_{or}(t \rightarrow \infty) = 0$, as displayed in Fig. 3.8, which yields

$$\Phi_P(t) = \frac{P_{or}(t)}{P_{or}(0)} . \quad (3.18)$$

$P_{or}(t)$ can now be expressed as (cf. Eq. 3.13)

$$P_{or}(t) = P_{or}(0) \cdot \Phi_P(t) = \varepsilon_0 \chi_{or} E(t=0) \cdot \Phi_P(t) . \quad (3.19)$$

One possible formulation of the FDT is the equivalence of the step response function with the autocorrelation function given in Eq. 3.5:

$$\Phi_P(t) = C_P(t) . \quad (3.20)$$

The time constant of autocorrelation and step response functions are defined via the integral

$$\tau = \int_0^\infty \Phi_P(t) dt = \int_0^\infty C_P(t) dt . \quad (3.21)$$

In order to mathematically tackle $P_{or}(t)$ for arbitrary time dependences of the external field, it is useful to introduce the pulse response function

$$\varphi_P(t) = -\frac{d\Phi_P(t)}{dt} . \quad (3.22)$$

The orientational polarization can now be calculated [44] to

$$P_{or}(t) = \varepsilon_0 \chi_{or} \int_{-\infty}^t \varphi_P(t-t') E(t') dt' . \quad (3.23)$$

The special case of harmonic external fields $E(t) = E_0 \cos \omega t$ yields

$$P_{or}(t) = \varepsilon_0 E_0 \chi_{or} \int_{-\infty}^t \varphi_P(t-t') \cos \omega t' dt' \quad (3.24)$$

leading to

$$\begin{aligned} P_{or}(t) &= \varepsilon_0 E_0 \chi_{or} \int_0^\infty \varphi_P(t') \cos(\omega(t-t')) dt' \\ &= \varepsilon_0 E_0 \chi_{or} \int_0^\infty \varphi_P(t') [\cos \omega t \cos \omega t' + \sin \omega t \sin \omega t'] dt', \end{aligned}$$

which finally contains the Fourier-transform of the pulse response function:

$$\begin{aligned} P_{or}(t) &= \varepsilon_0 E_0 \cos \omega t \cdot \chi_{or} \int_0^\infty \varphi_P(t') \cos \omega t' dt' + \\ &\quad + \varepsilon_0 E_0 \sin \omega t \cdot \chi_{or} \int_0^\infty \varphi_P(t') \sin \omega t' dt'. \end{aligned} \quad (3.25)$$

The orientational polarization thus consists of an in-phase contribution and a contribution in quadrature phase. The frequency-dependent susceptibility expressions, which determine the magnitude of each part, are defined like (cf. Eq. 3.25)

$$\begin{aligned} \chi'(\omega) &= \chi_{or} \int_0^\infty \varphi_P(t') \cos \omega t' dt' \\ \chi''(\omega) &= \chi_{or} \int_0^\infty \varphi_P(t') \sin \omega t' dt'. \end{aligned} \quad (3.26)$$

Similar to the polarization, one can consider the dielectric displacement in the case of harmonic external fields, yielding

$$\begin{aligned} \varepsilon'(\omega) &= \varepsilon_{or} \int_0^\infty \varphi_D(t') \cos \omega t' dt' \\ \varepsilon''(\omega) &= \varepsilon_{or} \int_0^\infty \varphi_D(t') \sin \omega t' dt' \quad \text{with} \quad \varepsilon_{or} \varphi_D(t) = \chi_{or} \varphi_P(t) + \delta(t), \end{aligned} \quad (3.27)$$

with $\delta(t)$ denoting the Dirac delta distribution. Now, complex properties may be defined like

$$\begin{aligned} \hat{\chi}(\omega) &= \chi'(\omega) - i\chi''(\omega) \\ \hat{\varepsilon}(\omega) &= \varepsilon'(\omega) - i\varepsilon''(\omega), \end{aligned} \quad (3.28)$$

allowing for a complex reformulation of eqs. 3.13:

$$\begin{aligned}\hat{P}(\omega, t) &= \varepsilon_0 \hat{\chi}(\omega) \hat{E}(\omega, t) \\ \hat{D}(\omega, t) &= \varepsilon_0 \hat{\varepsilon}(\omega) \hat{E}(\omega, t) = \varepsilon_0 \hat{E}(\omega, t) + \hat{P}(\omega, t) \\ \hat{\varepsilon}(\omega) &= \hat{\chi}(\omega) + 1.\end{aligned}\tag{3.29}$$

In accord with Eq. 3.12, the last equations have the consequence

$$\begin{aligned}\varepsilon'(\omega) &= \chi'(\omega) + 1 \\ \varepsilon''(\omega) &= \chi''(\omega).\end{aligned}\tag{3.30}$$

When results of dielectric experiments are shown in literature, the dielectric permittivity $\hat{\varepsilon}(\omega)$ is the quantity discussed preferably. In most cases the discussion is limited to the imaginary part $\varepsilon''(\omega)$, which is then called *dielectric susceptibility*. It can be shown that only the response in quadrature phase to the external field dissipates energy into the sample medium. Therefore $\varepsilon''(\omega)$ is further called *loss factor* or simply *dielectric loss*. Note again that $\chi_{or} = \varepsilon_{or} = \Delta\varepsilon$ are used equivalently. According to eqs. 3.26 and 3.28, the complex susceptibility is defined like

$$\begin{aligned}\hat{\chi}(\omega) &= \Delta\varepsilon \int_0^\infty \varphi_P(t') [\cos \omega t' - i \sin \omega t'] dt' \\ &= \Delta\varepsilon \int_0^\infty \varphi_P(t') \exp(-i\omega t') dt' .\end{aligned}\tag{3.31}$$

Integration by parts yields

$$\begin{aligned}\frac{\hat{\chi}(\omega)}{\Delta\varepsilon} &= 1 - i\omega \int_0^\infty \Phi_P(t') \exp(-i\omega t') dt' \\ \frac{\chi''(\omega)}{\Delta\varepsilon} &= -\Im \left\{ \frac{\hat{\chi}(\omega)}{\Delta\varepsilon} \right\} = \omega \cdot \int_0^\infty \Phi_P(t') \cos \omega t' dt' .\end{aligned}\tag{3.32}$$

Together with the Wiener-Khinchine theorem (Eq. 3.8) and the equivalence of step response and autocorrelation function (Eq. 3.20) another formulation of the FDT is given by

$$\frac{\chi''(\omega)}{\Delta\varepsilon\omega} = \frac{\chi_n''(\omega)}{\omega} = S_P(\omega)\tag{3.33}$$

with n denoting “normalized”. This connection between spectral density and susceptibility allows for an extensive comparison of experimental data stemming from different measurement techniques like dynamic light scattering (DLS; e.g. [36]) or

nuclear magnetic resonance spectroscopy (NMR, cf. [58]). Note that different experimental techniques measuring molecular reorientation probe reorientational autocorrelation functions of different Legendre polynomials. Some relaxation features appear then in different accentuations [36,64]. From the given definitions of the spectral density (Eqs. 3.8 and 3.33) it follows that

$$\lim_{\omega \rightarrow 0} \left(\frac{\chi_n''(\omega)}{\omega} \right) = S_P(0) = \int_0^{\infty} \Phi_P(t) dt = \tau. \quad (3.34)$$

From

$$\lim_{\omega \rightarrow 0} \left(\frac{d\chi_n''(\omega)}{d\omega} \right) = \lim_{\omega \rightarrow 0} S_P(\omega) + \underbrace{\lim_{\omega \rightarrow 0} \left(\omega \frac{dS_P(\omega)}{d\omega} \right)}_0 = S_P(0) = \tau \quad (3.35)$$

it follows that normalized susceptibility data show, when plotted versus ω , the slope τ in the low-frequency limit. When the data is plotted versus $\omega\tau$, the data show the slope 1 in the low-frequency limit. This fact is used to obtain mean relaxation times in a model independent way (see, e.g., Paper 2).

3.5.4 Measurement Setup

For all measurements of this work a parallel plate capacitor as shown in Fig. 3.9 was used as sample cell. The design of the cell corresponds to the descriptions given in [20], Fig. 3.9 is taken from Ref. [44].

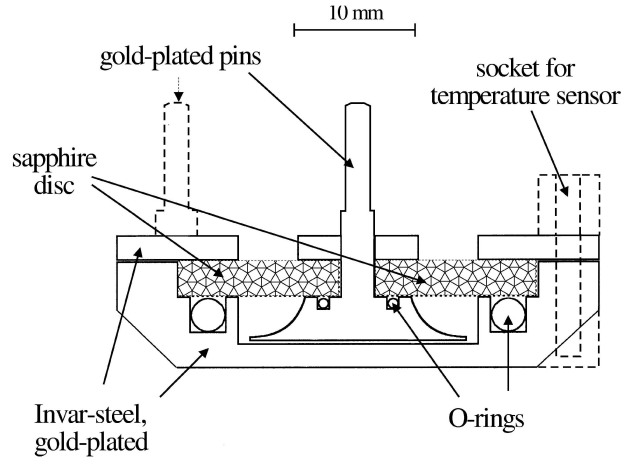


Figure 3.9: Measurement cell (figure taken from [44]).

The capacitor is made of gold-plated invar steel. A sapphire disc insulates the upper from the lower electrode. The mechanical contacts between the electrodes

and the sapphire disk secure a spacing of about $60\text{ }\mu\text{m}$ between both electrodes, where the liquid sample under investigation is placed. No additional spacer material like, e.g., fiber glass is required for this setup. The diameter of the upper electrode is about 18 mm, which leads to an empty capacity $C_0 \approx 38\text{ pF}$. As can be inferred from Fig.3.9, there is enough space above the upper electrode to collect excess sample material not fitting in the gap between the electrodes. When binary liquids were measured, the O-ring in the lower electrode was used to prevent evaporation of the volatile component and, thus, to keep the concentration of the mixture constant.

The sample capacitor was connected to the “Alpha-A Analyzer” by Novocontrol, which operates in the frequency range $\nu = 10^{-3}\text{--}10^7\text{ Hz}$. Since measuring below $\nu = 10^{-2}\text{ Hz}$ is very time consuming, the lower bound of the frequency range was limited to $\nu = 10^{-2}\text{ Hz}$ for most measurements. Since measurement artifacts around $\nu = 10^6\text{ Hz}$ tend to influence the results, data acquired in the range $\nu = 10^5\text{--}10^7\text{ Hz}$ are partially omitted in the figures. For the frequency-dependent measurement a harmonic voltage

$$\hat{U}(\omega, t) = U_0 \exp(i\omega t) \quad (3.36)$$

is applied to the sample. The phase-sensitive detection of the current $\hat{I}(\omega, t)$ allows for the measurement of the impedance

$$\hat{Z} = \frac{\hat{U}}{\hat{I}}. \quad (3.37)$$

For a capacitor $I = \dot{Q} = C\dot{U}$ holds, which can be adapted to the complex properties like

$$\hat{I}(\omega, t) = \hat{C}(\omega) \cdot i\omega \hat{U}(\omega, t) \quad (3.38)$$

finally leading to

$$\hat{\varepsilon}(\omega) = \frac{1}{i\omega C_0 \hat{Z}(\omega)}. \quad (3.39)$$

Note that any DC conductivity σ of the sample (now thought of as ohmic resistor), which appears solely in the real part of the impedance ($\hat{Z}(\omega) = R$), will contribute exclusively to the imaginary part of the dielectric function $\hat{\varepsilon}(\omega)$. Introducing the resistivity

$$\rho = R \frac{A}{d} = R \frac{C_0}{\varepsilon_0} = \frac{1}{\sigma} \quad (3.40)$$

leads to

$$\hat{\varepsilon}_{cond}(\omega) = \frac{1}{i\omega C_0 R} = \frac{\sigma}{i\omega \varepsilon_0} \quad (imaginary) \quad (3.41)$$

and

$$\varepsilon''_{cond}(\omega) = \frac{\sigma}{\varepsilon_0 \omega}. \quad (3.42)$$

The conductivity contribution to the dielectric susceptibility given in Eq. 3.42 appears in the form of a power law $\varepsilon''(\omega) \propto \omega^{-1}$.

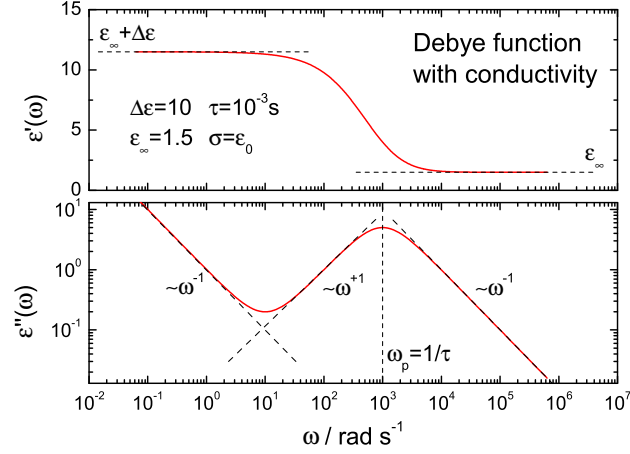


Figure 3.10: Sum of a Debye function and a typical DC conductivity contribution. Upper panel: real part $\varepsilon'(\omega)$ according to Eq. 3.45; lower panel: imaginary part $\varepsilon''(\omega)$ according to Eq. 3.46.

The simplest case of a step response function is a single exponential decay

$$\Phi_P(t) = \exp\left(-\frac{t}{\tau}\right). \quad (3.43)$$

According to Eq. 3.31, the corresponding dielectric function is given by

$$\begin{aligned} \hat{\varepsilon}(\omega) &= \Delta\varepsilon \int_0^\infty \left[-\frac{d}{dt} \exp\left(-\frac{t}{\tau}\right) \right] \exp(-i\omega t) dt + \varepsilon_\infty \\ &= \Delta\varepsilon \cdot \frac{1}{1 + i\omega\tau} + \varepsilon_\infty \end{aligned} \quad (3.44)$$

(cf. also Eq. 3.14) and called *Debye function*. The corresponding real and imaginary parts are

$$\begin{aligned} \varepsilon'(\omega) &= \Delta\varepsilon \cdot \frac{1}{1 + \omega^2\tau^2} + \varepsilon_\infty \quad \text{and} \\ \varepsilon''(\omega) &= \Delta\varepsilon \cdot \frac{\omega\tau}{1 + \omega^2\tau^2}. \end{aligned} \quad (3.45)$$

Adding a conductivity contribution (Eq. 3.42) to the imaginary part is in accord with a common approach, assuming an ohmic resistor connected in parallel to the

sample capacitor, and yields

$$\varepsilon''(\omega) = \Delta\varepsilon \cdot \frac{\omega\tau}{1 + \omega^2\tau^2} + \frac{\sigma}{\varepsilon_0\omega}. \quad (3.46)$$

Figure 3.10 displays real and imaginary part of a Debye function including a DC conductivity contribution. The corresponding parameters are given in the figure. In the upper panel the real part $\varepsilon'(\omega)$ according to Eq. 3.45 is shown, decaying monotonically from $\varepsilon_\infty + \Delta\varepsilon$ to ε_∞ . The step (maximum slope) is situated around $\omega = 1/\tau$. The lower panel of Fig. 3.10 displays the imaginary part $\varepsilon''(\omega)$ showing a peak at $\omega_p = 1/\tau$. Due to the double logarithmic representation the flanks of the peak, power laws $\propto \omega^1$ and $\propto \omega^{-1}$, appear as straight lines. Some frequency decades below ω_p a minimum is observed; left to the minimum the DC conductivity contribution is found. The conductivity contribution also appears as a straight line on the low frequency side of the peak (power law $\propto \omega^{-1}$; according to Eqs. 3.42 and 3.46).

When the isotropic molecular reorientation in supercooled liquids is probed, the observed susceptibility peak, the α -process, is broadened asymmetrically on the high-frequency side in comparison with the Debye peak. This broadening is usually interpreted as a signature of the cooperative nature of the α -process. A distribution of correlation times due to dynamic heterogeneities also corresponds to a broadened susceptibility peak. Several phenomenological fit functions quantifying the broadening, such as the Kohlrausch- or the Cole–Davidson-function [52], or modeled distributions of correlation times [44, 65] exist; a new function is discussed in Paper 1. Nevertheless, the special case of the exponential correlation decay and the corresponding Debye line shape of $\varepsilon''(\omega)$ is experimentally observed, too [66, 67]. A relaxation process found in monoalcohols like *n*-butanol [68], 2-ethyl-1-hexanol [69], ethanol [4] or water [68, 70], the mechanism of which is not fully elucidated yet, causes a typical Debye line shape of $\varepsilon''(\omega)$, and is thus usually referred to as *the Debye process*.

3.6 Contemporary Broadband Dielectric Spectroscopy

Historical dielectric experiments, which were limited to the determination of the temperature-dependent static dielectric constant or the measurement of the dielectric function $\hat{\varepsilon}(\nu = \text{const.}, T)$ at single frequencies, have been replaced by broadband techniques with a wide frequency range. Presenting data of isothermal measurements covering eight frequency decades has become the scientific standard. Combining several broadband setups (including time-domain setup, microwave reflectometry and Fourier-transform infrared spectroscopy), as done for example in the dielectric laboratory at the University of Augsburg run by A. Loidl and P. Lunkenheimer [19], makes it possible to measure the dielectric susceptibility

over the range of 16 frequency decades, which may be considered as the experimental state of the art (cf. also Fig. 3.1 (b)). Important to mention is also the application of high precision capacitance bridges as done, for example, by C. Gainaru et al. in order to obtain highly accurate susceptibility data even at lowest temperatures [53, 71]. The bridge used by Gainaru et al. has a narrower frequency range, but a higher accuracy, or sensitivity to low signals, than the broadband spectrometer applied within the present work.

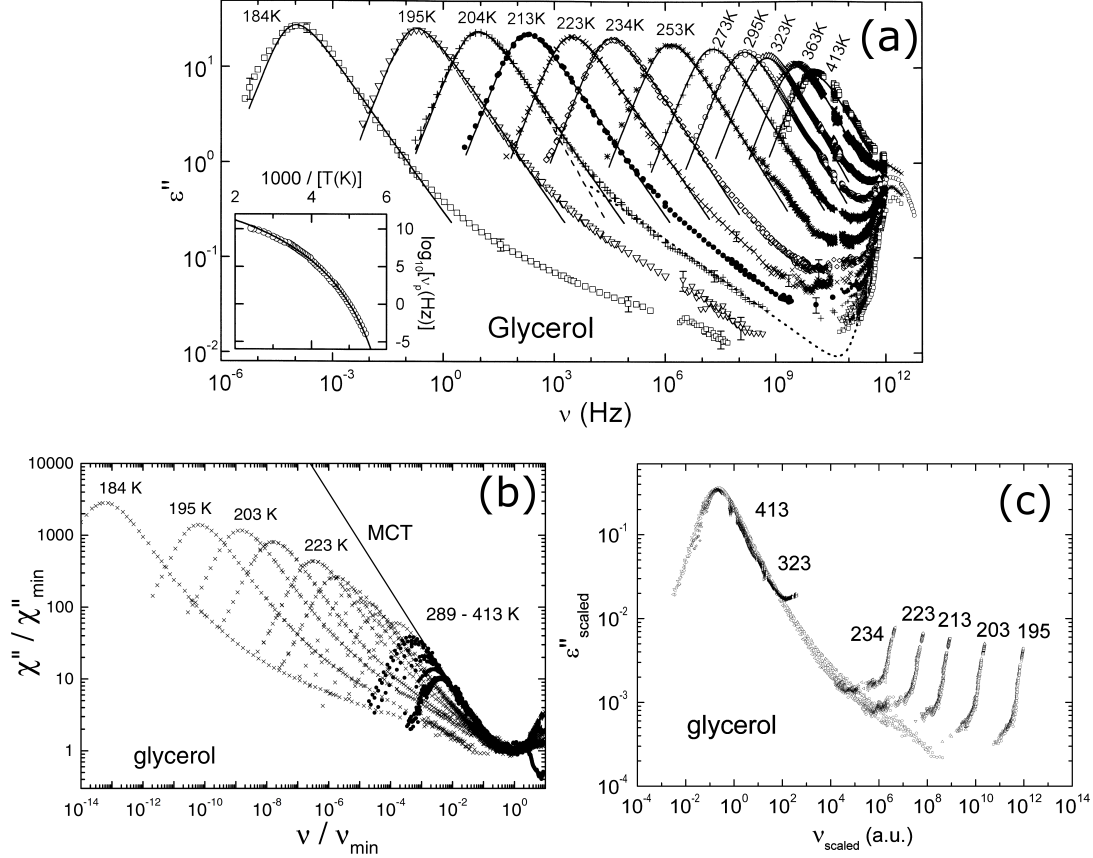


Figure 3.11: (a) Dielectric susceptibility of super-cooled glycerol, measured by the Augsburg group around P. Lunkenheimer. Figure taken from Ref. [72]. Inset: temperature dependence of the susceptibility peak positions. (b) The same data as in (a), rescaled to the susceptibility minimum according to the axes titling [73]. Crosses: data acquired in the temperature range $T = 184\text{--}273\text{ K}$. Circles: temperature range $T = 289\text{--}413\text{ K}$. (c) Selection of the data shown in (a), now scaled to the maxima [53].

In Figure 3.11 (a) dielectric susceptibility data of glycerol as published by the Lunkenheimer group [72] are shown, covering the frequency range $\nu \approx 10^{-5}\text{--}10^{12}\text{ Hz}$. The signal amplitudes reach from $\varepsilon'' \approx 0.01\text{--}20$, hence a wide dynamic range is accessed and even tiny spectral features can be resolved. For all isotherms shown in Fig. 3.11 (a) a prominent peak is observed, which shifts from $\nu_P = 10^{10}\text{ Hz}$

at $T \approx 400$ K to $\nu_P = 10^{-4}$ Hz at $T = 184$ K. The temperature dependence of the peak position ν_P is displayed in the inset of Fig. 3.11 and shows a strong curvature, i.e. a super-Arrhenius behavior of the time constant $\tau_P = 1/(2\pi\nu_P)$ typical for glassy dynamics [18, 26, 36, 74] is observed. Note that only in the case of the Debye peak $\tau = \tau_{max}$ holds exactly. In most cases there is yet no significant difference between the temperature dependences of $\tau_{max}(T)$, corresponding to the peak positions, and the mean correlation times $\tau(T)$ as defined by Eq. 3.21. Obviously an increase of the correlation time beyond any laboratory time scale is expectable when T is lowered further (cf. Sec. 3.3).

When the DS data are rescaled to the susceptibility minimum between α -relaxation and the so-called boson peak at highest frequencies (Fig. 3.11 (b)), the data of the temperature range $T = 289$ –413 K (circles) have a common envelope [73]. Data of temperatures below $T = 289$ K (crosses) deviate from the common envelope due to secondary relaxation features emerging between α - and boson peak in the form of excess susceptibility. For example, inspecting the $\varepsilon''(\nu)$ curve for $T = 184$ K in Fig. 3.11 (a), the high frequency side of the main relaxation peak has the shape of a power law in the range $\nu = 10^{-3}$ – 10^{-1} Hz. At higher frequencies ($\nu = 10^0$ – 10^2 Hz) a distinct positive curvature is observed, marking a crossover to another power law shape in the range ($\nu = 10^2$ – 10^7 Hz). The latter feature is usually referred to as *excess wing* (EW); glass formers showing an EW instead of secondary relaxation peaks are called *type-A* systems, according to the classification by Kudlik et al. [75].

All peaks shown in Fig. 3.11 (a) have nearly the same spectral shape, as demonstrated in Fig. 3.11 (c), where the data are scaled to the susceptibility maxima [53]. Thus, FTS (frequency domain equivalent of TTS, cf. Sec. 3.3) is obeyed in good approximation by the main relaxation peak. (As will be discussed in Paper 2 a slight sharpening of the peaks with increasing temperature can be quantified anyway.) TTS is also observed for the long-time decay of the correlation functions acquired by broadband DLS shown in Fig. 3.6 in Sec. 3.3. Remarkably, the data collapse shown in the master curve in Fig. 3.11 (c) also involves the EW contribution.

Besides the EW, as observed in the glycerol data (Fig. 3.11) and many other type-A glass formers (see Papers 2 & 3), explicit secondary relaxation (or β -) peaks are found in the susceptibility of *type-B* systems [75] (see Papers 4 & 5). In contrast to the α -relaxations, the time constants of which show non-Arrhenius behavior, the β -processes show thermally activated dynamics, i.e. their time constants follow Arrhenius laws [53, 75, 76]. Kudlik et al. [75] find mean activation energies of $\langle E \rangle \approx 24 T_g$ for most cases and attempt times in the range $\tau_0 = 10^{-18}$ – 10^{-15} s. The relaxation strengths of the β -processes $\Delta\varepsilon_\beta$ in relation to the respective α -relaxation strengths differ strikingly when several glass formers are compared [44]. Below T_g the $\Delta\varepsilon_\beta(T)$ are nearly constant, while they show a strong increase when temperature is increased above T_g [65, 77]. In Fig. 3.12 [44] DS data of the type-B systems (a) toluene (TOL) and (b) 3-fluoro aniline (or m-fluoro aniline; m-FAN) are collected, showing explicit β -peaks in addition to the α -relaxation peaks, ap-

pearing at clearly higher maximum frequencies than the latters. For TOL (Fig. 3.12 (a)) an immediate crossover from α - to β -peak is observed. In the case of m-FAN (Fig. 3.12 (b)) indications of an additional EW, appearing as a power law between α - and β -peak, are found.

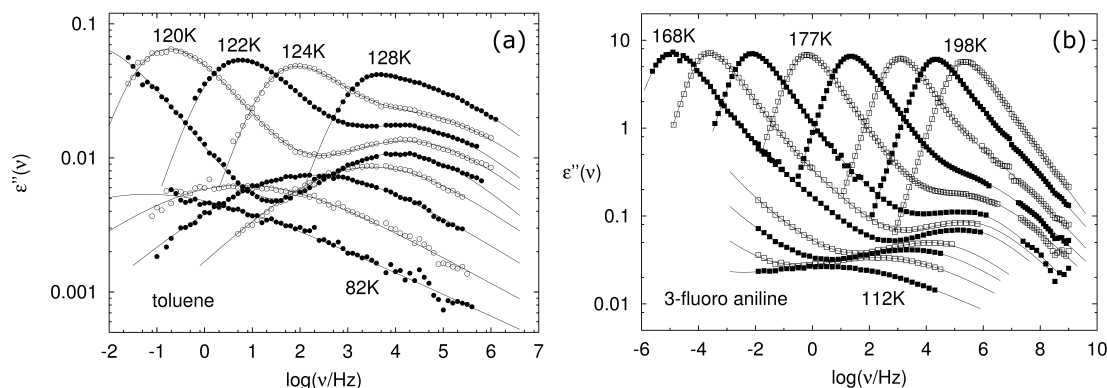


Figure 3.12: Dielectric susceptibility of type-B systems; figures taken from [44]. (a) Toluene ($T_g = 117$ K). (b) 3-fluoro aniline ($T_g = 172$ K).

The investigation of secondary relaxations in supercooled liquids has become an important task within the “glass community”, as well it is a significant issue of the present work. In Paper 4 an ensemble of chemically related systems consisting of six type-B glass formers are investigated. Since these systems contain phosphorus, they are very interesting systems for being also analyzed with the help of ^{31}P NMR as done by our group. In the Papers 5 & 6 binary mixtures of one of these systems (tripropyl phosphate; TPP) and polystyrene are investigated with DS as well as ^{31}P and ^2H NMR. A major strength of dielectric spectroscopy compared to other methods is the ability to resolve these secondary processes with high accuracy despite of their usually low signal compared to the primary relaxation. Due to the high sensitivity of the method, even subtle variations of the line shapes of primary as well as secondary relaxation features are detectable and quantifiable with the help of DS. Each publication included in this thesis thrives on this fact (Papers 1–6).

3.7 Existing Approaches to Describe Generic Relaxation Phenomena, Open Questions, and Major Results

Contemporary broadband DS on supercooled organic glass formers deals with the challenge of understanding the temperature evolution of the dynamic susceptibility, i.e. to phenomenologically comprehend the glass transition. An important step towards this understanding, which has been followed since long, is to establish an extensive data collection of different glass forming systems covering frequencies

from 0–1 THz. In this context, it is not less important to learn how to distinguish between system specific and generic phenomena by finding a conclusive way of disentangling the individual relaxation features. Today, several approaches are followed by different working groups, leading to different perceptions of EW, α - and β -relaxation. In the following section the most important interpretations are summarized.

α -relaxation The main process of molecular rearrangement in a liquid causes the so-called α -relaxation in the case of an external disturbance. This α -relaxation is responsible for the structural relaxation of the sample, which is accompanied by an isotropic and cooperative reorientation of the molecules (or, respectively, monomer units in polymers). This molecular reorientation manifests itself as the α -peak in the dynamic susceptibility. Orientational relaxation in plastic crystals shows a similar phenomenology [2–9].

One of the main experimental controversy concerning the α -relaxation is the question whether frequency-temperature superposition (FTS) holds for the α -relaxation at all temperatures $T \geq T_g$. Of course, any emerging secondary processes appearing close to T_g have to be separated adequately from the α -peak when this question is addressed. Schneider et al. [72] evaluated the data shown in Fig. 3.11 (a) by fitting exclusively the α -peaks and found a systematically temperature-dependent peak width, which is contrary to the results of the scaling analysis mentioned above (Fig. 3.11 (c)) presented ten years later [53] and actually reflecting the interpretation followed by the Bayreuth group since then. There are also earlier publications by this group explicitly showing systematic temperature dependences of the width parameter of the α -peak, yielded by fitting analyses [4, 58, 65, 73, 75, 78, 79]. These results were later put into perspective with the problem of a limited available fitting range (see below). Furthermore, in the context of a scaling analysis used by S. R. Nagel (University of Chicago) and co-workers [80–82], which applies within a certain approximation [83, 84], a failure of FTS is reported.

On the other hand, Olsen et al. [85] showed, for the system triphenyl phosphite, that FTS holds for the main relaxation peak even down to the glass transition temperature, as long as secondary processes are absent (EW) or at least well-separated (β -relaxation) from the α -peak. Based on this idea, Gainaru et al. introduced the approach of understanding the dielectric susceptibility as being composed additively of α -relaxation, excess wing (EW) and, if necessary, a β -relaxation [53, 76] (in this thesis often referred to as *the Gainaru approach*). Within this ansatz, besides a temperature-invariant line shape of the α -peak a temperature-independent exponent of the EW is assumed. Only τ_α and the amplitudes of α -peak and EW are temperature-dependent. This approach gives a much simpler picture of the evolution of the dynamic susceptibility than the straight forward fitting procedures presented by Blochowicz et al. [65, 79]. Furthermore, Brodin et al. showed that the typical temperature dependence of the line shape parameters of several

systems presented there may be merely an artifact due to the particular fitting strategy and the limited frequency range of the data [86]. The authors showed with the help of simple scaling representations, that actually FTS holds in good approximation for the α -relaxation peak, and even the comparison of α -peaks of different systems do not show significant differences. This new picture gives new input for, e.g., the advancement of theories like MCT. In addition to that, procedures of any analysis of data with a limited frequency range, e.g. the evaluation of fast field cycling NMR data, is based on FTS.

The following **open questions** concerning the α -relaxation are (re-)addressed in the present work:

- To which extent does FTS hold for the α -relaxation close to T_g ? (\rightarrow Papers 1 & 2.)
- Can apparent variations of the broadening of the α -peak be explained by a temperature-dependent excess wing amplitude? (\rightarrow Paper 2.)
- How can susceptibility spectra be interpolated adequately on the basis of the refined picture of the α -relaxation? (\rightarrow Papers 1 & 2.)
- How does the main relaxation peak of a plastic crystalline phase formed in the supercooled regime differ from the α -peak of the corresponding liquid? (\rightarrow Paper 3.)

The **major results** of the present work concerning the α -relaxation shall be summarized in the following. The first part of Paper 2 focuses on the temperature dependence of the dielectric susceptibility of glass formers with no resolved β -peak (type-A systems), i.e. the evolution of α -peak and EW under varying temperature. Plotting the normalized spectra versus $\omega\tau_\alpha$ leads to a collapse of the data on the low-frequency side of the α -peak (*low-frequency scaling*). While the line shape of the α -peak was considered to be essentially temperature-independent in the context of Gainaru's approach [53, 76, 86], a subtle but systematic variation in the high-frequency region of the master curves becomes obvious here. When the data sets are rescaled as demonstrated for PG in Fig. 3.13 (a), an almost perfect collapse on the high-frequency part of the data is observed, including the high-frequency flank of the α -peak as well as the EW. This *high-frequency scaling* suggests that temperature-affected changes of the line shape, which cannot be explained solely by the varying EW amplitude, concern merely the overall peak width instead of the high-frequency exponent of the α -peak. The subtle violation of FTS can thus be projected completely to the low-frequency region of the α -relaxation. This result is of high importance for the Gainaru approach itself since for this ansatz a temperature-independent high-frequency exponent of the α -peak is a necessary implication.

In order to quantify these findings, a phenomenological three parameter fit function for the normalized α -relaxation peak introduced in Paper 1 is applied. The

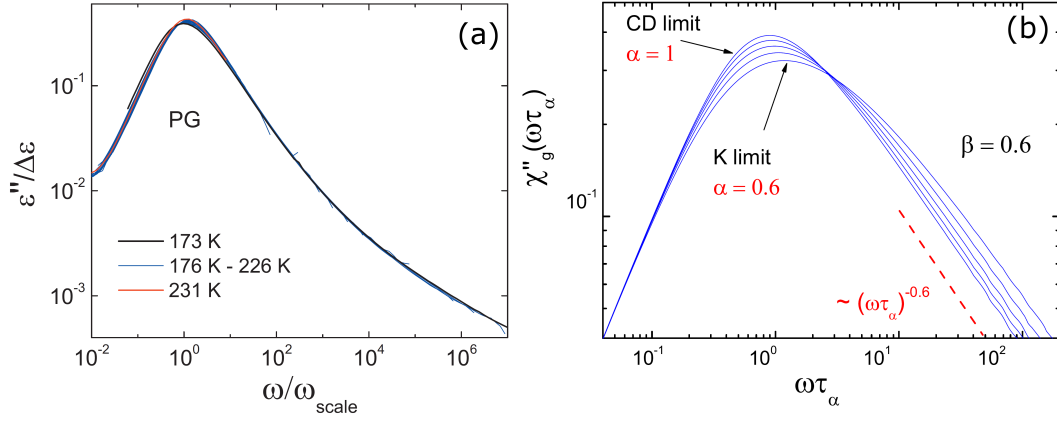


Figure 3.13: (a) Normalized susceptibility of propylene glycol (PG) plotted versus a reduced frequency (high-frequency scaling; figure taken from Paper 2). (b) Fit function introduced in Paper 1 for several values of the shape parameter α , normalized and plotted versus $\omega\tau_\alpha$.

function is defined as step-response function $\Phi_g(t)$ and has two shape parameters α and β besides the time constant τ_g . While the Cole-Davidson (CD) and Kohlrausch (K) functions have only one stretching parameter, which affects the broadening of the peak by determining the exponent of its high-frequency power law, the new function has a further shape parameter, which changes the shape of the tip of the relaxation peak without affecting the high-frequency exponent. The specialty of the new function is that the well-established K and CD functions are reproduced in the limiting cases $\alpha \rightarrow \beta$ and $\alpha \rightarrow 1$, respectively. In other words, the function $\Phi_g(t)$ interpolates continuously between K and CD peak shape (Fig. 3.13 (b)). Contrary to the Havriliak-Negami (HN) function, $\Phi_g(t)$ has a well-defined mean relaxation time τ_α due to the physically valid low-frequency limit $\varepsilon''(\nu) \propto \nu^1$ of its susceptibility representation. Finally it is shown in Paper 1 that $\Phi_g(t)$ has a non-negative distribution of correlation times $G(\ln \tau)$, which is the precondition for a physically valid relaxation function.

In Paper 2 dielectric susceptibilities of PC, PG, m-TCP, GLY and 4-TBP are fitted with this function, which is now extended to account also for the EW contribution. The results are displayed in Fig. 3.14. For basically all considered systems the shape parameter γ of the EW as well as the high-frequency parameter β of the α -peak are, in the spirit of the Gainaru approach, kept constant for all temperatures. The resulting parameters α (additional shape parameter of the α -peak) and C (relative relaxation strength of the EW) are found to be temperature-dependent: with increasing T α increases from $\alpha < 1$ to $\alpha = 1$, reflecting the peak assuming a Cole-Davidson (CD) shape above a certain temperature. At the same time $C > 0$ is nearly constant over a certain temperature range, before it decreases quickly to 0 when α assumes unity. The system 4-tert-butylpyridine (4-TBP), which is also discussed in Paper 2, cannot be analyzed in the same way. As can be inferred from Fig. 3.13 (inset), the shape parameter β is significantly

temperature-dependent (inset), further the temperature dependence of its shape parameter α differs from the behavior of the other analyzed systems. It turns out that this irregularity is caused by the presence of a weak β -process in the spectra of 4-TBP, which is hidden by the EW (see below).

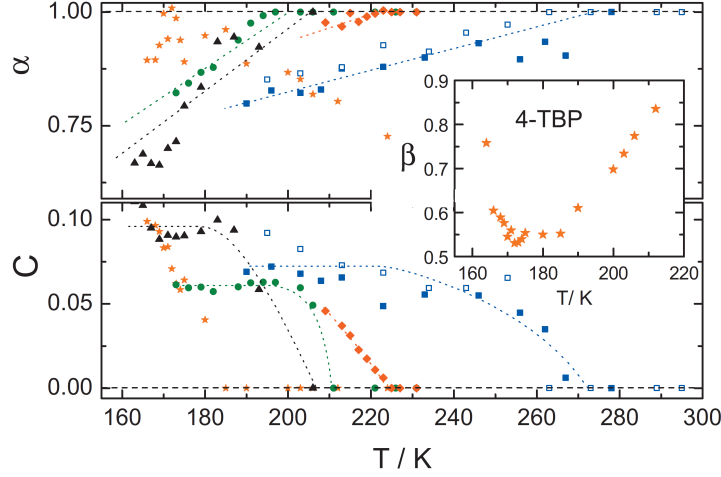


Figure 3.14: Fit parameters α and C as presented in Paper 2.

Quinaldine (2-methyl quinoline) is an exemplary type-A glass former [87]. In Paper 3 the three-parameter fit function introduced in Paper 1 is extended to account for EW and conductivity contribution and is now used to quantify the evolution of the dynamic susceptibility of quinaldine. Again, the high-frequency shape parameter β of the α -peak as well as the power law exponent γ describing the EW are found to be temperature-independent, while α and C show a weak variation with T . Further, the low-frequency scaling of the susceptibility curves reveals a temperature dependence of the line shape, which is limited to the EW region. The α -relaxation peak itself appears to obey FTS almost perfectly.

At temperatures well above $T_g = 180$ K (200 K $< T < T_m$) two subsequent phase transitions of liquid quinaldine (2mq1) into two dielectrically active phases (2mq2 and 2mq3) are observed. Paper 3 is funded through the project “Schwerpunktprogramm (SPP) 1415: Kristalline Nichtgleichgewichtsphasen - Präparation, Charakterisierung und in-situ-Untersuchung der Bildungsmechanismen” by Deutsche Forschungsgemeinschaft (DFG). Particular interest of the SPP lies in the mechanism of formation of the metastable crystalline phase. Thus, the analysis of the phase transitions and the phases itself is the actual main concern of Paper 3.

Figure 3.15 (a) displays results of a DS long-term measurement tracking the phase transition from the liquid phase 2mq1 to the dielectrically active crystalline phase 2mq2. A quantitative analysis of the time dependence of this phase transition reveals stretched exponential decays (Avrami laws, cf. Fig. 3.15 (b)) with temperature-dependent transformation time constants and exponents, the evaluation of which strongly suggests that the crystallization process is controlled by

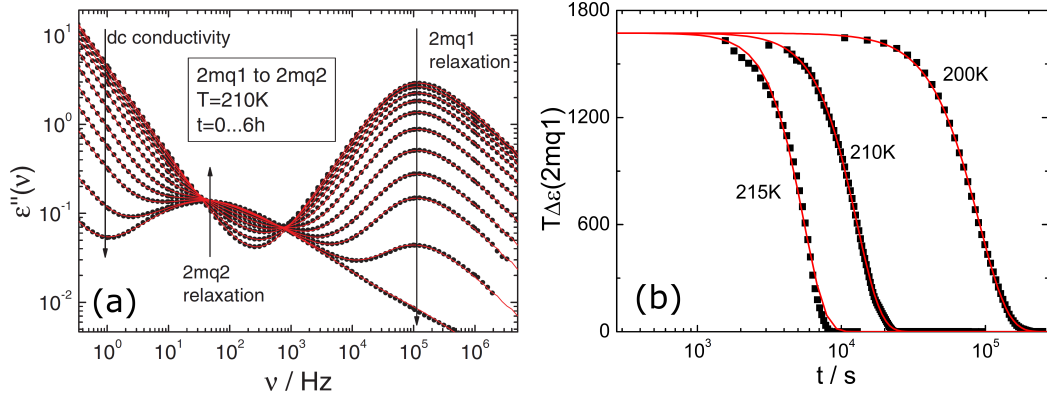


Figure 3.15: Liquid quinaldine (2mq1) transforming into the dielectrically active crystalline phase 2mq2. (a) Time-dependent dielectric spectra recorded at $T = 210$ K. (b) Decrease of the property $T\Delta\epsilon(T)$ during the phase transition from 2mq1 to 2mq2 at indicated temperatures, representing the time-dependent liquid fraction of the sample.

diffusion. Note that similar experiments concerning the crystallization kinetics of Nifedipine have been performed and are published in [88]. A phenomenology similar to the one of quinaldine (2-methyl quinoline) is also presented for 3-methyl quinoline in Paper 3.

In the context of the SPP 1415 a collaboration with the working groups around F. Emmerling (Bundesanstalt für Materialforschung und -prüfung; BAM) and K. Rademann (Humboldt-Universität zu Berlin) was established. X-ray diffraction (XRD) experiments on quinaldine presented in the present work were performed in BAM laboratories. Figure 3.16 (a) displays results of an XRD long-term measurement tracking the phase transition from the liquid phase 2mq1 to the dielectrically active crystalline phase 2mq2, clearly demonstrating a continuative emergence of Bragg reflexes out of the amorphous “halo” of 2mq1. The two crystalline phases show different X-ray diffractograms (Fig. 3.16 (b)) as well as dielectric relaxation peaks on longer time scales compared to the liquid, as has been already observed in a similar way for plastic crystalline ethanol [4, 7]. Both phase transitions manifest themselves as distinct peaks (or dips) in the DSC signal, comparable to the melting peak. They occur irreversibly, indicating that the intermediate phase 2mq2 is metastable like the supercooled liquid 2mq1.

As can be anticipated from Fig. 3.15 (a), the relaxation peaks of 2mq2 are more broadened than the α -peak of the liquid. Even broader relaxation peaks are observed for the third dielectrically active phase 2mq3 (cf. Paper 3). The relaxation strengths $\Delta\epsilon$ of the crystalline phases 2mq2 and 2mq3 are smaller than the $\Delta\epsilon$ of the liquid 2mq1. From this it can be concluded that the molecular reorientation in the two crystalline phases are spatially restricted. The EW contribution as found for the liquid (2mq1) is not observed in the same way for 2mq2. Only at lower temperatures excess susceptibility similar to an EW contribution is detected. In the case of 2mq3 no indications of an EW are observed.

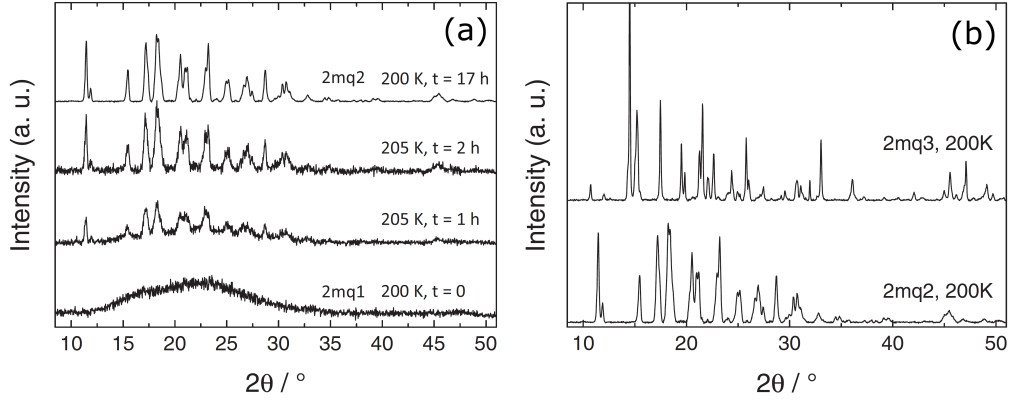


Figure 3.16: (a) Liquid quinaldine (2mq1) transforming into 2mq2, tracked by a XRD long-term measurement. (b) Comparison of X-ray diffractograms of the two crystalline phases 2mq2 and 2mq3.

β -relaxation Within this thesis the term “ β -process” means a secondary relaxation process which manifests itself as an explicit susceptibility peak at temperatures $T \lesssim T_g$. The β -processes are found to be thermally activated with a temperature-independent distribution of activation energies $g(E)$. As pointed out in Sec. 3.6, its maximum time constant $\tau_{max}(T) = 1/(2\pi\nu_{max}(T))$ follows an Arrhenius law below T_g . Kudlik et al. [75] have found mean activation energies of $\langle E \rangle \approx 24 T_g$ for most cases and attempt times in the range $\tau_0 = 10^{-18}$ – 10^{-15} s. The relaxation strengths of the β -processes $\Delta\varepsilon_\beta$ in relation to the respective α -relaxation strengths differ strikingly when several glass formers are compared [44]. Below T_g , the $\Delta\varepsilon_\beta(T)$ are nearly constant, while they show a strong increase when temperature is increased above T_g [65, 77].

β -relaxations have been known since long, usually attributed to internal motions of non-rigid molecules, or side-chain motions of polymer chains. In the seminal work of Johari and Goldstein [89] secondary relaxation peaks in the dielectric susceptibility of rigid polar molecules have been reported for the first time, thus the expression “Johari-Goldstein (JG) β -process” has become an established term denoting the β -relaxation of rigid molecules. Here, a big field of research has opened up in the past decades. The important work by Kudlik et al. [75, 78] gave the often-cited definition of type-A (no explicit β -peak) and type-B glass formers (explicit β -peak). Besides DS also other techniques have dealt with the β -process, like NMR [90–96] or solvation dynamics [97]. The main concern of these papers is the molecular mechanism of the β -process, which turns out to involve a spatially highly restricted reorientation of basically all molecules. Thus, at least for neat glass formers, the concept of “islands of mobility” introduced by Johari and Goldstein [89, 98], i.e. strong spatial heterogeneities (defects) leading to relaxational motion of a minority of molecules, is refuted. In a recent publication by our group [96] the concept is re-introduced for binary systems as the “emergence

of islands of rigidity”. Remarkably, typical β -relaxations are, in contrast to the EW, not detected by light scattering techniques [53, 76, 86].

Dielectric experiments under variable pressure [99–102] show different pressure dependences of secondary relaxations. Mierzwa et al. analyze the T - p -dependence of the dielectric susceptibility of the binary (type-B) system 2-picoline/tri-styrene as well as of the type-B glass former DGEBA [102]. In both cases the time constants of α - and β -process are temperature- and pressure-dependent. Spectra recorded at temperatures near T_g and at ambient pressure (p_{amb}) are compared to those recorded at elevated pressures (p_{elev}) and higher temperatures. For this purpose, temperature and pressure values are combined in the way that the $\tau_\alpha(T, p)$ of both measurements coincide. The spectral shapes of the α -peaks of both spectra (p_{amb} and p_{elev}) turn out to be nearly identical and, remarkably, the τ_β found at p_{amb} and p_{elev} coincide, suggesting that α - and β -relaxation are strongly coupled mechanisms. Pressure-dependent measurements on type-A systems presented in [100] reveal a similar scenario.

Paluch and co-workers perform similar experiments on decahydroisoquinoline (DHIQ) [101]. In this case, the β -relaxation found at ambient pressure turns out to be pressure-independent, hence measurements at elevated pressure lead to a separation of α - and β -process (see also [100]). The authors claim that there are two kinds of β -processes, namely those being strongly coupled to the α -relaxation (“true JG β -processes”) and those showing no sensitivity to a variation of pressure. In the framework of the so-called coupling model (CM) [74, 103] a correlation between the relaxation times of α - and β -process as well as the spectral shape of the α -peak is predicted, regardless of the applied T - p -combination. This is used by the authors of the above mentioned publications in order to identify the “true JG β -process”. As a consequence, the behavior of the EW under variable pressure may further suggest that the EW is a “true JG β -process” submerged below the α -peak [74, 103] (see below).

The following **open questions** concerning the β -relaxation are addressed within the present work:

- Is the $\langle E \rangle = 24 T_g$ rule maintainable? (\rightarrow Papers 2 & 4.)
- Is the behavior of the relaxation strength $\Delta\epsilon_\beta(T)$, as already observed for many type-B systems, universal? (\rightarrow Paper 4.)
- Is it reasonable to distinguish between JG and non-JG β -processes? In the case of flexible molecules: how do internal degrees of freedom influence the properties of the distribution of activation energies $g(E)$? (\rightarrow Paper 4.)
- Is the distribution of activation energies $g(E)$ of a β -process necessarily symmetric? (\rightarrow Papers 4 & 5.)
- What do we learn about the β -process by analyzing binary mixtures of a type-A and a type-B component? (\rightarrow Paper 5.)

- Does a cooperative process underlie the β -relaxation? (\rightarrow Papers 4 & 5.)
- Are all sample molecules involved in the β -relaxation? Which relevance does the concept of islands of mobility have for mixed glass formers? (\rightarrow Paper 5.)

Below a résumé of the **major results** concerning the β -process presented in the publications shall be given. In Paper 4 dielectric properties of a series of six molecular glass formers with a systematic chemical variation are investigated.¹ The goal of this study has been the search for a correlation between the chemical structure of the sample molecules and their dynamics. Since the molecules of all investigated systems, which all turn out to be good glass formers, are symmetric phosphoric acid esters, they are also conveniently probed by ^{31}P NMR as done by our group. This fact will be exploited in Papers 5 & 6, where the components of the binary system TPP/PS are probed selectively by ^2H and ^{31}P NMR.

Every β -process which is analyzed in this article shows time constants obeying an Arrhenius law (cf. Fig. 3.17 (a)). Similar to the findings presented in Paper 2 (cf. *ibid.*) a wide range of activation energies ($\langle E \rangle = 15 T_g - 24 T_g$) is found. Well below T_g , say $T < 0.9 T_g$, all β -processes of this study are determined by a thermally activated process (or better: by a plurality of thermally activated processes), governed by a temperature-independent distribution of activation energies $g(E)$, which completely defines the temperature evolution of the DS spectra via its relation to the distribution of correlation times $G(\ln \tau) d \ln \tau = g(E) dE$. This is evidenced by the application of a scaling procedure, which reconstructs $g(E)$ from the susceptibility data without the need of a fitting analysis (e.g. Gaussian fits as done in [75]). The resulting $g(E)$ are collected in Fig. 3.17 (b). Notably, most $g(E)$ -peaks, as well as the corresponding susceptibility peaks of the β -relaxations, are found to be asymmetric. When temperature approaches T_g ($T > 0.9 T_g$), the scaling fails due to an apparent increase of the most probable activation energy $E_{max} \approx \langle E \rangle$ or, as an alternative interpretation, due to a decrease of the attempt frequency ν_0 . Further, the scaling yields the relaxation strength $\Delta \varepsilon_\beta(T)$, which is nearly constant for all systems at temperatures $T < 0.9 T_g$. For higher temperatures a strong increase is observed (cf. Fig. 3.17 (c)).

The glass formers analyzed in Paper 4 are chemically related, i.e. the molecules of each system have a phosphate center, but side chains of different lengths. All molecules are expected not to be rigid, according to THz/far-infrared measurements on the gas phase of some of the systems [105, 106]. A weak correlation between the chain lengths and E_{max} , but no strict systematics is observed, which shows that $g(E)$ is not significantly influenced by internal degrees of freedom.

¹The three systems tributyl phosphate (TBP), tris(2-butoxyethyl) phosphate (T2BOEP) and tris(2-ethylhexyl) phosphate (T2EHP) were measured for this publication. Data of the two systems triethyl phosphate (TEP) and tripropyl phosphate (TPP) were measured for this thesis, but already published partially [104] (see also Paper 5). Note that data of TPP was also included in Paper 6. Data of trimethyl phosphate (TMP) was taken from literature [53, 73].

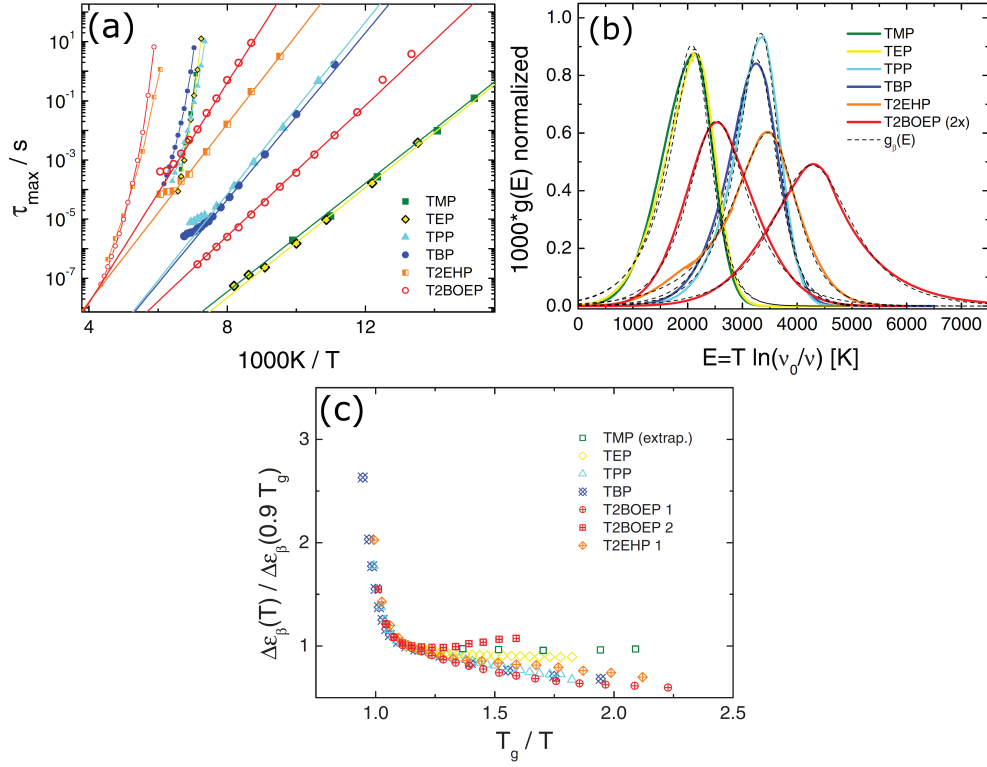


Figure 3.17: Figures presented in Paper 4. (a) Time constants of α - (smaller symbols) and β -relaxations (larger symbols) of all investigated samples. Lines are guides for the eye. (b) Distributions of activation energies underlying the β -relaxations as obtained by scaling the susceptibility (colored solid lines). Dashed lines: Fits with the $g_\beta(E)$ function [65]. (c) Temperature dependence of the relaxation strengths of the analyzed β -processes.

This suggests that all β -relaxations show the same phenomenology, which is further supported by the universal behavior of $\Delta\epsilon_\beta(T)$ mentioned above, which is also observed for liquids of rigid molecules as well as plastic crystals of flexible molecules [65,77]. The strong increase of $\Delta\epsilon_\beta(T)$ as well as the breakdown of $g(E)$ near T_g are finally interpreted as reflecting the “softening” of the glassy sample, probed by the molecules involved in the β -process. These results suggest that the β -relaxation is of cooperative nature and, further, a generic feature of the glass transition.

Papers 5 & 6 deal with the binary system TPP/PS, made of the two components tripropyl phosphate (TPP, $T_g = 134 \text{ K}$, cf. also Paper 4) and polystyrene with the molecular mass $M_w = 2250 \text{ g/mol}$ (PS, $T_g = 335 \text{ K}$). Besides the high T_g contrast ($\Delta T_g = 201 \text{ K}$), which is of particular importance for the analysis of the structural relaxation phenomena of the mixtures (cf. Paper 6), the molecules of the two components possess highly differing permanent dipole moments. As a consequence, one can say that dielectric spectroscopy monitors solely the dynamics of TPP. The β -process of TPP/PS, discussed in Paper 5, is found in DS

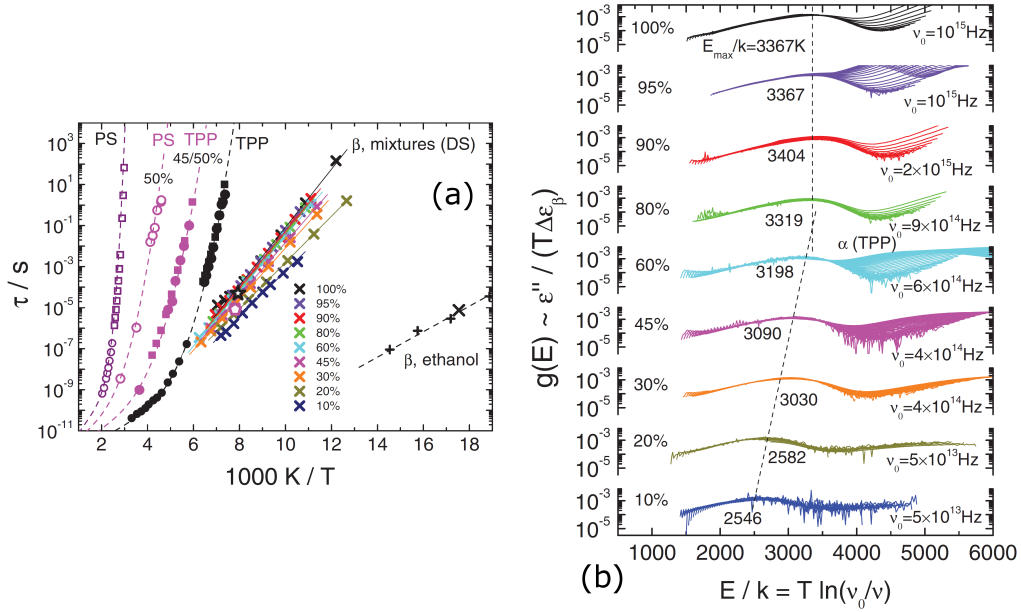


Figure 3.18: The β -process of TPP/PS mixtures analyzed by means of DS as well as ^2H and ^{31}P NMR as presented in Paper 5. (a) Time constants of primary relaxations (circles: NMR; squares: DS) and the β -relaxation (crosses: DS; stars: NMR). For comparison, time constants of the β -process of ethanol (plus: DS; crosses: NMR) are included. (b) Distributions of activation energies $g(E)$ of the β -processes.

spectra of all mixtures (except $c_{\text{TPP}} = 0\%$, i.e. neat PS). For all concentrations the susceptibility spectra of the β -process look very similar. As can be inferred from Fig. 3.18 (a), the time constants of the β -relaxations follow Arrhenius laws for any c_{TPP} . In the range $c_{\text{TPP}} = 50\%$ – 100% the activation energies $\langle E \rangle$ as well as the attempt rates ν_0 are found to be nearly concentration-independent. When concentration falls below 50% , $\langle E \rangle$ and ν_0 decrease weakly but steadily. This is demonstrated again with the scaling procedure already applied in Paper 4, revealing similar temperature-independent, asymmetric distributions of activation energies $g(E)$ underlying the thermally activated β -process in each mixture (Fig. 3.18 (b)). This systematic behavior supports the view of the β -process as being significantly determined by the surrounding of the relaxing molecules.

Selective ^{31}P NMR Hahn-echo experiments on neat TPP and the TPP molecules in the mixtures (Paper 5; actually to be part of D. Bock’s PhD thesis) identify the β -process as a spatially highly hindered motion, i.e. a small angle reorientation of the molecule, with time constants in accord with the dielectric findings (Fig. 3.18 (a)). Equivalent ^2H NMR solid-echo experiments on the PS molecules in the mixtures prove the participation of PS monomers in the β -process, although no β -relaxation is detected in neat PS. From that we conclude that the β -process in the mixtures is a cooperative process induced by the TPP subensemble, and imposed on the PS chains. A quantitative analysis of the NMR results reveals

that the fractions of PS monomers as well as TPP molecules participating in the β -process decrease with decreasing TPP concentration. This is interpreted as the emergence of “islands of rigidity”, as also observed for toluene/aroclor mixtures by our group [96]. Although the concept of “islands of mobility” [89,98] has been rejected for neat glass formers [93,97], these results suggest its re-introduction for binary systems.

excess wing (EW) As can be inferred from Fig. 3.11 (Sec. 3.6), the high-frequency flank of the α -relaxation peak bends over to show a lower dispersion at high frequencies. This high frequency feature, which can be described by a power law $\varepsilon''(\nu) \propto \nu^{-\gamma}$ (with γ being smaller than the high-frequency exponent of the α -peak) is called *excess wing* (EW), and if there is not a β -relaxation dominating the spectra, i.e. if a type-A glass former [75,78] is concerned, it is usually found in the dynamic susceptibility of supercooled liquids and glasses. There are three possible interpretations:

1. The excess wing is part of the α -process.
2. The excess wing is an individual relaxation process and has to be distinguished from α - and β -process.
3. The excess wing is a submerged β -relaxation peak.

The first interpretation is found primarily in the context of the scaling procedure applied by Nagel et al. [80–82]. In Ref. [107] it is stated explicitly that the EW exponent γ is strictly related to the exponent of the high frequency flank of the α -relaxation peak, and that FTS is not obeyed.

The second interpretation is followed in the framework of the analysis by Gainaru and co-workers [53,76,86]. Here, the shape parameters of α -peak and EW are found to be constant in the whole temperature range down to T_g , which is in contrast to the findings by Blochowicz et al. [65,79], and which implies that FTS is obeyed by the α -peak. Solely the relative amplitude of the EW in relation to the α -relaxation changes slightly with temperature, causing an apparent variation of the high frequency exponent of the α -peak. The assumption that β -process and EW are separate processes is supported by the fact that the EW is resolved in DLS experiments, where the β -relaxation is invisible [36,108,109]. Moreover, it is demonstrated in [110] that the EW obscures the $g(E)$ -scaling of the thermally activated β -process described above (Fig. 3.17 (b) and 3.18 (b)), which again points into the direction that EW and β -process have to be distinguished. Further, contrary to the temperature-dependent peak shape of β -processes, the EW exponent γ shows no significant temperature dependence. Thus, by means of the Gainaru approach aging experiments performed by Schneider et al. [19,111] can be reinterpreted by assuming the high-frequency susceptibility contribution as being composed additively of EW and β -process (the authors themselves prefer the third

interpretation; see below). Similar aging experiments on 4-tert-butylpyridine (4-TBP) are shown in Paper 2 (see below), where they are also interpreted according to this interpretation.

The third interpretation is supported by the results of dielectric aging experiments performed by Schneider et al. [19, 111]. Here, the sample is cooled to temperatures few Kelvin below T_g and, hence, pushed out of thermal equilibrium, which is reached only on time scales of 10^6 s. While waiting the α -relaxation peak (not observed directly below T_g) becomes more separated from the EW. The latter starts to show a distinct curvature and develops continuously into a relaxation peak. The authors conclude that this peak is the “real face” of the EW, which, thus, is nothing else than a β -relaxation, usually submerged below the α -peak. This is supported by Casalini et al. [112], performing pressure-dependent DS experiments on a type-B glass former. With increasing pressure an initially absent EW emerges and, finally, develops into a further well-resolved peak.

Note that up to now the origin of EW as well as β -process are still to be clarified. NMR measurements on type-A glass formers below T_g do not reveal indications of restricted molecular motion like in the case of type-B systems [36]. However, slightly above T_g the spectra start to resemble those of type-B glass formers [36, 113], which makes a clear distinction between the two processes again appear difficult. Learning about commonalities, similarities and differences between both processes, and finding the answer to the question if there are two different kinds of secondary processes at all, are issues of current and future research.

In the present work the second interpretation in the spirit of the Gainaru approach is favored. Concerning the EW, the following **open questions** are addressed in the publications:

- How can the EW be described within the Gainaru approach refined according to the subtle line shape variations of the α -peak? (\rightarrow Paper 2.)
- Are there further examples of type-A systems which have a β -relaxation covered by the EW? (\rightarrow Paper 2.)
- Which commonalities among type-A systems may indicate that the EW has a microscopic origin different from that of β -processes? (\rightarrow Paper 2.)
- How does the EW found for the liquid phase of quinaldine behave, and is it also observed for the other dielectrically active phases? (\rightarrow Paper 3.)

It was already stated in the context of the α -process that the EW is not observed in the usual way in the crystalline phases of quinaldine, all the same it is pointed out above how dielectric spectra of type-A systems can generally be quantified by accounting for the EW contribution. In the following, the **major results** presented in the second part of Paper 2 concerning the EW shall be summarized at this point.

Aging experiments on supercooled 4-TBP at temperatures closely below T_g monitor the susceptibility approaching thermal equilibrium within a number of

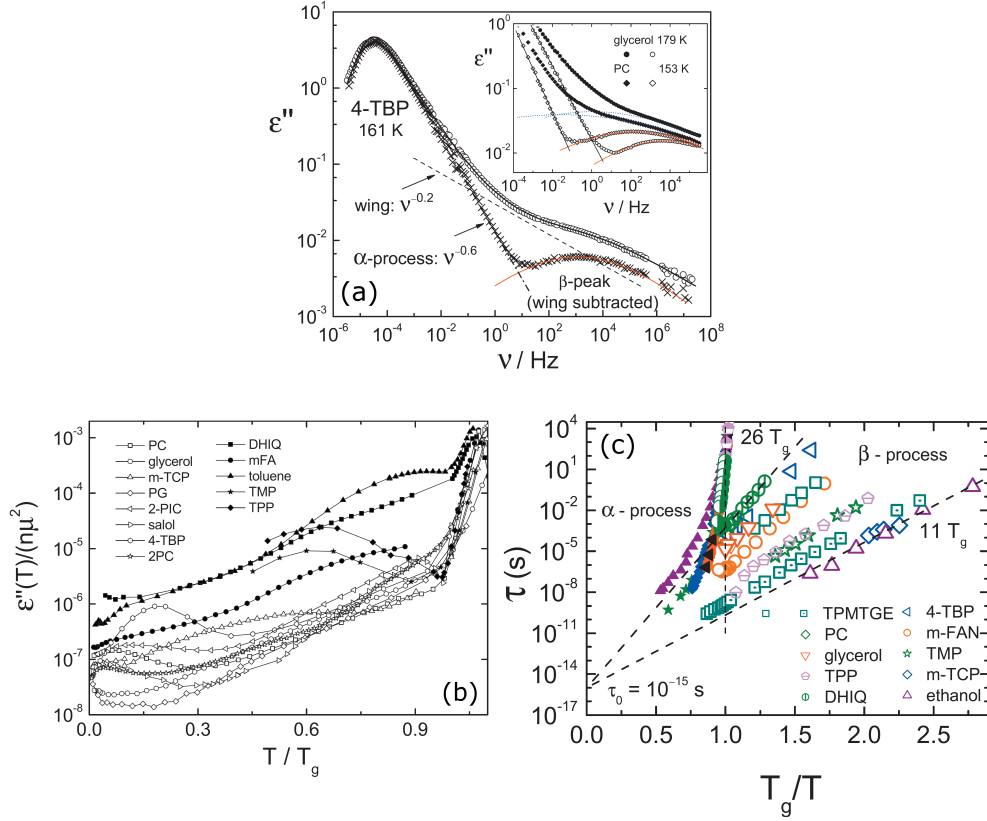


Figure 3.19: (a) Equilibrium spectrum of 4-TBP at $T = 161$ K (circles). Crosses: the same data after subtraction of a power law $\propto \nu^{-0.2}$ (dashed line). Inset: DS data of glycerol (full circles; $T = 179$ K) and propylene carbonate (PC, full diamonds; $T = 153$ K). Open symbols: data sets after subtraction of a power law $\propto \nu^{-0.2}$. (b) Temperature dependence of the normalized dielectric susceptibility of several type-A (open symbols) and type-B systems (full symbols) at fixed frequency $\nu = 1$ kHz, plotted versus reduced temperature. (c) Time constants of α and β -processes of several glass formers.

days. Since the analysis of type-A systems has shown (high-frequency scaling; EW amplitude $C \approx \text{const.}$ near T_g , see Fig. 3.14) that the EW contribution is strongly coupled to the α -relaxation peak, the susceptibility variation of 4-TBP during aging (for details see Paper 2) is interpreted, consequently within the ideas of the Gainaru approach, as a vanishing of the spectral contribution of the EW. The latter withdraws together with the α -peak, which shifts slowly to longer time scales. The curvature in $\epsilon''(\nu)$ of 4-TBP, which is already present in the non-equilibrium spectra, but gets more pronounced upon aging, is interpreted as the signature of a hidden β -relaxation. Finally, the β -peak is completely revealed by subtracting the EW contribution in the form of a power law $\epsilon''(\nu) \propto \nu^{-\gamma}$ with $\gamma \approx 0.2$. The resulting β -peak is symmetric, and its time constants show typical Arrhenius behavior with the activation energy $\langle E \rangle = 24 T_g$ as often found for β -

processes (cf. Fig. 3.19 (c)). Figure 3.19 (a) illustrates this procedure of spectral decomposition, displaying the susceptibility of 4-TBP at $T = 161$ K before and after the subtraction of the EW contribution.

Dielectric measurements on several molecular glass formers (type-A and -B) down to lowest temperatures of $T \approx 2$ K have been performed in the framework of Paper 2. In Fig. 3.19 (b) a comparison of resulting $\varepsilon''(T)$ data at fixed frequency $\nu = 1$ kHz, normalized by the relaxation strength of the α -relaxation near T_g , is displayed. For all systems the signature of the α -peak is found near T_g . At lowest temperatures ($0 < T/T_g < 0.3$) low-temperature anomalies interpretable as thermally activated dynamics in asymmetric double well potentials (ADWP) [71] appear as peaks. In the intermediate temperature range susceptibility contributions of excess wings as well as β -relaxations or, respectively, their low-temperature signatures, are observed. Here, almost identical amplitudes within different type-A systems are found, suggesting that α -relaxation and EW have strongly correlated molecular origins. On the other hand, higher and strongly varying loss amplitudes are found for type-B glass formers, suggesting that the β -relaxation has a microscopic origin different from that of the EW phenomenon. This finding also justifies the Gainaru approach used for the spectral decomposition of 4-TBP: any β -process contribution in Fig. 3.19 (b) appears as *additional* contribution to a generic, “basic” susceptibility. This result supports strongly the Gainaru approach, i.e. the overall susceptibility may, thus, be interpreted as a superposition of α -process, β -process, and EW.

A compilation of time constants describing β -processes of a variety of glass formers, including also 4-TBP and other type-A systems where the β -process was revealed by subtracting the EW contribution, is shown in Fig. 3.19 (c). Their activation energies vary within $\langle E \rangle = 11 T_g - 26 T_g$. Thus, the $\langle E \rangle = 24 T_g$ rule introduced by Kudlik et al. [75, 78] seems obsolete (cf. also Fig. 3.17 (a) and (b), as well as Paper 4).

relaxation processes in binary systems Two-component mixtures of organic glass formers are called binary systems in this thesis. Providing a comprehensive description of the phenomenology of the primary relaxations in binary systems may become quite challenging, as documented by several contributions on polymer-plasticizer systems [114–118] and mixtures of low molecular weight glass formers [119–121]. Only in the case of *asymmetric* binary systems, i.e. mixtures of components with a high T_g contrast [35, 122], two primary relaxations are well resolved and attributed to the molecular dynamics of each component. Principally, FTS does not hold in binary systems since broad temperature-dependent distributions of correlation times caused by strong dynamic heterogeneity underlie the primary relaxations [38, 45]. Moreover, in the recent work by Blochowicz et al. [35, 122] a temperature-dependent fraction of plasticizer molecules attributed to the matrix dynamics is identified. However, the effect of a low- T_g component on the structural relaxation of the high- T_g component (plasticizer effect) as well

as the effect of the high- T_g component on the primary relaxation of the low- T_g component (anti-plasticizer effect) are well known, e.g. from differential scanning calorimetry (DSC) experiments showing two glass transition temperatures for binary mixtures [123–128] (cf. also Fig. 3.20).

Besides a complex phenomenology concerning the primary relaxation features of the components “in the mixture”, and the existence of two concentration dependent T_g , binary systems offer another viewpoint on secondary relaxations. If a β -relaxation is present, it may be found for almost all investigated mixing proportions [96, 122, 129]. In some cases, at high concentrations of the low T_g component ($c \rightarrow 1$), α - and β -peak approach each other and the β -relaxation even submerges below the α -peak, i.e. the β -peak develops continuously into an EW [44, 119, 122].

The investigation of binary glass forming systems is a quite new, wide field of research. Since many combinations of components are possible and each combination has to be analyzed for several concentrations, much effort is required for the complete characterization of a binary system, and, hence, comparably little knowledge on the molecular dynamics of binary systems has been accumulated. In the context of the analysis of a highly asymmetric binary system within the present work, the following open questions are addressed:

- How are the primary relaxations of each component affected by the presence of the other component in the mixture? (\rightarrow Paper 6.)
- Are there additional dynamics in the mixture, which were not observed in the neat components? (\rightarrow Paper 6.)
- Do the microscopic mechanisms (isotropic vs. spatially hindered) of the primary relaxations or their appearance (thermally activated vs. non-Arrhenian $\tau(T)$; FTS) vary with concentration? (\rightarrow Paper 6.)
- How do the T_g depend on concentration? (\rightarrow Paper 6.)
- How can the geometry of molecular motion be characterized for both components? (\rightarrow Papers 5 & 6.)

The **major results** concerning the primary relaxation phenomena of the asymmetric binary system TPP/PS (tripropyl phosphate, $T_g = 134$ K; polystyrene, $M_w = 2250$ g/mol, $T_g = 335$ K) shall be summarized here. As already pointed out above, the molecules of the two components possess highly differing permanent dipole moments. As a consequence, DS monitors solely the dynamics of TPP. The results for TPP/PS mixtures of 13 concentrations are presented in detail in Paper 6, which is a joint study by dielectric spectroscopy (DS), ^{31}P and ^2H nuclear magnetic resonance spectroscopy (NMR) and, actually, also differential scanning calorimetry (DSC) and depolarized light scattering (DLS) experiments.

Due to the high T_g contrast of the components, two distinct glass steps are observed in the DSC traces of the mixtures, situated at the two concentration-dependent glass transition temperatures $T_{g1}(c_{\text{TPP}})$ and $T_{g2}(c_{\text{TPP}})$. ^2H NMR experiments on the PS monomers and, equivalently, ^{31}P NMR measurements on the

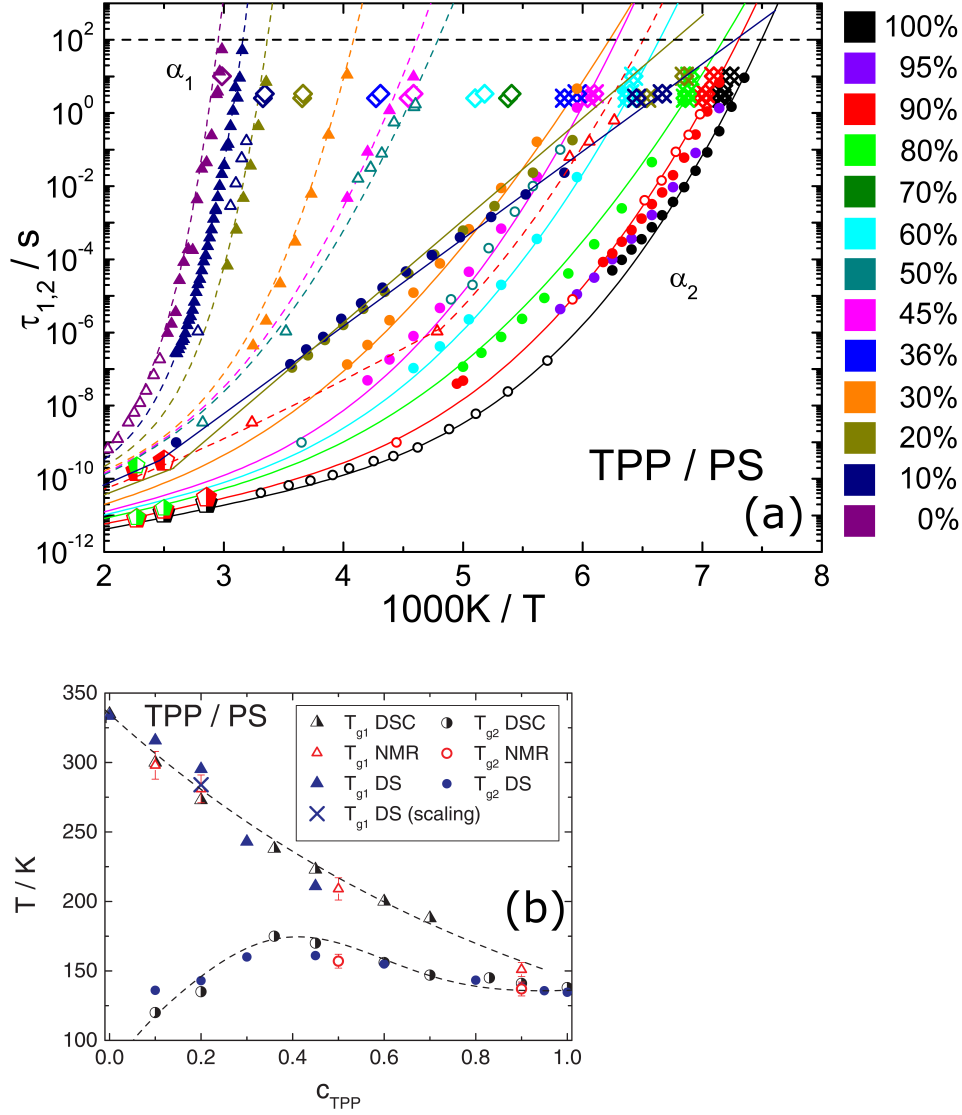


Figure 3.20: (a) Time constants from DS (full triangles: α_1 ; full circles: α_2), NMR (open triangles: α_1 ; open circles: α_2), DSC (open diamonds: α_1 ; crossed diamonds: α_2) and DLS (left pentagons: α_1 ; right pentagons: α_2) for all investigated concentrations (cf. color code). Lines are guides for the eye. For details see Paper 6. (b) Glass transition temperatures T_g as yielded by DSC, NMR and DS for all investigated mixtures. Dashed lines: guides for the eye.

TPP molecules assign T_{g1} to PS (“matrix”) dynamics, and T_{g2} to TPP dynamics occurring on shorter time scales. DLS experiments demonstrate, that the time scales of the TPP and PS dynamics are separated up to highest concentrations and temperatures. DS measurements probing, as said above, solely dynamics of the polar TPP molecules reveal two primary TPP relaxations on different time scales. The time constants τ_2 of the faster relaxation (α_2 -process) correspond with the TPP dynamics observed by NMR and identified as T_{g2} in the DSC traces for

the respective concentrations. The τ_1 of the slow α_1 -relaxation agree with the time constants of PS dynamics observed by NMR, as well as the T_{g1} of the DSC experiments. We conclude that two sub-ensembles of TPP molecules exist, one of which is dynamically “trapped” by (or attributed to) the PS matrix. The other TPP sub-ensemble performs “free” TPP dynamics, yet under the concentration dependent anti-plasticizing effect of the PS matrix.

A quantitative analysis of the dielectric relaxation strengths $\Delta\epsilon_1$ and $\Delta\epsilon_2$ of the α_1 - and α_2 -process, respectively, reveals that the fraction of TPP molecules associated with the high- T_g component (i.e. the *matrix* component) decreases with increasing T and, finally, vanishes at a temperature T_c . This phenomenon was also observed by Blochowicz et al. [35], who interpreted it as the signature of a so-called *type-A glass transition* as predicted by MCT.

The combination of methods yields time constants of both relaxations in a wide temperature and concentration range and, therefore, gives an unprecedented overview over the quite complex dynamics of the binary system (Fig. 3.20 (a)). The time constants $\tau_2(T)$ of the α_2 -process are found to develop from VFT behavior at high TPP concentrations to an Arrhenian temperature dependence at low concentrations, i.e. a transition from fragile to strong behavior under decreasing concentration is observed. This leads, by applying the definition $\tau_2(T_{g2}) = 100\text{ s}$, to a maximum in $T_{g2}(c_{TPP})$, which is confirmed by the DSC results, but has, up to our knowledge, not been observed before (Fig. 3.20 (b)).

The α_2 -peak has a typical α -peak shape at high TPP concentrations. Here, the failure of FTS is restricted to the low-frequency side of the peak. When c_{TPP} is lowered, the α_2 -peak assumes a broad shape increasing its width with decreasing temperature, which reminds of the behavior of a thermally activated β -process. Indeed, the scaling procedure also used in Papers 4 and 5 works, and proves that the α_2 -process is thermally activated at low additive concentrations, yielding temperature independent distributions of activation energies $g(E)$. However, ^{31}P NMR spectra of the $c_{TPP} = 20\%$ mixture identify the α_2 -relaxation as a process of isotropic, liquid-like molecular reorientation, even in the case of low TPP concentrations.

4 Publications

List of publications forming this thesis:

- Paper 1** Generalization of the Cole–Davidson and Kohlrausch Functions to Describe the Primary Response of Glass-Forming Systems.
R. KAHLAU, D. KRUK, T. BLOCHOWICZ, V. N. NOVIKOV,
AND E. A. RÖSSLER,
Journal of Physics: Condensed Matter **22**, 365101 (2010).
- Paper 2** Evolution of Excess Wing and β -Process in Simple Glass Formers
C. GAINARU, R. KAHLAU, E. A. RÖSSLER, AND R. BÖHMER,
The Journal of Chemical Physics **131**, 184510 (2009).
- Paper 3** Quinaldine: Accessing Two Crystalline Polymorphs via the Supercooled Liquid
R. KAHLAU, T. GNUTZMANN, F. EMMERLING,
K. RADEMANN, AND E. A. RÖSSLER,
The Journal of Chemical Physics **137**, 054505 (2012).
- Paper 4** Secondary Relaxations in a Series of Organic Phosphate Glasses Revealed by Dielectric Spectroscopy
R. KAHLAU, T. DÖRFLER, AND E. A. RÖSSLER,
The Journal of Chemical Physics **139**, 134504 (2013).
- Paper 5** On the Cooperative Nature of the β -Process in Neat and Binary Glasses: A Dielectric and Nuclear Magnetic Resonance Spectroscopy Study
D. BOCK, R. KAHLAU, B. MICKO, B. PÖTZSCHNER,
G. J. SCHNEIDER, AND E. A. RÖSSLER,
The Journal of Chemical Physics **139**, 064508 (2013).
- Paper 6** Dynamics of Asymmetric Binary Glass Formers. I. A Dielectric and Nuclear Magnetic Resonance Spectroscopy Study
R. KAHLAU, D. BOCK, B. SCHMIDTKE, AND E. A. RÖSSLER,
The Journal of Chemical Physics **140**, 044509 (2014).

Individual contribution to each publication:

- Paper 1** I had the idea of applying the introduced modifications to the step-response representation of the Cole–Davidson function. The properties of the resulting fit function were analyzed by me, and I calculated the mean correlation time. I showed that the Kohlrausch function is the second limiting case of the function (besides the Cole–Davidson function). Following the advice given by T. Blochowicz, I applied Bernstein’s theorem to show that the new function is a physically valid relaxation function, and proved its complete monotonicity. The distribution of correlation times was calculated and numerically evaluated by D. Kruk.
- Paper 2** I reanalyzed previously published DS spectra of molecular glass formers by applying the low-frequency and the high-frequency scaling, as demonstrated in Fig. 2. For this purpose, I normalized the data by the relaxation strength, which is demonstrated in Fig. 3. I finally fitted the data of propylene carbonate (PC), propylene glycol (PG), m-tricresyl phosphate (m-TCP), 4-tert-butylpyridine (4-TBP), and glycerol with the function introduced in Paper 1. The results of this analysis are collected in Fig. 4, corresponding data interpolations are shown in Fig. 3. The second part of Paper 2 is basically the work by C. Gainaru. Data of decahydroisoquinoline (DHIQ) were measured by me, but already shown in my Diploma thesis. Besides some modifications, Fig. 8 as well as related measurements are also part of my Diploma thesis.
- Paper 3** I executed DS measurements on liquid quinaldine and liquid 3-methyl quinoline, which finally led to the discovery of the dielectrically active phases 2mq2 and 2mq3, as well as 3mq2 and 3mq3. I conducted all further experiments, including frequency resolved dielectric spectroscopy on the dielectrically active phases of 2-methyl quinoline and 3-methyl quinoline, time resolved DS experiments monitoring the time dependent phase transformations, time resolved X-ray diffraction (XRD) experiments (together with T. Gnutzmann in the laboratory of Bundesanstalt für Materialforschung und -prüfung in Berlin) and differential scanning calorimetry (DSC) experiments. All analyses shown in this paper, except the processing of XRD data (T. Gnutzmann), were executed by me.

-
- Paper 4** I measured triethyl phosphate (TEP), tripropyl phosphate (TPP) and tributyl phosphate (TBP). Data of TEP and TPP are partially published in [104], data of TPP are further used in Papers 5 & 6. The systems tris(2-butoxyethyl) phosphate (T2BOEP) and tris(2-ethylhexyl) phosphate (T2EHP) were measured, under my guidance, by T. Dörfler in the framework of his Bachelor thesis. All analyses shown in this paper were done by me.
- Paper 5** I executed all DS measurements for this publication. Data were also used in Paper 6, data of neat TPP were also shown in Paper 4 and in [104]. I further did all analyses of dielectric data. All NMR experiments and related analyses on TPP, PS, and TPP/PS mixtures were done by D. Bock.
- Paper 6** I performed all DS measurements for this publication. Data were also used in Paper 5, data of neat TPP were also shown in Paper 4 and in [104]. I further did all analyses of dielectric data. All NMR and DSC experiments as well as related analyses on TPP, PS, and TPP/PS mixtures were done by D. Bock.

Further publications:

- Dynamics of Asymmetric Binary Glass Formers. II. Results from Nuclear Magnetic Resonance Spectroscopy
D. BOCK, R. KAHLAU, B. PÖTZSCHNER, T. KÖRBER, E. WAGNER, AND E. A. RÖSSLER,
The Journal of Chemical Physics **140**, 094505 (2014).
- Reorientational Dynamics in Molecular Liquids as Revealed by Dynamic Light Scattering: From Boiling Point to Glass Transition Temperature
B. SCHMIDTKE, N. PETZOLD, R. KAHLAU, AND E. A. RÖSSLER,
The Journal of Chemical Physics **139**, 084504 (2013).
- Evolution of the Dynamic Susceptibility in Molecular Glass Formers: Results from Light Scattering, Dielectric Spectroscopy, and NMR
N. PETZOLD, B. SCHMIDTKE, R. KAHLAU, D. BOCK, R. MEIER, B. MICKO, D. KRUK, AND E. A. RÖSSLER,
The Journal of Chemical Physics **138**, 12A510 (2013).
- Crystal Growth Rates and Molecular Dynamics of Nifedipine
T. GNUTZMANN, R. KAHLAU, S. SCHEIFLER, F. FRIEDRICHS, E. A. RÖSSLER, K. RADEMANN, AND F. EMMERLING,
CrystEngComm **15**, 4062 (2013).
- From Boiling Point to Glass Transition Temperature: Transport Coefficients in Molecular Liquids Follow Three-Parameter Scaling
B. SCHMIDTKE, N. PETZOLD, R. KAHLAU, M. HOFMANN, AND E. A. RÖSSLER,
Physical Review E **86**, 041507 (2012).
- Reorientational Dynamics of Organophosphate Glass Formers—a Joint Study by ^{31}P NMR, Dielectric Spectroscopy and Light Scattering
S. ADISHCHEV, D. BOCK, C. GAINARU, R. KAHLAU, B. MICKO, N. PETZOLD, B. PÖTZSCHNER, AND E. A. RÖSSLER,
Zeitschrift für Physikalische Chemie **226**, 1149 (2012).

-
- Energy Landscape in Molecular Glasses Probed by High-Resolution Dielectric Experiments
C. GAINARU, R. BÖHMER, R. KAHLAU, AND E. RÖSSLER,
Physical Review B **82**, 104205 (2010).
 - Comparative Studies of the Dynamics in Viscous Liquids by Means of Dielectric Spectroscopy and Field Cycling NMR
R. MEIER, R. KAHLAU, D. KRUK, AND E. A. RÖSSLER,
Journal of Physical Chemistry A **114**, 7847 (2010).
 - From Rouse to Fully Established Entanglement Dynamics: A Study of Polyisoprene by Dielectric Spectroscopy
A. ABOU ELFADL, R. KAHLAU, A. HERRMANN,
V. N. NOVIKOV, AND E. A. RÖSSLER,
Macromolecules **43**, 3340 (2010).
 - Molecular Weight Dependence of Glassy Dynamics in Linear Polymers Revisited
J. HINTERMEYER, A. HERRMANN, R. KAHLAU, C. GOICEANU,
AND E. A. RÖSSLER,
Macromolecules **41**, 9335 (2008).
 - On the Nature of the High-Frequency Relaxation in a Molecular Glass Former: A Joint Study of Glycerol by Field Cycling NMR, Dielectric Spectroscopy, and Light Scattering
C. GAINARU, O. LIPS, A. TROSHAGINA, R. KAHLAU,
A. BRODIN, F. FUJARA, AND E. A. RÖSSLER,
The Journal of Chemical Physics **128**, 174505 (2008).

Paper 1

Generalization of the Cole–Davidson and Kohlrausch Functions to Describe the Primary Response of Glass-Forming Systems

R. KAHLAU, D. KRUK, T. BLOCHOWICZ, V. N. NOVIKOV, AND
E. A. RÖSSLER,
Journal of Physics: Condensed Matter **22**, 365101 (2010).

© 2010 IOP Publishing Ltd
doi:10.1088/0953-8984/22/36/365101

Generalization of the Cole–Davidson and Kohlrausch functions to describe the primary response of glass-forming systems

R Kahlau¹, D Kruk^{1,2}, Th Blochowicz¹, V N Novikov¹ and E A Rössler¹

¹ Experimentalphysik II, Universität Bayreuth, D-95440 Bayreuth, Germany

² Institute of Physics, Jagiellonian University, Reymonta 4, 30-059 Krakow, Poland

Received 13 May 2010, in final form 1 July 2010

Published 11 August 2010

Online at stacks.iop.org/JPhysCM/22/365101

Abstract

We introduce a three-parameter step-response function which is based on a generalization of the Cole–Davidson (CD) and Kohlrausch (K) functions, and which provides a highly flexible susceptibility description for viscous liquids. A second parameter α characterizing the overall width, in addition to a parameter β determining the high-frequency behavior of the susceptibility, allows for a continuous change of the spectral shape from the CD-type to the K-type. We prove that the function fulfills mathematical conditions required for a step-response function. When applying the function to interpolate dielectric spectra of neat (pure) glass formers, it is possible to keep the high-frequency parameter β temperature-independent while varying the parameter α to account for the change of the overall width. This analysis might suggest that the failure of frequency–temperature superposition in glass formers is reflected by a broadening in the low-frequency region instead of in the high-frequency one.

(Some figures in this article are in colour only in the electronic version)

1. Introduction

The structural or primary α relaxation of (super-cooled) liquids slows down from picoseconds around the melting point ($T \geq T_m$) to about 100 s near the glass transition temperature T_g . The relaxation is markedly non-exponential, i.e. stretched in time, and describes the long-time decay of structural fluctuations for small-molecule glass formers [1–3]. In dielectric spectra, for example, the corresponding relaxation peak is asymmetrically broadened, that is its high-frequency flank does not follow a Debye law but rather a power-law behavior with an exponent $\beta < 1$. Discarding for the moment further (‘secondary’) relaxation processes which appear with low amplitudes at high frequencies [4–6], the main relaxation peak is, due to missing theoretical guidance, usually modeled by empirical susceptibility or step-response functions. Prominent examples of such functions are the Cole–Davidson (CD) susceptibility and the Kohlrausch (K) step-response function [7]. Both functions contain a single width parameter and work fairly well in one-component glass formers but may fail in binary systems for which broad relaxation peaks are typically observed [8, 9]. Essentially, they allow for determining the time constant and

estimating the width of the relaxation peak. Such a one-parameter description is usually assumed in studies looking for correlations between the super-Arrhenius temperature behavior of the time constant τ_α and the non-Debye character of the α process: however, such a correlation is not generally accepted [10–12].

A quantitative description of the evolution of the relaxation (including secondary relaxation processes) while cooling down to T_g is an important task, yet not fully achieved. For example, the validity of frequency–temperature superposition (FTS) introduced a long time ago is still debated. While FTS is assumed to be an essential feature of ‘glassy dynamics’ by mode coupling theory [13], at temperatures close to T_g it is often observed that the apparent spectral shape is temperature-dependent [14]. Some studies emphasize that, via an appropriate spectral analysis, the validity of FTS can be preserved, at least asymptotically [11, 15]. While such a spectral analysis relies on a proper model for disentangling the main and secondary relaxations, they also rely on a proper description of the lineshape of the main relaxation itself. Recently, Gainaru *et al* [16] demonstrated that actually one width parameter is not enough to fully account for the

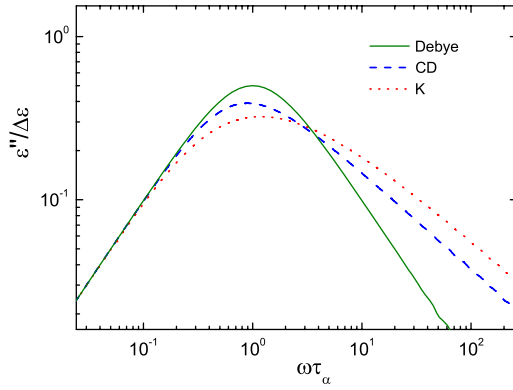


Figure 1. Comparison of Debye, Cole–Davidson (CD) and Kohlrausch (K) susceptibility as a function of reduced frequency; the corresponding stretching parameters are set to 0.6.

spectral shape of the α process even in simple glass formers, a result already anticipated by Olsen *et al* [15] as well as by Blochowicz *et al* [14]. Moreover, they observed that an interpolation by the CD function works well at high temperatures, whereas usually the Kohlrausch function gives a better description at low temperatures. Thus, looking for a susceptibility function which contains both CD and K functions as special cases is a starting point for an improved description of the measured susceptibilities.

In the present contribution we shall introduce a three-parameter step-response function encompassing the CD and K functions, which allows for a straightforward interpolation of the experimental α -relaxation peak (excluding any secondary relaxation processes). As will be demonstrated, the function is sufficiently flexible to provide almost perfect fits for both simple as well as binary glass formers.

The most widely applied three-parameter susceptibility is given by the Havriliak–Negami (HN) function [7]. However, the HN function exhibits an unphysical low-frequency ($\omega\tau \ll 1$) behavior, i.e. its time constant (or the first moment of the corresponding distribution of relaxation times) diverges. Thus, the function is not adequate to describe the main relaxation in liquids, and there is a need for a physically well-behaved (and simply implemented) three-parameter susceptibility function.

As discussed in a preliminary study [16], applying this susceptibility function for simple liquids reveals a crossover from a CD susceptibility at high temperature to a K susceptibility at low temperatures while the high-frequency parameter β may be kept temperature-independent.

2. Generalization of the Cole–Davidson and Kohlrausch step responses

Before introducing a generalization of CD and K susceptibility functions we briefly recall the definitions of both. The CD susceptibility is given by

$$\chi_{CD}(\omega) = \frac{1}{(1 + i\omega\tau_{CD})^\beta} \quad 0 < \beta \leq 1 \quad (1)$$

with β describing the imaginary part $\chi''_{CD}(\omega)$ of the complex susceptibility. The corresponding pulse response function is

given by [7]

$$\varphi_{CD}(t) = -\frac{d\phi_{CD}(t)}{dt} = \frac{1}{\tau_{CD}\Gamma(\beta)} \left(\frac{t}{\tau_{CD}}\right)^{\beta-1} \exp\left(-\frac{t}{\tau_{CD}}\right) \quad (2)$$

and the step-response function by

$$\phi_{CD}(t) = \frac{1}{\Gamma(\beta)} \int_0^t x^{\beta-1} \exp(-x) dx = \frac{\Gamma(\beta, \frac{t}{\tau_{CD}})}{\Gamma(\beta)} \quad (3)$$

with

$$\Gamma(\beta) = \int_0^\infty x^{\beta-1} \exp(-x) dx \quad (4)$$

denoting the Gamma function and

$$\Gamma(\beta, y) = \int_y^\infty x^{\beta-1} \exp(-x) dx \quad (5)$$

being the upper incomplete Gamma function [18].

The K function represents a step response:

$$\phi_K(t) = \exp\left[-\left(\frac{t}{\tau_K}\right)^\alpha\right] \quad (6)$$

with the corresponding stretching parameter α . Both the K as well as the CD functions converge to a Debye susceptibility when the corresponding stretching parameter reaches 1.

Figure 1 shows the CD and K functions, the latter after (numerically calculated) Fourier transformation into the frequency domain, with the same relaxation time τ_α and stretching parameter $\alpha = \beta$. Generally, for a given stretching parameter the Kohlrausch relaxation peak is broader than the Cole–Davidson peak. For the realistic value of $\alpha = \beta = 0.6$ this difference is expected to be resolvable in experiments (cf below). Most experimental works analyzing, for example, dielectric spectra of glass-forming systems use the CD or K functions, and some deficiencies of the interpolation are accepted when a large temperature range is covered. As mentioned in section 1, indications have been found that actually two lineshape parameters are needed to fully reproduce the primary relaxation peak [14, 15]. This is once again demonstrated in figures 2(a) and (b) where the normalized dielectric spectra of propylene carbonate (PC) [5] and propylene glycol (PG) [14] are rescaled to agree at the high-frequency flank of the relaxation peak. Figure 2(a) shows the full spectral range for which the dielectric data have been measured. In figure 2(b) we focus on the data around the relaxation maximum, as the function to be introduced describes the relaxation peak only. Indeed, the data coincide over a substantial frequency range at high frequencies, indicating that the high-frequency parameter does not change significantly with temperature. We note that at the highest frequencies (figure 2(a)) indications for the so-called excess wing are recognized which may change its amplitude upon cooling [5, 6, 17]. At the low-frequency flank and around the peak (figure 2(b)) no agreement is found. Here, the peak appears to broaden when lowering temperature. The overall change of the width is also reflected in a decreasing height of the peak. Moreover, as demonstrated by the fits in

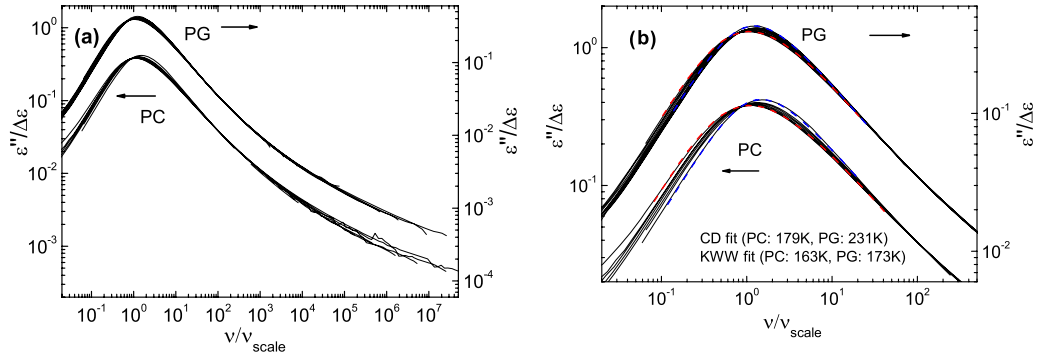


Figure 2. (a) Propylene carbonate (PC, left axis) and propylene glycol (PG, right axis) susceptibility data normalized by the relaxation strength and plotted versus a reduced frequency to allow for an overlapping of the data at high frequencies (PG data: [14]; PC data: [5]). (b) The same plots shown for the frequency range of the main relaxation peak only. In addition Cole–Davidson and Kohlrausch interpolations, respectively, are shown for the indicated temperatures.

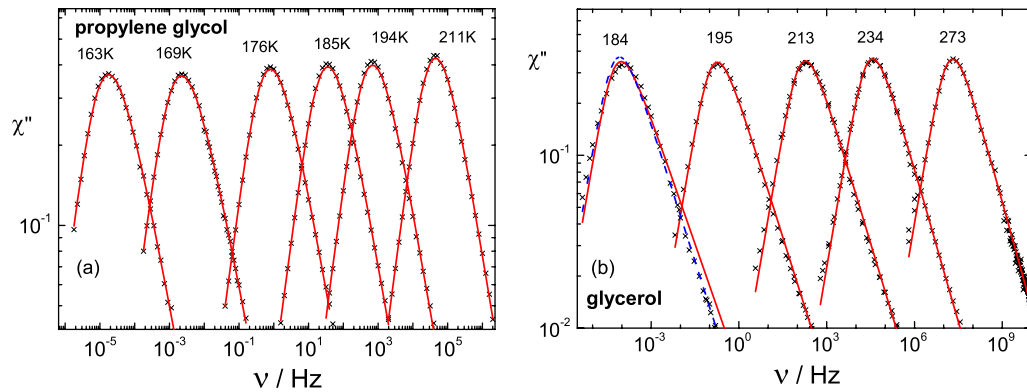


Figure 3. (a) Interpolation of the main relaxation of propylene glycol (crosses) with a Kohlrausch susceptibility function (red lines, fit weighted, data from [14]); note deviations around peak at high temperature. (b) Main relaxation of glycerol (crosses) interpolated with the Cole–Davidson (CD) function (red lines) without weighting. Blue dotted line: CD fit (weighted fit, data from [1]); systematic deviations occur at low temperatures.

figure 2(b) a crossover from a CD spectral shape towards a K shape is suggested, i.e. a CD function works better at high temperature whereas a K function is better at low temperature. Consequently, a fit over a large temperature range by the CD or K functions yields systematic deviations independent of the applied fitting strategy. This is demonstrated in figure 3. Once again we focus only on the data around the relaxation peak.

Next, we present a function $\phi_g(t)$ which may be called a generalization of K and CD functions; it includes the CD and K functions as special cases. The function $\phi_g(t)$ can be introduced by modifying $\phi_{CD}(t)$ in equation (3):

$$\phi_g(t) = \frac{\int_{\frac{t}{\tau_g}}^{\infty} x^{\beta-1} \exp(-x^\alpha) dx}{\int_0^{\infty} x^{\beta-1} \exp(-x^\alpha) dx} \quad (7)$$

by adding a stretching parameter α to the exponential expression, i.e. changing the exponential term in equation (3) to a Kohlrausch expression (cf equation (6)). An alternative definition of $\phi_g(t)$ which is more suitable for a numerical implementation of the model function is given by

$$\phi_g(t) = \frac{1}{\Gamma(\frac{\beta}{\alpha})} \int_{(\frac{t}{\tau_g})^\alpha}^{\infty} y^{\frac{\beta}{\alpha}-1} \exp(-y) dy = \frac{\Gamma(\frac{\beta}{\alpha}, (\frac{t}{\tau_g})^\alpha)}{\Gamma(\frac{\beta}{\alpha})}. \quad (8)$$

This formula has been obtained by substituting $y = x^\alpha$ in equation (7).

It is obvious that $\phi_g(t) = \phi_{CD}(t)$ if $\alpha = 1$ and $\beta = \beta_{CD}$ (cf equation (3)), and one can easily prove that the condition $\alpha = \beta$ gives again the K function:

$$\begin{aligned} \phi_g(t) &= \frac{1}{\Gamma(1)} \int_{(\frac{t}{\tau_g})}^{\infty} \exp(-y) dy = \exp\left[-\left(\frac{t}{\tau_g}\right)^\alpha\right] = \phi_K(t) \\ &= \exp\left[-\left(\frac{t}{\tau_K}\right)^\alpha\right] \quad \text{for } \alpha = \beta. \end{aligned} \quad (9)$$

By integrating $\phi_g(t)$ (equation (8)) one gets the mean correlation time (cf the appendix):

$$\tau_\alpha = \tau_g \frac{\Gamma(\frac{1+\beta}{\alpha})}{\Gamma(\frac{\beta}{\alpha})}. \quad (10)$$

Again, the limits of CD and K susceptibility [7, 19] are recovered:

$$\tau_{\alpha,CD} = \lim_{\alpha \rightarrow 1} \tau_\alpha = \tau_g \frac{\Gamma(1+\beta)}{\Gamma(\beta)} = \tau_g \beta \quad (11)$$

$$\tau_{\alpha,K} = \lim_{\alpha \rightarrow \beta} \tau_\alpha = \tau_g \frac{\Gamma(\frac{1+\alpha}{\alpha})}{\Gamma(1)} = \tau_g \Gamma\left(\frac{1}{\alpha} + 1\right) = \frac{\tau_g}{\alpha} \Gamma\left(\frac{1}{\alpha}\right). \quad (12)$$

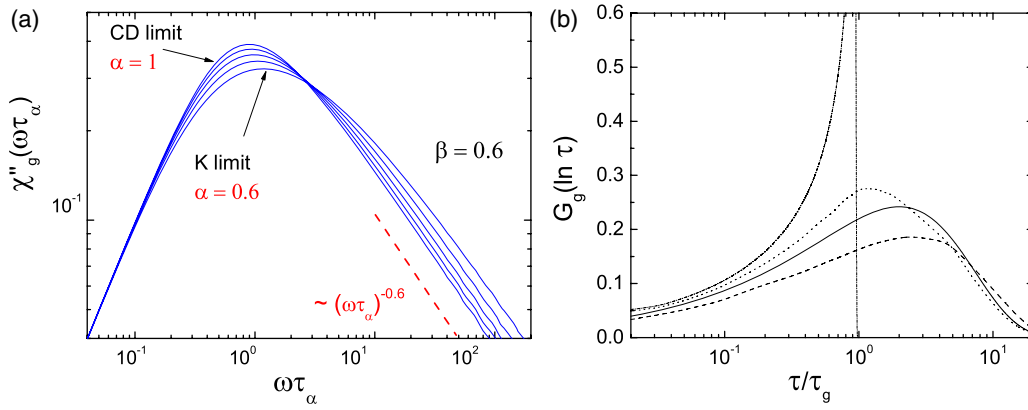


Figure 4. (a) Graphs of the susceptibility function $\chi''_g(\omega\tau_\alpha)$ (cf equation (8)) for $\alpha = 0.6, 0.7, 0.8, 0.9, 1.0$ and $\beta = 0.6$. Dashed red line: power law proportional to $(\omega\tau_\alpha)^{-0.6}$. (b) Corresponding distribution of correlation times $G(\ln \tau)$; solid line: $\alpha = \beta = 0.5$ (Kohlrausch distribution); dashed line: $\alpha = 0.4, \beta = 0.5$; dotted line: $\alpha = 0.6, \beta = 0.5$; dashed-dotted line: Cole–Davidson distribution for $\beta = 0.5$.

Figure 4(a) shows the susceptibility $\chi''_g(\omega)$ calculated from equation (8) via Fourier transformation for the parameter $\beta = 0.6$ and several α values ranging between 0.6 ($\alpha = \beta$) and 1.0. A continuous crossover of the spectral shape from CD to K type is illustrated. The parameter β determines the high-frequency slope of the peak, in analogy to the CD stretching parameter, and α is responsible for its flattening. The corresponding distribution $G(\ln \tau)$ is displayed in figure 4(b) (cf the appendix). With respect to the CD distribution with its clear cutoff at long correlation times the new function allows us to vary its long-time flank continuously.

Any valid relaxation function $\phi(t)$ of a system in thermodynamic equilibrium can be expressed in terms of a non-negative distribution of relaxation times representing ϕ as a sum of single exponential decays [7, 20]. This is equivalent to ϕ being completely monotonic, which in turn, by virtue of Bernstein's theorem, is the equivalent of [21–23]

$$(-1)^n \phi^{(n)}(t) \geq 0 \quad \text{for } 0 \leq t < \infty \quad (13)$$

with $\phi^{(n)}(t) = \frac{d^n \phi(t)}{dt^n}$ being the n th derivative of $\phi(t)$. In the case of $\phi_g(t)$, it is easily seen that

$$\phi_g^{(0)}(t) > 0 \quad \text{for } 0 \leq t < \infty \quad (14)$$

(equations (7) and (8)). Using the properties of the regularized incomplete Gamma function [18] the first derivative can be calculated:

$$\begin{aligned} \phi_g^{(1)}(t) &= \frac{d}{dt} \left[1 - \frac{1}{\Gamma(\frac{\beta}{\alpha})} \int_0^{\left(\frac{t}{\tau_g}\right)^\alpha} x^{\frac{\beta}{\alpha}-1} \exp(-x) dx \right] \\ &= -\frac{\frac{\alpha}{\tau_g}}{\Gamma(\frac{\beta}{\alpha})} \left(\frac{t}{\tau_g}\right)^{\beta-1} \exp\left[-\left(\frac{t}{\tau_g}\right)^\alpha\right] \leq 0 \end{aligned} \quad (15)$$

for $\alpha, \beta, \tau_g > 0$ and $0 \leq t < \infty$.

From Bernstein's theorem it follows that the higher-order derivatives ($n \geq 2$) of $\phi_g^{(n)}(t)$ will be of opposite signs if and only if the expression

$$\left(\frac{t}{\tau_g}\right)^{\beta-1} \exp\left[-\left(\frac{t}{\tau_g}\right)^\alpha\right] \quad (16)$$

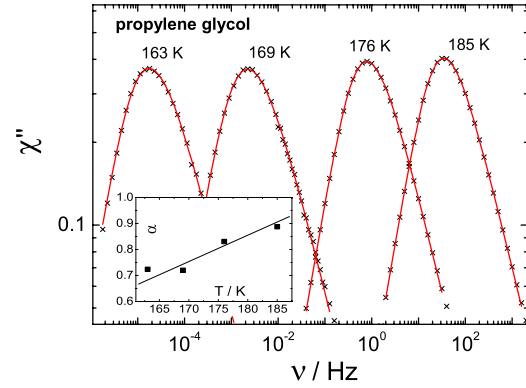


Figure 5. Susceptibility data of propylene glycol (crosses) interpolated by the $\chi''_g(\omega)$ function (red lines, β fixed to 0.72). Inset: temperature dependence of the parameter α (boxes); straight line: guide for the eye.

is completely monotonic in t . Since it is well known [21, 22] that the product of two completely monotonic functions is again completely monotonic, and for the factors $\exp[-(\frac{t}{\tau_g})^\alpha]$ as well as $(\frac{t}{\tau_g})^{\beta-1}$ equation (13) is obviously fulfilled for $\tau_g > 0$ and $\alpha, \beta \leq 1$, the complete monotonicity of ϕ_g is proven. Therefore $\phi_g(t)$ is a physically valid relaxation function for $\alpha, \beta, \tau_g > 0$ and $\alpha, \beta \leq 1$.

3. Applications

In figure 5 we show dielectric spectra of propylene glycol (PG) [14] interpolated by the new function $\phi_g(t)$ given as a Fourier transform $\chi''_g(\omega)$. A perfect interpolation is provided and the deficiencies of the CD function are removed. Of course, this is of no surprise as a second shape parameter has been introduced. However, the interpolations shown are achieved by keeping the high-frequency parameter $\beta = 0.72$ temperature-independent and changing only the parameter α . In other words, as suggested by the high-frequency scaling in figure 2 the susceptibility keeps its high-frequency flank while it broadens on the low-frequency side. When inspecting the

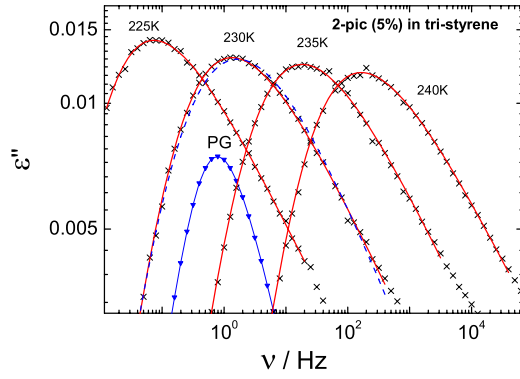


Figure 6. α -relaxation peaks of 2-picoline (5%) in tri-styrene (crosses) compared to propylene glycol (PG) at 176 K (blue triangles, shifted arbitrarily). Interpolations by the model function $\phi_g(t)$ (red lines, cf equation (8)); for comparison interpolation by Kohlrausch function (dashed blue line) showing systematic deviations.

temperature evolution of the parameter α (cf inset of figure 5), it decreases starting from 0.89 at the highest temperature to 0.72 at the lowest temperature, i.e. a trend towards the K function ($\alpha = \beta$) is recognized while cooling.

In order to demonstrate the flexibility of the introduced function $\phi_g(t)$ we try to interpolate broad α peaks as they are typically observed in binary glass formers [8, 9]. Figure 6 shows the dielectric spectra of the binary system 2-picoline (5%) in tri-styrene in comparison to the spectra of the simple liquid PG. Clearly, the relaxation peak in the binary system is much broader than in the simple liquid PG. Again, the interpolation by $\phi_g(t)$ is superior to a fit by, for example, a K function. In contrast to neat glass formers the parameter α stays virtually constant with $\alpha = 0.57$ while β drops from 0.3 to 0.18 with increasing temperature.

4. Discussion and conclusions

The introduced three-parameter step-response function $\phi_g(t)$ provides a highly flexible description which allows for ‘interpolating’ between the CD-type and K-type spectral shapes of the susceptibility in neat as well as binary glass formers. Three-parameter descriptions of the main relaxation have already been introduced, such as the gamma distribution [14, 24] or the HN susceptibility [7]. Regarding the HN susceptibility, often applied for interpolating, for example, the spectra of polymers, as already mentioned in section 1, the function does not show the physically correct low-frequency limit, i.e. its time constant is not defined. Thus it is not expected that the HN function provides a correct interpolation of any main relaxation in complex liquids. In the case of the gamma distribution the susceptibility has to be calculated via a Laplace transform of the distribution of correlation times whereas the presently introduced function applies directly for the step-response function.

As suggested by the high-frequency scaling of the experimental susceptibility in neat glass formers (cf figure 2(b)), the function enables one to keep the high-frequency parameter β temperature-independent while varying the parameter α to account for the experimentally documented changes of the

linewidth. Thus, it appears that the failure of FTS in neat glass formers might also be reflected by a low-frequency broadening. Generalizing the results, the invariance of the high-frequency flank of the main relaxation peak might be a generic property of neat glass-forming liquids, and could become an essential input for a full lineshape analysis including main and secondary relaxation. Independent of such conclusions the presented function offers a new tool for interpolating relaxation peaks in complex fluids.

Appendix

A.1. Mean correlation time

Starting from the definition of $\phi_g(t)$:

$$\phi_g(t) = \frac{1}{\Gamma(\frac{\beta}{\alpha})} \int_{(\frac{t}{\tau_g})^\alpha}^{\infty} y^{\frac{\beta}{\alpha}-1} \exp(-y) dy = \frac{\Gamma(\frac{\beta}{\alpha}, (\frac{t}{\tau_g})^\alpha)}{\Gamma(\frac{\beta}{\alpha})} \quad (\text{A.1})$$

one can calculate the mean correlation time of $\phi_g(t)$ by changing the variable $z = (\frac{t}{\tau_g})^\alpha$:

$$\begin{aligned} \tau_\alpha &= \int_0^\infty \phi_g(t) dt = \frac{1}{\Gamma(\frac{\beta}{\alpha})} \int_0^\infty \Gamma\left(\frac{\beta}{\alpha}, \left(\frac{t}{\tau_g}\right)^\alpha\right) dt \\ &= \frac{1}{\Gamma(\frac{\beta}{\alpha})} \int_0^\infty \int_{(\frac{t}{\tau_g})^\alpha}^{\infty} y^{\frac{\beta}{\alpha}-1} \exp(-y) dy dt \\ &= \frac{\tau_g}{\Gamma(\frac{\beta}{\alpha})} \int_0^\infty z^{\frac{1}{\alpha}-1} \Gamma\left(\frac{\beta}{\alpha}, z\right) dz. \end{aligned} \quad (\text{A.2})$$

This expression can be converted [18] to

$$\tau_\alpha = \tau_g \frac{\Gamma(\frac{1+\beta}{\alpha})}{\Gamma(\frac{\beta}{\alpha})}. \quad (\text{A.3})$$

A.2. Distribution of correlation times

A step-response function $\phi(t)$ can be explicitly rewritten as $\phi(t, \tilde{\tau})$ with $(\tilde{\tau} = \tau_{CD}, \tau_{KKW}, \tau_g)$ and related to a distribution function $G(\tau, \tilde{\tau})$ defined as

$$\phi(t, \tilde{\tau}) = \int_0^\infty G(\tau, \tilde{\tau}) \exp\left(-\frac{t}{\tau}\right) d\tau \quad (\text{A.4})$$

and connected with the often-used form $G(\ln \tau)$ via $G(\ln \tau, \tilde{\tau}) = \tau G(\tau, \tilde{\tau})$.

Substituting $s = \tau^{-1}$ one can write equation (A.4) in the form

$$\begin{aligned} \phi(t, \tilde{\tau}) &= \int_0^\infty \frac{G(s, \tilde{\tau})}{s^2} \exp(-st) ds \\ &= \int_0^\infty k(s, \tilde{\tau}) \exp(-st) ds. \end{aligned} \quad (\text{A.5})$$

This implies that the distribution function $G(\tau, \tilde{\tau}) = s^2 k(s, \tilde{\tau}) = \frac{k(\tau^{-1}, \tilde{\tau})}{\tau^2}$ can be obtained by taking the inverse Laplace transform of the step-response function $\phi(t, \tilde{\tau})$: $L_s^{-1}[\phi(t, \tilde{\tau})] = k(s, \tilde{\tau})$. Detailed calculations show that it is convenient to express the distribution function in terms of $u = \frac{\tau}{\tilde{\tau}}$: $G(u) = s^2 k(s, \tilde{\tau})$. The distribution function $G_{CD}(u)$

associated with the Cole–Davidson step-response function, $\phi_{\text{CD}}(t, \tau_{\text{CD}}) \equiv \phi_{\text{CD}}(u)$, is given as [7]

$$G_{\text{CD}}(u) = \frac{\sin(\pi\beta)}{\pi} \frac{1}{u} \left(\frac{u}{1-u} \right)^\beta \quad (\text{A.6})$$

while the distribution function $G_{\text{K}}(u)$ corresponding to the Kohlrausch step-response function $\phi_{\text{K}}(t, \tau_{\text{K}}) \equiv \phi_{\text{K}}(u)$ is given by the formula [19]

$$G_{\text{K}}(u) = -\frac{1}{\pi} \sum_{k=0}^{\infty} \frac{(-1)^k}{k!} \sin(\pi k \alpha) \Gamma(\alpha k + 1) u^{\alpha k - 1}. \quad (\text{A.7})$$

The $\phi_{\text{g}}(t, \tau_{\text{g}}) \equiv \phi_{\text{g}}(u)$ is related to a distribution function $G_{\text{g}}(u)$ which can be obtained in a ‘semi-analytical’ form by taking the following steps:

$$\begin{aligned} G_{\text{g}}(u) &= \tau_{\text{g}} s^2 k_{\text{g}}(s, \tau_{\text{g}}) = \tau_{\text{g}} s^2 L_s^{-1}[\phi(t, \tau_{\text{g}})] \\ &= -\tau_{\text{g}} s L_s^{-1} \left[\frac{d}{dt} \phi(t, \tau_{\text{g}}) \right] \\ &= \frac{\tau_{\text{g}} s}{\Gamma(\frac{\beta}{\alpha})} L_s^{-1} \left[\frac{d}{dt} \int_0^{\left(\frac{t}{\tau_{\text{g}}}\right)^\alpha} x^{\frac{\beta}{\alpha}-1} \exp(-x) dx \right] \\ &= \frac{\tau_{\text{g}} s \alpha}{\Gamma(\frac{\beta}{\alpha})} L_s^{-1} \left\{ \left(\frac{t}{\tau_{\text{g}}} \right)^{\beta-1} \exp \left[- \left(\frac{t}{\tau_{\text{g}}} \right)^\alpha \right] \right\}. \end{aligned} \quad (\text{A.8})$$

Since the distribution function anyway depends on $u = \frac{t}{\tau_{\text{g}}}$, it is convenient at this stage to set $\tau_{\text{g}} = 1$. The inverse Laplace transform can be obtained by applying the rule for a Laplace transform of a product of two functions, which yields

$$L_s^{-1}\{t^{\beta-1} \exp(-t^\alpha)\} = \int_0^s g(s-\sigma) h(\sigma) d\sigma \quad (\text{A.9a})$$

where

$$g(s-\sigma) = \frac{(s-\sigma)^{-\beta}}{\Gamma(1-\beta)} \quad (\text{A.9b})$$

is the inverse Laplace transform of $t^{\beta-1}$, while $h(\sigma)$ is given by equation (A.4) with $\sigma = u^{-1}$. Finally, the distribution function $G_{\text{g}}(s)$ takes the form

$$\begin{aligned} G_{\text{g}}(s) &= \frac{s \alpha}{\Gamma(\frac{\beta}{\alpha}) \Gamma(1-\beta)} \left(-\frac{1}{\pi} \right) \sum_{k=0}^{\infty} \frac{(-1)^k}{k!} \sin(\pi \alpha k) \\ &\quad \times \Gamma(\alpha k + 1) \int_0^s (s-\sigma)^{-\beta} \sigma^{-(\alpha k+1)} d\sigma. \end{aligned} \quad (\text{A.10})$$

For the special case of $\alpha = 0.5$ the distribution function is given by a simpler expression:

$$\begin{aligned} G_{\text{g}}(s) &= \frac{s}{4\sqrt{\pi} \Gamma(2\beta) \Gamma(1-\beta)} \\ &\quad \times \int_0^s (s-\sigma)^{-\beta} \sigma^{-3/2} \exp\left(-\frac{1}{4\sigma}\right) d\sigma. \end{aligned} \quad (\text{A.11})$$

Examples for the corresponding $G(\ln \tau)$ distribution are plotted in figure 4.

References

- [1] Lunkenheimer P, Schneider U, Brand R and Loidl A 2000 *Contemp. Phys.* **41** 15
- [2] Ediger M D 2002 *Annu. Rev. Phys. Chem.* **51** 99
- [3] Blochowicz T, Brodin A and Rössler E A 2006 *Adv. Chem. Phys.* A **133** 127
- [4] Johari G P and Goldstein M 1970 *J. Chem. Phys.* **53** 2372
- [5] Kudlik A, Benkhof S, Blochowicz T, Tschirwitz C and Rössler E 1999 *J. Mol. Struct.* **479** 201
- [6] Ngai K L and Paluch M 2004 *J. Chem. Phys.* **120** 857
- [7] Böttcher C J and Bordewijk P 1978 *Theory of Electric Polarization* vol 2 (Amsterdam: Elsevier)
- [8] Blochowicz T and Rössler E A 2004 *Phys. Rev. Lett.* **92** 225701
- [9] Capaccioli S, Kessairi K, Prevosto D, Lucchesi M and Ngai K L 2006 *J. Non-Cryst. Solids* **352** 4643
- [10] Böhmer R, Ngai K L, Angell C A and Plazek D J 1993 *J. Chem. Phys.* **99** 4201
- [11] Brodin A, Gainaru C, Porokhonsky V and Rössler E A 2007 *J. Phys.: Condens. Matter* **19** 205104
- [12] Nielsen A I, Pawlus S, Paluch M and Dyre J C 2008 *Phil. Mag.* **88** 4101
- [13] Götze W and Sjögren L 1992 *Rep. Prog. Phys.* **55** 241
- [14] Blochowicz T, Gainaru C, Medick P, Tschirwitz C and Rössler E A 2006 *J. Chem. Phys.* **124** 134503
- [15] Olsen N B, Christensen T and Dyre J C 2001 *Phys. Rev. Lett.* **86** 1271
- [16] Gainaru C, Kahlau R, Rössler E A and Böhmer R 2009 *J. Chem. Phys.* **131** 184510
- [17] Hofmann A, Kremer F, Fischer E W and Schönhals A 1994 *Disorder Effects on Relaxational Processes* (Berlin: Springer) chapter 10
- [18] Abramowitz M and Stegun I A 1972 *Handbook of Mathematical Functions* (New York: Dover)
- [19] Lindsey C P and Patterson G D 1980 *J. Chem. Phys.* **73** 3348
- [20] Wagner K W 1913 *Ann. Phys. (Leipzig)* **40** 817
- [21] Alzer H and Berg C 2002 *Ann. Acad. Sci. Fenn. Math.* **27** 445
- [22] Alzer H and Berg C 2006 *Ramanujan J.* **11** 225
- [23] Widder D V 1972 *The Laplace Transform* (Princeton: Princeton University Press)
- [24] Nicolai T, Gimel J C and Johnsen R 1996 *J. Physique* **6** 695

Paper 2

Evolution of Excess Wing and β -Process in Simple Glass Formers

C. GAINARU, R. KAHLAU, E. A. RÖSSLER, AND R. BÖHMER,
The Journal of Chemical Physics **131**, 184510 (2009).

© 2009 American Institute of Physics
doi:10.1063/1.3258430

Evolution of excess wing and β -process in simple glass formers

Catalin Gainaru,^{1,2,a)} Robert Kahlau,¹ Ernst A. Rössler,¹ and Roland Böhmer²¹*Physikalisches Institut, Universität Bayreuth, Bayreuth 95440, Germany*²*Fakultät für Physik, Technische Universität Dortmund, Dortmund 44221, Germany*

(Received 1 August 2009; accepted 12 October 2009; published online 13 November 2009)

Dielectric loss spectra of glass forming liquids are analyzed, with emphasis on systems for which a peak due to a secondary relaxation is not immediately obvious. Thus, glass formers are considered for which the high-frequency flank of the α -relaxation peak appears to be dominated by a so-called wing contribution. It is shown that even for such supercooled liquids the shape of the α -peak has to be characterized by two parameters. By performing a series of aging experiments it is demonstrated that the high-frequency flank of the α -relaxation, assumed to follow a power-law behavior, is superimposed by contributions from an excess wing and from a β -relaxation peak. In particular, the excess wing, previously associated with either the α - or the β -relaxation, is identified as a feature that evolves in its own right. It is argued that excess wing and β -relaxation are always present albeit with relative strengths that may vastly differ from glass former to glass former.

© 2009 American Institute of Physics. [doi:10.1063/1.3258430]

I. INTRODUCTION

When cooling or compressing glass forming liquids their dynamic susceptibilities evolve in a complicated fashion. The structural or primary α -relaxation slows down from picoseconds at $T \gg T_g$ to about 100 s near the glass transition temperature T_g . This relaxation is markedly nonexponential, i.e., stretched in time, and defines the ultimate long-time decay of structural fluctuations in small-molecule glass formers. At shortest times microscopic dynamics are observed as an oscillation dephasing with typical frequencies in the terahertz range at all temperatures. In the enormous range of more than 14 decades in time or frequency which separate the time scale of the α -relaxation near T_g from that of the microscopic dynamics a variety of other relaxation processes emerges. In dielectric loss spectra these features manifest themselves as so-called excess wing (EW) and more often as secondary relaxation peaks. The last were first studied systematically by Johari and Goldstein.^{1,2} Primary and secondary relaxations can often, but not always, be distinguished from each other on the basis of their different spectral, aging, pressure, and temperature evolutions. Whether the excess wing is a feature separate from those relaxations is debated,^{3,4} because a generally accepted procedure allowing one to disentangle the wing contributions from those of the primary and/or of the secondary relaxations is currently not available.^{5–11}

Clarifying the role of the secondary peak and/or of the wing contributions is important since any assumption regarding their spectral shapes may affect the result for that of the primary relaxation. For example, taking results from neutron¹² or from light scattering measurements¹³ as well as from other experimental¹⁴ or computational work,^{15,16} frequency temperature superposition (FTS) has been reported to be obeyed by the α -process of glass formers at high tempera-

tures for which neither secondary peaks nor wing relaxations significantly interfere. While FTS is assumed to be an essential feature of glassy dynamics by certain theories,¹⁷ at temperatures close to T_g it was often found that the spectral shape probed, e.g., by dielectric spectroscopy is temperature dependent.^{3,18,19} Some studies emphasize that via appropriate spectral analyses FTS can be recovered, at least asymptotically,^{14,20,21} throughout the supercooled regime. Recently, based on high-pressure experiments as well as on theoretical work it was argued that the spectral shape should remain invariant neither along a line of constant temperature nor under constant-pressure conditions, but merely along an isochronal line in the temperature-volume plane.^{22–24} However, different phenomenological approaches for disentangling the contribution of the α -peak from the other relaxation processes were proposed,^{18,19,25–28} without leading to an overall consensus regarding the situation.

Disregarding secondary processes for the moment, it may be asked whether a single parameter is sufficient to describe the shape of the dielectric α -relaxation close to its peak frequency at a given temperature. Such a one-parameter description was assumed in studies inquiring into correlations between the super-Arrhenius with the non-Debye character of the α -process.²⁹ In the meantime there are some indications that more than one shape parameter may be necessary to describe the spectral profile of the α -relaxation even in relatively simple low molecular weight glass formers.^{14,18,27} Such a case obviously complicates the search for straightforward correlations among various parameters and could rationalize reports suggesting shortcomings of simple correlations.^{21,30} To clarify the nature of β -processes themselves, an unambiguous separation of them from the primary relaxation is sometimes considered desirable, too. In view of the connectivity between the α - and β -process^{31,32} it is not clear, however, to which extent such a separation can

^{a)}Electronic mail: catalin.gainaru@uni-dortmund.de.

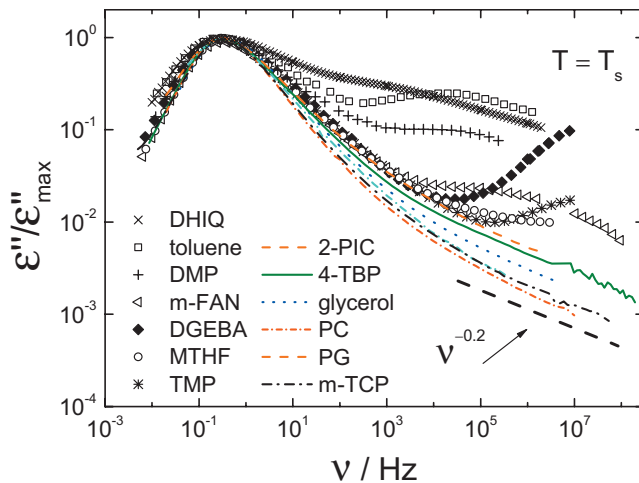


FIG. 1. Dielectric loss spectra for various glass formers recorded for comparable peak frequencies and scaled to the same peak height. The spectra exhibit a succession of decreasing high-frequency contributions thus illustrating a continuous transition from type B to type A profiles. This representation is compatible with β -process and excess wing always being simultaneously present, albeit with different relative intensities. The spectral shape of this glass former is thus intermediate between so-called type A and other type B systems. References and information regarding the measurement temperatures and ε''_{\max} are provided in Table I.

be achieved not only phenomenologically, but under which circumstances a separate consideration is permissible in principle.

The temperature at which secondary relaxation peaks or excess wing first appear upon cooling is sometimes taken to signal a crossover in the dynamics of supercooled liquids.^{9,33} Yet, its clear-cut manifestation in susceptibility spectra well above T_g remains a matter of debate.

In order to disentangle the various processes, dielectric studies monitoring pressure^{22,34} and aging dependences^{28,35} turned out to be particularly useful. In aging experiments Schneider *et al.*³⁵ found subtle spectral changes in the high-frequency wing of the α -peak for glycerol and propylene carbonate (PC). These results were interpreted as arising from an emerging secondary relaxation peak and led those authors to suggest that the excess wing is a relaxation process of the JG type.^{2,35} The cited aging study was important in pointing out that β -relaxations may exist in glass formers in which their presence is not obvious, at first glance. However, as already suggested on the basis of high-pressure experiments we will argue “that the excess wing and the β relaxation cannot be treated on the same footing.”²²

To put these results in a broader perspective and to address the question whether secondary relaxations may be universally present in glass formers, in Fig. 1 we compile dielectric loss spectra of several supercooled liquids for scaling temperatures $T_s \approx T_g$. The data are normalized to their maximum loss, see Table I for ε''_{\max} , T_s , and references to the original works. For some substances such as toluene or dimethylphthalate (DMP), a β -relaxation peak is clearly discernible at about 5 decades above the α -peak frequency. These liquids are thus typical examples of type B systems.¹¹ For glass formers like diglycyl ether of bisphenol A (DGEBA) or trimethylphosphate (TMP) only the low-frequency flank of a secondary peak is recognized in Fig. 1. Here the separation from the α -peak is larger than 8 decades and we will show below that in fact all degrees of separation are observed. For methyl-tetrahydrofuran (MTHF) a β -process is barely resolved.³⁶ For other supercooled liquids the β -relaxation amplitude is even smaller and a β -peak seemingly absent. Glass formers in this limit have been called type A systems¹¹ with glycerol, propylene glycol (PG), and propylene carbonate³⁷ usually considered as classical examples.³⁸ We point out that for systems such as m-fluoroaniline (m-FAN), TMP, and DGEBA both a well resolved EW and a β -peak are observed, suggesting that the two processes are independent relaxation phenomena. As revealed in Fig. 1, slightly stronger high-frequency contributions are exhibited by 2-picoline (2-PIC) and 4 tert-butyl pyridine (4-TBP). In all type A systems collected in Fig. 1 the high-frequency loss asymptotically varies as $\varepsilon'' \propto \nu^{-\gamma}$ with $\gamma \approx 0.2$. Although 2-PIC and 4-TBP appear relatively similar in this plot, in Sec. IV we will point out that the behaviors of these glass formers are in fact to be distinguished. Here, we mention that the excess wing is equivalent³⁹ to what has been termed the intermediate power-law on the basis of optical Kerr effect studies.^{21,40,47} There, again a very similar exponent close to $\gamma \approx 0.2$ has been reported.

The main point of the present article is that near T_g the EW and the β -relaxation are to be considered as universally present but distinguishable features of varying relative strengths. Thus, we do not view the EW as a special (submerged) β -process. Merely, the high-frequency wing in most type A glass former will be interpreted to involve an EW and a very weak β -process. As will be demonstrated this interpretation also allows one to describe the aging experiments presented in Refs. 35 and 51, and in Sec. III, below.

Before discussing our aging results, we first present a

TABLE I. The scaling parameters ε''_{\max} and T_s used for Fig. 1 are summarized. Typically, T_s is slightly higher than T_g as defined by $T_g = T(\tau_\alpha = 100 \text{ s})$. The line shape parameters β and γ from the fits are reported here, if they were kept constant, while the temperature dependence of the free parameters is presented in Fig. 4. The γ exponents of m-TCP and TMP are those given in Fig. 9.

	Glycerol	PC	2-PIC	PG	4-TBP	m-TCP	TMP	DHIQ	Toluene	m-FAN	MTHF	DGEBA	DMP
ε''_{\max}	22.5	30.3	4.5	26.5	4	2	16.6	0.063	0.06	7	6.3	2.7	0.15
T_s (K)	196	163	133	173	168	213	140	183	119	177	94	256	198
T_g (K)	189	158	130	168	166	205	136	179.5	117	172	92	251	195
β	0.66	0.78	0.6	0.74	...	0.6	0.52
γ	0.23	0.23	0.2	0.23	0.2	0.19	0.17	0.23
References	10, 11	11	11	27	27	27	68	(This work)	11	28, 11	54	69	70

scaling analysis (Sec. II A) which implies that a one-parameter description is sometimes insufficient to describe the shape of the α -process. This is even the case in the region where we may disregard the contributions from the excess wing and from the β -process. Then, in Sec. II B we quantify these indications using a phenomenological fitting approach which supports the notion that α -relaxation and excess wing are governed by different behaviors. In Sec. III these indications are further confirmed by investigating the aging-induced change of the spectral shape of 4-TBP, PC, and glycerol, glass formers that were already well studied under equilibrium conditions.^{27,41} Finally, in Secs. IV and V we discuss and summarize our main findings.

II. SHAPE OF THE RELAXATION PEAK $T > T_g$

A. Scaling features

Line shape parameters that change with temperature are often used to describe the evolution of the main relaxation over a broad frequency range.² However, if no secondary relaxation peak interferes, temperature independent line shape parameters were extracted from some spectral analyses.^{14,21} The determination of these parameters depends on the extent to which contributions from the α -peak region and from the EW were included in the analysis. This ambiguity demonstrates the difficulty encountered when using different fitting strategies, a problem that is particularly acute at high temperatures. Here, the spectral range in which secondary relaxation features are observable becomes smaller and smaller so that the power laws originating from the α -peak may become indistinguishable from those of the EW. This situation may adversely affect the outcome of “free fits” in the sense that it is likely that artificial temperature dependences are introduced. To circumvent such problems, let us resort to studying the scaling properties of dielectric susceptibility data from a wide temperature range in a model independent way.

In order to detect possible changes of the loss shape we consider normalized susceptibility spectra, $\chi''(\nu) = \varepsilon''(\nu)/\Delta\varepsilon$. Here the relaxation strength $\Delta\varepsilon$ was extracted from the corresponding $\varepsilon'(\nu)$ data by taking their low- and high-frequency limits ε_s and ε_∞ into account. ε_∞ was considered constant in the entire temperature range $T > T_g$. At temperatures close to T_g the plateau associated with ε_s is no longer fully reached. To obtain the plateau value in those cases the $\varepsilon'(\nu)$ curves were extrapolated to lower frequencies, according to their behavior at higher temperatures. The integral of such normalized spectra yielded $\pi/2 \pm 0.05$ for all the data we will present below. In a next step we plotted them as a function of reduced frequency $\omega\tau_\alpha$ with τ_α denoting the time constant of the α -relaxation. τ_α was determined in a model-free way as follows: It is an intrinsic property of the normalized spectral density $J(\omega)$ of simple liquids that

$$\left. \frac{d\chi''(\omega)}{d\omega} \right|_{\omega\tau_\alpha \rightarrow 0} = J(0) = \tau_\alpha, \quad (1)$$

and hence

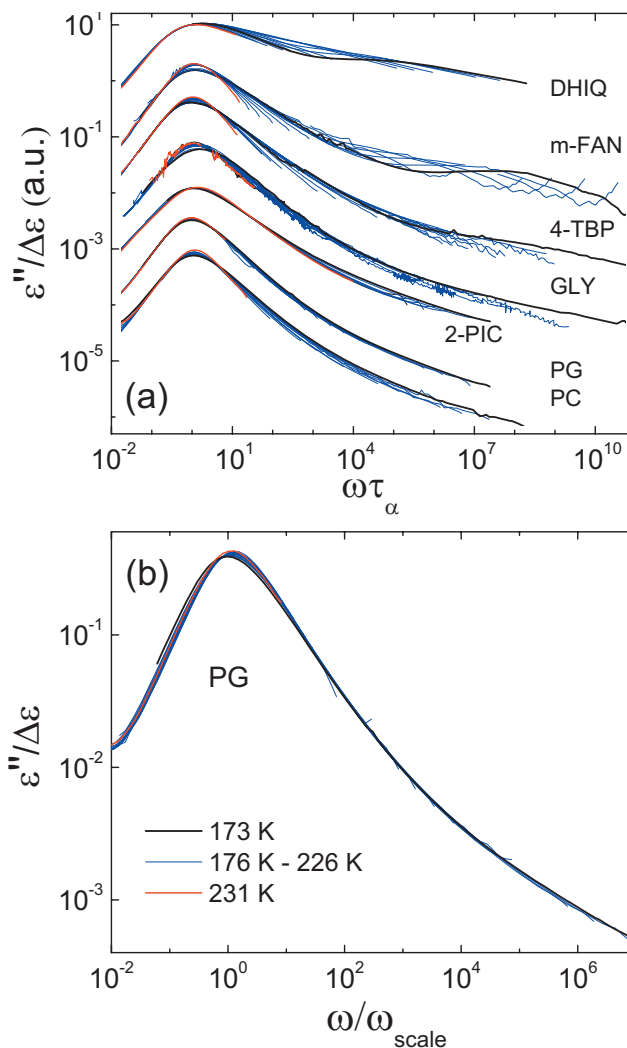


FIG. 2. (a) Normalized dielectric susceptibility spectra plotted vs reduced frequency for glass formers previously categorized as type B (DHIQ and m-FAN) or type A systems (all others). The data were taken from the references quoted in Table I. After scaling by $\Delta\varepsilon$ the data set for each glass former was shifted vertically for clarity. The red and the black lines refer to the highest and to the lowest temperatures, respectively, for each set of data. While in frame (a) a “low-frequency scaling” procedure was implemented, frame (b) involves “high-frequency scaling” for the example of PG.

$$\chi''(\omega\tau_\alpha)|_{\omega\tau_\alpha \rightarrow 0} = \omega\tau_\alpha. \quad (2)$$

Therefore, as a function of temperature, the low-frequency flank of the normalized susceptibility should collapse when plotting χ'' versus $\omega\tau_\alpha$. This low-frequency scaling is demonstrated in Fig. 2(a) for a variety of systems. Let us focus first on glass formers that were previously categorized as being of type A such as PG, glycerol, 2-PIC, 4-TBP, and PC. For several of these systems the peak systematically becomes narrower and, since the area under the peak is conserved, the peak amplitude becomes higher with increasing temperature. To quantify the width changes we note that, e.g., for PC at half the peak value of ε'' the horizontal shift of the loss curves is about 0.2 decades, while for the other systems, like 2-PIC, such effects are less pronounced. All curves in Fig. 2(a) intersect at a frequency slightly higher than that corresponding to the peak maximum. Furthermore, the high-

frequency flanks of PG, glycerol, 2-PIC, and PC do not collapse but appear to be shifted parallel to each other at high reduced frequencies. Thus, it appears that for those systems the exponents describing the high-frequency slope of the α -peak and the excess wing are temperature independent over a wide temperature range. This is explicitly demonstrated in a “high-frequency scaling” plot, Fig. 2(b). There, using a scaling frequency ω_{scale} , the high-frequency flanks of the PG spectra completely collapse whereas at low frequencies discrepancies are recognized. All data except those of 4-TBP follow the same behavior for $\omega\tau_\alpha \gg 1$.

Figure 2 thus shows that a temperature dependence of the overall width of the relaxation profile is obvious from the high-frequency flanks and that the overlap of the data near the peak maxima is far from being perfect. From these observations we conclude that the shape of the α -relaxation peak, even in some glass formers that were previously categorized as type A, is characterized by at least two shape parameters. However, the choice of these parameters is certainly not unambiguous. Hence, in the absence of a well-founded theory, this choice should be guided by the requirement that a minimum number of parameters are to be used to describe each glass former. In the next paragraph we choose these parameters in a phenomenological fashion (i) to reflect a high-frequency power law, $\nu^{-\beta}$, of the α -peak and (ii) to account for its overall width.

As representatives of type B systems we included decahydroisoquinoline (DHIQ) (this work) and m-FAN in Fig. 2(a). In particular for DHIQ one clearly recognizes that at the highest (red line) and at the lowest temperature (black) for which the α - and the β -relaxations are well separated, the high-frequency slope of the primary process is relatively steep. Close to the temperature at which both processes tend to coalesce, that high-frequency slope indicates an “artificial” broadening. For DHIQ and m-FAN the scaled curves appear not just shifted parallel to each other as for type A systems, but they intersect several times, as highlighted by the black curves in Fig. 2. The same is observed for 4-TBP, hence, based on this curve-crossing criterion, the latter substance should also be categorized as a type B system. This conjecture is substantiated by the aging experiments presented in Sec. III, below.

B. Quantitative description

In order to parametrize the line shape of the α -peak we apply the step response function⁴²

$$\Phi_\alpha(t) = 1 - \Gamma\left[\left(\frac{t}{\tau_\alpha}\right)^\alpha, \frac{\beta}{\alpha}\right] = \frac{\int_{t/\tau_\alpha}^{\infty} x^{\beta-1} e^{-x^\alpha} dx}{\int_0^{\infty} x^{\beta-1} e^{-x^\alpha} dx}. \quad (3)$$

Here $\Gamma(\dots, \dots)$ designates the regularized lower incomplete gamma function.⁴³ The parameter $\beta \leq 1$ determines the exponent of the high-frequency flank, $\varepsilon'' \propto \nu^{-\beta}$, in the peak region of the α -process while the parameter $\alpha \leq 1$ is a measure for its overall width. For $\alpha=1$ Eq. (3) reduces to the step-response of the Cole–Davidson⁴⁴ approach with $\beta=\beta_{\text{CD}}$. It

can be shown⁴² that Φ_α reduces to the well-known Kohlrausch relaxation function provided that $\beta=\alpha$. This function thus accommodates for changes of the spectral shape, which for many glass formers turns from the Cole–Davidson form at high temperatures to the Kohlrausch form close to the calorimetric glass transition.

For a more complete description of the overall spectral shape, even of type A systems, an EW contribution needs to be included into the relaxation function. The phenomenological ansatz chosen here for the overall step response function is

$$\Phi(t) = \Phi_\alpha(t)[C\Phi_{\text{EW}}(t) + (1 - C)], \quad (4)$$

with $\Phi_{\text{EW}}(t) = 1 - \Gamma(t/\tau_\alpha, \gamma)$ being of the Cole–Davidson type ($\alpha=1$), i.e., the time constant of the EW is assumed to be the same as that of the α -relaxation. Hence, the EW is characterized by a high-frequency power-law exponent, $0 < \gamma < 1$, and is always connected to the α -process.⁴⁵ For the following quantitative description of the data the parameter C is introduced as a measure for the strength of the excess wing relative to that of the α -process. The dielectric spectrum is obtained from $\Phi(t)$ via

$$\varepsilon''/\Delta\varepsilon = 2\pi\nu \operatorname{Re}\{F(\Phi(t))\}, \quad (5)$$

where F symbolizes the Fourier transform.⁴⁶ The fitting parameters of this function are $\Delta\varepsilon$, τ_α , C , α , β , and γ . In order to reduce the number of free variables, fits were performed applying constraints on $\Phi_\alpha(t)$. For example, with α kept fixed and the other parameters being free, one always finds systematic deviations between fits and data (not shown). On the other hand, for all systems that at first glance behave like type A glass formers, but not for 4-TBP, good fits were achieved with a fixed β for $T > T_g$. The value chosen for β was that from fits to the spectra at the highest temperatures. Here Eqs. (3)–(5) were used together and $C=0$ as well as $\alpha=1$ were always chosen. The fact that good fits are obtained with $\beta=\text{const.}$ may have been already anticipated in view of the validity of the “high-frequency scaling” demonstrated in Fig. 2(b). Under these constraints, γ was found to be only weakly changing with temperature in a large T range above T_g . Our decision was then to keep both β and γ fixed. The value for γ was chosen after fitting the spectra at temperatures close to T_g with a constant β . We thus assumed that the high-frequency flank of the α -relaxation, and in addition the exponent of the EW, is independent of temperature, but not the relaxation strength C . We just mention here that unconstrained fits lead to a continuous increase in both exponents β and γ with increasing T , in accord with previous investigations using such a fitting procedure.²⁷

Figure 3(a) shows that the $\varepsilon''/\Delta\varepsilon$ data for PG are perfectly described by such fits with the β - and γ -values given in Table I and α as well as C varying as summarized in Fig. 4. The decrease in the peak height evident in Fig. 3(a) [and already discussed in connection with Fig. 2(a)] is a clear indication that the α -peak broadens with decreasing temperature. This effect is less visible in a double-logarithmic plot, see Fig. 3(b), where we show data for 4-TBP. To obtain good

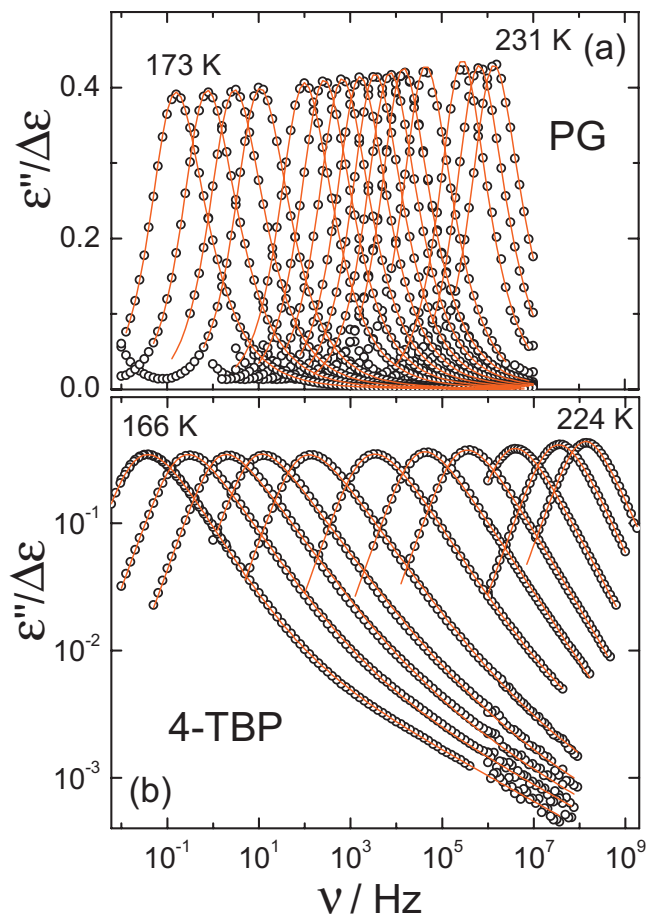


FIG. 3. (a) Susceptibility spectra of PG ($T=173, 176, 179, 182, 188, 191, 194, 197, 200, 203, 206, 211, 221, 226$, and 231 K) (Ref. 18). Fits using Eq. (4) in conjunction with Eq. (3) are represented as lines. The parameters $\beta=0.74$ and $\gamma=0.23$ were kept constant. (b) The same for 4-TBP ($T=166, 168, 170, 172, 175, 180, 185, 190, 200, 212$, and 224 K) but with only $\gamma=0.2$ fixed. The different representations in frames (a) and (b) are chosen to document the quality of the fits in both types of plot.

fits, for this substance α and β had to be treated as adjustable variables, only γ could be kept fixed. The parameters for 4-TBP are also given in Table I and Fig. 4.

The same fitting procedure was applied to glycerol, PG, PC, and m-tricresylphosphate (m-TCP) yielding always perfect fits. Figure 4 summarizes the temperature dependence of the fitting parameters α and C for these glass formers. In all cases C is practically constant in a wide temperature range and drops quickly at higher temperatures while, on the other hand, α approaches 1 upon heating. This means that the spectral shape of the α -process approaches that of the Cole-Davidson type and that the signature of the EW eventually disappears upon heating. Such a disappearance, or appearance upon cooling, is also known from OKE (Ref. 47) as well as from light scattering experiments.³⁹ We thus conclude that FTS is not generally valid for the α -relaxation. However, the fact that the “high-frequency scaling” of α -peak and EW works so well rationalizes why C is constant in a large range near T_g for most glass formers shown in Fig. 2(a). To summarize, for an accurate description of the shape of the α -relaxation peak two parameters are in general required.⁴⁸

III. PHYSICAL AGING AND SUSCEPTIBILITY AT TEMPERATURES $T \leq T_g$

The compilation of dielectric loss data shown in Fig. 1 contains also systems such as 4-TBP, for which a β -peak is not obvious and for which an EW characterized by a power law with $\gamma \approx 0.2$ seems to prevail. However, inspecting the loss spectra for lower temperatures in Fig. 2(a) traces of a β -relaxation peak may be recognized for 4-TBP. As will be shown in this section using aging experiments a β -peak becomes clearly visible for this substance. Similar observations were made for glycerol and PC by Schneider *et al.*³⁵ who interpreted their finding, however, as indicating that the EW evolves into a β -process with a well defined average relaxation time. This scenario may also be anticipated in the case of glycerol at the lowest temperature in Fig. 2(a). Here we wish to check whether a β -process with a tiny relaxation strength can be separated from an EW while cooling the sample very close to T_g . If so this would imply that EW and β -process exist simultaneously.

In order to investigate further whether or not a β -peak might exist in what seems to be a type A system, such as 4-TBP, we attempted a quantitative line shape analysis. In the spirit of the above discussion, we consider the loss spectra close to T_g to be composed of three contributions: the α -peak, the EW, and the β -relaxation. To achieve a simple phenomenological description let us, in the present context, consider them for simplicity as additive. The following assumptions are then made to disentangle dielectric loss data with the goal to isolate a β -relaxation frequency $1/\tau_\beta$:

- The high-frequency flank of the structural relaxation is characterized by a power law $\varepsilon'' \propto \nu^{-\beta}$ with an exponent β .
- The excess wing is also characterized by a power law with an exponent γ and relative amplitude C , cf. Eq. (4).
- The β -relaxation peak is characterized by a symmetric shape on a logarithmic frequency scale.

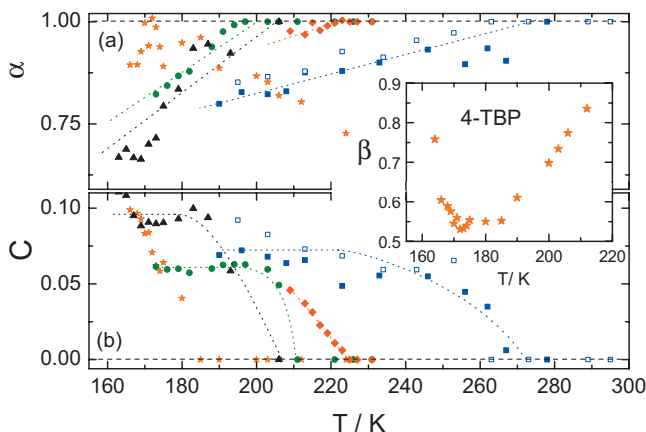


FIG. 4. Temperature dependence of the parameters (a) α and (b) C of PC (triangles, Ref. 18), PG (circles, Ref. 27), m-TCP (asterisks, Ref. 27), 4-TBP (stars, Ref. 27), and glycerol (closed squares from Ref. 10, open squares from Ref. 11). For 4-TBP the parameter β is given in the inset. Note that the temperature at which the excess wing vanishes ($C=0$) is close to the one marking the crossover to the Cole-Davidson susceptibility ($\alpha=1$) that is observed when increasing T . The dashed lines are guide to the eye.

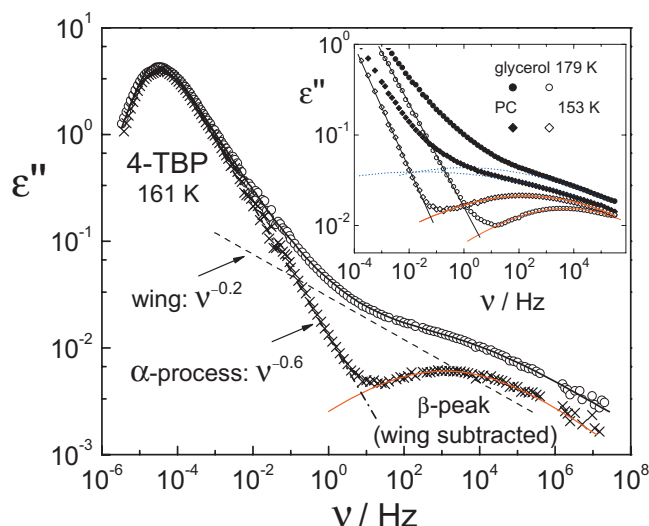


FIG. 5. Circles: the dielectric loss spectrum of 4-TBP as measured at 161 K under equilibrium conditions. Crosses: the same data but with the excess wing contribution $\propto \nu^{-0.2}$ (dashed line) subtracted on a phenomenological basis so that a symmetric β -peak results (solid line). The dash-dotted line highlights the power law on the high-frequency side of the α -peak. Inset: a similar subtraction analysis was performed for published data of glycerol and PC (Ref. 35). The solid lines show the resulting β -peaks with those previously obtained by Schneider *et al.* (Ref. 35) (dotted lines).

When choosing the high-frequency slope of the EW to be $\gamma=0.2$, for the 4-TBP data shown in Fig. 5 the conditions (i) and (iii) can only be fulfilled simultaneously if β is chosen to be 0.6 near T_g . The same β is obtained for this system at the highest temperatures where no EW contribution is evident. We applied this type of line-shape analysis⁴⁹ also to the glycerol and to the PC data measured by Schneider *et al.*³⁵ In all cases this procedure leads to β -relaxation peaks with very small amplitudes and much higher peak frequencies than previously reported (cf. inset of Fig. 5). Hence, at temperatures well above T_g these β -peaks have practically no impact on the manifestation of the high-frequency wing. For PC and glycerol the quite substantial differences between the time constants of the β -process previously obtained and those obtained by using the current analysis are presented in Fig. 7(a): whereas the mean time constants of the β -process from the present analysis are in the microsecond regime the previously reported ones³⁵ are in the ms...s regime [cf. the arrows in Fig. 7(a)].⁵⁰

In order to check whether a β -relaxation peak can unambiguously be resolved for 4-TBP without employing subtraction procedures, we carried out physical aging experiments at 153 and 151 K, i.e., somewhat below the calorimetric $T_g=163$ K. At these temperatures equilibrium was reached only after the number of days (d) as labeled in Fig. 6(a). There we show the equilibrium spectra as solid lines. As compared to the data recorded at the same temperatures under nonequilibrium conditions [symbols in Fig. 6(a)], the equilibrium spectra exhibit a minimum slope $s_{\min} = \min[d \log \epsilon'' / d \log \omega]$ with its absolute value significantly reduced in the low-frequency regime. However, a discernible peak maximum corresponding to a zero crossing of s_{\min} did not evolve during the aging of 4-TBP.⁵¹

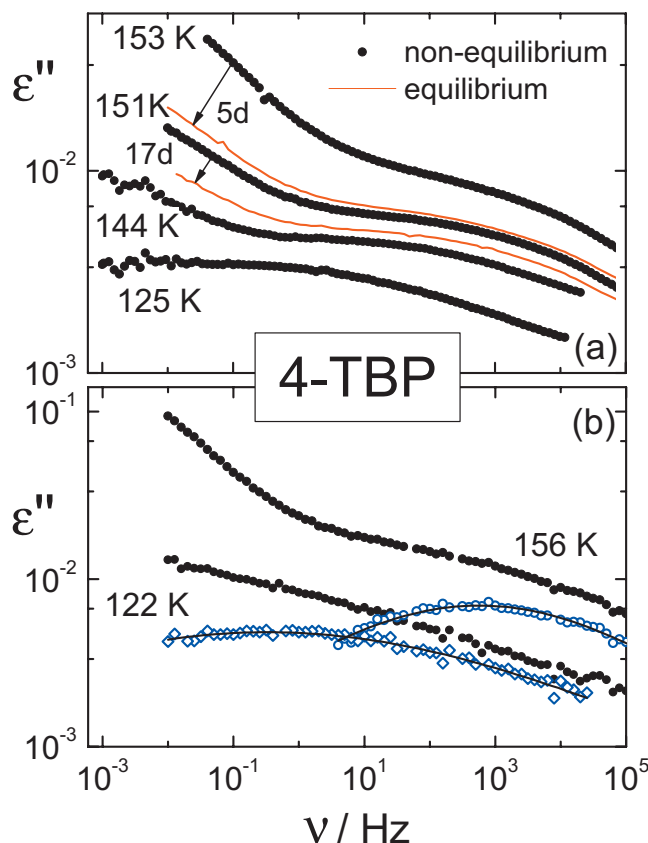


FIG. 6. (a) Aging data for 4-TBP as recorded in this work in equilibrium (lines) and out of equilibrium (symbols). (b) Loss data for 4-TBP from Ref. 27 as measured (dots) and as obtained after subtraction of a power-law contribution, $\epsilon'' \propto \nu^{-0.2}$, which again yields symmetric β -peaks (diamonds).

Additional nonequilibrium loss spectra were recorded considerably below the calorimetric glass temperature subsequent to the prolonged aging at higher temperatures. These data are included in Fig. 6(a) and are seen to exhibit slopes with $s_{\min} \rightarrow 0$. This suggests that the β -relaxation peak is in the experimental frequency window in the T range covered by the data in Fig. 6(a).

In order to separate the β -peaks we also re-evaluated previously published nonequilibrium spectra of 4-TBP (Ref. 27) which are shown as filled circles in Fig. 6(b). These data were measured without prior aging and exhibit low-frequency losses which are larger than the current ones. To analyze the data we extrapolated the above conditions (i) through (iii) to the range $T < T_g$ assuming *additionally* that the exponents β and γ as well as the amplitude $\Delta\epsilon$ remain unchanged from their values near T_g .⁵² The resulting spectra are shown in Fig. 6(b) as open circles. The spectrum accordingly obtained by subtraction at 122 K almost coincides with that recorded at 125 K after prolonged aging at 151 K.

The time constants $\tau_{\beta}^{\text{non}}(T)$ of 4-TBP resulting from the analysis of the nonequilibrium spectra are included in Fig. 7(a). Here one recognizes that the activation energy (measured in temperature units) determined from the temperature dependence of $\tau_{\beta}^{\text{non}}$ is $\approx 24T_g$. To this Arrhenius plot, we also added the time constants τ_{β}^{eq} obtained in equilibrium, cf., Fig.

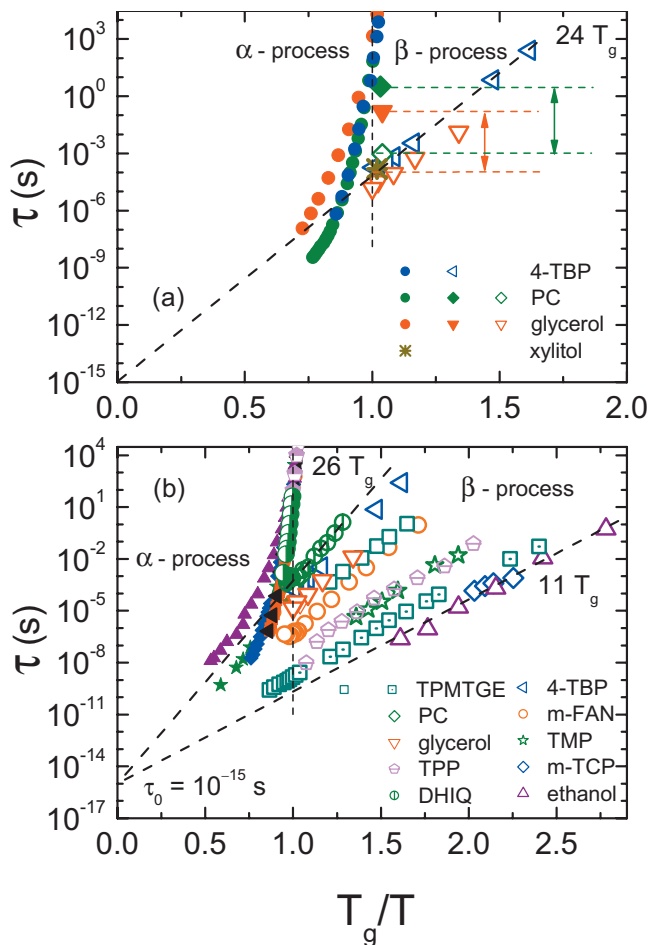


FIG. 7. (a) T_g -scaled Arrhenius plot comparing the time scales for the α -relaxation (dots) with those of the β -process for 4-TBP, PC, glycerol, and xylitol. The open symbols are the time constants obtained using the phenomenological subtraction procedure illustrated in Figs. 5 and 6 and are compatible with an E/T_g ratio of about 24 and a pre-exponential factor of 10^{-15} s. The closed symbols for glycerol, and PC were obtained from the analysis of Schneider *et al.* (Refs. 35 and 51) who did not take into account a separate EW. The arrows indicate the difference (of about 3 decades!) between the β time scales obtained by the two kinds of analysis. Frame (b) is similar to frame (a), but it includes more data. Except for TPMTGE τ_β was obtained using the subtraction procedure illustrated in Figs. 5 and 6. The data for m-FAN (Ref. 28), TPMTGE (Ref. 59), and ethanol (Ref. 56) were taken from the literature, those for m-TCP and TMP are from the present work. The dashed lines are Arrhenius laws calculated with the same prefactor ($\tau_0 = 10^{-15}$ s) and the T_g -scaled activation energies indicated in the figure.

5. The compatibility of τ_β^{non} and τ_β^{eq} indicates that τ_β is essentially unaffected by aging. This is in accord with previous data.⁵³

IV. DISCUSSION

The time constants τ_β , corresponding to the β -peak, determined either directly from the data or via the procedure outlined above are shown in Fig. 7(b) for a range of glass formers. For some systems the spectra were measured as part of this work and for others the data are taken from literature (see Table I for details). The data fall into the E/T_g range of $11 \cdots 26$. This is true also for glass formers with a “nonresolved” β -process, e.g., 4-TBP, glycerol, MTHF⁵⁴ or

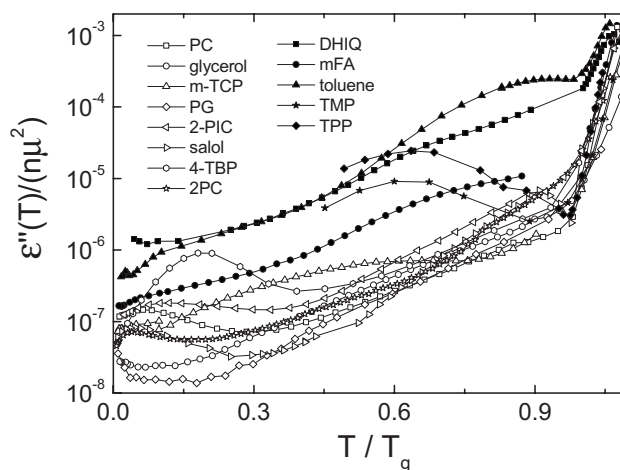


FIG. 8. Dielectric loss of several glass formers focusing on the range $T < T_g$. The ordinate axis is normalized by $n\mu^2$ (Ref. 65). While type A glass formers show a relatively uniform behavior for $0.6 < T/T_g < 0.9$, type B systems exhibit a larger normalized loss. The normalization parameters are given in Table II.

xylitol.⁵¹ One reassuring aspect of the current analysis is not only the magnitude of the obtained E/T_g ratios, but also that a physically plausible pre-exponential factor of the order of $\tau_0 = 10^{-15}$ s is recovered for all glass formers. This is highlighted by extrapolating the Arrhenius lines in Figs. 7(a) and 7(b) to infinite temperatures. Note that much smaller pre-exponential factors are found if the EW is assumed to be a submerged β -process.⁵⁵

Data for triphenylphosphite (TPP), TMP, m-TCP, and ethanol⁵⁶ that exhibit relatively fast secondary processes are also included in Fig. 7(b) (cf. also Table I). For these systems the resulting energy barrier E_β is $\leq 16T_g$. The criterion implied here in terms of the E/T_g ratio, which can be related to other parameters describing the degree of decoupling,⁵⁷ is to some extent arbitrary. This is because the degree of decoupling is known to vary more or less continuously if a large array of glass formers is considered.⁵⁸ A relatively slow and a relatively fast β -relaxation can in fact coexist as is, e.g., the case for triepoxy triphenylolmethane triglycidyl ether (TPMTGE),⁵⁹ see Fig. 7(b). Furthermore, the application of high pressures may help render the presence of two distinct processes, which are faster than the α -relaxation, visible.³⁴

As compiled in Table I the exponent characterizing the EW is $\gamma = 0.2 \pm 0.03$.⁶⁰ However, there is an apparent exception, TPP,¹⁴ for which no EW is observed in the studied frequency range. Here the high-frequency flank of the α -peak follows a $\nu^{-0.5}$ behavior up to the frequencies at which a fast beta process sets in Ref. 61. But the onset of an excess wing is difficult to detect in the presence of a comparably broad α -relaxation as it is typical for TPP.²¹ We also mention that an excess wing with a pressure-independent exponent of $\gamma = 0.22$ was recently identified in the dielectric response of an ionic liquid.⁶²

To check which other common features and differences might exist in the low-temperature regime ($T < T_g$), we compile $\epsilon''(T/T_g)$ data measured at 1 kHz for various glass formers in Fig. 8. The main difference to a previous version of that figure (cf. Ref. 63) is that it contains more data sets⁶⁴

and that the loss axis has been scaled to the dispersion step related to the α -process. The dispersion step is proportional to the square of the molecular dipole moment, μ^2 , and the dipole number density, n .

The quantity $n\mu^2$ was determined by assuming that a Curie law $n\mu^2 = 3\varepsilon_0 k_B T_{\text{ref}} \Delta\varepsilon_{\text{ref}}$ holds at temperatures $T \gg T_g$.⁶⁵ Here $\Delta\varepsilon_{\text{ref}}$ is the dispersion step at a reference temperature T_{ref} and ε_0 is the permittivity of free space. In Fig. 8 we plotted $\varepsilon''/(n\mu^2)$ versus T/T_g with the values for T_{ref} and $\Delta\varepsilon_{\text{ref}}$ summarized in Table II. Figure 8 reveals a remarkable similarity of behavior for various systems including PC, PG, and glycerol. These glass formers (represented by open symbols in Fig. 8) exhibit the lowest loss in the range⁶⁶ from about $0.6T_g$ to $0.9T_g$ and also the lowest high-frequency wings in the representation of Fig. 1. The similarity of the scaled loss in the $0.6T_g$ to $0.9T_g$ range in these so-called type A systems is remarkable because it suggests that α -process and wing derive from the same dipolar entities. In passing we note that the best agreement is found below 4 K, possibly indicating an universal low-temperature relaxation of molecular glasses as expected, e.g., in the tunneling regime.⁶³

Systems previously classified as type B are represented by solid symbols in Fig. 8. In the temperature range covered by Fig. 8 they show a considerably larger loss suggesting that this has its origin in the presence of a secondary process. 4-TBP or m-TCP with their very small or very fast secondary process, respectively, exhibit an intermediate amplitude in Fig. 8. Hence, the strength of the β -process does not scale with the molecular dipole moment, and this distinguishes this process from the EW. Since the view taken in this article implies that, in principle, all glass formers are type B systems in the sense that a β -relaxation is ubiquitously present, we conclude that this should also apply for 2-PIC which exhibits a relatively large amplitude in the representation of Fig. 8 but so far no indications for a β -peak could be resolved. Extended aging experiments are underway to clarify this issue.

β -relaxations are thermally activated and hence the corresponding loss peaks broaden continuously for decreasing temperatures.⁶⁷ If, for $T < T_g$, one would identify the EW with a β -relaxation then such a monotonous broadening of the shape of the EW would be expected. This should manifest itself in a steady decrease in the power law exponent γ , cf. Eq. (4). However, experimental results indicate that below T_g this exponent remains constant over a wide range and then typically decreases in a more or less stepwise fashion.^{63,65} As examples for this “constant-exponent” behavior we present loss spectra of m-TCP and TMP in Fig. 9. Here one clearly recognizes that the low-frequency part of the spectra stays temperature independent in a large range below T_g .

To conclude the discussion on the distinction between

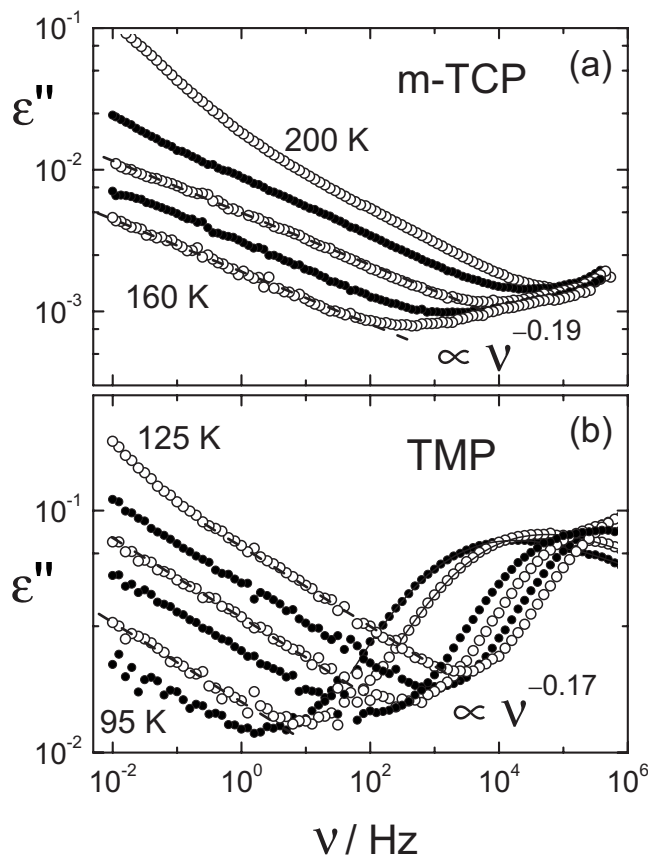


FIG. 9. Dielectric loss spectra for (a) m-TCP recorded at $T=160, 170, 180, 190$, and 200 K and (b) TMP recorded at $T=95, 100, 110, 115, 120$, and 125 K. The solid lines represent power laws $\propto \nu^{-0.19}$ in frame (a) and $\propto \nu^{-0.17}$ in frame (b). After subtraction of the high-frequency flank, $\varepsilon'' \propto \nu^{-0.6}$, from the α -process of m-TCP the exponent $\gamma=0.19$ is recovered also for 200 K (not shown).

so-called type A and type B glass formers let us consider again the temperature range $T \geq T_g$ where recently the α -time dependent minimum slopes $s_{\text{min}}(\tau_\alpha)$ have been scrutinized for more than 50 glass formers.²⁰ That was done with the goal to check whether $s_{\text{min}} = -0.5$ plays a special role. In this context the s_{min} parameter may be taken as a measure of the high-frequency stretching of the α -process. In Fig. 10 we selected xylitol and PG from Ref. 20 as two representative examples to highlight the characteristic behaviors of s_{min} for so-called type A versus type B glass formers. For regular type B systems a trend opposite to that of type A glass formers is observed. Since the relatively broad β -relaxation in typical type B systems is usually observed to gain amplitude with increasing temperature this renders $|s_{\text{min}}|$ smaller upon heating. For type A glass formers $|s_{\text{min}}|$ gets smaller and hence $\varepsilon''(\nu)$ less steep when approaching T_g because, in our interpretation, the excess wing with its frequency insensitive

TABLE II. Parameters used to normalize the data shown in Fig. 8.

	Glycerol	PC	2-PIC	PG	4-TBP	m-TCP	TMP	DHIQ	Toluene	m-FAN	Salol	2PC	TPP
$T_{\text{ref}}(\text{K})$	301	231	202	175	301	307	230	206	120	290	240	350	212
$\Delta\varepsilon_{\text{ref}}$	43	106	6.5	61	7.8	4.6	23	2.2	0.3	13	5	7.7	0.83

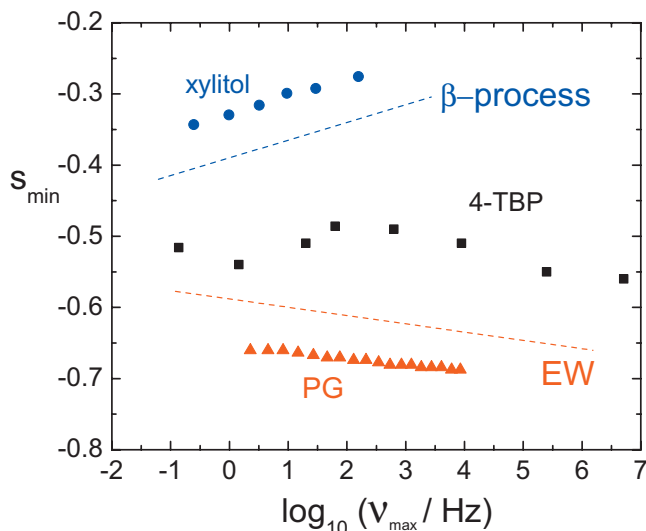


FIG. 10. Typical dependences of the minimum slope s_{\min} as a function of the primary relaxation time τ_{α} . Out of the wide range of possible dependences (cf. Ref. 20) only a few typical cases are selected and shown as symbols. The dashed lines illustrate $s_{\min}(\tau_{\alpha})$ dependences expected on the basis of the current analysis for systems for which either a β -relaxation or an EW dominates above the region of the α -peak. The behavior of 4-TBP is intermediate between the two cases.

slope gains amplitude upon cooling. Thus, this model-independent observation is in agreement with the $C(T)$ dependence discussed in relation to Fig. 4 and is different from the behavior observed for systems with strong β -contributions.

For intermediate systems with weak or fast β -processes a mixture of the two kinds of behaviors is observed. As an example in Fig. 10 we show s_{\min} as evaluated from the current 4-TBP data. At the lowest temperatures, at which the amplitude of the β -process is small, a behavior similar to that of type A systems is obtained. At higher temperatures or shorter τ_{α} , however, the trend in s_{\min} reverses as a signature that in this regime the β -process gains amplitude. At even higher temperatures, the β -process merges with the α -process and a type A behavior is recovered. Again, within the view taken in the current article, the β -process appears to interfere with the clear-cut trend observed for glass formers in which an EW dominates the high-frequency behavior.

V. SUMMARY

By re-examining the evolution of the dielectric spectra of low-molecular weight glass formers we conclude that the structural relaxation does not obey FTS and that for a detailed description of the α -peak shape sometimes two parameters have to be used. A suitable fitting function was applied which accommodates for a change from a Cole–Davidson-like to a Kohlrausch-like spectral profile that is typically observed when cooling a liquid through the viscous regime. The present phenomenological addition of primary relaxation and high-frequency wing renders their relative amplitude temperature dependent. On the quantitative level it is found within this framework that the exponents α and β which parametrize the shape and width of the α -relaxation in and near the peak region do in general depend on tempera-

ture. However, for most glass formers investigated in the present study the exponent β could be kept fixed. For these systems the only parameter that describes the evolution of the entire high-frequency flank of the α -peak is the relative amplitude of the excess wing with respect to that peak. The power-law exponent γ describing the high-frequency wing is of the order of 0.2 for virtually all systems studied in harmony with previous reports. For many systems this exponent is obtained above and also well below T_g .

Our phenomenological procedure to subtract an EW contribution from the overall dielectric loss of glass formers, for which no secondary relaxation is immediately obvious, yields secondary relaxation peaks for practically all investigated systems. The temperature dependence for many of them conforms to that expected for secondary relaxations. We thus argue that β -relaxations are universal features of glass formers which due to their low, relative to the EW contribution, relaxation strength sometimes cannot be resolved and then remain undetected. More direct evidence for a β -relaxation peak in 4-TBP, a glass former that has previously been called a type A system was obtained using aging experiments. These results as well as the analysis of the data of several other glass formers show that EW and β -process can be present simultaneously. In that sense, the EW is not a submerged β -relaxation but has to be treated on a different footing. The scaling presented in Fig. 8 also supports this result since it reveals that the EW and the β -relaxation exhibit different signatures.

To summarize, we presented an alternative way of analyzing the dynamic susceptibility in simple glass formers. It allows one to isolate β -processes in virtually any glass former, making obvious the limitations of the type A versus type B classification scheme. Furthermore, the present work shows that the E_{β}/T_g ratios span an even larger range than previously thought. The current analysis has the added advantage that the pre-exponential factors associated with the β -peaks thus obtained exhibit physically reasonable values, no matter whether they are determined under equilibrium conditions or from aging experiments.

¹G. P. Johari and M. Goldstein, *J. Chem. Phys.* **53**, 2372 (1970).

²K. L. Ngai and M. Paluch, *J. Chem. Phys.* **120**, 857 (2004).

³P. K. Dixon, L. Wu, S. R. Nagel, B. D. Williams, and J. P. Carini, *Phys. Rev. Lett.* **65**, 1108 (1990).

⁴A. Hofmann, F. Kremer, E. W. Fischer, and A. Schönhal, in *Disorder Effects on Relaxation Processes*, edited by R. Richert and A. Blumen (Springer, Berlin, 1994), p. 309.

⁵H. Z. Cummins, G. Li, Y. H. Hwang, G. Q. Shen, W. M. Du, J. Hernandez, and N. J. Tao, *Z. Phys. B: Condens. Matter* **103**, 501 (1997).

⁶C. A. Angell, K. L. Ngai, G. B. McKenna, P. F. McMillan, and S. W. Martin, *J. Appl. Phys.* **88**, 3113 (2000).

⁷K. L. Ngai, *J. Non-Cryst. Solids* **275**, 7 (2000).

⁸W. Götze, *J. Phys.: Condens. Matter* **11**, A1 (1999).

⁹T. Blochowicz, A. Brodin, and E. A. Rössler, *Adv. Chem. Phys.* **133**, 127 (2006).

¹⁰P. Lunkenheimer, A. Pimenov, B. Schiener, R. Böhmer, and A. Loidl, *Europhys. Lett.* **33**, 611 (1996); P. Lunkenheimer, U. Schneider, R. Brand, and A. Loidl, *Contemp. Phys.* **41**, 15 (2000).

¹¹A. Kudlik, S. Benkhof, T. Blochowicz, C. Tschirwitz, and E. A. Rössler, *J. Mol. Struct.* **479**, 201 (1999).

¹²A. Tölle, *Rep. Prog. Phys.* **64**, 1473 (2001).

¹³A. Brodin and E. A. Rössler, *Eur. Phys. J. B* **44**, 3 (2005).

¹⁴N. B. Olsen, T. Christensen, and J. C. Dyre, *Phys. Rev. Lett.* **86**, 1271 (2001).

- ¹⁵W. Kob and H. C. Andersen, *Transp. Theory Stat. Phys.* **24**, 1179 (1995).
- ¹⁶S. Kämmerer, W. Kob, and R. Schilling, *Phys. Rev. E* **58**, 2131 (1998); **58**, 2141 (1998).
- ¹⁷W. Götze and L. Sjögren, *Rep. Prog. Phys.* **55**, 241 (1992).
- ¹⁸T. Blochowicz, C. Tschirwitz, S. Benkhof, and E. A. Rössler, *J. Chem. Phys.* **118**, 7544 (2003).
- ¹⁹K. L. Ngai, P. Lunkenheimer, C. León, U. Schneider, R. Brand, and A. Loidl, *J. Chem. Phys.* **115**, 1405 (2001).
- ²⁰A. I. Nielsen, T. Christensen, B. Jakobsen, K. Niss, N. B. Olsen, R. Richert, and J. C. Dyre, *J. Chem. Phys.* **130**, 154508 (2009); A. I. Nielsen, S. Pawlus, M. Paluch, and J. C. Dyre, *Philos. Mag.* **88**, 4101 (2008).
- ²¹A. Brodin, C. Gainaru, V. Porokhonskyy, and E. A. Rössler, *J. Phys.: Condens. Matter* **19**, 205104 (2007).
- ²²S. Hensel-Bielowka and M. Paluch, *Phys. Rev. Lett.* **89**, 025704 (2002).
- ²³K. L. Ngai, R. Casalini, S. Capaccioli, M. Paluch, and C. M. Roland, *J. Phys. Chem. B* **109**, 17356 (2005).
- ²⁴U. R. Pedersen, N. P. Bailey, T. B. Schröder, and J. C. Dyre, *Phys. Rev. Lett.* **100**, 015701 (2008).
- ²⁵R. V. Chamberlin, *Phys. Rev. B* **48**, 15638 (1993).
- ²⁶G. Tarjus, D. Kivelson, and P. Viot, *J. Phys.: Condens. Matter* **12**, 6497 (2000).
- ²⁷T. Blochowicz, C. Gainaru, P. Medick, C. Tschirwitz, and E. A. Rössler, *J. Chem. Phys.* **124**, 134503 (2006).
- ²⁸C. Gainaru, A. Brodin, V. N. Novikov, and E. A. Rössler, arXiv:cond-mat/0604597.
- ²⁹R. Böhmer, K. L. Ngai, C. A. Angell, and D. J. Plazek, *J. Chem. Phys.* **99**, 4201 (1993).
- ³⁰K. Niss, C. Dalle-Ferrier, G. Tarjus, and C. Alba-Simionesco, *J. Phys.: Condens. Matter* **19**, 076102 (2007).
- ³¹R. Böhmer, G. Diezemann, B. Geil, G. Hinze, A. Nowaczyk, and M. Winterlich, *Phys. Rev. Lett.* **97**, 135701 (2006).
- ³²K. Kessairi, S. Capaccioli, D. Prevosto, M. Lucchesi, S. Sharifi, and P. A. Rolla, *J. Phys. Chem. B* **112**, 4470 (2008).
- ³³V. N. Novikov and A. P. Sokolov, *Phys. Rev. E* **67**, 031507 (2003).
- ³⁴R. Casalini and C. M. Roland, *Phys. Rev. Lett.* **91**, 015702 (2003).
- ³⁵U. Schneider, R. Brand, P. Lunkenheimer, and A. Loidl, *Phys. Rev. Lett.* **84**, 5560 (2000).
- ³⁶F. Qi, T. El Goresy, R. Böhmer, A. Döb, G. Diezemann, G. Hinze, H. Sillescu, T. Blochowicz, C. Gainaru, E. Rössler, and H. Zimmermann, *J. Chem. Phys.* **118**, 7431 (2003).
- ³⁷This does not necessarily imply that local (internal) motions are absent. From NMR and calorimetry a CH₃ rotation was identified for PC, see F. Qi, R. Böhmer, and H. Sillescu, *Phys. Chem. Chem. Phys.* **3**, 4022 (2001).
- ³⁸A pattern similar to that shown in Fig. 1 is also observed for a series of polyalcohols, see A. Döb, M. Paluch, H. Sillescu, and G. Hinze, *Phys. Rev. Lett.* **88**, 095701 (2002); A. Döb, M. Paluch, H. Sillescu, and G. Hinze, *J. Chem. Phys.* **117**, 6582 (2002).
- ³⁹A. Brodin and E. A. Rössler, *J. Chem. Phys.* **125**, 114502 (2006); **126**, 244508 (2007).
- ⁴⁰M. Ricci, P. Bartolini, and R. Torre, *Philos. Mag. B* **82**, 541 (2002).
- ⁴¹K. Kessairi, S. Capaccioli, D. Prevosto, M. Lucchesi, and P. A. Rolla, *J. Chem. Phys.* **127**, 174502 (2007).
- ⁴²R. Kahlau *et al.* (unpublished).
- ⁴³*Handbook of Mathematical Functions*, edited by M. Abramowitz and I. A. Stegun (National Bureau of Standards, Washington, D.C., 1964), Chap. 26.
- ⁴⁴C. J. F. Böttcher and P. Bordewijk, *Theory of Electric Polarization: Dielectrics in Time-Dependent Fields* (Elsevier, Amsterdam, 1978), Vol. 2.
- ⁴⁵Note that this connection of α -process and EW does not imply that these processes are identical. Recent studies show that while the α -process is isotropic, the excess wing originates from a spatially highly restricted motion, see M. Vogel, C. Tschirwitz, S. Schneider, C. Koplin, P. Medick, and E. Rössler, *J. Non-Cryst. Solids* **307–310**, 326 (2002); C. Gainaru, O. Lips, A. Troshagina, R. Kahlau, A. Brodin, F. Fujara, and E. A. Rössler, *J. Chem. Phys.* **128**, 174505 (2008).
- ⁴⁶The Fourier transformation was carried out numerically using a program written by Dr. A. Brodin whom we thank for making this program available to us.
- ⁴⁷The emergence of the EW at high temperatures is best recognized in optical Kerr effect as well as in light scattering experiments, see Ref. 21 and H. Cang, V. N. Novikov, and M. D. Fayer, *J. Chem. Phys.* **118**, 2800 (2003).
- ⁴⁸Note that for polymeric glass formers two parameters are in general required for a description of the main relaxation, albeit there for a different reason, see A. Schönhals, F. Kremer, and E. Schlosser, *Phys. Rev. Lett.* **67**, 999 (1991).
- ⁴⁹The conditions (i) through (iii) can be fulfilled with $\beta=0.63$ and $\gamma=0.21$ for glycerol and with $\beta=0.78$ and $\gamma=0.23$ for PC. Here the β -parameters are those resulting from previous scaling analyses of glycerol (Ref. 68) and of PC (Ref. 27), respectively.
- ⁵⁰A recent study on glycerol at ultrahigh pressure also reports more “normal” β time constants below the α - β merging region, see A. A. Pronin, M. V. Kondrin, A. G. Lyapin, V. V. Brazhkin, A. A. Volkov, P. Lunkenheimer, and A. Loidl (unpublished).
- ⁵¹For xylitol extended aging led to a resolved β -peak, see R. Wehn, P. Lunkenheimer, and A. Loidl, *J. Non-Cryst. Solids* **353**, 3862 (2007).
- ⁵²It is clear that at the lowest temperatures the high-frequency part of the α -process is irrelevant for determining τ_β .
- ⁵³G. P. Johari, *Ann. N. Y. Acad. Sci.* **279**, 117 (1976).
- ⁵⁴For MTHF the E/T_g ratio was reported to be $1650/91=18.1$, see Ref. 36. Since in that article a different method of analysis was employed the data are not included in Fig. 7.
- ⁵⁵T. Blochowicz and E. A. Rössler, *Phys. Rev. Lett.* **92**, 225701 (2004).
- ⁵⁶R. Brand, P. Lunkenheimer, U. Schneider, and A. Loidl, *Phys. Rev. B* **62**, 8878 (2000) (and references cited therein).
- ⁵⁷See, e.g., T. El Goresy and R. Böhmer, *J. Phys.: Condens. Matter* **19**, 205134 (2007) and references cited therein.
- ⁵⁸K. L. Ngai, *Phys. Rev. E* **57**, 7346 (1998).
- ⁵⁹D. Pisignano, S. Capaccioli, R. Casalini, M. Lucchesi, P. A. Rolla, A. Justl, and E. A. Rössler, *J. Phys.: Condens. Matter* **13**, 4405 (2001).
- ⁶⁰The same value for the exponent γ was used by U. Buchenau, *J. Chem. Phys.* **131**, 074501 (2009); see also R. Casalini and C. M. Roland, *Phys. Rev. B* **69**, 094202 (2004).
- ⁶¹The behavior of TPP was rationalized in Ref. 21.
- ⁶²A. Rivera-Calzada, (private communication), see also Fig. 3 in A. Rivera-Calzada, K. Kaminski, C. León, and M. Paluch, *J. Phys.: Condens. Matter* **20**, 244107 (2008).
- ⁶³C. Gainaru, A. Rivera, S. Putselyk, G. Eska, and E. A. Rössler, *Phys. Rev. B* **72**, 174203 (2005).
- ⁶⁴Apart from the data of Refs. 63 and 65 we included data on 3,3,4,4-benzophenonetetracarboxylic dianhydride (2PC) from Ref. 2 and data on DHIQ from this work.
- ⁶⁵C. Gainaru, Dissertation, Universität Bayreuth, 2007.
- ⁶⁶The peaks observed for $T<0.3T_g$ in Fig. 8 are due to the relaxation in asymmetric double well potentials, see the discussion in Ref. 63.
- ⁶⁷A. Kudlik, C. Tschirwitz, T. Blochowicz, S. Benkhof, and E. Rössler, *J. Non-Cryst. Solids* **235–237**, 406 (1998).
- ⁶⁸S. Adichtchev, T. Blochowicz, C. Gainaru, V. N. Novikov, E. A. Rössler, and C. Tschirwitz, *J. Phys.: Condens. Matter* **15**, S835 (2003).
- ⁶⁹C. Gainaru *et al.* (unpublished).
- ⁷⁰A. Brodin, R. Bergman, J. Mattsson, and E. A. Rössler, *Eur. Phys. J. B* **36**, 349 (2003).

Paper 3

Quinaldine: Accessing Two Crystalline Polymorphs via the Supercooled Liquid

R. KAHLAU, T. GNUTZMANN, F. EMMERLING, K. RADEMAN, AND
E. A. RÖSSLER,
The Journal of Chemical Physics **137**, 054505 (2012).

© 2012 American Institute of Physics
doi:10.1063/1.4738583

Quinaldine: Accessing two crystalline polymorphs via the supercooled liquid

Robert Kahlau,¹ Tanja Gnutzmann,^{2,3} Franziska Emmerling,² Klaus Rademann,³ and Ernst A. Rössler¹

¹Physikalisches Institut, Universität Bayreuth, Bayreuth 95440, Germany

²BAM Federal Institute for Materials Research and Testing, Berlin 12489, Germany

³Department of Chemistry, Humboldt-Universität, Berlin 12489, Germany

(Received 6 March 2012; accepted 6 July 2012; published online 3 August 2012)

Quinaldine (2-methyl quinoline) is a liquid at room temperature, which can be supercooled to reach finally the glassy state. By heating the glass above the glass transition temperature $T_g = 180$ K the sample performs two subsequent transitions into, likewise, dielectrically active phases. Thus, the reorientational relaxations of these phases as well as the kinetics of the phase transitions can be tracked in a highly resolved way by dielectric spectroscopy. X-ray diffraction analysis clearly shows two structurally different crystalline phases in addition to the supercooled liquid. Calorimetric measurements support the notion of first order phase transitions, occurring irreversibly in the supercooled regime, and suggest that the intermediate crystalline phase is metastable, too. Analyzing the quite distinct dielectric relaxation strengths, we discuss the possible nature of the two crystalline phases. Additionally, a very similar behavior to quinaldine is observed for 3-methyl quinoline, indicating a broad field of polymorphism among the quinoline derivatives. © 2012 American Institute of Physics. [<http://dx.doi.org/10.1063/1.4738583>]

I. INTRODUCTION

Organic compounds are commonly known for showing the phenomenon of polymorphism,^{1–8} i.e., they may exist in structurally different crystalline phases. For example, in the case of the compound ROY, at least seven polymorphs have been identified.² Under the given conditions, only a single phase can be thermodynamically stable whereas the others are all metastable. Finding the routes to obtain and capture such metastable phases has thus become an important issue in materials science.

Many liquids can be supercooled leading to a strong increase of their transport coefficients like viscosity or diffusion coefficient. At temperatures around the glass transition temperature T_g , the crystallization process of the deeply supercooled liquid is typically diffusion controlled and therefore avoided on laboratory time scales.¹ Then the liquid is in a metastable state. Considering the chemical potential $\mu_l(T)$ of the highly supercooled liquid as a function of temperature, usually a large gap opens with respect to the potential $\mu_c(T)$ of the thermodynamically stable crystalline phase (cf. Fig. 1). A metastable crystalline phase with its potential $\mu_m(T)$, if present, will appear within this gap. In other words, by increasing the temperature of the highly viscous liquid and thus again facilitating diffusion the usually occurring phase transition does not necessarily have to end up with the thermodynamic equilibrium phase but may yield metastable phases. Thus, strongly supercooling a liquid opens the possibility for searching unknown metastable phases of molecular systems.

A prominent example is liquid ethanol,^{9,10} which transforms into a metastable crystal if it is kept close to $T_g = 97$ K, i.e., well below the melting point $T_m = 159$ K. Regarding its

orientational degrees of freedom, this crystal exhibits “glassy” dynamics, i.e., highly cooperative molecular rotation above the corresponding T_g . Upon heating, the glassy crystal phase of ethanol transforms into the orientationally ordered and thermodynamically stable phase, which melts at T_m .

Studying the regime of a supercooled liquid or even the glass ($T < T_g$) with respect to possible phase transitions is also an important issue in understanding how to stabilize glasses against crystallization. For some applications, for example, pharmaceuticals, the glassy state is advantageous over the crystalline state, and it is important to avoid crystallization or at least to minimize the rate of crystal growth. In a recent application, Ediger and co-workers¹¹ have investigated the diffusion coefficient D of the supercooled liquid indomethacin ($T_g = 315$ K). The authors have found that the temperature dependence of the diffusion is significantly weaker than that of viscosity, and that it is indeed $D(T)$, which controls the transformation into the three identified^{12,13} crystalline polymorphs of indomethacin.

In the present contribution, the polymorphism of the compound quinaldine (2-methyl quinoline, 2mq, see Fig. 3) is examined. Quinaldine is a liquid at room temperature, which can easily be supercooled below its melting temperature $T_m \approx 264$ – 270 K as demonstrated by Capaccioli *et al.*¹⁴ Like in other glass-forming liquids, the structural relaxation becomes very slow upon cooling, i.e., the reorientational correlation time of a molecule rises from $\tau = 10^{-12}$ s at the melting point to $\tau = 100$ s at the glass temperature T_g . Since the quinaldine molecule is polar, this behavior is well verifiable by means of dielectric spectroscopy,¹⁵ and we have determined the glass transition temperature to be $T_g \approx 180$ K. We demonstrate that

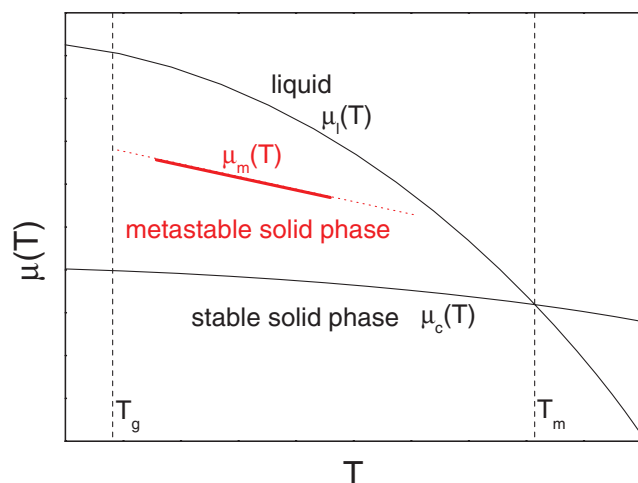


FIG. 1. Searching for metastable phases: chemical potential of stable and metastable solid phases together with that of the (supercooled) liquid phase; melting (T_m) and glass transition temperatures (T_g) are indicated.

two phase transitions can be monitored with the help of dielectric spectroscopy, x-ray diffractometry (XRD) and differential scanning calorimetry (DSC) upon heating the highly supercooled liquid. Here, we benefit from the fact that all the three phases of quinaldine are dielectrically active and thus allow to probe the dynamics in each phase as well as both phase transitions. Moreover, as quinaldine is a rigid molecule of low symmetry, any dynamics has to involve the total molecule. This is likely to result in some kind of cooperative dynamics in the crystalline state, the nature of which we are interested in. Finally, we show that similar polymorphs are identified for 3-methyl quinoline.

II. EXPERIMENTAL

A. Chemicals

2-methyl quinoline (“quinaldine,” CAS 91-63-4, 97+%) was purchased from Alfa Aesar, 3-methyl quinoline (CAS 612-58-8, 99%) was delivered by Sigma-Aldrich. Both substances were used as received without any further treatment.

B. Dielectric spectroscopy

Dielectric measurements were carried out with the Alpha-A analyzer by Novocontrol, which allows for frequency resolved measurements of the dielectric susceptibility in the range of $\nu = 10^{-2}$ – 10^6 Hz. During a frequency scan, the sample temperature was kept constant within ± 0.2 K with the help of a Quatro-H temperature controller by Novocontrol.

In order to interpolate the main relaxation peak in the dielectric spectra of the (supercooled) liquid phase (2mq1), we used a step response function, which generalizes the Kohlrausch and the Cole-Davidson spectral shape and has turned out to be a versatile response function for supercooled liquids.¹⁶ Explicitly,

$$\phi_g(t) = \frac{1}{\Gamma(\frac{\beta}{\alpha})} \int_{(\frac{t}{\tau_g})^\alpha}^{\infty} y^{\frac{\beta}{\alpha}-1} \exp(-y) dy = \frac{\Gamma(\frac{\beta}{\alpha}, (\frac{t}{\tau_g})^\alpha)}{\Gamma(\frac{\beta}{\alpha})} \quad (1)$$

was used for the structural relaxation or α -peak. Here $\Gamma(\dots)$ denotes the gamma function and $\Gamma(\dots, \dots)$ the upper incomplete gamma function as defined by Eq. (1), respectively. This (normalized) step response function is connected with the susceptibility spectra in the frequency domain by the one-sided Fourier transform $F(\dots)$

$$\varepsilon''(\omega) = \Delta\varepsilon \chi''(\omega) = \Delta\varepsilon \omega \text{Re}\{F[\phi(t)]\} \quad (2)$$

with $\Delta\varepsilon$ being the dielectric relaxation strength. The integral of $\phi_g(t)$ (Eq. (1)) yields the mean relaxation time

$$\tau_\alpha = \tau_0 \frac{\Gamma(\frac{\beta+1}{\alpha})}{\Gamma(\frac{\beta}{\alpha})}. \quad (3)$$

The interpolation of the so-called excess wing (EW), appearing on the high-frequency flank of the α -relaxation peak as a kind of power-law, was obtained by including the step response of the Cole-Davidson function (CD function)

$$\phi_{CD}(t) = \frac{\Gamma(\gamma, \frac{t}{\tau_{CD}})}{\Gamma(\gamma)} \quad (4)$$

together with the Williams-Watts approach¹⁷

$$\phi(t) = [C\phi_{CD}(t) + (1 - C)]\phi_g(t) \quad (5)$$

with C being a measure for the amplitude of the EW. The time constants of both contributions are set equal ($\tau_g = \tau_{CD}$) so that only the high-frequency power-law with the exponent γ of the Cole-Davidson contribution remains visible.¹⁸

The second observed quinaldine phase (2mq2) exhibits a relaxation peak, which has again the spectral shape of a structural relaxation peak rather than the shape of a secondary process. Since its low-frequency flank, however, has an exponent slightly smaller than 1 we used the normalized Havriliak-Negami susceptibility function as fit function,

$$\hat{\chi}_{HN}(\omega) = \frac{1}{[1 + (i\omega\tau)^\alpha]^\beta}. \quad (6)$$

The third phase (2mq3) shows a broad relaxation peak, which is best interpolated by the distribution of correlation times usually applied for secondary relaxations in glasses.¹⁹ Explicitly,

$$G_\beta(\ln \tau) = N_\beta(a, b) \frac{1}{b(\frac{\tau}{\tau_\beta})^a + (\frac{\tau}{\tau_\beta})^{-ab}} \quad (7)$$

with the normalization factor

$$N_\beta(a, b) = \frac{a(1+b)}{\pi} b^{\frac{b}{1+b}} \sin\left(\frac{\pi b}{1+b}\right). \quad (8)$$

The parameter a causes a symmetric broadening of the distribution while b only affects its short time flank. Therefore b can also be called “asymmetry parameter.” After Laplace transforming $G_\beta(\ln \tau)$ into frequency domain, the resulting susceptibility peak is broadened symmetrically by a , which is also the exponent of the power-law approached asymptotically by the peak’s low frequency flank. The exponent of the power-law asymptote of the high-frequency flank is given by the product ab .

For all phases, a power-law accounts additively for the dc conductivity contribution

$$\chi''_{\text{DC}}(\omega) = A\omega^{-1.2 \dots -0.8}. \quad (9)$$

C. Differential scanning calorimetry

For the DSC measurements, we used a Netzsch DSC 200. Its temperature scale was calibrated within the range of interest with the help of the first order phase transitions of six reference samples (cyclohexane, chloroform, mercury, carbon tetrachloride, water, benzene). The DSC-signal intensity was not calibrated; yet, any conclusions can be drawn in a qualitative way. Throughout the DSC studies within this work, temperature has either been kept constant (isothermal measurement) or heating/cooling rates of 20 K/min (ramp experiments) were applied. Any temperature scan shown below was compiled of a cooling stage from room temperature to 120 K, an isothermal stage lasting 10 min and a heating run back to room temperature. If additional stages were applied in order to induce phase transitions, it will be explained explicitly.

D. X-ray structure analysis

The x-ray diffraction (XRD) experiments were carried out using Cu-K α 1 radiation and a curved position sensitive detector (INEL CPS120) and a furnace (MRI) as sample environment. The sample was kept on a temperate stage in a thermally isolating vacuum. Using this setup, it was possible to gain diffractograms on short time scales in order to obtain several snapshots of the phase transition processes in the sample. In order to gain higher signal qualities for characterizing the neat crystalline phases, the data accumulation time could be increased and adapted to the experimental situation.

III. RESULTS

A. Dielectric spectra

1. Supercooled liquid (2mq1)

Typical dielectric susceptibility spectra of the supercooled quinaldine's liquid phase (2mq1, $T > T_g$) are shown in Fig. 2. In addition to a main (α -) relaxation peak, an EW is observed on the high-frequency flank of the relaxation peak. Since no secondary β -relaxation peak can be resolved, the system can be categorized as type-A glass former.¹⁵ Both spectral features shift to lower frequencies with decreasing temperature without any significant spectral changes.

In order to fit the full spectra, including the EW, the relaxation function is made up of a convolution of the generalized Kohlrausch/Cole-Davidson function (α -process, Eq. (1)) with a CD function with width parameter γ (Eq. (4)) applying the Williams-Watts ansatz (Eq. (5)); the CD function accounts for the EW, which follows a power-law behavior ($\epsilon_{\text{EW}}''(\nu) \propto \nu^{-\gamma}$). The decomposition of the spectra is indicated in Fig. 2. The high-frequency shape parameter of the α -peak is found to be temperature independent with $\beta = 0.71$, and also

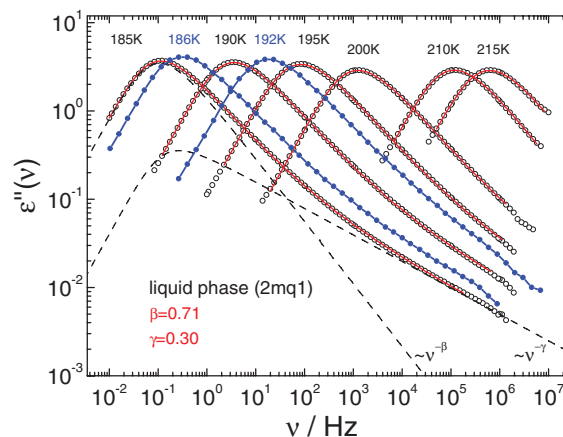


FIG. 2. Dielectric spectra of supercooled liquid quinaldine (2mq1, open symbols; this work, connected dots: data taken from Ref. 14). Continuous lines: fits including relaxation peak and EW (Eqs. (1)–(5)). Dashed lines: decomposed fit of the spectrum at 185 K. The shape parameters β and γ have been kept fixed for all temperatures (numbers); the shape parameter α and the EW amplitude C vary weakly (inset in Fig. 3).

the exponent of the EW $\gamma = 0.30$ can be kept constant at all measured temperatures. The parameters α (low-frequency shape parameter) and C (amplitude of the EW) vary weakly with temperature (cf. inset Fig. 3). In other words, frequency-temperature superposition (FTS) holds in good approximation for the full spectra. This is verified once again with the help of the corresponding master curve shown in Fig. 3 where the normalized susceptibility is plotted versus $\omega\tau_\alpha$. No significant changes in the spectral shape of both main relaxation and EW are observed. The spectral shape is in almost perfect agreement with that reported by Capaccioli *et al.*¹⁴ as demonstrated in Fig. 2. A small discrepancy in amplitude (factor 1.1) and frequency position (factor 1.4) exists, which is barely recognized on logarithmic scale and probably due to a tiny mismatch in temperature calibration.

The extracted relaxation times τ_α (cf. Eq. (3)) are shown in Fig. 4(a) (squares). Their non-Arrhenius temperature

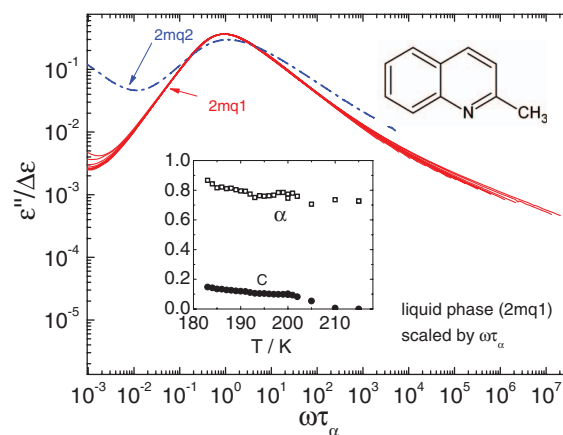


FIG. 3. Susceptibility spectra (182 K–215 K) of supercooled liquid quinaldine normalized by the relaxation strength $\Delta\epsilon$ and plotted versus $\omega\tau_\alpha$ (continuous lines). For comparison: main relaxation of the second phase 2mq2 (at 215 K, dashed line). Inset: temperature dependence of the fit parameters α and C (cf. Eqs. (1), (4), and (5)).

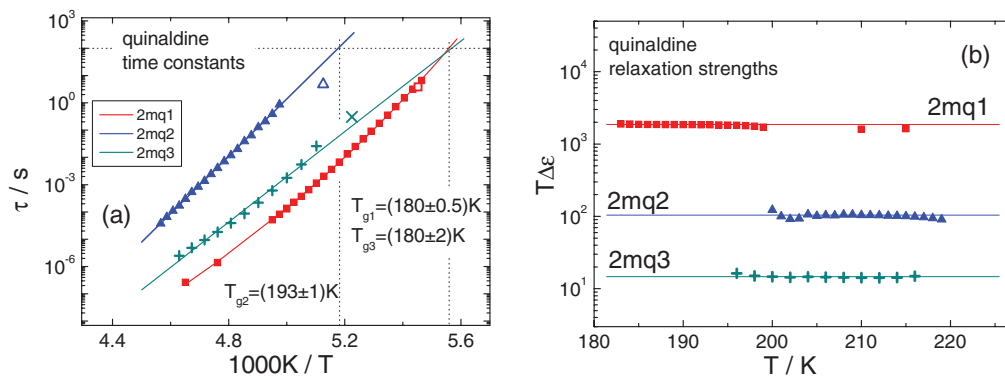


FIG. 4. (a) Time constants τ of the three dielectrically active phases of quinaldine; τ of 2mq1 (liquid, squares) are interpolated by a VFT law (Eq. (10)); τ of 2mq2 (triangles) and 2mq3 (crosses) are fitted by Arrhenius laws. The corresponding values of T_g (defined by $\tau(T_g) = 100$ s) are indicated. Larger open symbols: time constants as obtained by DSC. (b) Testing the Curie law: product $T\Delta\epsilon$ versus temperature for each phase.

dependence being typical of supercooled liquids, indicating cooperative molecular dynamics, can be interpolated by a Vogel-Fulcher-Tammann (VFT) law, explicitly

$$\tau = \tau_0 \exp\left(\frac{B}{T - T_0}\right). \quad (10)$$

We define the glass transition temperature as $T_g = T(\tau_\alpha = 100$ s), which is determined as $T_{g1} = 180$ K (cf. Fig. 4(a)). In order to compare the effective dipole moments μ_{eff} participating in the relaxation processes of the different quinaldine phases, we analyze the relaxation strengths (see also Eq. (2)) via the Curie law

$$\Delta\epsilon = \frac{N\mu_{\text{eff}}^2}{3k_B T} \quad (11)$$

with N being the number density of dipoles. In Fig. 4(b), the product $T\Delta\epsilon$ for phase 2mq1 is plotted versus temperature and compared to that of the other phases (cf. below). In agreement with Eq. (11), a constant value is obtained all over the analyzed temperature range.

2. Second phase (2mq2)

When the supercooled liquid of quinaldine is kept at temperatures above, say, 200 K, the dielectric spectra become time dependent, cf. Fig. 5. Here the sample was kept at $T = 210$ K. The time interval between two shown data sweeps was about 35 min. With advancing time, the amplitude of the α -relaxation of the liquid decreases monotonically, while the dc-conductivity contribution at low frequencies is lowered similarly. At intermediate frequencies a second, weaker relaxation peak is revealed. Its amplitude increases monotonically with time (arrows in Fig. 5(a)). Finally, the dielectric response becomes again temperature independent, and the transformation was completed after 6 h. Since the amplitude of the relaxation peak in the dielectric susceptibility is proportional to the density of rotationally mobile dipoles (cf. Eq. (11)), the strong decrease of the signal in the frequency range of the main relaxation of the liquid indicates the disappearance of the liquid phase. We conclude that the sample is performing a phase transition to another phase (2mq2) with different rotational degrees of freedom, which results in a new relaxation peak at lower frequencies.

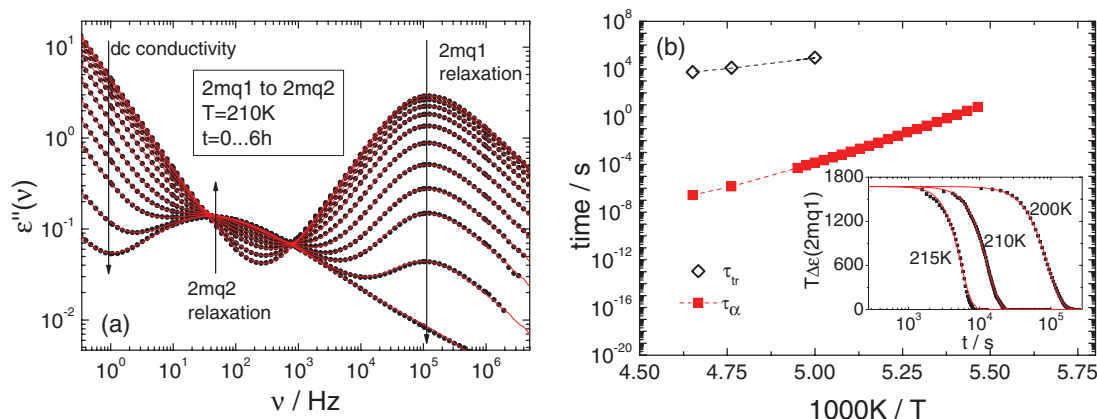


FIG. 5. (a) Monitoring dielectric spectra (symbols) at $T = 210$ K over 6 h demonstrating the phase transition from the liquid (2mq1) to a second phase (2mq2); arrows: progress of time. Lines: fits made up of the sum of the contributions of 2mq1 relaxation (Eqs. (1), (4) and (5)), of 2mq2 relaxation (Eq. (6)) and of conductivity contribution (Eq. (9)). (b) Transition times τ_{tr} (open diamonds) compared to the structural relaxation times τ_α of 2mq1 (full squares). Inset: decrease of the property $T\Delta\epsilon(t)$ of the liquid phase 2mq1 during transition to phase 2mq2 versus time at different temperatures (squares). Lines: fits according to the Avrami law (Eq. (12)).

In Fig. 5(a), the overall susceptibility curves at different times are compared and interpolated by the sum of three spectral contributions: the 2mq1 relaxation described by Eqs. (1), (4), and (5), the 2mq2 relaxation (Havriliak-Negami, Eq. (6)), and the conductivity contribution given by Eq. (9). During fitting, all time constants and spectral shape parameters were kept constant. Only the relaxation strength parameter $\Delta\epsilon$ of both phases and the conductivity parameters were adjusted. For the sake of clarity, only every sixth susceptibility scan is shown in Fig. 5(a). In order to access the phase transition kinetics, the time dependence of the relaxation strength of the liquid's spectral contribution shall be quantified. In the inset of Fig. 5(b) the obtained decay curves $T\Delta\epsilon(t)$ are interpolated with the Avrami law

$$T\Delta\epsilon(t) = T\Delta\epsilon(t=0) \exp \left[- \left(\frac{t}{\tau_{tr}} \right)^n \right], \quad (12)$$

which is often used to describe crystallization kinetics.²⁰ Any induction period is neglected since the preparation time of each experiment is short compared to the transformation process, which itself set in already during the first frequency scans. Here $T\Delta\epsilon(t)$ is assumed to be proportional to the fraction of untransformed liquid. The resulting exponents n show some variation: $n(200 \text{ K}) = 2.2$, $n(210 \text{ K}) = 2.6$ and $n(215 \text{ K}) = 2.9$. Dantuluri *et al.*²¹ have found values of the same range for the crystallization kinetics of supercooled celecoxib. In Fig. 5(b), the obtained transformation times τ_{tr} (open diamonds) are compared to the structural relaxation times τ_α (full squares) of the liquid phase 2mq1 (cf. Fig. 4(a)). Obviously, τ_{tr} shows a temperature dependence different from that of the structural relaxation, following the relation $\tau_{tr} \propto \tau_\alpha^{0.44}$. According to Ref. 22, the Avrami transition time τ_{tr} is connected with the linear crystallization velocity u via

$$u \propto \tau_{tr}^{-\frac{n}{n-1}} \propto (\tau_\alpha^{0.44})^{-\frac{n}{n-1}} = \tau_\alpha^{-0.72}, \quad (13)$$

assuming a time and cluster-size independent rate of thermal nucleation at constant temperature. The last equality was obtained after inserting the average exponent of the three Avrami interpolations $\langle n \rangle = 2.57$ (see text above). Since a decoupling of the diffusion coefficient D from viscosity η , explicitly

$$D \propto \eta^{-\xi} \propto \tau_\alpha^{-\xi} \text{ with } \xi \leq 1, \quad (14)$$

is well established,²³ diffusion controlled crystal growth is expected to lead to $u \propto D \propto \tau_\alpha^{-\xi}$. This has been confirmed by Sun *et al.*² for the crystallization of different (supercooled) liquids ($\xi = 0.7\text{--}0.8$). As we find a similar exponent, we assume that the phase transition from 2mq1 to 2mq2 is controlled by diffusion, too.

The dielectric spectra of the phase 2mq2 at different temperatures can be monitored as demonstrated in Fig. 6. In order to account for the low-frequency exponent of the relaxation peak, which is smaller than one, interpolations have been done by applying the Havriliak-Negami function (Eq. (6)). The dc conductivity contribution has been included in the fitting procedure by adding a power law according to Eq. (9). At low temperatures, the susceptibility deviates from the Havriliak-Negami shape due to an emerging high-frequency contribution reminding of an EW. Since this feature is not resolved well in the whole temperature range,

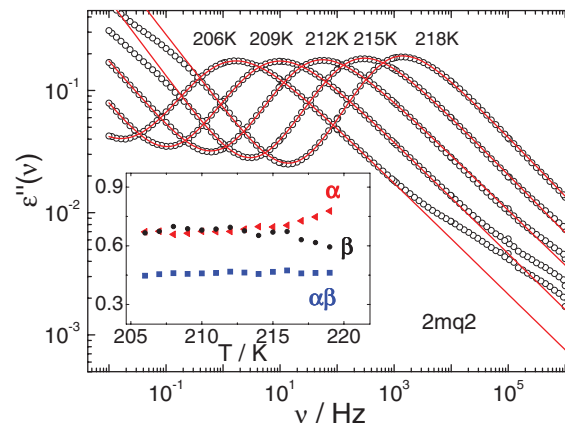


FIG. 6. Dielectric susceptibility spectra of the second phase of quinaldine 2mq2 at indicated temperatures; interpolation (solid lines) by Havriliak-Negami function (Eq. (6)) including a dc-conductivity contribution (Eq. (9)). Inset: temperature dependence of the corresponding shape parameters α (triangles; exponent of the low frequency peak flank) and β (dots). The product $\alpha\beta$ (squares) represents the high-frequency flank's exponent.

it has been excluded from the fits. At higher temperatures, the conductivity contribution deviates from a simple power-law behavior. Here the fitting range was limited to frequencies one decade below the minimum position. As shown in Fig. 6, a small increase of the low-frequency exponent β of the relaxation peak is observed. This is reflected once again by the increase of α (low frequency exponent) with a constant product $\alpha\beta$ (high-frequency exponent, cf. inset of Fig. 6). The resulting time constants τ_{HN} are included in Fig. 4(a). In contrast to the supercooled liquid, τ_{HN} of 2mq2 seems to show an Arrhenius temperature behavior yielding an activation energy $E_a/k_B = 24\,100 \text{ K}$. Considering the exponential prefactor $\tau_0 = 7.10 \times 10^{-53} \text{ s}$ of the Arrhenius fit, which is not a physically reasonable value for a single particle attempt time, we expect the $\tau(T)$ curve to flatten at higher temperatures. Since the permittivity curves are presented on logarithmic scale, it shall be pointed out that the second phase's relaxation strength is strikingly smaller than the one of the liquid. In Fig. 4(b) the product $T\Delta\epsilon$ is plotted in order to be compared with the findings for the liquid (2mq1). We find again a temperature independent value with $T\Delta\epsilon(2mq2) \approx 0.06 T\Delta\epsilon(2mq1)$.

3. Third phase (2mq3)

Similar to the above described transformation of the supercooled liquid, the dielectric spectra of 2mq2 become time dependent at high temperatures, say, $T = 210 \text{ K--} 230 \text{ K}$. The phase transformation evolves on a slower time scale compared to that from phase 2mq1 to 2mq2, therefore, slightly higher temperatures are considered. The transformation leading to the third phase (2mq3) at $T = 218 \text{ K}$ is displayed in Fig. 7. The time interval between two shown spectra is now about 158 min. The complete transformation took 130 h. In contrast to the transformation shown in Fig. 5, the appearing relaxation peak of phase 2mq3 is situated at slightly higher frequencies, compared to the diminishing peak of phase 2mq2.

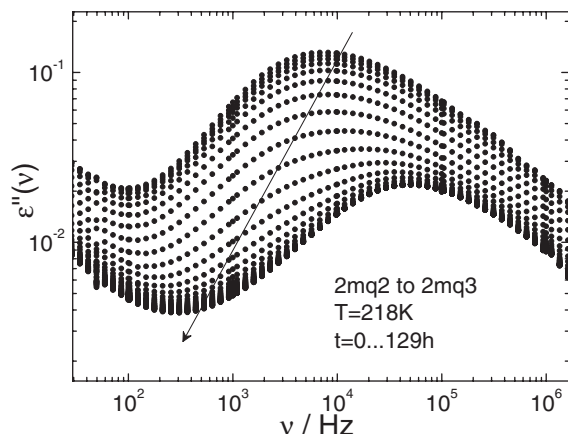


FIG. 7. Time evolution of the dielectric spectra documenting the phase transition from phase 2mq2 to 2mq3 at $T = 218$ K; (arrow) progress of time.

The spectra of phase 2mq3 at different temperatures are shown in Fig. 8. Here the best interpolations of the quite broad peaks can be obtained with the help of a distribution of correlation times $G_\beta(\ln \tau)$ (Eq. (7); constant $b = 0.36$), typically applied to interpolate a secondary relaxation process in molecular glasses.¹⁹ The resulting time constants τ_β show approximate Arrhenius behavior with a mean activation energy of $E_a/k_B = 19\,100$ K (cf. Fig. 4(a)). For a thermally activated process governed by a distribution of activation energies, the width of the relaxation peak is expected to diminish until the peak assumes Debye shape at infinite temperature, since here the temperature dependent $G_\beta(\ln \tau)$ becomes a δ -distribution. The time constant then approaches the attempt time τ_0 of the Arrhenius law. As shown in the inset of Fig. 8, the reciprocal width parameter $1/a$ does not vanish at infinite but rather at a finite temperature. This may be explained¹⁵ by writing the Eyring expression for each correlation time of the distribution

$$\tau = \tau_0 \exp\left(-\frac{\Delta S_a}{k_B}\right) \exp\left(\frac{E_a}{k_B T}\right) \quad (15)$$

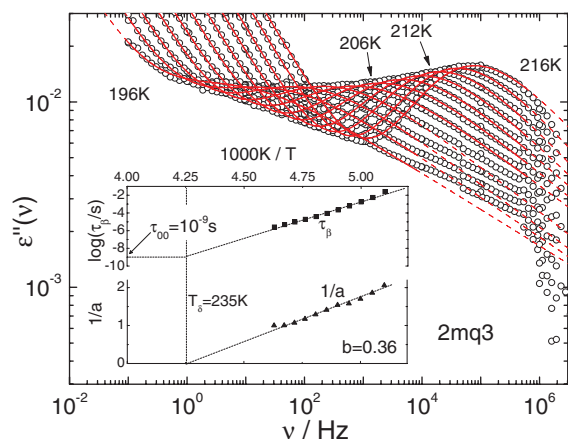


FIG. 8. Relaxation peaks of the third quinaldine phase 2mq3 at temperatures as indicated (2K-increment, open symbols). Dashed lines: Interpolations with a distribution of correlation times $G_\beta(\ln \tau)$ (Eqs. (7) and (8)) and a dc conductivity contribution (Eq. (9)). Inset: Temperature dependence of the time constant τ_β (squares) and the width parameter $1/a$ (triangles). The asymmetry parameter could be kept fixed to $b = 0.36$.

with E_a being the activation enthalpy and ΔS_a the activation entropy. Introducing now the so-called Meyer-Neldel rule,²⁴ which assumes a linear relationship between entropy and enthalpy, explicitly

$$\Delta S_a = \frac{E_a}{T_\delta}, \quad (16)$$

leads to the expression

$$\tau = \tau_0 \exp\left[\frac{E_a}{k_B} \left(\frac{1}{T} - \frac{1}{T_\delta}\right)\right], \quad (17)$$

which explains the limit $\tau_\beta(T) = \tau_0$ to be reached at $T = T_\delta$. The width of the relaxation peak, and thus the property $1/a$, follows the temperature dependence¹⁹

$$\frac{1}{a} \propto \frac{1}{T} - \frac{1}{T_\delta} \quad (18)$$

and consequently vanishes when T_δ is reached. We find for 2mq3 $T_\delta = 235$ K, being actually quite a low value, and $\tau_\beta(T = T_\delta) = \tau_0 = 10^{-9}$ s, which is at least somewhat closer to a physically reasonable value for a single molecule attempt time (cf. inset of Fig. 8).

B. Differential scanning calorimetry

The transitions observed by dielectric spectroscopy were investigated further with DSC. DSC heating scans applying a heating rate $Q = 20$ K/min of the supercooled quinaldine (2mq1) in the temperature range from 120 K to room temperature revealed an endothermal step with an onset at 183 K (“glass step,” see Fig. 9, topmost line). Additionally, an exothermal peak was observed at 235 K followed by an endothermal peak at 255 K. Finally, at 266 K the endothermal melting peak is found in accordance with the literature ($T_m \approx 264$ –270 K). Tentatively, we attribute the two peaks observed in the DSC scan below the regular melting point to phase transitions to the phases 2mq2 and 2mq3, respectively.

The relaxation times probed by DSC can be compared with those from dielectric spectroscopy after calculating the

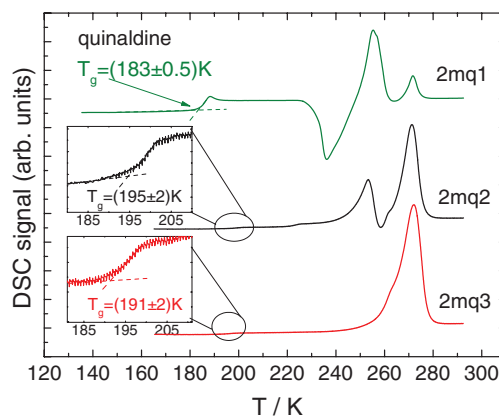


FIG. 9. DSC scans of the quinaldine phases 2mq1 (topmost line), 2mq2 (central line), and 2mq3 (lowermost line)—see text. Straight dotted lines: Guides for the eye, indicating the onsets of the endothermal steps.

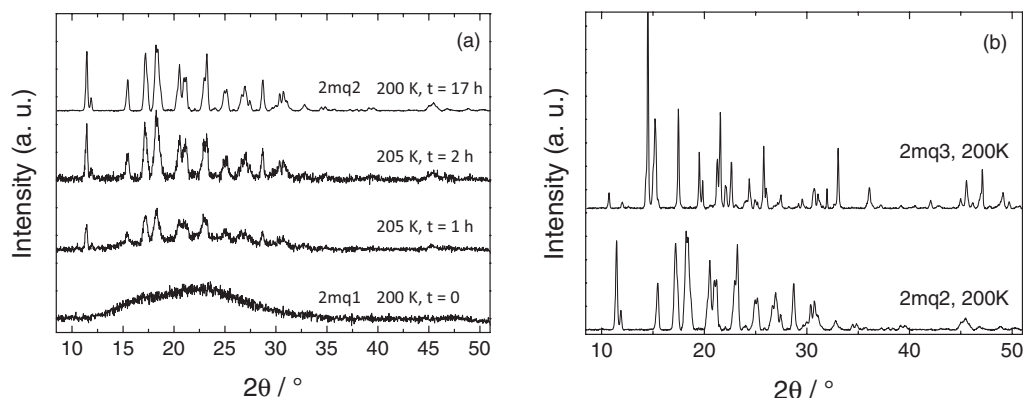


FIG. 10. (a) XRD data of quinaldine monitored during the phase transition from 2mq1 to 2mq2 (evolution times and recording temperatures as indicated). (b) Comparison of the long-time diffractograms (15 h accumulation time) of both crystalline quinaldine phases 2mq2 and 2mq3 after presumably complete transformation.

calorimetric time constant via^{25,26}

$$\tau_{\text{cal}} = \frac{k_B T_g^2}{\Delta H_{\text{eff}} Q}. \quad (19)$$

ΔH_{eff} denotes the activation enthalpy taken from the dielectric data at the calorimetric T_g . Thus,

$$\Delta H_{\text{eff}} = k_B \left. \frac{\partial \ln \tau}{\partial \frac{1}{T}} \right|_{\frac{1}{T_g}} = \frac{k_B B}{\left(1 - \frac{T_0}{T_g}\right)^2} \quad (20)$$

holds in the case of a VFT temperature dependence (Eq. (10)), and $\Delta H_{\text{eff}} = E_a = \text{const.}$ for the case of an Arrhenius temperature dependence. The extracted DSC time constants for all three phases (see below) are plotted in Fig. 4(a) as open symbols and show fair accordance with the dielectric time constants.

In order to further clarify the nature of the phase transition, in the next step the heating scan starting below T_g is interrupted at, e.g., $T = 218$ K. Now the phase transition from 2mq1 to 2mq2 starts and will be completed in less than 30 min. Afterwards, a cooling to 120 K, 10 min of waiting, and reheating to room temperature results in the central trace in Fig. 9. As expected, the exothermal peak is missing now, only a very weak step in the same temperature region remains. The endothermal peaks at higher T are found at the same positions as in the former measurement. This proves that the central curve in Fig. 9 results from probing the 2mq2 phase of quinaldine. At $T = 195$ K, a weak step is found in the DSC signal (cf. inset) which we interpret, similar to the glass transition of the liquid, as an indication of a “freezing” of motional degrees of freedom within phase 2mq2. Calculating the corresponding calorimetric time constant according to Eq. (19) leads to the result included in Fig. 4(a).

The experiment can be repeated with 2mq2 by introducing an additional isothermal stage at, for instance, $T = 255$ K. After subsequent cooling, waiting, and heating again to room temperature, the lowermost line in Fig. 9 is obtained. The missing of the first endothermal peak is proof of the second phase transition from QN2 to QN3 to have already proceeded during the isothermal stage. We now find a weak DSC-step at

$T = 191$ K (cf. inset), which is situated about 4 K below the step in 2mq2 and in accordance with the dielectric findings (cf. Fig. 4(a)).

C. X-ray diffraction

XRD experiments provide a straightforward way to identify the observed quinaldine phases. The experiment is started with cooling the liquid below $T_g = 180$ K. Afterwards, the sample temperature was increased in 5 K steps. After each increment, XRD data were accumulated isothermally for ca. 15–20 minutes. In Fig. 10(a), the amorphous “halo” of the supercooled liquid (2mq1) is shown (“ $t = 0$ ”). After increasing the temperature up to 205 K, the sample was kept for 1 h while several diffractograms were recorded. The last one is shown in Fig. 10(a) (“ $t = 1$ h”). As can clearly be seen, Bragg reflexes from some crystalline phase, most probably 2mq2, have emerged on top of the diffractogram of the liquid. After 2 h, the amorphous contribution has decreased further (“ $t = 2$ h”). Since this last signal did not seem to evolve anymore even after further temperature increments up to 215 K, the sample was cooled again to 200 K in order to conserve the present phase of the sample. Here another diffractogram was accumulated for 15 h (Fig. 10(a), “ $t = 17$ h”). There is no recognizable change but an improved S/N ratio due to longer accumulation time.

Subsequently, the same strategy as described above was repeated with the present crystalline sample at higher temperatures. At 220 K–225 K, the signal becomes time dependent again: new peaks appear and old peaks start to shrink or even vanish, respectively. This is interpreted as the phase transition from 2mq2 to 2mq3. After keeping the sample at 225 K for ca. 6 h and at 230 K for another hour, no more change in the signal could be observed. The sample was then cooled again to 200 K, where another diffractogram was accumulated for 15 h. Figure 10(b) shows the comparison of the measurements with long accumulation times of both, significantly different, crystalline phases of quinaldine.

Due to the isolation vacuum in the chamber where the sample is situated during the measurement, it was not pos-

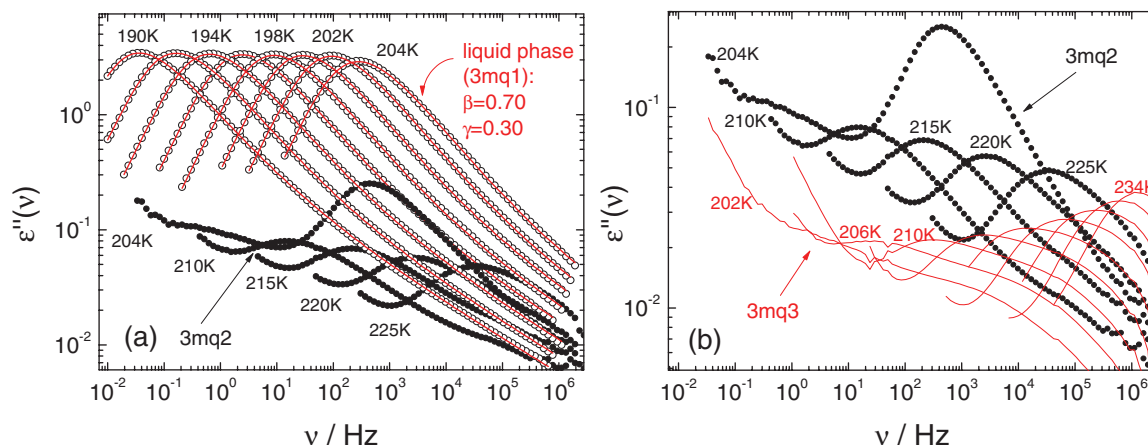


FIG. 11. Susceptibility data of the three phases of 3-methyl quinoline, namely, 3mq1 (liquid, open symbols in (a)), 3mq2 (full symbols in (a) and (b)), and 3mq3 (lines in (b)) as indicated. Temperature was incremented in 2 K-steps (3mq1), 5 K-steps additionally to $T = 204$ K (3mq2), and 4 K-steps (3mq3). Lines on top of open symbols in (a): fits including relaxation peak and EW of 3mq1 (Eqs. (1)–(5), $\beta = 0.7$, $\gamma = 0.3$).

sible to watch the melting process, i.e., the phase transition from 2mq3 to 2mq1. Instead, the 2mq3 signal disappears in the range of 240–250 K until the sublimation of the sample is terminated.

D. 3-methyl quinoline

At this point, it shall be mentioned that the findings presented above for quinaldine (2-methyl quinoline) are not at all unique for the quinoline family. Quite similar phenomena are observed for 3-methyl quinoline (molecule cf. Fig. 12(b)), and a corresponding analysis of their dielectric spectra shall be presented briefly here. Figure 11 shows a compilation of dielectric susceptibility data of three phases found for 3-methyl quinoline. The liquid phase (3mq1, open symbols) can be supercooled like 2mq1 and its susceptibility data is again interpolated by the same response function (thin lines on top of the open symbols) given by Eqs. (1)–(5). Here, the shape parameters $\beta = 0.70$ and $\gamma = 0.30$ were kept fixed and α and C showed only small changes with temperature. All in all, the dielectric spectra of the supercooled liquid are very similar to

those of quinaldine, i.e., FTS holds and indications of an EW are observed.

The supercooled phase 3mq1 performs a phase transition to phase 3mq2 (Fig. 11, full symbols) when the sample is kept at temperatures higher than, say, 200 K. The full-symbol curve for $T = 204$ K shows the relaxation peaks of both 3mq1 and 3mq2 with reduced amplitudes since the phase transition is presumably not completed. At higher temperatures only the 3mq2 relaxation remains visible and can be interpolated by the Havriliak-Negami model function (Eq. (6)) with $\alpha = 0.73$ and $\beta = 0.49$ kept constrained. After a temperature excursion to $T > 240$ K, a third phase, 3mq3, appears (Fig. 11(b), lines). The susceptibility of phase 3mq3 consists of two broad peaks, which merge with increasing temperature and cannot be decomposed easily. In order to determine some time constant and relaxation strength, the fitting range was limited to the larger low-frequency relaxation peak. Interpolations were obtained by applying the $G_\beta(\ln \tau)$ distribution (cf. Eqs. (7) and (8)) with an additional conductivity contribution (Eq. (9)). The asymmetry parameter was fixed to $b = 0.36$.

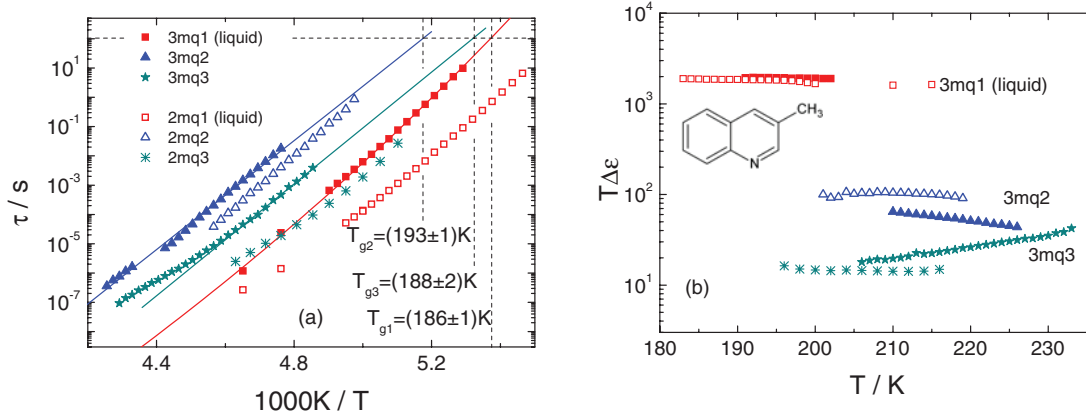


FIG. 12. Comparison of the dynamics in phases 3mq1 (full squares), 3mq2 (full triangles), and 3mq3 (full stars); and 2mq1 (open squares), 2mq2 (open triangles), and 2mq3 (asterisks), respectively. (a) Time constants with Arrhenius fits (3mq2, 3mq3) and VFT fit (3mq1). T_g as indicated by dashed lines. (b) Testing the Curie law: product $T\Delta\epsilon$ versus temperature for each phase.

Figure 12(a) summarizes the time constants found for all 3-methyl quinoline phases. The structural relaxation time of the liquid (3mq1) was fitted by a VFT law yielding a $T_g = 186$ K, which is 6 K higher than for the liquid 2-methyl quinoline phase. The τ of 3mq2 ($E_a/k_B = 21\,400$ K) and 3mq3 ($E_a/k_B = 22\,000$ K), respectively, were fitted by an Arrhenius law. Again they are shifted to somewhat higher temperatures compared to those of 2-methyl quinoline. In Fig. 12(b), the products $T\Delta\epsilon$ for all phases are plotted versus temperature. Both liquids, 2mq1 and 3mq1, yield the same constant value. This is not surprising since both molecules are almost identical (Figs. 3 and 12(b)) and, thus, have almost the same molecular dipole moment. The relaxation strengths for 3mq2 and 3mq3 are, within a factor of two, the same as for 2mq2 and 2mq3. The continuous increase of the relaxation strength of 3mq3 can be explained with the merging of two susceptibility peaks of comparable amplitude.

IV. DISCUSSION/CONCLUSIONS

Deeply supercooled liquid quinaldine transforms via an intermediate metastable crystalline polymorph (2mq2) into a structurally distinct and, presumably, thermodynamically stable phase (2mq3). The time scale of the phase transition can be controlled by choosing temperature properly. In addition to the liquid, the two crystalline phases are dielectrically active, i.e., molecular dynamics is present in all phases, the nature of which, however, is not easily identified. As the molecule is rigid and of low symmetry, motion always involves reorientation of the entire molecule and one expects cooperative dynamics for each crystalline phase. Very similar phase behavior is observed for the isomer 3-methyl quinoline.

The dynamics in phase 2mq2 exhibits Arrhenius temperature dependence with an exponential pre-factor, which is beyond any physically reasonable value for a single particle motion. In other words, at higher temperatures, due to the fast transformation into phase 2mq3, actually not accessible experimentally, the $\tau(T)$ curve is expected to bend over, exhibiting some decreasing apparent activation energy. Thus, one can speculate whether phase 2mq2 in analogy to the case of ethanol is a plastic crystal in which still cooperative dynamics occurs. However, inspecting the significantly lower apparent dipole moment with respect to that of the liquid (cf. Fig. 4(b)), the geometry of the motion has to be significantly reduced, i.e., the degree of spatial hindrance is highly increased. This conclusion holds, provided that the corresponding Kirkwood factors included in μ_{eff} , reflecting static correlations among the dipoles, are not significantly different. As the molecule is sterically flat, one expects a reorientation around an axis perpendicular to the molecular plane. Yet, a full rotation around this axis is not possible as this cannot explain the strong reduction of the effective dipole moment.²⁷ In contrast, in the case of ethanol being a non-rigid molecule, the glassy crystal exhibits isotropic reorientational dynamics. Its dielectric spectra are virtually indistinguishable in shape and amplitude; only the time constant slows down in the glassy crystalline with respect to the liquid phase. Although the spectral shape in phase 2mq2 is distinct from that in the supercooled liquid (cf. Fig. 3), it changes only weakly with temperature (cf.

Fig. 6), a behavior typical of cooperative dynamics. In addition, one may speculate that a similar high-frequency wing is found in the dielectric spectra of phase 2mq2 like in phase 2mq1 (cf. Fig. 6). In conclusion, we argue that phase 2mq2 is a glassy crystal with an in-plane cooperative dynamics.

The molecular motion in phase 2mq3 exhibits even smaller relaxation strength and for a given temperature its motion is faster than in the case of 2mq2. The spectra exhibit features, which are well known from secondary relaxation processes in molecular glasses. In this case, the spectral width increases with lowering temperature and the time constant follows an approximate Arrhenius behavior. This behavior is usually explained by assuming a distribution of activation energies. Although in phase 2mq3, indeed, the spectra broaden linearly with the reciprocal temperature, however, no proper Arrhenius behavior is observed. The motion in phase 2mq3 is still expected to show some extent of cooperativity, but the spatial hindrance of the dynamics has to be rather large since the relaxation strength is significantly smaller than that in phase 2mq2. A particularity of phase 2mq3 is the transformation enthalpy from phase 2mq2 to 2mq3 appearing to be positive (cf. Fig. 9), i.e., an endothermic phase transition is involved. Here we note that the DSC results are difficult to be fully reproduced; they are highly dependent on the temperature/time protocol.

Clearly, XRD identifies two crystalline phases. In accordance with the dielectric and DSC experiments, we attribute the diffractogram at $T \leq 215$ K to phase 2mq2 and the one at $220 \text{ K} \leq T \leq 230 \text{ K}$ to phase 2mq3, as is shown in Fig. 10(b). The number of Bragg reflexes in phase 2mq2 is not significantly smaller than in phase 2mq3. Thus, we cannot say that the symmetry of the crystal is higher in phase 2mq2, a behavior often found in orientationally disordered crystals like ethanol, cyanoadamantane^{28,29} or caffeine.^{30,31} XRD as well as dielectric spectroscopy and DSC experiments indicate both phase transitions to be monotropic in quinaldine, since no reversal can be observed after having cooled down the corresponding new phase.

Concluding, the two crystalline phases of quinaldine show cooperative dynamics, the nature of which cannot be fully assessed, however. Currently, NMR as well as high resolution XRD studies are under way to further dwell on identifying the motional mechanism involved. Finally, we note that the family of methyl quinoline derivatives show a rich phenomenology of different dielectrically active phases and may become a playground for investigating a variety of metastable phases.

ACKNOWLEDGMENTS

The authors appreciate the financial support by Deutsche Forschungsgemeinschaft (DFG) through project RO 907/14 (SPP 1415) for this study.

¹Y. Sun, H. Xi, M. D. Ediger, and L. Yu, *J. Phys. Chem. B (Letters)* **112**, 661 (2008).

²Y. Sun, H. Xi, M. D. Ediger, R. Richert, and L. Yu, *J. Chem. Phys.* **131**, 074506 (2009).

³K. Winkel, W. Hage, Th. Loerting, S. L. Price, and E. Mayer, *J. Am. Chem. Soc.* **129**, 13863 (2007).

- ⁴M. Bauer, M. S. Elsaesser, K. Winkel, E. Mayer, and T. Loerting, *Phys. Rev. B* **77**, 220105 (2008).
- ⁵J. Leiterer, F. Emmerling, U. Panne, W. Christen, and K. Rademann, *Langmuir* **24**, 7970 (2008).
- ⁶M. Klimakow, J. Leiterer, J. Kneipp, E. Rössler, U. Panne, K. Rademann, and F. Emmerling, *Langmuir* **26**, 11233 (2010).
- ⁷M. Klimakow, K. Rademann, and F. Emmerling, *Cryst. Growth Des.* **10**, 2693 (2010).
- ⁸C. Tschirwitz, S. Benkhof, T. Blochowicz, and E. Rössler, *J. Chem. Phys.* **117**, 6281 (2002).
- ⁹S. Benkhof, A. Kudlik, T. Blochowicz, and E. Rössler, *J. Phys.: Condens. Matter* **10**, 8155 (1998).
- ¹⁰O. Haida, H. Suga, and S. Seki, *J. Chem. Thermodyn.* **9**, 1133 (1979).
- ¹¹S. F. Swallen and M. D. Ediger, *Soft Matter* **7**, 10339 (2011).
- ¹²T. Wu and L. Yu, *J. Phys. Chem. B* **110**, 15694 (2006).
- ¹³L. Carpentier, R. Decressain, S. Deprez, and M. Descamps, *J. Phys. Chem. B* **110**, 457 (2006).
- ¹⁴S. Capaccioli, M. S. Thayyil, and K. L. Ngai, *J. Phys. Chem. B* **112**, 16035 (2008).
- ¹⁵A. Kudlik, S. Benkhof, T. Blochowicz, C. Tschirwitz, and E. Rössler, *J. Mol. Struct.* **479**, 201 (1999).
- ¹⁶R. Kahlau, D. Kruk, T. Blochowicz, V. N. Novikov, and E. A. Rössler, *J. Phys.: Condens. Matter* **22**, 365101 (2010).
- ¹⁷G. Williams and D. C. Watts, *Trans. Faraday Soc.* **67**, 1971 (1971).
- ¹⁸C. Gainaru, R. Kahlau, E. A. Rössler, and R. Böhmer, *J. Chem. Phys.* **131**, 184510 (2009).
- ¹⁹T. Blochowicz, C. Tschirwitz, S. Benkhof, and E. A. Rössler, *J. Chem. Phys.* **118**, 7544 (2003).
- ²⁰M. Avrami, *J. Chem. Phys.* **7**, 1103 (1939).
- ²¹A. K. R. Dantuluri, A. Amin, V. Puri, and A. K. Bansal, *Mol. Pharmaceutics* **8**, 814 (2011).
- ²²I. Gutzow and J. Schmelzer, *The Vitreous State* (Springer, Berlin, 1995).
- ²³D. Ehlich and H. Sillescu, *Macromolecules* **23**, 1600 (1990).
- ²⁴W. Meyer and H. Neldel, *Z. Tech. Phys.* **12**, 588 (1937).
- ²⁵T. Blochowicz, S. A. Lusceac, P. Gutfreund, S. Schramm, and B. Stühn, *J. Phys. Chem. B* **115**, 1623 (2011).
- ²⁶I. M. Hodge, *J. Non-Cryst. Solids* **169**, 211 (1994).
- ²⁷T. Blochowicz, A. Kudlik, S. Benkhof, J. Senker, and E. Rössler, *J. Chem. Phys.* **110**, 12011 (1999).
- ²⁸M. Foulon, J. P. Amoureux, J. L. Sauvajol, J. P. Cavrot, and M. Muller, *J. Phys. C: Solid State Phys.* **17**, 4213 (1984).
- ²⁹J. F. Willart, M. Descamps, and J. C. van Miltenburg, *J. Chem. Phys.* **112**, 10992 (2000).
- ³⁰M. Descamps, N. T. Correia, P. Derollez, F. Danede, and F. Capet, *J. Phys. Chem. B* **109**, 16092 (2005).
- ³¹A. A. Decroix, L. Carpentier, and M. Descamps, *Philos. Mag.* **88**, 3925 (2008).

Paper 4

Secondary Relaxations in a Series of Organic Phosphate Glasses Revealed by Dielectric Spectroscopy

R. KAHLAU, T. DÖRFLER, AND E. A. RÖSSLER,
The Journal of Chemical Physics **139**, 134504 (2013).

© 2013 AIP Publishing LLC
doi:10.1063/1.4822002

Secondary relaxations in a series of organic phosphate glasses revealed by dielectric spectroscopy

R. Kahlau, T. Dörfler, and E. A. Rössler^{a)}

Experimentalphysik II, Universität Bayreuth, 95440 Bayreuth, Germany

(Received 18 July 2013; accepted 9 September 2013; published online 3 October 2013)

Dielectric susceptibility spectra of six chemically similar organic phosphate glass formers are analyzed in order to elucidate the spectral evolution of a multitude of secondary (β) relaxation processes dominating the dielectric loss below the glass transition temperature T_g . By doing the spectral analysis we forgo any data fitting procedure and apply a model independent scaling approach instead. This approach assumes a constant distribution of activation energies $g(E)$ underlying a plurality of thermally activated processes, which determine the β -relaxation. The scaling reveals temperature independent, asymmetric distributions $g(E)$ for temperatures well below T_g . Simultaneously, the temperature dependence of the relaxation strength of the β -processes $\Delta\epsilon_\beta(T)$ is yielded, being nearly constant well in the glassy state. Already somewhat below T_g the spectral scaling fails and reveals an apparent increase of the mean activation energy, leading to a weaker temperature dependence of the mean relaxation times $\tau_\beta(T)$. In the same temperature regime $\Delta\epsilon_\beta(T)$ starts to increase drastically, i.e., the softening of the glass near T_g is reflected directly in the loss of temperature independence of $g(E)$ and $\Delta\epsilon_\beta(T)$. Comparing the different glasses made from phosphate molecules with increasing number of internal degrees of freedom we do not see systematic changes in the spectral evolution. In some cases even identical distributions $g(E)$ are found. © 2013 AIP Publishing LLC. [<http://dx.doi.org/10.1063/1.4822002>]

I. INTRODUCTION

With the technical progress of broadband methods of dielectric spectroscopy it has become possible to measure structural (α) as well as secondary (β) relaxations of glass forming systems with high accuracy and over a wide frequency range.^{1–4} Like the α -process secondary relaxations are believed to be generic features which are observed in all molecular glasses. They emerge above T_g and determine the relaxation in the glass, i.e., below the glass transition temperature T_g . According to the phenomenological appearance of their secondary relaxations glass forming liquids have been categorized by our group as either type-A or type-B systems.⁵ Type-B systems show a discernible secondary relaxation peak, while type-A systems do not. The latter only show a susceptibility contribution on the high-frequency side of the structural relaxation peak in the shape of a power-law $\sim \nu^{-\gamma}$ with a relatively low exponent around $\gamma \cong 0.2$.^{1,2,6} This susceptibility contribution is usually called excess wing (EW). In some cases both EW and a β -process, or even two β -processes can be identified.

Regarding the motional mechanism, the β -process has been investigated thoroughly by means of ²H NMR, in structural glass formers^{7–9} as well as in glassy crystals.^{10,11} It has been demonstrated that in neat systems essentially all molecules participate (cf. also Ref. 12) and perform highly hindered reorientations which can be described by a wobbling-on-a-cone model. Recent NMR studies on binary glasses, however, have demonstrated that in mixtures

of type-A and type-B glass formers, there is a remarkable fraction of molecules belonging to the type-B component but not performing the β -relaxation.¹³ Thus, the concept of islands of mobility (or rigidity), first introduced by Johari and Goldstein¹⁴ (and rejected for neat glass formers), gains new momentum for binary systems. Moreover, in such mixtures molecules of the type-B component induce the participation of type-A component molecules in the β -process.¹⁵ This, together with earlier NMR findings in binary glasses, which have shown that molecules of both components participate independently of size and shape,¹⁶ may be taken as indications for the nature of the β -process to be to some extent of co-operative kind – like the α -process. Possibly, this applies for systems comprising rigid molecules as well as molecules with internal degrees of freedom.

The cooperative nature of the β -process, in structural glasses as well as glassy crystals, might be also signaled by the fact that the relaxation strength strongly increases above T_g , i.e., the β -process probes the “softening” of the glass above T_g .^{10,11,17} This fact cannot easily be explained by a simple internal degree of freedom which would have to change its nature above T_g . It has been shown by ²H NMR that indeed the angular displacement of the molecular C–²H bonds becomes significantly larger above T_g , thus leading to “motionally averaged” spectra in the case of a comparatively fast β -process.^{10,11,13,18}

In the present study we focus on a group of six organic phosphates with ester groups being of alkyl and branched alkyl type (cf. Table I), which all show a well resolved β -process. The alkyl rests are increasingly longer, or “more complex,” which allows to search for a correspondence between the chemical structure and the manifestation of the

^{a)} Author to whom correspondence should be addressed. Electronic mail: ernst.roessler@uni-bayreuth.de.

secondary process. Organic phosphate glass formers are also well suited to be investigated by ^{31}P NMR.^{15,19} Due to their high molecular dipole moment these systems show a strong dielectric response, too. The spectral analysis will focus on scaling the data in an appropriate way to allow for extracting the distribution of activation energies $g(E)$ as well as the relaxation strength underlying the dynamics of the β -processes in a rather model independent way, i.e., without applying any particular fitting procedure. We will demonstrate that a strong increase of the relaxation strengths of all β -processes above T_g is observed, which again signals the “non-local” character of secondary processes in glasses. In addition, comparing the different glasses containing ester groups with increasing number of internal degrees of freedom, we do not see systematic changes in the spectral evolution, i.e., in the distribution $g(E)$; in some cases even identical distributions $g(E)$ are found.

II. EXPERIMENTAL DETAILS

Triethyl phosphate (TEP),¹⁹ tripropyl phosphate (TPP),^{15,19} tributyl phosphate (TBP), *tris*(2-butoxyethyl) phosphate (T2BOEP), and *tris*(2-ethylhexyl) phosphate (T2EHP) were purchased from Sigma-Aldrich and used without further treatment (cf. Table I). Data of trimethyl phosphate (TMP) is taken from Ref. 20. For the dielectric measurements performed within this work an Alpha-A analyzer by Novocontrol was used in combination with a sample cell design described in Ref. 21. Absolute temperature was assumed to be accurate within ± 1 K and was kept constant within ± 0.2 K by using a Quatro-H temperature controller by Novocontrol in combination with an Oxford cryostat, cooled with liquid Nitrogen. Dielectric measurements on TMP²⁰ were performed with a SI1260 spectral analyzer by Schlumberger with a similar temperature controlling and sample cell setup.

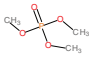
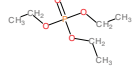
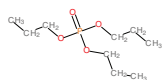
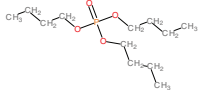
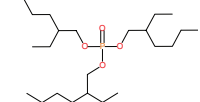
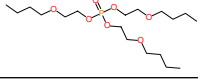
III. RESULTS

A. Measurements

The dielectric susceptibility data of TBP, TPP, T2EHP, and TEP (cf. Table I) are compiled in Fig. 1. In all four cases the α -relaxation peak is observable as the most prominent relaxation feature above T_g , while below T_g a β -relaxation is recognized. The maximum value ε''_{\max} of the α -peak is about 2 for T2EHP, while in the other cases values around 10 are found. When temperature is increased, the α -relaxation shifts to higher frequencies without essentially changing its spectral shape. At the same time a loss contribution caused by ionic conductivity (for most datasets in Fig. 1 omitted for the sake of clarity) moves into the frequency window and shows the same temperature dependence as the α -peak. At least as long as it is observable its onset is situated 1–2 frequency decades below the frequency of the α -peak in the cases TBP, TPP, and TEP. T2EHP shows an exceptionally low conductivity contribution at frequencies three decades below the α -relaxation peak frequency.

At high temperatures, when the α -relaxation reaches peak frequencies in the kHz regime, TBP, TPP, as well as TEP start to crystallize, and no more permittivity data of the supercooled liquid can be acquired. Again T2EHP is exceptional

TABLE I. Molar masses and structural formulae of the investigated glass formers.

System	M (10^{-3} kg/mol)	T_g (K)	Structure
TMP	140	137	
TEP	182	137	
TPP	224	134	
TBP	266	140	
T2EHP	435	159	
T2BOEP	398	167	

since no crystallization tendency is observed up to highest peak frequencies.

Clearly, all systems in Fig. 1 show a secondary (β -) relaxation peak on the high-frequency side of the α -peak, which survives below T_g down to lowest measured temperatures (about 80 K). Thus, all systems of Fig. 1 may be called type-B systems. Slightly above T_g , when the α -peak is situated close to the edge of the accessible frequency range, this β -peak is situated about 3–4 frequency decades above the α -peak frequency of TBP, TPP, and T2EHP; in the case of TEP both peaks are spectrally more distant.

Figure 2 shows the dielectric data of TMP and T2BOEP (cf. Table I). The temperature evolution of the α -relaxation of these systems is again similar to the others discussed above. The maximum value ε''_{\max} is about 10 for TMP and 5 for T2BOEP. TMP starts to crystallize when the α -peak is situated in the kHz regime, while T2BOEP shows no crystallization tendency. In contrast to the systems shown in Fig. 1 TMP and T2BOEP show a more complex secondary relaxation pattern. In the susceptibility data of TMP an EW is clearly observable in addition to a β -relaxation, i.e., on the high-frequency side of the α -peak (about 2 frequency decades right to the peak position) $\varepsilon''(\nu)$ follows a power law with an exponent of, as typical for the excess wing phenomenon, $-\gamma \cong -0.2$ (cf. Fig. 2(a)). At even higher frequencies this EW is followed by a β -relaxation peak similar to the one of TEP (cf. Fig. 1(d)). T2BOEP even shows two secondary relaxation peaks, which are well resolved at temperatures below T_g (cf. Fig. 2(d)), so TMP as well as T2BOEP, and hence all measured systems, may be called type-B systems. It shall be mentioned that all presented systems may have an excess wing contribution which is obscured by the explicitly observable β -peaks. Since this cannot be clarified without a model dependent quantitative analysis, we focus on the relaxation peaks of α - and β -relaxation. We assume further that the dielectric spectra below T_g are dominated by the contribution of the β -relaxation.

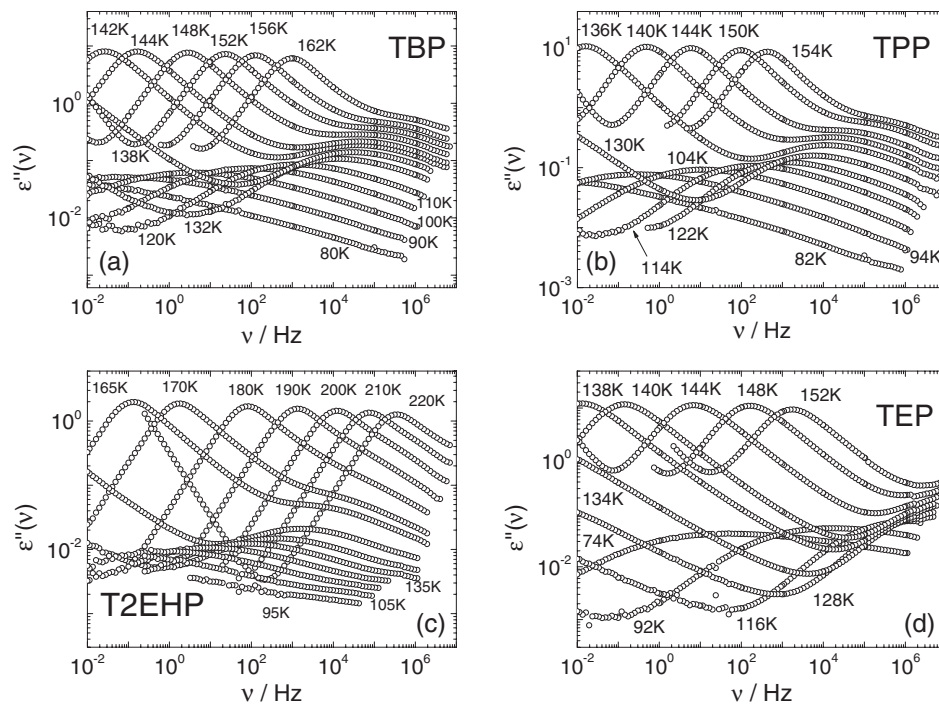


FIG. 1. Dielectric loss data of (a) TBP ($T_g = 140$ K), (b) TPP ($T_g = 134$ K), (c) T2EHP ($T_g = 159$ K), and (d) TEP ($T_g = 137$ K) at indicated temperatures. See Table I for chemical structures.

Time constants of all α - and β -relaxation peaks from Figs. 1 and 2 as given by $\tau_{max} = 1/(2\pi\nu_{max})$ are compiled in Fig. 3. Due to similar glass temperatures the α -relaxation times τ_α of TMP, TEP, TPP, and TBP almost coincide. A similar statement can be made for τ_α of T2EHP and T2BOEP, yet their T_g differs considerably in comparison with the other systems. The time constants τ_β follow Arrhenius temperature

dependences at temperatures well below T_g (straight lines in Fig. 3, cf. Sec. III B). The corresponding activation energies (given in K) vary from $E \approx 2100 - 4200$ K, while the attempt times are settled at $\nu_0 = 10^{-13} - 10^{15} \text{ s}^{-1}$ (cf. Table II). Note that a representation on T_g/T scale does not lead to a collapse of the data and does not yield further information. When T_g is approached the temperature dependence of τ_β

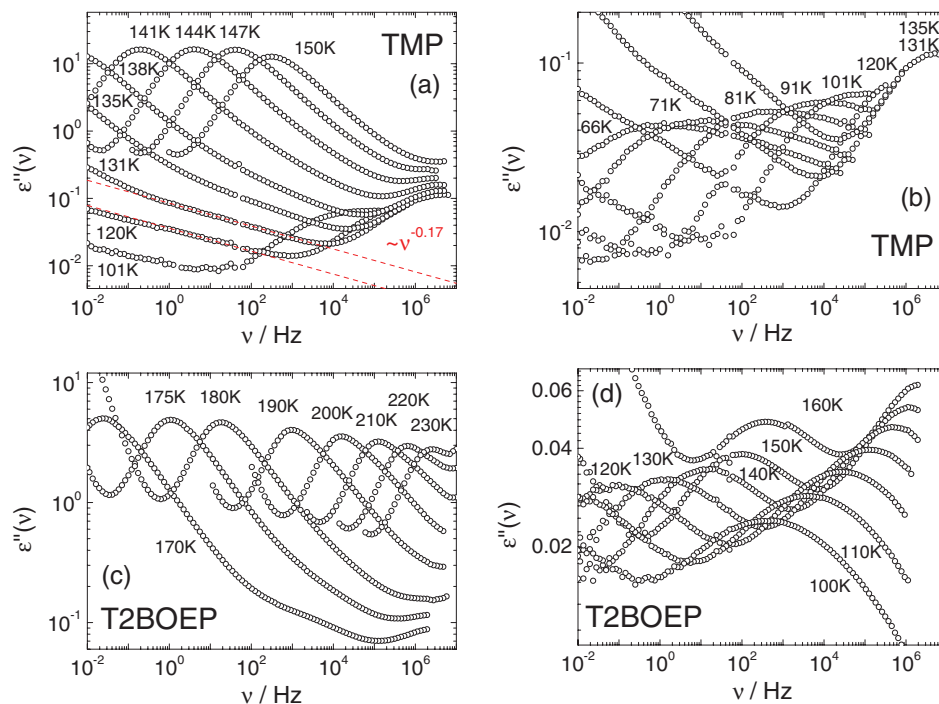


FIG. 2. Dielectric loss data of TMP ((a) and (b), $T_g = 137$ K) and T2BOEP ((c) and (d), $T_g = 167$ K) at indicated temperatures (cf. Table I for chemical structures). Dashed lines in (a) represent power laws $\sim \nu^{-\gamma}$ with $\gamma = 0.17$ attributed to the excess wing.

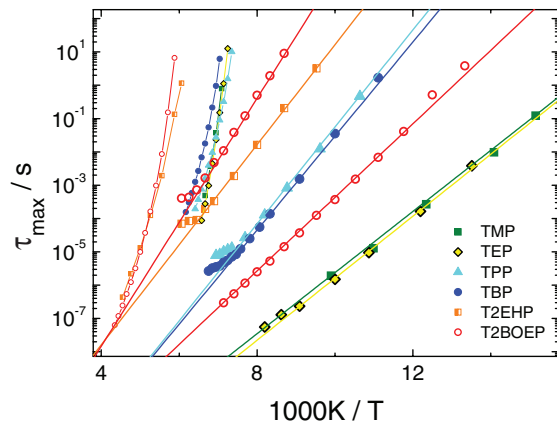


FIG. 3. Time constants of α and β -process determined from the relaxation peak positions of all investigated systems (cf. symbol map). Small symbols: α -relaxations. Here, curved lines are guides for the eye. Large symbols: β -relaxations. Here, straight lines are calculated from the distributions of activation energies $g(E)$ introduced in Sec. III B. Note the change of the $\tau_\beta(T)$ around T_g .

becomes weaker (actually a kink is observed near T_g , best recognized for TBP), which is caused by an apparent increase of the mean activation energy near T_g (see Sec. III B, cf. also Refs. 22 and 23). Interestingly, the time constants $\tau_\beta(T)$ of TMP and TEP as well as TPP and TBP coincide, which may suggest that the mean activation energy as well as the attempt time τ_0 are determined rather by intermolecular interactions than by intramolecular interactions dependent on the different (flexible^{24,25}) ester groups. As we will demonstrate in Sec. III B, the spectra of the β -process can be scaled according to the assumption that it is governed by a broad distribution of activation energies, i.e., the β -relaxation is governed by a multitude of thermally activated processes well below T_g .

B. Scaling analysis of the β -process spectra

In this section a scaling procedure for thermally activated processes will be applied to the β -relaxations found in the investigated systems.^{26–28} If a temperature independent distribution of activation energies $g(E)$ forms the basis of a relaxation process, i.e., for a given “site” in the glass with activation energy E (given in K) a simple Arrhenius law

TABLE II. Scaling parameters (maximum activation energy E_m and attempt frequency ν_0) and fit parameters (E_m , c , and b according to Eqs. (5) and (6)) of the investigated β -relaxations.

System	T_g (K)	Scaling		$g_\beta(E)$ fits		
		E_m (K)	ν_0 (s ⁻¹)	E_m (K)	c	b
TMP	137	2113	10^{14}	2074	0.00411	0.5067
TEP	137	2143	2×10^{14}	2127	0.0043	0.45646
TPP	134	3350	10^{15}	3333	0.00417	0.5318
TBP	140	3251	7×10^{14}	3250	0.00356	0.5908
T2EHP	159	3458	10^{13}	3472	0.00277	0.49246
T2BOEP 1	167	2541	4×10^{13}	2526	0.00176	1.32432
T2BOEP 2	167	4284	3×10^{14}	4267	0.0015	1.05335

$\tau = \tau_0 \exp(\frac{E}{T})$ holds, the corresponding distribution of correlation times can be calculated via

$$G(\ln \tau) d(\ln \tau) = g(E) d(E), \quad (1)$$

$$G(\ln \tau) = T \cdot g(E). \quad (2)$$

The corresponding susceptibility measured by dielectric spectroscopy is then calculated to

$$\varepsilon''(\nu) = \Delta\varepsilon \int_{-\infty}^{\infty} G(\ln \tau) \frac{2\pi\nu\tau}{1 + (2\pi\nu\tau)^2} d(\ln \tau) \cong T \Delta\varepsilon \frac{\pi}{2} \cdot g(E). \quad (3)$$

Here, the approximation in the last part of the equation can be made in the case of a broad distribution $G(\ln \tau)$ (leading to a broad $g(E)$), which is usually observed for β -processes in molecular glass formers.⁵ After substituting the variable E with the Arrhenius expression $\tau = \tau_0 \exp(\frac{E}{T})$, the distribution of activation energies can be expressed like²⁸

$$g(E) = g(T \ln(\nu_0/\nu)) = \frac{2}{\pi} \frac{\varepsilon''(\nu)}{T \Delta\varepsilon}. \quad (4)$$

In other words, plotting the right hand side expression of Eq. (4) versus $T \ln(\nu_0/\nu)$ reveals a master curve which yields the distribution of activation energies $g(E)$. Here, the attempt frequency ν_0 is assumed to be constant for all E . Since the dependence of $g(E)$ on ν_0 is logarithmic, any dependence of ν_0 on E as, e.g., assumed for a kind of Meyer-Neldel relation,^{5,29} can be neglected in the scaling procedure. In the following this scaling is applied to the dielectric loss spectra of all β -peaks of the investigated systems in order to clarify if indeed a temperature independent distribution of activation energies is present.

Figure 4 displays the susceptibility of TBP after the scaling along Eq. (4). Instead of dividing the susceptibility $\varepsilon''(\nu)$ by T and $\Delta\varepsilon_\beta$, the latter of which would have had to be determined in advance independently, the data was normalized only by T as a first step. Afterwards, the $\varepsilon''(\nu)/T$ curves were plotted vs. $T \ln(\nu_0/\nu)$, and remaining systematic deviations in

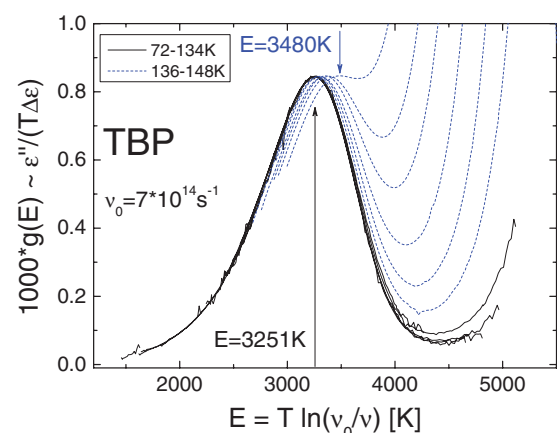


FIG. 4. Susceptibility data of TBP (72-134 K; $T_g = 140$ K) scaled according to Eq. (4) (black lines); susceptibility data for $T = 136-148$ K (dashed lines). Arrows indicate maximum positions, the corresponding values are given. Attempt frequency ν_0 indicated.

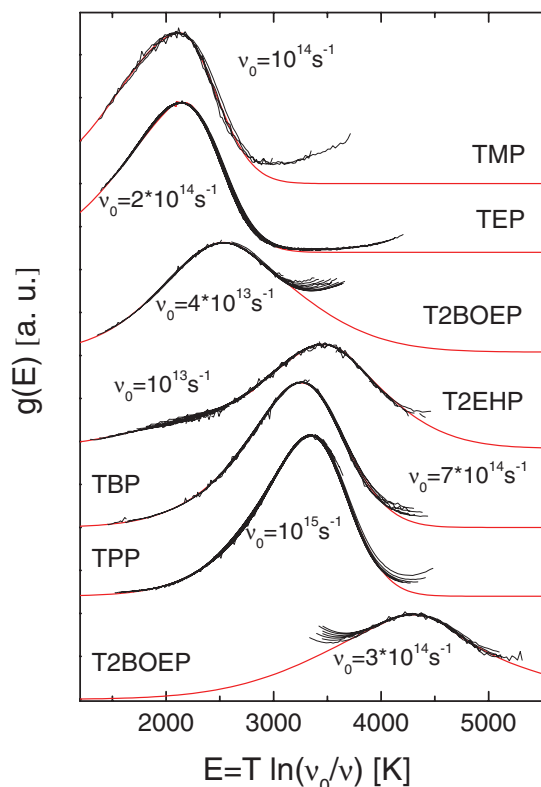


FIG. 5. Distribution of activation energies $g(E)$ for the indicated systems. Red lines: interpolations serving as guides for the eye. Note that T2BOEP exhibits two secondary relaxations.

height were corrected by dividing the curves by their maximum values. The latter are proportional to $\Delta\varepsilon_\beta(T)$ and will be discussed below. Actually, this allows to determine the relative temperature evolution of $\Delta\varepsilon_\beta(T)$ not assuming any particular spectral shape of the β -relaxation. As a third step, the master curve was normalized by its area. As can be inferred from Fig. 4, a very good collapse of the data for $T = 72$ – 134 K is observed for an attempt frequency $\nu_0 = 7 \times 10^{14} \text{ s}^{-1}$. The scaling works very well for the spectra below T_g for all investigated systems, even in the cases of T2BOEP, for which two β -processes are identified. All master curves are compared in Fig. 5. In order to cross check the validity of the scaling procedure, for all β -relaxations the mean logarithmic $\tau_\beta(T)$ were calculated along the Arrhenius law using $\tau_0 = 1/(2\pi\nu_0)$ and the most probable E values taken from $g(E)$ displayed in Fig. 5. They are included in Fig. 3, and good coincidence is found for all datasets well below T_g , i.e., all straight lines interpolate the measured points.

Above 134 K, 6 K below T_g , the scaling (Fig. 4) starts to fail and the relaxation peaks shift to higher E with increasing temperature, which may correspond to a distinct increase of the mean activation energy near T_g . Alternatively, a decrease of ν_0 near T_g might also be a possible reason for the bend in $\tau_\beta(T)$ in Fig. 3 (cf. Sec. IV). The change of $g(E)$ is also observed for TPP, T2EHP, and T2BOEP, when temperature gets close to T_g .

Figure 5 compiles the distributions $g(E)$ of all investigated β -processes as obtained by applying the discussed scaling procedure. Here, only the datasets well below T_g are

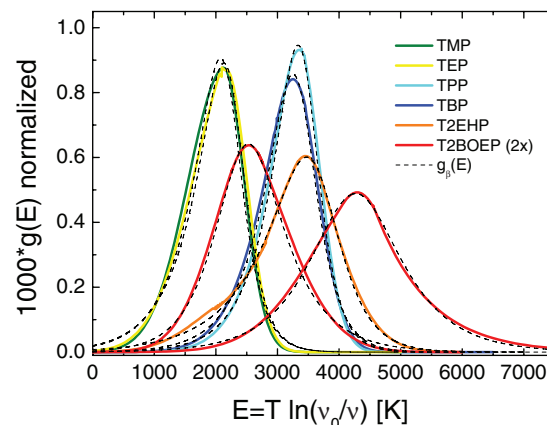


FIG. 6. $g_\beta(E)$ function (dashed lines) fitted to the experimentally obtained $g(E)$ distributions. Solid lines taken from Fig. 5; cf. symbol map). Note: the glass T2BOEP exhibits two β -processes.

shown. In all cases, clearly asymmetric distributions $g(E)$ are revealed. Most probable energies $E_m = 2100$ – 4200 K are found, while ν_0 varies from 10^{13} s^{-1} to 10^{15} s^{-1} . Again, striking coincidence in peak position and shape of $g(E)$ between TMP and TEP, as well as between TBP and TPP, respectively, is observed (cf. also Figs. 3 and 6). We note that a further plot of all $g(E)$ versus a reduced energy scale E/T_g does not yield additional information. Instead, the coincidence between TMP/TEP and TPP/TBP is corrupted. The distribution $g(E)$ of T2EHP shows some excess contribution at $E \approx 2000$ K, potentially indicating another β -relaxation (cf. Figs. 5 and 6).

In the following the distributions of activation energies shall be analyzed in a more quantitative way. Since the distributions of activation energies are found to be asymmetric, the model function for $g(E)$ introduced in Ref. 30 (there also applied to interpolate secondary relaxation spectra)

$$g_\beta(E) = N_\beta(c, b) \frac{1}{b \exp[c(E - E_m)] + \exp[-cb(E - E_m)]} \quad (5)$$

with the normalization factor

$$N_\beta(c, b) = \frac{c(1+b)}{\pi} b^{\frac{b}{1+b}} \sin\left(\frac{\pi b}{1+b}\right) \quad (6)$$

is adequate and shall be fitted to the normalized $g(E)$ of Fig. 5. Note that a susceptibility function such as Havriliak-Negami is not suitable for describing a relaxation process determined by thermally activated dynamics.^{30,31} The results are displayed in Fig. 6 and allow a direct comparison of the $g(E)$ of the systems investigated. All in all, good fits with few minor deviations are obtained. The strongest deviations are found for TMP, TEP, and, due to the excess amplitude at $E = 2000$ K, for T2EHP. Table II summarizes all parameters characterizing the β -process. Obviously the parameter c , which reflects the inverse overall width of the distributions, is lowest for both relaxation processes of T2BOEP and the process of T2EHP. The parameter b is a measure for the asymmetry of the distribution. Values around $b = 0.5$ are found for TMP, TEP, TPP, TBP, and T2EHP, reflecting the high energy slope being steeper than the low energy slope. The relaxation of T2BOEP

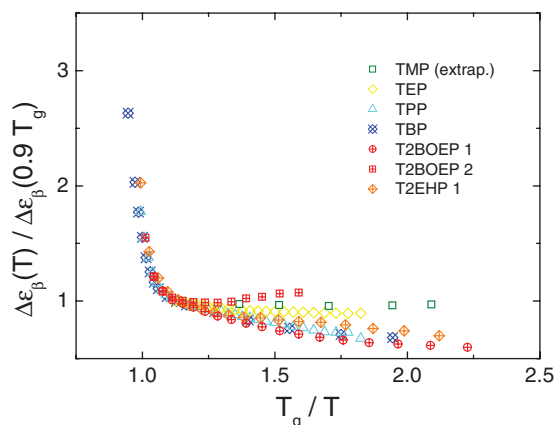


FIG. 7. Relaxation strengths $\Delta\epsilon_\beta(T)$ of the investigated β -relaxations (cf. Table I) normalized with $\Delta\epsilon_\beta(0.9 T_g)$ and plotted versus the reduced temperature scale T_g/T . As the TMP values are nearly constant, $\Delta\epsilon_\beta(T)$ was extrapolated linearly to $T = 0.9 T_g$.

with $E_m = 2500$ K has a $b > 1$, which reflects a converse tilt of the peak. The other T2BOEP peak is rather symmetric and thus has a $b = 1$.

As explained above, the temperature dependence of a quantity which is proportional to the relaxation strengths $\Delta\epsilon_\beta(T)$ is obtained by producing the master curves of Fig. 5. In Fig. 7 the $\Delta\epsilon_\beta(T)$ of all β -relaxations are compiled, normalized to the respective value $\Delta\epsilon_\beta(T = 0.9 T_g)$, and plotted versus a reduced temperature scale T_g/T . Below T_g the values are either constant (TMP and TEP) or decrease slightly with decreasing temperature. The only exception is the relaxation process of T2BOEP with $E_m = 4300$ K (“T2BOEP 2”, cf. Table II), the $\Delta\epsilon_\beta(T)$ of which increases slightly with decreasing T . Strikingly, all $\Delta\epsilon_\beta(T)$ data accessible at higher temperatures increase strongly when T_g is approached. This increase sets in already 13–16 K below the conventionally defined glass transition temperature, which is given by $T_g = T(\tau_\alpha = 100 \text{ s})$. As discussed in the Introduction, we take the strong increase of $\Delta\epsilon_\beta$ above T_g as an indication for all β -processes to be coupled to the α -process, in the sense that $g(E)$ changes above T_g when the glass “softens.” According to the interpretation suggested by the ^2H NMR studies^{10,11,13,18} the increase of $\Delta\epsilon_\beta$ reflects the increasing angular displacement of the molecules involved in the β -process.

IV. SUMMARY AND DISCUSSION

Dielectric loss spectra of six phosphate glass formers with different ester groups have been analyzed. A model independent scaling procedure reveals a temperature independent distribution of activation energies $g(E)$ for all investigated β -relaxations well below T_g . We note that the scaling procedure yielding $g(E)$ has already been applied successfully to several molecular glass formers.^{15,26–28} In particular, a version of the scaling has been used to identify the low temperature dielectric and mechanical losses assumed to originate from defects leading to the tunneling systems at very low temperatures (so-called Gilroy-Phillips approach).³²

The distributions $g(E)$ of different β -relaxations vary in maximum position, width, and asymmetry and are cat-

egorized quantitatively with an adequate model distribution $g_\beta(E)$. Yet, for two pairs of systems identical distributions are found, although different ester groups are involved. Already somewhat below the glass temperature ($T \approx 0.9 T_g$) the $g(E)$ appears to change. Here, an apparent increase of the mean activation energy (at constant attempt frequency ν_0) can be inferred from the systematic shift of the scaled data peaks. This is formally in accord with a reduced temperature dependence of the time constants τ_β , a phenomenon well observed in the data and which has also been reported in, e.g., Refs. 22 and 23. The effect can alternatively be interpreted as a reduction of the attempt frequency of the Arrhenius law (at constant activation energy E), which may be explained by a softening of the potential landscape caused by the thermally induced increase of molecular mobility near T_g . One may think of broadened potential wells, leading to lower oscillation frequencies in a harmonic approximation.

This apparent change of $g(E)$ is accompanied by a drastic increase of the relaxation strengths $\Delta\epsilon_\beta(T)$, which has also been observed for many structural glasses as well as glassy crystals.¹⁷ Thus, the appearance of the change of ν_0 or mean E and the strong increase of $\Delta\epsilon_\beta(T)$ may be considered as a generic behavior of β -processes observed in molecular glasses. The idea of the surrounding glassy matrix governing the relaxing center has already been presented by Johari and Goldstein.¹⁴ Here, the authors state that intermolecular interactions make up the potential barrier landscape, no matter if the relaxing groups of molecules have internal degrees of freedom or move rigidly. The phosphate systems investigated in this work are known to have different conformational states, depending on the length of the side chains,^{24,25} which implies the presence of internal motional degrees of freedom. One could expect each (chemical) prolongation of the alkyl side chain, leading to an increase of internal degrees of freedom, to cause a change of the activation energy distribution of the β -relaxation, if the latter is significantly determined by intramolecular potentials. Instead, the $g(E)$ is sometimes affected ($E_{\max}(\text{TPP}) > E_{\max}(\text{TEP})$) and sometimes not ($E_{\max}(\text{TMP}) = E_{\max}(\text{TEP})$; $E_{\max}(\text{TPP}) = E_{\max}(\text{TBP})$). Hence, the interpretations given above concerning the temperature independent $g(E)$ and the influence of the softening glassy matrix on the relaxation process appear to be unaffected by the character of the intramolecular degrees of freedom being present. Clearly, since the relaxation strength changes above T_g , the β -process is not governed by a simple thermally activated process as it is paradigmatically found in crystalline rotor phases (e.g., solid benzene). Here, the motional mechanism is caused by the (high) symmetry of the molecule, thus the quality of the motion does not change above and below T_g .³³ We think that in the dense matrix of the glass as well as the super-cooled liquid a significant, yet hindered motion is only possible if some extent of cooperativity is present as in the case of the α -process. This is signaled by the generic change of $\Delta\epsilon_\beta(T)$ above T_g .

¹P. Lunkenheimer, U. Schneider, R. Brand, and A. Loidl, *Contemp. Phys.* **41**, 15 (2000).

²F. Kremer and A. Schönhal, *Broadband Dielectric Spectroscopy* (Springer, Berlin, 2003).

- ³T. Blochowicz, C. Gainaru, P. Medick, C. Tschirwitz, and E. A. Rössler, *J. Chem. Phys.* **124**, 134503 (2006).
- ⁴K. L. Ngai, *Relaxation and Diffusion in Complex Systems* (Springer, New York, 2011).
- ⁵A. Kudlik, S. Benkhof, T. Blochowicz, C. Tschirwitz, and E. Rössler, *J. Mol. Struct.* **479**, 201 (1999).
- ⁶C. Gainaru, R. Kahlau, E. A. Rössler, and R. Böhmer, *J. Chem. Phys.* **131**, 184510 (2009).
- ⁷M. Vogel and E. Rössler, *J. Phys. Chem. B* **104**, 4285 (2000).
- ⁸M. Vogel and E. Rössler, *J. Chem. Phys.* **114**, 5802 (2001).
- ⁹M. Vogel and E. Rössler, *J. Chem. Phys.* **115**, 10883 (2001).
- ¹⁰B. Micko, S. A. Lusceac, H. Zimmermann, and E. A. Rössler, *J. Chem. Phys.* **138**, 074503 (2013).
- ¹¹B. Micko, D. Kruk, and E. A. Rössler, *J. Chem. Phys.* **138**, 074504 (2013).
- ¹²H. Wagner and R. Richert, *J. Non-Cryst. Solids* **242**, 19 (1998).
- ¹³B. Micko, C. Tschirwitz, and E. A. Rössler, *J. Chem. Phys.* **138**, 154501 (2013).
- ¹⁴G. Johari and M. Goldstein, *J. Chem. Phys.* **53**, 2372 (1970).
- ¹⁵D. Bock, R. Kahlau, B. Micko, B. Pötzschner, G. J. Schneider, and E. A. Rössler, *J. Chem. Phys.* **139**, 064508 (2013).
- ¹⁶M. Vogel, C. Tschirwitz, G. Schneider, C. Koplin, P. Medick, and E. Rössler, *J. Non-Cryst. Solids* **307–310**, 326 (2002).
- ¹⁷C. Tschirwitz, S. Benkhof, T. Blochowicz, and E. Rössler, *J. Chem. Phys.* **117**, 6281 (2002).
- ¹⁸M. Vogel, P. Medick, and E. A. Rössler, *Annu. Rep. NMR Spectrosc.* **56**, 231 (2005).
- ¹⁹S. Adichtchev, D. Bock, C. Gainaru, R. Kahlau, B. Micko, N. Petzold, B. Pötzschner, and E. A. Rössler, *Z. Phys. Chem.* **226**, 1149 (2012).
- ²⁰S. Adichtchev, T. Blochowicz, C. Gainaru, V. N. Novikov, E. A. Rössler, and C. Tschirwitz, *J. Phys.: Condens. Matter* **15**, S835 (2003).
- ²¹H. Wagner and R. Richert, *J. Phys. Chem. B* **103**, 4071 (1999).
- ²²N. B. Olsen, *J. Non-Cryst. Solids* **235–237**, 399 (1998).
- ²³N. B. Olsen, T. Christensen, and J. C. Dyre, *Phys. Rev. E* **62**, 4435 (2000).
- ²⁴I. N. Smirnova, A. Cuisset, F. Hindle, G. Mouret, R. Bocquet, O. Pirali, and P. Roy, *J. Phys. Chem. B* **114**, 16936 (2010).
- ²⁵A. Cuisset, G. Mouret, O. Pirali, P. Roy, F. Cazier, H. Nouali, and J. De-maison, *J. Phys. Chem. B* **112**, 12516 (2008).
- ²⁶L. Wu and S. Nagel, *Phys. Rev. B* **46**, 11198 (1992).
- ²⁷J. Wiedersich, S. V. Adichtchev, and E. Rössler, *Phys. Rev. Lett.* **84**, 2718 (2000).
- ²⁸C. Gainaru, R. Böhmer, R. Kahlau, and E. Rössler, *Phys. Rev. B* **82**, 104205 (2010).
- ²⁹W. Meyer and H. Neldel, *Z. Tech. Phys.* **12**, 588 (1937).
- ³⁰T. Blochowicz, C. Tschirwitz, S. Benkhof, and E. A. Rössler, *J. Chem. Phys.* **118**, 7544 (2003).
- ³¹C. F. J. Böttcher and P. Bordewijk, *Theory of Electric Polarization* (Elsevier, Amsterdam, 1996), Vol. II.
- ³²K. S. Gilroy and W. A. Phillips, *Philos. Mag. B* **43**, 735 (1981).
- ³³E. Rössler, M. Taupitz, and H. M. Vieth, *J. Phys. Chem.* **94**, 6879 (1990).

Paper 5

On the Cooperative Nature of the β -Process in Neat and Binary Glasses: A Dielectric and Nuclear Magnetic Resonance Spectroscopy Study

D. BOCK, R. KAHLAU, B. MICKO, B. PÖTZSCHNER, G. J. SCHNEIDER, AND
E. A. RÖSSLER,
The Journal of Chemical Physics **139**, 064508 (2013).

© 2013 AIP Publishing LLC
doi:10.1063/1.4816374

On the cooperative nature of the β -process in neat and binary glasses: A dielectric and nuclear magnetic resonance spectroscopy study

D. Bock,¹ R. Kahlau,¹ B. Micko,¹ B. Pötzschner,¹ G. J. Schneider,² and E. A. Rössler¹

¹Experimentalphysik II, Universität Bayreuth, 95440 Bayreuth, Germany

²Jülich Centre for Neutron Science JCNS, Outstation at FRM2, Forschungszentrum Jülich GmbH, 85747 Garching, Germany

(Received 28 May 2013; accepted 9 July 2013; published online 14 August 2013)

By means of dielectric as well as ^2H and ^{31}P nuclear magnetic resonance spectroscopy (NMR) the component dynamics of the binary glass tripropyl phosphate (TPP)/polystyrene (PS/PS- d_3) is selectively investigated for concentrations distributed over the full range. We study the secondary (β -) relaxation below T_g , which is found in all investigated samples containing TPP, but not in neat polystyrene. The dielectric spectrum of the β -process is described by an asymmetric distribution of activation energies, essentially not changing in the entire concentration regime; its most probable value is $E/k \cong 24 T_g$. Persistence of the β -process is confirmed by ^{31}P NMR Hahn-echo and spin-lattice relaxation experiments on TPP, which identify the nature of the β -process as being highly spatially hindered as found for other (neat) glasses studied previously, or re-investigated within this work. The corresponding ^2H NMR experiments on PS- d_3 confirm the absence of a β -process in neat PS- d_3 , but reveal a clear signature of a β -process in the mixture, i.e., polystyrene monomers perform essentially the same type of secondary relaxation as the TPP molecules. Yet, there are indications that some fractions of PS- d_3 as well as TPP molecules become immobilized in the mixture in contrast to the case of neat glasses. We conclude that in a binary glass the β -process introduced by one component induces a highly similar motion in the second component, and this may be taken as an indication of its cooperative nature. © 2013 AIP Publishing LLC. [<http://dx.doi.org/10.1063/1.4816374>]

I. INTRODUCTION

Since the works of Johari and Goldstein (JG)¹ a second (or β -) relaxation peak is a well documented relaxation feature observed in many liquids at frequencies higher than those of the primary α -relaxation upon (super-) cooling.^{2–7} In some cases, for type-A glass formers⁸ (in contrast to type-B systems with a well resolved secondary process), such a β -peak is missing and only an “excess wing” appears on the high-frequency flank of the α -peak. Even two resolved secondary relaxation peaks may be found.^{9,10} Photon correlation spectroscopy (PCS) studies of type-B glass formers have identified only an excess wing, which is masked by a strong β -peak in the dielectric spectrum.^{10–12} Why PCS does not probe the β -process while it is clearly detected in dielectric and mechanical relaxation as well as in nuclear magnetic resonance (NMR) experiments remains a challenge to be understood. Thus, the situation is quite puzzling since there exists no final conclusion concerning the nature of these processes and their relevance with regard to the glass transition phenomenon.

As a β -process is also observed for molecules without internal degrees of freedom, it is assumed to be generic to the glassy state. In contrast to the α -process the β -process is often loosely called a “local” process. This classification may suggest that the extent of cooperativity of the dynamics typical of the α -process is not found for secondary relaxations. Actually, however, all correlation lengths discussed for the α -process are, if at all present, on the order of a few nanometers which still is rather local. A prominent feature which might point to a local character of the dynamics is the fact that be-

low T_g the most probable relaxation time τ_β of the β -process follows an Arrhenius temperature dependence, the peak width increases with reciprocal temperature as expected for a temperature independent distribution of activation energies, and the relaxation strength changes only weakly.^{8,13} Yet, the mean activation energies are quite high, usually in the range $E/k \cong 11\text{--}26 T_g$.^{5,7} Its generic nature is also signaled by the fact that the relaxation strength strongly increases above T_g , i.e., the β -process probes the “softening” of the glass above T_g . Important to note is that a β -process is also observed in super-cooled plastic crystals (glassy crystals) with activation energies almost not altered with respect to that of the corresponding structural glass.^{13,14}

Systematic ^2H NMR solid-echo studies on structural glass formers such as toluene, decalin, and polybutadiene^{15–18} as well as on glassy crystals like ethanol¹⁹ or cyano cyclohexane^{20,21} have been carried out in the past. Due to its high sensitivity on small-angle reorientations, the solid-echo technique yields a clear picture of the nature of the β -process in terms of its single-particle dynamics.^{22,23} Spatially highly restricted reorientation of essentially all molecules prevails in the glassy state of neat systems. As suggested by random walk simulations,^{22,24} the β -process is a multi-step process (like the α -process), so that the overall loss of correlation is not achieved before a number of elementary steps with a jump time $\tau_J \ll \tau_\beta$ are performed. The wobbling-on-a-cone model allows to reproduce the salient features of the NMR spectra as well as to quantify the extent of spatial

restriction with a full opening cone angle $\chi < 10^\circ$.^{22,23} The NMR manifestation of the β -process in plastic crystals is essentially indistinguishable from that in canonical glasses.^{19–21} Investigating the β -process in binary glass formers has shown that in a certain concentration range both components exhibit the same highly hindered (slow) wobbling of their molecular axis independent of size and shape of the molecules.¹⁷ These experimental findings may allow to speculate that the β -process displays some extent of cooperativity, too.

In the present study the binary glass tripropyl phosphate (TPP)/(deuterated) polystyrene (PS/PS- d_3 , $M_w \approx 2 \times 10^3$ g/mol) is investigated well below T_g by means of dielectric spectroscopy, ^2H and ^{31}P NMR. Nine concentrations spread over the complete range are chosen. The system is characterized by a large T_g contrast of the pure components ($\Delta T_g \cong 200$ K). Caused by the choice of this system the application of ^{31}P and ^2H NMR allows to probe selectively the dynamics of TPP and PS- d_3 , respectively. Beyond that, dielectric spectroscopy (DS) provides information on the evolution of the distribution of activation energies when changing concentration. For comparison we included unpublished ^2H NMR results on ethanol for which a β -process is well identified by DS¹⁴ (cf. also Ref. 17). As the molecular dipole moment of TPP is significantly higher than that of PS, the DS experiment of the mixture probes, in reasonable approximation, solely the TPP dynamics. For the first time we probe the characteristics of the β -process also by a ^{31}P NMR Hahn-echo sequence. As will be demonstrated, in binary glasses the type-B component causes the other component to participate in a common β -process. Yet, a fraction of both components becomes immobilized, i.e., in binary glasses – in contrast to neat systems – islands of rigidity appear, as already reported previously.²⁵ Our results clearly favor the interpretation that the β -process is a cooperative process – as is the α -process.

II. EXPERIMENTAL DETAILS AND DATA ANALYSIS

A. Systems

A polystyrene sample with the molecular mass $M_w = 2250$ g/mol (PS) and another polystyrene sample, partially deuterated at the backbone, with very similar mass $M_w = 2440$ g/mol (PS- d_3) were purchased from Polymer Standards Service (Mainz, Germany) and used without further treatment. Since the chains consist of more than 20 monomer units, we assume that any specific end group of the polymer chains will not have a considerable effect on the investigation of the segmental dynamics. For the dielectric experiments PS was used for the preparation of the mixtures, while PS- d_3 was used for the NMR measurements. Tripropyl phosphate (TPP, 99%) was bought from Sigma Aldrich and used as received, too (cf. also Ref. 26). A list of mass concentrations $c = m_{\text{TPP}}/(m_{\text{TPP}} + m_{\text{PS/PS-}d_3})$ of the mixtures measured by DS and/or NMR is given by Table I. Ethanol- d_2 (deuterated at the methylene group) was purchased from Aldrich. We do not find any indication that phase separation or crystallization occurs in the binary glasses. Among other tests, light scattering experiments show a homogeneous sample.

TABLE I. Mass concentrations of systems measured by DS and/or NMR.

c	0	0.1	0.2	0.3	0.45	0.5	0.6	0.8	0.9	0.95	1
DS	x	x	x	x	x	...	x	x	x	x	x
^2H NMR	x	x	x	x	...	x	x
^{31}P NMR	...	x	x	x	x

B. Dielectric spectroscopy

Dielectric measurements were carried out with the Alpha-A analyzer by Novocontrol while temperature was kept constant within ± 0.2 K by using the Quatro-H temperature controller by Novocontrol. The absolute accuracy is assumed to be better than ± 1 K. The sample cell has the design published by Wagner and Richert and assures a constant sample volume.²⁷ All β -relaxation peaks have an asymmetric shape and can be interpolated with the $G_\beta(\ln \tau)$ distribution introduced in Ref. 28. Actually, the time constant is the only parameter discussed in this article, which can also be obtained in good approximation via $\tau_\beta = 1/(2\pi\nu_{\text{max}})$ by determining the maximum positions ν_{max} . In order to obtain the time constants of the α -relaxation of neat PS a Kohlrausch function is used for the data interpolation. In the case of neat TPP a Cole-Davidson model is preferred. Time constants of the α -process in the mixtures, where the primary relaxation peak is significantly broadened in relation to neat TPP, were defined by the peak positions like $\tau_\alpha = 1/(2\pi\nu_{\text{max}})$. A more detailed analysis of the structural relaxation peaks of all investigated mixtures will be presented in a forthcoming publication.

C. NMR

The ^{31}P NMR experiments were carried out using a Bruker Avance III console and a Spectrospin 400 MHz cryomagnet. The field strength of 9.4 T corresponds to a Larmor frequency $\nu_L = 161.98$ MHz for ^{31}P . The length of the $\pi/2$ -pulse was 2.2 μs . A home-built (in cooperation with Bruker Biospin GmbH) double resonance probe was cooled by liquid nitrogen using an Oxford CF1200 cryostat, controlled by an Oxford ITC-503. Temperature accuracy was ± 2 K, stability was better than ± 0.2 K. The ^2H NMR experiments were carried out on a Bruker Avance DSX spectrometer and an Oxford 300 MHz cryomagnet. The field strength of 7 Tesla corresponds to a ^2H Larmor frequency of $\nu_L = 46.067$ MHz; the length of the $\pi/2$ -pulse was 2.8 μs . A home-built probe was cooled by liquid nitrogen using a CryoVac Konti cryostat and an Oxford ITC-503 temperature controller. Temperature accuracy was better than ± 1 K, stability was better than ± 0.2 K.

At temperatures below its minimum the spin-lattice relaxation time $T_1(T)$ was measured via a saturation recovery sequence. Above the T_1 minimum temperature the inversion recovery sequence was applied. In the case of ^{31}P the spin-lattice relaxation was found to be in non-exponential, as in this ^2H NMR the relaxation below T_g is non-exponential as in this case spin-diffusion can be neglected at least at short relaxation times. Therefore the mean value $\langle T_1 \rangle$ is given, which is obtained by interpolating the relaxation function by

a Kohlrausch decay (stretched exponential). This decay function is also used to interpolate the decay of the solid-echo (cf. below and Eq. (3)).

The NMR frequency depends on the angle θ between the principal interaction tensor axis and the magnetic field direction:

$$\nu_{\text{local}}(\theta) = (\pm)(3 \cos^2 \theta - 1) \cdot \delta_{\text{CSA}/Q}/2, \quad (1)$$

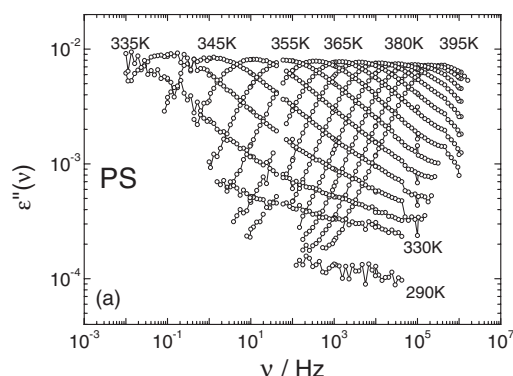
where ν_{local} is the shift of the resonance frequency with respect to the Larmor frequency ν_L . The parameter $\delta_{\text{CSA}/Q}$ (in kHz) specifies the anisotropy of the interaction tensor, which is given by the interaction of the nuclear quadrupolar moment (Q) with the electrical field gradient in the case of ^2H NMR. In the case of PS- d_3 , the orientation of the ^2H -C bonds at the chain backbone is probed. Due to the spin $I = 1$ two transitions occur and positive as well as negative signs are valid. In the case of ^{31}P NMR (spin $I = 1/2$) the rigid lattice spectrum is determined by the chemical shift anisotropy (CSA), and in Eq. (1) δ_{CSA} is used and only the negative sign is found. Both interaction tensors CSA and Q are axially symmetric in the present case. In the case of an isotropic distribution of tensor orientations (e.g., in glasses) characteristic powder spectra are observed, a (symmetric) Pake spectrum in the case of ^2H NMR whereas the CSA spectrum is asymmetric.

The solid-state spectra were collected by applying a Hahn-echo (^{31}P NMR) or a solid-echo sequence (^2H NMR) preceded by a saturation sequence of five $\pi/2$ pulses; the buildup time was chosen to be $2.5 T_1$ or 1 s at least. In the case of ^{31}P NMR ^1H decoupling was applied during the echo sequence. Appropriate 8-fold (^2H) and 16-fold (^{31}P) phase cycling was applied.²⁹ Fits to the solid-echo Pake spectra were corrected for finite pulse excitation.^{30,31} Simulations have shown that in the case of small angle reorientations as typically found for the β -process the largest effect in the solid-echo spectrum is found for the condition $\tau_{\beta} \delta_{\text{local}} \cong 1$.³²

III. RESULTS

A. Neat components—Dielectric spectra

The susceptibility spectra of PS ($T_g = 335$ K) are shown in Fig. 1(a). Above T_g a pronounced peak is visible, which



is identified as the structural or α -relaxation. The low amplitude reflects the rather non-polar nature of the PS monomer. Close to T_g , the high-frequency side of the α -peak is made up of a crossover from one power-law behavior to another one usually called excess wing. This spectral shape is typical for a type-A glass former, where no explicit secondary relaxation peak is resolvable. While temperature is increased the main relaxation peak shifts to higher frequencies. When the sample is cooled below T_g the α -peak moves out of the frequency window and the signal, now consisting only of the excess wing contribution, drops close to the resolution limit of the spectrometer. No indications for a secondary (β -) relaxation peak are observed.

The dielectric spectra of neat TPP ($T_g = 134$ K) are displayed in Fig. 1(b). As in the case of PS above T_g an α -relaxation peak can be identified, the amplitude of which exceeds the one of PS by a factor of about 1000, i.e., the TPP molecule carries a strong dipole moment. At frequencies several decades above the maximum position of the α -peak a secondary relaxation is well resolved (type-B glass former). This secondary peak survives at temperatures below T_g when the α -peak has already left the frequency window. Its spectrum broadens significantly when temperature is lowered. When temperature is increased above, say, $T = 150$ K, both peaks approach each other until above $T = 156$ K the measurement of the super-cooled liquid cannot be continued due to the crystallization of the sample.

The time constants of both α - and β -process are shown in Fig. 2. In the case of neat PS we added the results of Ediger and co-workers,³³ and for TPP we included the ^{31}P NMR results obtained by applying the stimulated echo technique as well as the data from an analysis of the spin-lattice and spin-spin relaxation.²⁶ Good agreement is found between the NMR and DS results. While the τ_{α} show the typical super-Arrhenius temperature dependence, the β -process in TPP exhibits an Arrhenius behavior. The mean activation energy is found to be $E/k = 3240$ K $= 24 T_g$.

B. Neat components— ^{31}P and ^2H NMR results

As seen in Fig. 3(a), below T_g the spin-lattice relaxation time $T_1(T)$ of PS- d_3 displays a rather weak temperature

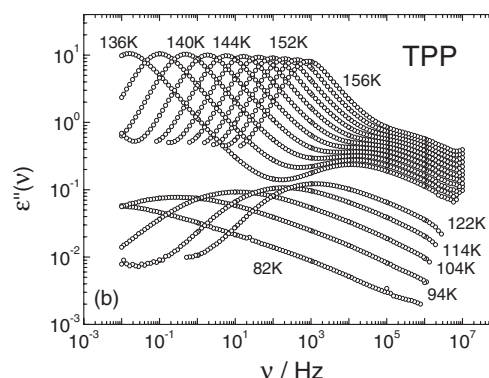


FIG. 1. (a) Dielectric spectra of neat PS; $T = 290$ K and $T = 330 - 395$ K in 5 K steps (some temperatures indicated). (b) Susceptibility spectra of neat TPP revealing a well resolved β -process (some temperatures indicated; data above T_g partially taken from Ref. 26).

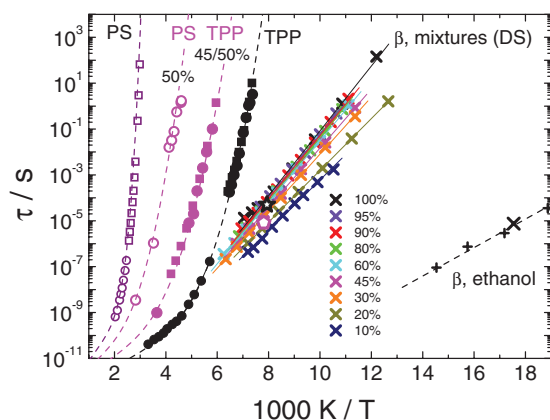


FIG. 2. Structural relaxation times τ_α in neat PS (DS: open squares, NMR: open circles³³), and neat TPP (DS: full squares, NMR: full circles²⁶) and in the mixtures $c = 45\%$ (DS probing TPP, full squares) and $c = 50\%$ (^{31}P NMR probing TPP, full circles; and ^2H NMR probing PS dynamics, open circles); time constant τ_β of the β -process in neat TPP and in the mixtures as revealed by DS (crosses, color code for the concentrations given in legend), τ_β of TPP yielded by ^{31}P Hahn-echo (open star) and of PS in the mixture by ^2H solid-echo (open pentagon). For comparison, time constants of the β -process of ethanol as given by DS (plus signs)¹⁴ and NMR (cross). Solid lines: Arrhenius-fits (see Fig. 7), dashed lines: guides for the eye.

dependence typical of an excess wing determining the relaxation in the glass as indicated by the dielectric spectra (cf. Fig. 1(a)). Approximately an exponential temperature dependence $\langle T_1 \rangle \propto e^{-T/T_0} \propto 1/J(\omega = \text{const.})$ with $T_0 = 96$ K is observed (dashed line), as also found for the spectral density $J(\omega)$ of many type-A glasses by dielectric spectroscopy.^{7,8,34,35} We note that dynamic mechanical analysis appears to show a β -process in high molecular mass polystyrene,³⁶ yet, we do not see any indication of this in our NMR as well as dielectric experiments on our sample. Despite of the low molecular dipole moments of polystyrene samples dielectric spectroscopy is principally able to detect a β -relaxation in polystyrene.³⁷ Above T_g the α -process dominates and T_1 decreases, yet a relaxation minimum is not observed as it occurs at even higher temperatures.

In the case of ^{31}P NMR on TPP, a well resolved T_1 -minimum is found and attributed to the α -process. The corresponding time constant $\tau_\alpha(T) = 1/(2\pi\nu_L)$ agrees with the results from a full T_1/T_2 analysis.²⁶ Below T_g the temperature dependence of T_1 becomes weaker, yet, it is much stronger than in the case of PS- d_3 due to the β -process controlling the relaxation. As the ^{31}P relaxation is controlled by the chemical shift anisotropy (CSA; cf. Sec. II C) the relation $1/T_1 \propto \varepsilon''(\omega_L)$ ^{26,38,39} is expected to hold and one can check this relationship by inserting the intensity of the dielectric spectra of the respective temperatures (cf. Fig. 1(b)) extrapolated to the Larmor frequency ($\nu_L = 161.98$ MHz) of the ^{31}P NMR experiment. As indicated by the dashed line in Fig. 3(a), indeed, the temperature dependence of $T_1(T)$ is well reproduced by that of ε'' . A different situation is found for the comparison of the ^2H and ^{31}P T_1 data of the mixtures (Fig. 3(b)), which will be discussed in detail in Sec. III D.

The β -process can also be accessed by analyzing the NMR spectra via the application of a two-pulse echo sequence, namely the Hahn-echo (^{31}P) or the solid-echo (^2H) sequence. The majority of former NMR studies on the β -process in molecular glasses are based on ^2H solid-echo experiments.^{15–22} There, subtle spectral changes characteristic of a highly hindered molecular reorientation have been identified by varying the inter-pulse delay t_p . In Fig. 4(a) this is first documented for the structural glass of neat ethanol- d_2 for which DS has identified a comparatively fast β -process with $E/k = 15 T_g$ (cf. also Fig. 2).¹⁴ While at low as well as high temperatures (yet below $T_g = 92$ K) rather weak spectral changes are recognized and the spectra display more or less the typical solid-state ^2H NMR powder (Pake) shape, at intermediate temperatures ($T_g - 30$ K) a strong decrease of the spectral intensity around zero frequency is observed for long delay time t_p , yet the singularities prevail. We conclude that well in the glassy state of ethanol the β -process passes through the NMR time window.

Fig. 4(b) shows the results of an analogue experiment on TPP. Due to the different spin dynamics for the $I = 1/2$ nucleus ^{31}P , in contrast to the $I = 1$ spin systems in the case

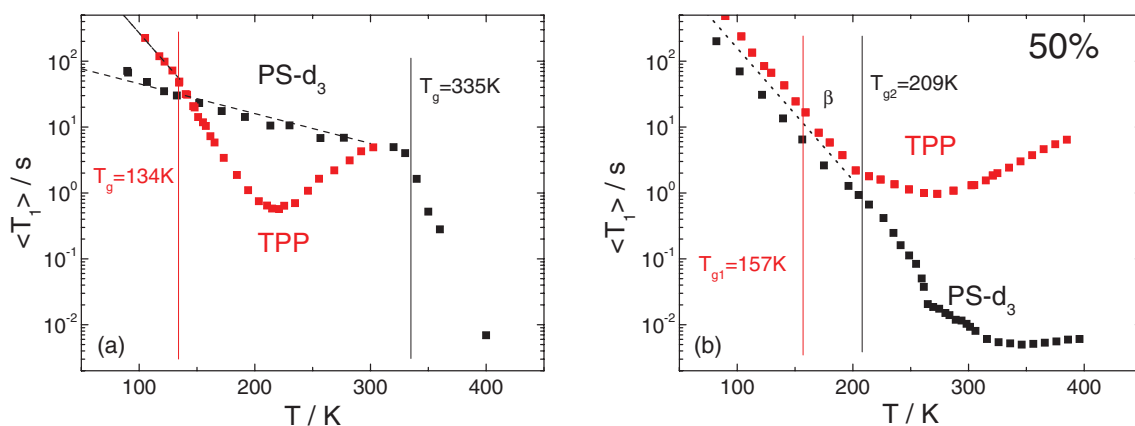


FIG. 3. (a) Spin-lattice relaxation times of neat TPP (^{31}P NMR) and neat PS- d_3 (^2H NMR). ^2H relaxation is non-exponential below T_g and therefore the mean relaxation time (T_1) is given. Glass transition temperatures T_g are indicated by vertical lines; dashed line: interpolation by an exponential relaxation law for PS- d_3 ; dashed line below T_g of TPP: estimate of T_1 of TPP from the dielectric spectral density. (b) Spin lattice relaxation times of 50% TPP/PS- d_3 (^{31}P NMR and ^2H NMR; dashed line: estimate from the dielectric spectral density; vertical solid lines indicate T_g (for a detailed assessment cf. Sec. III D).

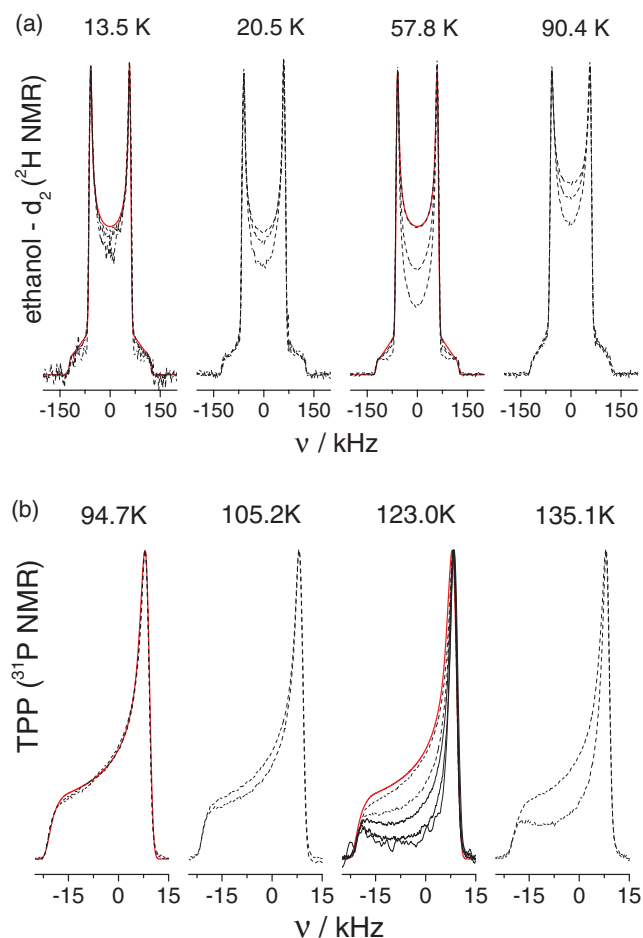


FIG. 4. (a) Solid-echo spectra of ethanol- d_2 at indicated temperatures, each set representing inter-pulse delays of 20 μ s, 100 μ s, and 200 μ s; for shortest inter-pulse delay t_p a fit with a Pake model is shown as solid line ($\delta_Q = 123$ kHz); (b) Hahn-echo spectra of neat TPP, each set with inter-pulse delays of 20 μ s and 200 μ s, at 123 K additionally 400 μ s, 800 μ s, and 1600 μ s (solid lines). A fit to the powder spectrum is included for shortest t_p as solid line ($\delta_{CSA} = 20.5$ kHz). All datasets are normalized to their maximum values.

of ^2H , a Hahn-echo sequence was applied. Like in Fig. 4(a), all spectra are normalized to their maximum values. As mentioned the relevant spin interaction in TPP is given by the CSA, which leads to an intrinsically asymmetric solid-state powder spectrum. The heteronuclear ^1H - ^{31}P coupling was removed by ^1H decoupling, and the homonuclear ^{31}P - ^{31}P coupling can be ignored safely due to the large distance between the nuclei in different molecules. Again, spectral intensity is lost mainly at the center of the spectra. In contrast to ethanol the effect is most prominent close to $T_g = 134$ K. Qualitatively, this is understood as the β -process in TPP is much slower than the one in ethanol (cf. Fig. 2). At $T = 123$ K extremely large inter-pulse delays (spectra marked by solid line) were applied. Here the intensity around $\nu = -5$ kHz almost vanishes, indicating that essentially all molecules participate in the β -process.

The spectral changes observed for neat ethanol ($T < T_g$) as well as TPP are very similar to those reported previously for pure toluene, decalin or polybutadiene or a de-

calin/chlorobenzene mixture;^{17,23} even for the glassy crystalline phases of ethanol¹⁹ or cyano cyclohexane.²⁰ The NMR spectrum loses intensity in the center of the spectrum, as said, a characteristic of a highly hindered motion. Assuming a wobbling-on-a-cone model, one finds for all examples that the angular displacement does not exceed 10° , which is therefore a rather generic feature of the β -process.^{21,22} The second Legendre polynomial, determining the NMR frequency shift in the solid state, exhibits the highest sensitivity on a small angle reorientation at $\theta = 45^\circ$ or $\nu = \delta_{CSA}/4$, respectively, because here the derivative $|\text{d}\nu_{\text{local}}/\text{d}\theta|$ is maximal. This is seen directly in the case of ^{31}P NMR. Since in ^2H NMR the contributions of both signs in Eq. (1) are combined (two NMR transitions are involved), due to reasons of symmetry the highest sensitivity is found at $\nu = 0$.

The spectral effect can be quantified by measuring the intensity at the center of the spectrum with respect to that at the singularity,¹⁸ explicitly a quantity R is defined by

$$\begin{aligned} R &= I(\nu = 0)/I(\nu = \delta_Q/2) && ^2\text{H NMR}, \\ R &= I(\nu = -\delta_{CSA}/4)/I(\nu = \delta_{CSA}/2) && ^{31}\text{P NMR}. \end{aligned} \quad (2)$$

In Fig. 5(a) the R values for long t_p (200 μ s) (solid symbols) measured in ethanol (^2H NMR) and TPP (^{31}P NMR) are displayed as a function of the reduced temperature T/T_g . As expected a minimum is observed for ethanol at which the condition $\tau_\beta \delta_Q \cong 1$ applies with δ_Q specifying the quadrupolar interaction (cf. Sec. II C).²⁰ We note that in the case of short t_p values (e.g. $t_p = 20$ μ s) no such minima are found in $R(T)$ as essentially no dephasing of the NMR frequencies (due to molecular reorientation involved in the β -process) is monitored; i.e., the spectrum has the undistorted powder shape (cf. Fig. 4). An analysis of the undisturbed low-temperature Pake spectrum (cf. Fig. 4) yields $\delta_Q = 123$ kHz for ethanol- d_2 . From this an estimate of the time constant of the β -process can be given. The resulting τ_β is included in Fig. 2 and fits well into the DS findings.

In Fig. 5(a) we also included the ^2H NMR results on the glassy crystalline phase of cyano cyclohexane.²⁰ Again a minimum is observed in $R(T)$, however, at higher reduced temperature, which correlates well with the fact that $E/k = 19 T_g$ is larger than in ethanol (15 T_g). In the case of TPP, with its much slower β -process, i.e., with higher activation energy $E/k = 24 T_g$, a minimum can only be anticipated at highest temperatures, as above T_g the α -process interferes. Still, the time constant extracted via $\tau_\beta \delta_{CSA} \cong 1$ with $\delta_{CSA} = 20.5$ kHz is compatible with those from DS (cf. Fig. 2). The results for TPP are very similar to those of toluene (cf. again Fig. 5(a)), the paradigmatic glass former without internal (DS active) degrees of freedom, the β -process of which has been systematically investigated by ^2H NMR.¹⁵⁻¹⁷ It turns out that the mean activation energy is the same as for TPP.⁵ Finally, the result for PS- d_3 is included in Fig. 5(a). Here, essentially no temperature dependence is observed in agreement with the results from DS where no β -process is resolvable. In conclusion, the NMR spectra clearly reflect the β -process in the different glasses. Depending on the value of the mean activation energy E the quantity R reveals a minimum more or less below T_g .

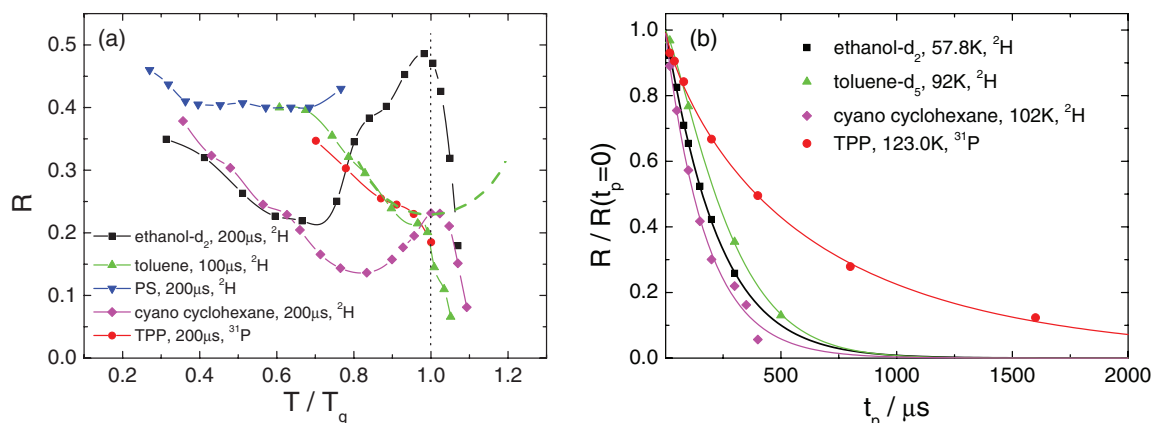


FIG. 5. (a) The parameter $R(T)$ at (high) $t_p = 200 \mu$ s quantifying the spectral changes occurring in the solid-state NMR spectra for glassy ethanol, PS and plastically crystalline cyano cyclohexane (CNC),²⁰ TPP, as well as toluene- d_5 ¹⁵ at $t_p = 100 \mu$ s. Lines are guides for the eye. For toluene (as well as TPP) a minimum above T_g , as would be expected without the influence of the α -process, is anticipated (dashed line). (b) Parameter R normalized to $R(t_p = 0)$ characterizing the spectral changes of the NMR spectra of ethanol, toluene, CNC, and TPP as a function of the inter-pulse delay t_p for temperatures as indicated; lines: Kohlrausch fits.

Figure 5(b) displays the dependence $R(t_p)$, normalized by $R(t_p = 0)$, for the temperatures of the minima found in Fig. 5(a). For ethanol, toluene¹⁵ and cyano cyclohexane²⁰ $R(t_p)$ reaches almost zero at longest time t_p , which signals that essentially all molecules participate in the β -process. Again, $R(t_p)$ completely decays to zero. In the case of TPP, $R(t_p)$ shows a very similar behavior, yet, on somewhat longer inter-pulse times which are not accessible by 2 H NMR due to its faster spin-spin relaxation. We can conclude that essentially all TPP molecules participate in the β -process of neat TPP glass.

C. Characterizing the β -process in the TPP/PS mixtures by dielectric spectroscopy

In order to gain information about the β -relaxation in the mixture, PS molecules are now added stepwise to the TPP. By producing mixtures with $c = 0\%$, 10%, 20%, 30%, 45%, 60%, 80%, 90%, 95%, 100% mass fraction of TPP (cf. Table I), the entire concentration range is covered by DS experiments (as well as by NMR, cf. below). As the dielectric signal of PS is significantly smaller than that of TPP, we can safely assume that in the mixtures only the TPP dipoles are probed by DS.

For the concentration $c = 45\%$ dielectric spectra are compiled in Fig. 6. At temperatures above $T = 160$ K a peak is observed, which shifts to higher frequencies when temperature is increased. This peak is caused by the α -relaxation of TPP in the mixture. The corresponding time constants lie between those of the two neat systems as is seen in Fig. 2. Adding PS to TPP always ends up in a slowing down of the structural relaxation of the TPP ensemble due to the anti-plasticizer effect. The α -peak is strongly broadened; especially the low-frequency power-law exponent is reduced to values much smaller than 1, which is not found in the neat systems. In Fig. 2 we included the results of 2 H and 31 P NMR obtained from analyzing stimulated echo decays, for $c = 50\%$, which probe the structural relaxations of PS and TPP, respectively. Clearly, the time constant τ_α of PS is significantly longer than that of TPP, i.e., the dynamics of the two components are de-

coupled and two T_g can be defined, T_{g1} (PS) and T_{g2} (TPP). As stated before, a detailed assessment of the structural relaxations of the TPP/PS mixtures is given in a forthcoming publication; here we focus on the β -relaxation.

Below 160 K, when the α -peak has left the low-frequency limit of the spectrometer (Fig. 6), a β -relaxation is found like in the case of neat TPP. In particular, no essential change of the time constant is observed. This rather weak concentration dependence of the β -process is reflected in the Arrhenius plot of the time constants extracted from the maximum positions of the β -relaxation (Fig. 2). As in neat TPP the time constants τ_β follow Arrhenius laws for any concentration. For all TPP concentrations higher than $c \cong 60\%$ the $\tau_\beta(T)$ curves are essentially the same, yielding a mean activation energy $E/k = 24 T_g$. At lower concentrations a slight reduction of E is observed, and the attempt frequency ν_0 is reduced, too. This is best seen in Fig. 7 where ν_0 and E are plotted as a function of concentration. Below $c = 60\%$ both E and ν_0 show a weak linear decrease. The slight extent of the concentration dependence of E is rather surprising, and one could argue that it points to the interpretation of the β -relaxation to be an intramolecular process due to some particularity of the TPP

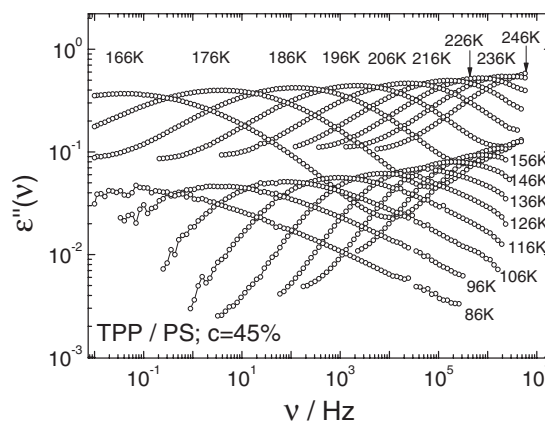


FIG. 6. Dielectric spectra of 45% TPP in PS at indicated temperatures.

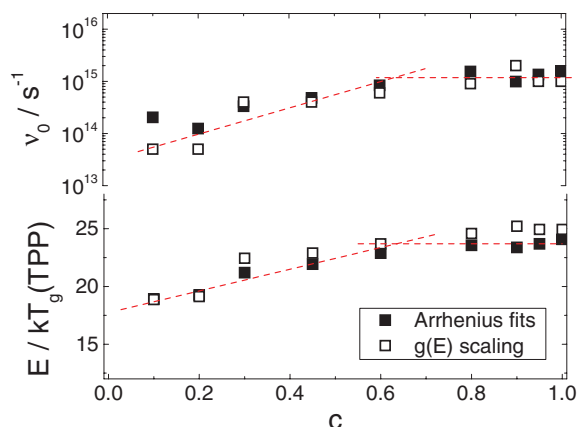


FIG. 7. Attempt rates ν_0 (upper panel) and activation energies (lower panel) for the whole concentration range of TPP. Full symbols: yielded by Arrhenius fits of $\tau_\beta(T)$ data in Fig. 2. Open symbols: yielded by $g(E)$ scaling (cf. text).

molecule. As we will demonstrate, however, this interpretation is misleading. Comparing the time constants of the β - and α -process in the mixtures one recognizes that their separation grows when PS is added (cf. Fig. 2). In other words, as the β -process essentially does not change but T_g of the mixture grows with the amount of PS, no structural relaxation of any considered mixture interferes with the analysis of the secondary relaxation carried out here.

The concentration dependence of the τ_β shown in Fig. 2 is also seen directly from the peak positions: comparing the β -peak of different mixtures, its spectral position shifts only weakly when PS molecules are added (cf. Fig. 8(a)). The only obvious change is a decrease of its amplitude. Next we consider the spectral shape of the β -peaks. As a first attempt, in Fig. 8(a) a symmetric log-Gaussian function, as usually found for β -processes,⁵ is fitted to the data set for $c = 45\%$. However, the fit is not fully successful; the spectra do not appear symmetric. The asymmetric shape becomes even more obvious in Fig. 8(b), where data of the $c = 45\%$ sample at different temperatures are scaled onto their maximum height and position.

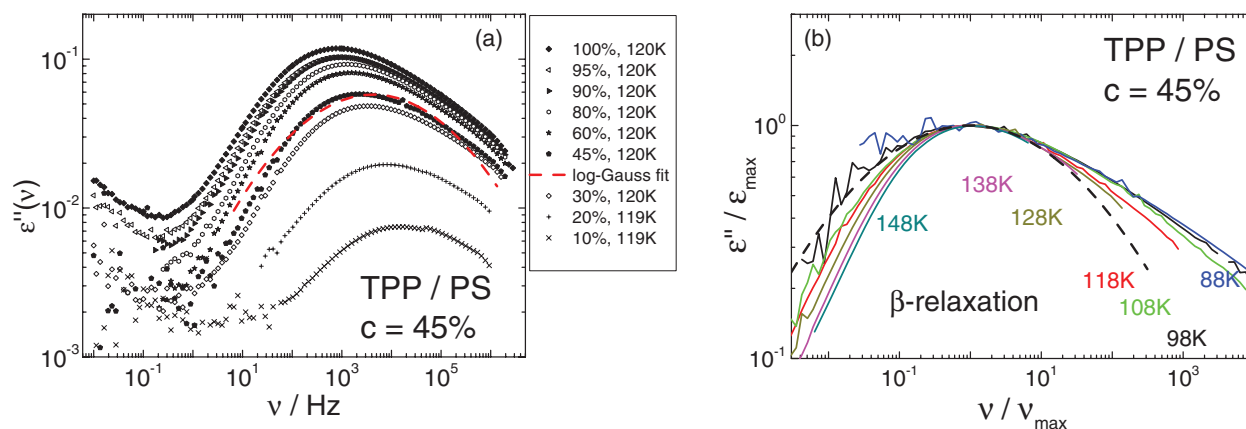


FIG. 8. (a) Susceptibility data of several mixtures of TPP in PS at similar temperature (119–120 K; mass fractions and temperatures indicated). Dashed line: Symmetric model function (log-Gauss) fit to the $c = 45\%$ data. (b) Data of the 45% sample at indicated temperatures, scaled to match maximum height and position. Dashed line: Fit from Fig. 5(a) scaled to maximum.

tion. Here, a temperature dependent broadening of the peak is observed, which is typical of a thermally activated process.

If a relaxation process is governed by a temperature independent distribution of activation energies $g(E)$ (which is actually a characteristic of a thermally activated process) the resulting distribution of correlation times $G(\ln\tau/\tau_0)$ can be calculated via the Arrhenius law $\ln\tau/\tau_0 = E/kT$, leading to $G(\ln\tau/\tau_0) = kT g(kT \ln\tau/\tau_0)$. Here, a constant attempt time τ_0 is assumed. In the case of a broad function $g(E)$, the shape of the resulting distribution $G(\ln\tau/\tau_0)$ is reproduced by the corresponding susceptibility in good approximation, $G(\ln\nu_0/\nu) \cong \chi''(\ln\nu_0/\nu)$. As a consequence, the susceptibility peak must increase with temperature, while it shifts to higher frequencies and decreases its width, exactly as it is observed experimentally in the case of most β -processes.⁷ Thus, a re-scaling of the susceptibility spectra can be applied to yield a master curve representing the distribution $g(E)$.^{35,40,41} Plotting $\varepsilon''/T\Delta\varepsilon_\beta$ as a function of $T\ln\nu_0/\nu$ is expected to yield master curves, provided that the $g(E)$ is indeed temperature independent. The only free parameter of this scaling is the attempt rate ν_0 of the relaxation, which is assumed to be constant for all spectra, i.e., temperature independent.

The results of the scaling procedure applied to the data of the TPP/PS mixtures are shown in Fig. 9. In all samples a broad but asymmetric $g(E)$ is revealed, justifying to identify the β -relaxation in all mixtures as thermally activated. This is in accord with the time constants τ_β following Arrhenius laws (Fig. 2). While $g(E)$ in Fig. 9 are very similar for all concentrations, the peak position (most probable energy barrier) is only constant for concentrations $c > 60\%$. For $c \leq 60\%$ a trend to lower activation energies becomes obvious. This corresponds to the above findings, where activation energies of the Arrhenius laws (Fig. 2) and peak positions at a fixed temperature (Fig. 8(a)) became concentration dependent below $c = 60\%$. This is once again demonstrated in Fig. 7, where activation energies and attempt rates ν_0 gained from the $g(E)$ scaling (Fig. 9) as well as from the Arrhenius fits (Fig. 2) are compared. Both analyses yield comparable results and the same concentration dependences. Summarizing, we can state that the β -relaxation of all investigated mixtures is

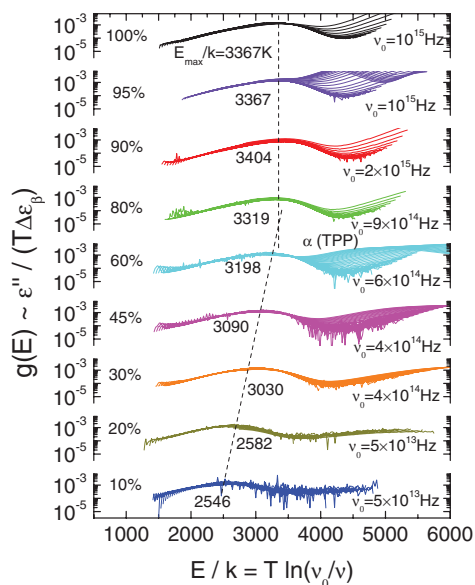


FIG. 9. Distribution of activation energies $g(E)$ obtained from scaling the susceptibility (cf. text) of the sub- T_g measurements of all investigated mixtures (concentrations, attempt rates, and most probable activation energies indicated). Dashed lines: Guides to the eye. Note: At high E/k deviations are observed due to the α -process of TPP.

governed by asymmetric but temperature independent distributions of activation energies $g(E)$. As a consequence, all time constants τ_β follow Arrhenius laws. All susceptibility data can be collapsed in order to reveal $g(E)$, making a detailed discussion of shape parameters, as obtainable by data fitting, needless in the context of this work.

D. Characterizing the β -process in the TPP/PS- d_3 mixtures by NMR experiments

As documented by the dielectric spectra, the β -process in the TPP/PS mixtures is well separated from the α -process. This is an important prerequisite for probing it by NMR, in particular, by applying a Hahn-echo (^{31}P) or a solid-echo (^2H) two-pulse sequence. The concentration selection of TPP/PS- d_3 mixtures investigated with these techniques can be inferred from Table I. Figure 10(a) shows the Hahn-echo spectra of TPP of the $c = 20\%$ mixture. A series of spectra, again normalized to their maximum values, is collected at three selected temperatures with a pulse delay $t_p = 40 \mu\text{s}$, $80 \mu\text{s}$, and $200 \mu\text{s}$. While at high as well as low temperature no spectral changes are recognized, a weak but well discernible decrease of intensity around $\nu = -\delta_{\text{CSA}}/4$ is recognized at the intermediate temperature $T = 121.0 \text{ K}$. Again, the characteristic spectral changes associated with a β -process are well identified. In the case of the $c = 50\%$ sample a similar evolution of the ^{31}P spectra is observed (cf. Fig. 10(b)), here, even longer t_p values have been applied at $T = 120.3 \text{ K}$ (solid lines) and the intensity around $\nu = -\delta_{\text{CSA}}/4$ almost vanishes at longest time t_p as in the case of neat TPP (cf. Figs. 4(b) and 5(b)).

As before for the neat components the spectral effect can be quantified by measuring the intensity close to the center of the spectrum with respect to the singularity, i.e., the quan-

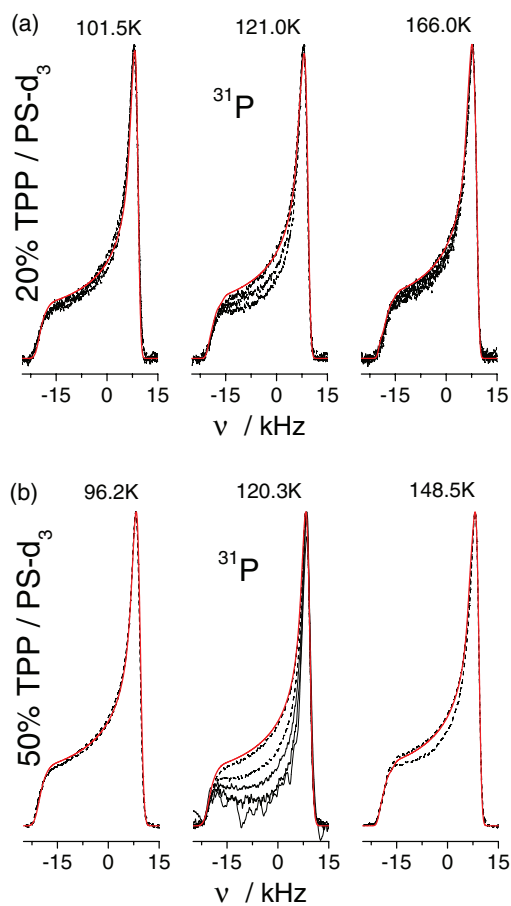


FIG. 10. ^{31}P Hahn-echo spectra of TPP/PS- d_3 glass at indicated temperatures, (a) $c = 20\%$, each set with $t_p = 40 \mu\text{s}$, $80 \mu\text{s}$, and $200 \mu\text{s}$ (b) $c = 50\%$, $20 \mu\text{s}$ and $200 \mu\text{s}$ each, at $T = 120.3 \text{ K}$ very long interpulse delays were applied additionally (solid lines, $t_p = 400 \mu\text{s}$, $800 \mu\text{s}$, and $1600 \mu\text{s}$) and the intensity at $\nu = -\delta_{\text{CSA}}/4$ almost vanishes. For shortest t_p a fit by a CSA powder spectrum is included (solid line).

tity $R(t_p)$ (cf. Eq. (2)). In Fig. 11(a) the R values for long t_p ($200 \mu\text{s}$) (solid symbols) measured for three TPP concentrations ($c = 10\%$, 20% , 50% , and for comparison 100%) are plotted versus temperature. Except for $c = 100\%$ (as discussed before) a distinct minimum, essentially not shifting, is displayed. This signals immediately that the time constant of the process does not significantly change in the mixtures, a result already known from our DS study (cf. Fig. 2). In contrast to the $c = 100\%$ sample the minimum in $R(t_p)$ is well resolved due to the larger separation of α - and β -process in the mixtures. Also the depth of the minimum is very similar, at lowest concentration $c = 10\%$ it is somewhat less deep.

The decays of $R(t_p)$ for the different TPP concentrations at very similar temperatures are displayed in Fig. 11(c) and compared to the data of neat TPP. While for the $c = 50\%$ sample the decay of $R(t_p)$ is similar to that of $c = 100\%$, the situation for $c = 20\%$ is different. The $R(t_p)$ appears not to relax completely down to zero, indicating that at low TPP concentrations only a fraction of TPP molecules participates in the β -process, i.e., some molecules have become immobilized. Yet, in all cases the decay is described by a Kohlrausch function (cf. Eq. (3), below) with $\beta = 0.95$, and the apparent

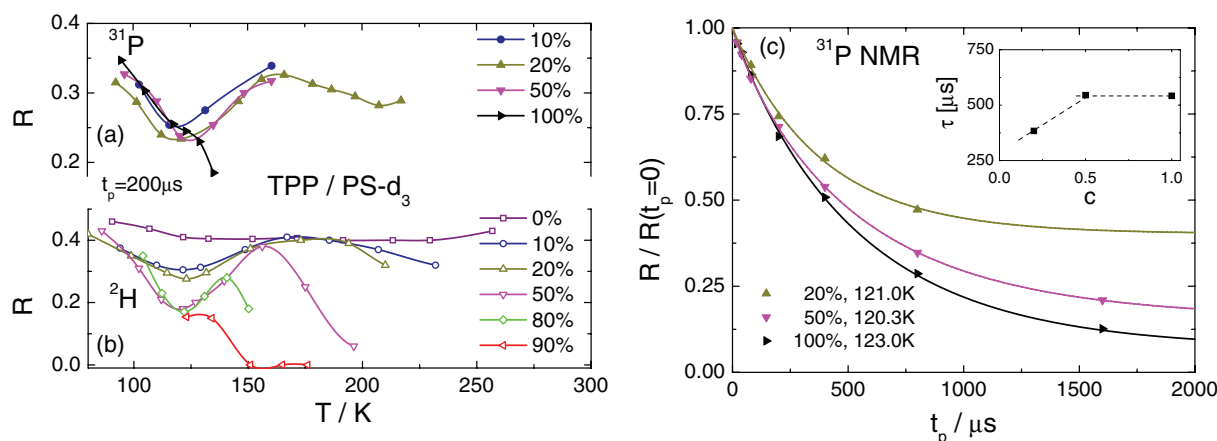


FIG. 11. Temperature dependence of line-shape parameter R at $t_p = 200 \mu\text{s}$ for (a) TPP and (b) PS- d_3 ; mass fractions as indicated. Lines serve as guides for the eye. (c) Dependence of $R(t_p)$, normalized to short t_p values, on the inter-pulse delay t_p as revealed by ^{31}P Hahn-echo; mass fractions, and temperatures as indicated; inset: time constant as a function of concentration, dashed lines: a possible interpretation.

time constant (Fig. 11(b), inset) becomes somewhat shorter as also observed in the dielectric spectra (cf. Fig. 2).

Neat PS is a type-A glass former not showing any spectrally resolved β -process in the DS spectra. This is also confirmed by ^2H spin-lattice relaxation measurements, which display only a weak temperature dependence in the glassy state as discussed before (cf. Fig. 3). Here, the question arises whether polystyrene in the mixture exhibits a β -process. Due to the selectivity of ^2H NMR probing solely the dynamics of the PS- d_3 molecules ^2H solid-echo spectra can give a clear-cut answer. Figure 12 shows a series of solid-echo spectra of TPP/PS- d_3 with $c = 50\%$ taken at different t_p values for three temperatures. A pronounced spectral change is observed at intermediate temperature $T = 121.5 \text{ K}$. Similar results are observed for the $c = 20\%$ sample, in particular, the largest spectral change is again observed at 123.0 K . Moreover, the effect is found at similar temperatures as in the case of TPP studied by ^{31}P NMR. It seems that PS in the mixture shows some secondary relaxation, too, which passes through the solid-echo time window well below T_g at similar temperatures as in the case of TPP. The corresponding $R(T)$ values (at long inter-pulse delay $t_p = 200 \mu\text{s}$) are included in Fig. 11(b). While no distinct temperature dependence is observed in neat PS- d_3 ($c = 0\%$), a minimum emerges when TPP molecules are added. Up to $c = 50\%$ the minimum depth increases monotonously. Remarkably, the minima do not shift with concentration and they are positioned roughly at the same temperature as the minima resulting from the ^{31}P Hahn-echo experiment on TPP (Fig. 11(a)). Actually, the minimum of $R(T)$ is slightly shifted to higher temperatures in the case of the ^2H spectra of PS- d_3 , which is expected due to the higher coupling constant δ_Q . Taking $\delta_Q = 122.4 \text{ kHz}$ from an analysis of the low-temperature ^2H solid-state spectra of PS- d_3 , the extracted time constant τ_β agrees well with those determined by DS as well as by ^{31}P Hahn-echo experiment (cf. Fig. 2). These findings strongly suggest that in the mixtures polystyrene monomers participate in the highly hindered re-orientation of the β -process introduced by the TPP molecules. In other words, the β -process is not solely an intramolecular process. It appears that the TPP molecules cause the monomer

units of polystyrene to wobble in a rather similar way and on the same time scale as the TPP molecules do.

In order to further investigate the t_p dependence of the ^2H solid-echo spectra, Fig. 13(a) shows the solid-echo spectra at very similar temperatures for the different investigated

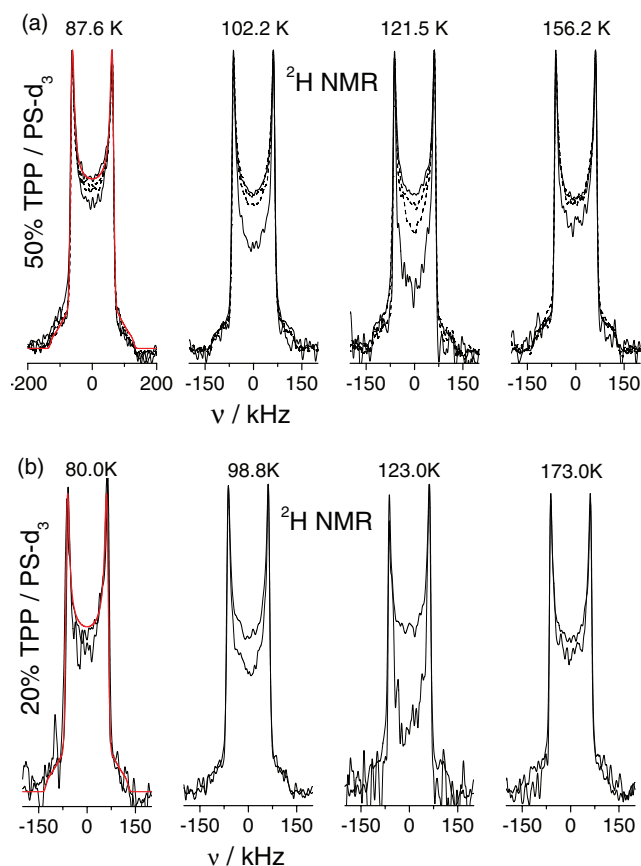


FIG. 12. ^2H NMR spectra of TPP/PS- d_3 , normalized to maxima, at indicated temperatures. (a) $c = 50\%$; each set with $t_p = 20 \mu\text{s}$, $200 \mu\text{s}$ (solid lines), $40 \mu\text{s}$ and $80 \mu\text{s}$ (dashed lines), (b) $c = 20\%$, $t_p = 20 \mu\text{s}$ and $200 \mu\text{s}$. For lowest temperatures fits with Pake spectral shape are included (solid red line, $\delta_Q = 122.4 \text{ kHz}$).

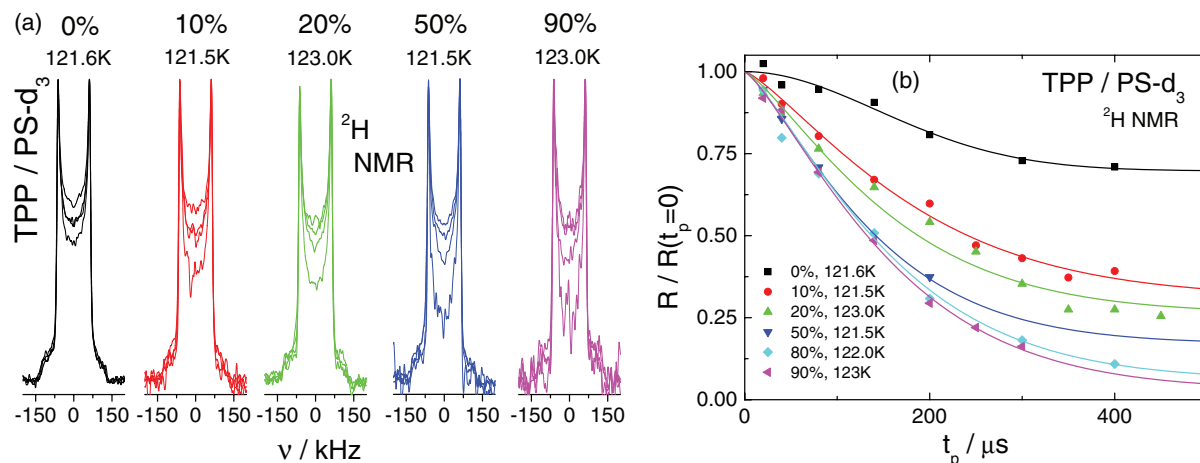


FIG. 13. (a) ^2H NMR spectra of TPP/PS- d_3 for various concentrations of TPP at indicated temperatures; each set with $t_p = 20 \mu\text{s}$, $40 \mu\text{s}$, $80 \mu\text{s}$, and $200 \mu\text{s}$. (b) R values as a function of inter-pulse delay, normalized to short t_p value. Lines are fits according to Eq. (3).

concentrations. For neat PS- d_3 one recognizes only weak spectral changes, which is actually due to some other relaxation mechanism, while the spectral changes induced by large t_p values significantly grow with increasing TPP concentration. Explicitly, at $t_p = 200 \mu\text{s}$ the spectral intensity at zero frequency is the lower, the higher c is. It seems as if the fraction of PS molecules participating in the β -process grows with the fraction of TPP molecules present in the mixture. Figure 13(b) displays the corresponding evolution of $R(t_p)$. For all concentrations $c > 0$ $R(t_p)$ decays on similar t_p time scale ($\tau = (170 \pm 20) \text{ ms}$ and $\beta = 1.28$), while for $c = 0$ (neat PS- d_3) a qualitatively different, slower decay is observed. The latter finding is in accordance with the fact that actually neat PS does not exhibit a β -process and another relaxation process may be active. For $c = 90\%$ and $c = 80\%$ $R(t_p)$ decays down to very low values at long delay times, while for $c \leq 50\%$ $R(t_p)$ appears to level off at different plateaus at longest t_p . In particular, a systematic trend of the final plateau to increase with decreasing concentration is recognized.

To access quantitatively the decay $R(t_p)$ and in particular the plateau at longest times t_p we describe the normalized decay by the following expression²⁵

$$R_n(t_p, c) = f_\beta(c) \cdot \exp\left(-\left(\frac{t_p}{\tau}\right)^\beta\right) + (1 - f_\beta(c)), \quad (3)$$

where $f_\beta(c)$ is interpreted as a fraction of molecules which contributes to the β -process, and τ and β are parameters describing the effective time evolution of the echo spectra. We note that the latter time constant is not identical with τ_β as determined from the DS spectra. In the case of TPP, a free fit by Eq. (3) to $R(t_p)$ (cf. Fig. 11) provides similar relaxation times τ (and similar $\beta = 0.95 \pm 0.05$) with a small trend to become somewhat shorter at low $c = 20\%$. Since a correlation between τ and τ_β is expectable, this is in accordance with the DS result where a weak trend to shorter τ_β is revealed for $c < 60\%$ (cf. Fig. 3). The long-time value $1 - f_\beta$ is not any longer zero but increases with decreasing TPP concentration. The corresponding value $f_\beta(c)$ reflecting the fraction of TPP molecules participating in the β -process is found in Fig. 14.

The higher is the TPP concentration, the higher is the fraction of TPP molecules participating in the β -process. We note that in the case of ethanol, cyano cyclohexane, and toluene (Fig. 5(a)) we find a plateau value $1 - f_\beta = 0.0 \pm 0.04$ while in the case of neat TPP we find $f_\beta = 0.93$, i.e., $1 - f_\beta = 0.07 \pm 0.04$ putting our above given statement on a quantitative basis: in neat glasses essentially all molecules take part in the β -process while this is no longer the case in a binary system.

In the case of PS- d_3 a corresponding analysis of $R(t_p)$ along Eq. (3) (solid lines in Fig. 13(b)) provides essentially the same time constants, but, nevertheless, varying fractions of PS molecules participating in the β -process. The result is included in Fig. 14. With increasing TPP concentration also the fraction of PS molecules participating in the β -process grows quickly. It even appears that the fraction f_β of PS is higher than that of TPP. This excess fraction becomes most conspicuous at $c = 0$, where a plateau value of $f_\beta(c = 0) = 0.25$ is found. This is somewhat unreasonable, since, due to the absence of TPP molecules, no contribution to the β -relaxation is expected at all. One can argue that, due to some further

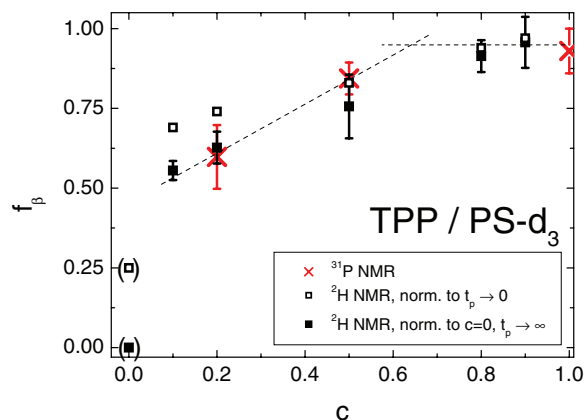


FIG. 14. Fraction of molecules of TPP (crosses) and PS- d_3 (full squares: normalized to behavior of neat PS- d_3 ; open squares: normalized to short t_p value) participating in the β -process as estimated by the Hahn-echo and solid-echo experiments. Dashed straight lines: A possible interpretation.

relaxation process in neat PS, $R(t_p)$ decays to some plateau which has to be taken into account also in the mixture. Thus renormalizing $1 - f_\beta$ by $1 - f_\beta(\text{neat PS})$, the fraction f_β decreases and becomes similar to that of TPP. Thus the fractions of TPP and PS molecules participating in the β -process coincide for each concentration.

As discussed above, the dynamics of neat PS- d_3 and TPP have also been characterized by the spin-lattice relaxation monitored as a function of temperature (cf. Fig. 3(a)). No indication of a β -process shows up for PS- d_3 while below T_g in TPP the ^{31}P relaxation is clearly controlled by the β -process. The findings for the TPP/PS mixture with $c = 50\%$ are shown in Fig. 3(b). With respect to the neat components, the results are now quite different. Below T_g the temperature dependences $T_1(T)$ of TPP and PS- d_3 run parallel, i.e., the same strong temperature dependence is observed in both methods. Above T_g a minimum is found for TPP which reflects the isotropic reorientation of the TPP molecules in the mixture. A similar minimum occurring yet at higher temperatures is found for PS- d_3 . This difference directly reflects the decoupling of the primary (isotropic) dynamics of the components: in the mixture PS reorients much slower than TPP, a fact well known from results on asymmetric binary glass formers.^{42,43} There is a further feature the detailed discussion of which is postponed to a forthcoming publication: At temperatures for which the T_1 minimum of TPP occurs, particularities are also observed in the ^2H relaxation of PS- d_3 . This shows that the fast isotropic dynamics of TPP affects the polystyrene monomers leading to a highly hindered (i.e., non-isotropic) dynamics, however, occurring at similar time scale as the TPP molecules. These findings demonstrate that a plasticizer molecule does not only change the T_g but also induces additional dynamics on the polymer.

As in the case of neat TPP the temperature dependence of the spin-lattice relaxation can be understood on a quantitative level by taking the dielectric results into account. These provide the dynamic susceptibility determined by a temperature independent distribution of activation energies, which actually does not change significantly in the mixture. Analogously to the case of ^{31}P dielectric susceptibility data can be compared to $T_1(T)$ of ^2H NMR after extrapolating it to higher frequencies. As can be seen in Fig. 3(b) (dashed line) the slope of $T_1(T)$ of TPP as well as PS- d_3 is reproduced.

IV. DISCUSSION AND CONCLUSION

We have studied the secondary (β -) relaxation process in the binary glass mixture TPP/PS by dielectric spectroscopy as well as TPP/PS- d_3 by ^{31}P and ^2H NMR. While neat TPP exhibits a β -process (type-B glass former) and neat polystyrene shows none (type-A), in the mixture also PS- d_3 molecules clearly participate in the β -relaxation. Here, for both TPP and PS- d_3 , NMR spectra reveal a spatially highly restricted motion as identified by NMR in other type-B systems, like toluene^{16,22} or ethanol.^{17,23} Up to our knowledge a Hahn-echo sequence (here for ^{31}P) has been applied for the first time to monitor the subtle spectral changes deep in the glass characteristic of the β -process. The dielectric spectra reflect a distribution of activation energies which is temperature in-

dependent; yet, its asymmetric shape is rather unusual for β -processes and does not change with concentration, a phenomenon observed also in other binary glass formers.^{25,43,44} Even at a TPP concentration of $c = 10\%$ the mean activation energy is still similar to that of neat TPP. The β -process introduced by the type-B component survives in the mixture and induces the type-A molecule to participate in the relaxation process. Yet, in contrast to neat systems not all molecules participate in the β -process; islands of rigidity or immobility appear. The higher the concentration of the type-B component the higher is the fraction of both components which participate. We emphasize, as we do not find any indication for the mixed glasses to decompose, the immobilized molecules are not part of crystalline regions. Instead the mixtures become glasses with inhomogeneously distributed dynamics. In a recent ^2H NMR study of another binary system (toluene/aroclor) an indication of a threshold concentration has been found below which immobile type-B molecules appear.²⁵ Although not sufficient NMR data at various concentrations has been collected in the present study a similar behavior can be anticipated also for TPP/PS- d_3 . Only below, say, $c = 60\%$ some relevant fraction of TPP or PS- d_3 appear to become immobilized. This corresponds with the (slight) change of the mean activation energy below 60% (cf. Figs. 7 and 9).

All together the presented experimental findings point into the direction that also the β -process exhibits some cooperative nature. When mixed with type-B molecules, type-A molecules do react to the highly hindered motion introduced by the β -process, actually a behavior expected in (dense) condensed matter. A similar phenomenon is observed for the decoupled isotropic reorientation of the TPP molecules in the vitrified matrix of polystyrene. Whether the extent of spatial hindrance is the same for the two molecules is yet to be investigated. In any case both components show dynamics on the same time scale.

ACKNOWLEDGMENTS

The authors acknowledge financial support by Deutsche Forschungsgemeinschaft (DFG) under Grant No. RO 907/10.

¹G. Johari and M. Goldstein, *J. Chem. Phys.* **53**, 2372 (1970).

²G. Williams and D. C. Watts, *Trans. Faraday Soc.* **67**, 1971 (1971).

³L. Wu, *Phys. Rev. B* **43**, 9906 (1991).

⁴A. Arbe, D. Richter, J. Colmenero, and B. Farago, *Phys. Rev. E* **54**, 3853 (1996).

⁵A. Kudlik, C. Tschirwitz, S. Benkhof, T. Blochowicz, and E. Rössler, *Europhys. Lett.* **40**, 649 (1997).

⁶K. L. Ngai and M. Paluch, *J. Chem. Phys.* **120**, 857 (2004).

⁷C. Gainaru, R. Kahlau, E. A. Rössler, and R. Böhmer, *J. Chem. Phys.* **131**, 184510 (2009).

⁸A. Kudlik, S. Benkhof, T. Blochowicz, C. Tschirwitz, and E. Rössler, *J. Mol. Struct.* **479**, 201 (1999).

⁹M. Paluch, S. Pawlus, S. Hensel-Bielowka, E. Kaminska, D. Prevosto, S. Cappacioli, P. A. Rolla, and K. L. Ngai, *J. Chem. Phys.* **122**, 234506 (2005).

¹⁰N. Petzold, B. Schmidtke, R. Kahlau, D. Bock, R. Meier, B. Micko, D. Kruk, and E. A. Rössler, *J. Chem. Phys.* **138**, 12A510 (2013).

¹¹L. Comez, D. Fioretto, L. Palmieri, L. Verdini, P. A. Rolla, J. Gapinski, T. Pakula, A. Patkowski, W. Steffen, and E. W. Fischer, *Phys. Rev. E* **60**, 3086 (1999).

¹²A. Brodin, E. A. Rössler, R. Bergman, and J. Mattsson, *Eur. Phys. J. B* **36**, 349 (2003).

- ¹³C. Tschirwitz, S. Benkhof, T. Blochowicz, and E. Rössler, *J. Chem. Phys.* **117**, 6281 (2002).
- ¹⁴S. Benkhof, A. Kudlik, T. Blochowicz, and E. Rössler, *J. Phys.: Condens. Matter* **10**, 8155 (1998).
- ¹⁵M. Vogel and E. Rössler, *J. Phys. Chem. B* **104**, 4285 (2000).
- ¹⁶M. Vogel and E. Rössler, *J. Chem. Phys.* **114**, 5802 (2001).
- ¹⁷M. Vogel, C. Tschirwitz, G. Schneider, C. Koplin, P. Medick, and E. Rössler, *J. Non-Cryst. Solids* **307–310**, 326 (2002).
- ¹⁸S. A. Lusceac, C. Gainaru, M. Vogel, C. Koplin, P. Medick, and E. A. Rössler, *Macromolecules* **38**, 5625 (2005).
- ¹⁹G. Schneider, Diploma thesis, Universität Bayreuth, 2001.
- ²⁰B. Micko, S. A. Lusceac, H. Zimmermann, and E. A. Rössler, *J. Chem. Phys.* **138**, 074503 (2013).
- ²¹B. Micko, D. Kruk, and E. A. Rössler, *J. Chem. Phys.* **138**, 074504 (2013).
- ²²M. Vogel and E. Rössler, *J. Chem. Phys.* **115**, 10883 (2001).
- ²³M. Vogel, P. Medick, and E. A. Rössler, *Annu. Rep. NMR Spectrosc.* **56**, 231 (2005).
- ²⁴M. Vogel and E. Rössler, *J. Magn. Reson.* **147**, 43 (2000).
- ²⁵B. Micko, C. Tschirwitz, and E. A. Rössler, *J. Chem. Phys.* **138**, 154501 (2013).
- ²⁶S. Adishchev, D. Bock, C. Gainaru, R. Kahlau, B. Micko, N. Petzold, B. Pötzschner, and E. A. Rössler, *Z. Phys. Chem.* **226**, 1149 (2012).
- ²⁷H. Wagner and R. Richert, *J. Phys. Chem. B* **103**, 4071 (1999).
- ²⁸T. Blochowicz, C. Tschirwitz, S. Benkhof, and E. A. Rössler, *J. Chem. Phys.* **118**, 7544 (2003).
- ²⁹D. Schaefer, J. Leisen, and H. W. Spiess, *J. Magn. Reson., Ser. A* **115**, 60 (1995).
- ³⁰M. Bloom, J. H. Davis, and M. I. Valic, *Can. J. Phys.* **58**, 1510 (1980).
- ³¹K. Schmidt-Rohr and H. W. Spiess, *Multidimensional Solid-State NMR and Polymers* (Academic Press, New York, 1994) p. 66.
- ³²S. A. Lusceac, Ph.D. thesis, Universität Bayreuth, 2005.
- ³³Y. He, T. R. Lutz, and M. D. Ediger, *Macromolecules* **37**, 5032 (2004).
- ³⁴C. Gainaru, A. Rivera, S. Putselyk, G. Eska, and E. A. Rössler, *Phys. Rev. B* **72**, 174203 (2005).
- ³⁵C. Gainaru, R. Böhmer, R. Kahlau, and E. Rössler, *Phys. Rev. B* **82**, 104205 (2010).
- ³⁶N. G. McCrum, B. E. Read, and G. Williams, *Anelastic and Dielectric Effects in Polymer Solids* (Wiley, London, 1967).
- ³⁷J. Hintermeyer, A. Herrmann, R. Kahlau, C. Goiceanu, and E. A. Rössler, *Macromolecules* **41**, 9335 (2008).
- ³⁸E. Rössler and P. Eiermann, *J. Chem. Phys.* **100**, 5237 (1994).
- ³⁹T. Blochowicz, A. Kudlik, S. Benkhof, J. Senker, and E. A. Rössler, *J. Chem. Phys.* **110**, 12011 (1999).
- ⁴⁰L. Wu and S. Nagel, *Phys. Rev. B* **46**, 11198 (1992).
- ⁴¹J. Wiedersich, S. V. Adichtchev, and E. Rössler, *Phys. Rev. Lett.* **84**, 2718 (2000).
- ⁴²D. Bingemann, N. Wirth, J. Gmeiner, and E. A. Rössler, *Macromolecules* **40**, 5379 (2007).
- ⁴³T. Blochowicz, S. A. Lusceac, P. Gutfreund, S. Schramm, and B. Stühn, *J. Phys. Chem. B* **115**, 1623 (2011).
- ⁴⁴D. Cangialosi, A. Alegría, and J. Colmenero, *J. Chem. Phys.* **128**, 224508 (2008).

Paper 6

Dynamics of Asymmetric Binary Glass Formers. I. A Dielectric and Nuclear Magnetic Resonance Spectroscopy Study

R. KAHLAU, D. BOCK, B. SCHMIDTKE, AND E. A. RÖSSLER,
The Journal of Chemical Physics **140**, 044509 (2014).

© 2014 AIP Publishing LLC
doi:10.1063/1.4861428

Dynamics of asymmetric binary glass formers. I. A dielectric and nuclear magnetic resonance spectroscopy study

R. Kahlau, D. Bock, B. Schmidtke, and E. A. Rössler^{a)}

Experimentalphysik II, Universität Bayreuth, 95440 Bayreuth, Germany

(Received 30 October 2013; accepted 20 December 2013; published online 29 January 2014)

Dielectric spectroscopy as well as ^2H and ^{31}P nuclear magnetic resonance spectroscopy (NMR) are applied to probe the component dynamics of the binary glass former tripropyl phosphate (TPP)/polystyrene (PS/PS- d_3) in the full concentration (c_{TPP}) range. In addition, depolarized light scattering and differential scanning calorimetry experiments are performed. Two glass transition temperatures are found: $T_{g1}(c_{\text{TPP}})$ reflects PS dynamics and shows a monotonic plasticizer effect, while the lower $T_{g2}(c_{\text{TPP}})$ exhibits a maximum and is attributed to (faster) TPP dynamics, occurring in a slowly moving or immobilized PS matrix. Dielectric spectroscopy probing solely TPP identifies two different time scales, which are attributed to two sub-ensembles. One of them, again, shows fast TPP dynamics (α_2 -process), the other (α_1 -process) displays time constants identical with those of the slow PS matrix. Upon heating the α_1 -fraction of TPP decreases until above some temperature T_c only a single α_2 -population exists. Inversely, below T_c a fraction of the TPP molecules is trapped by the PS matrix. At low c_{TPP} the α_2 -relaxation does not follow frequency-temperature superposition (FTS), instead it is governed by a temperature independent distribution of activation energies leading to correlation times which follow Arrhenius laws, i.e., the α_2 -relaxation resembles a secondary process. Yet, ^{31}P NMR demonstrates that it involves isotropic reorientations of TPP molecules within a slowly moving or rigid matrix of PS. At high c_{TPP} the super-Arrhenius temperature dependence of $\tau_2(T)$, as well as FTS are recovered, known as typical of the glass transition in neat systems. © 2014 AIP Publishing LLC. [<http://dx.doi.org/10.1063/1.4861428>]

I. INTRODUCTION

The evolution of the dynamic susceptibility in neat glass formers is well documented starting at temperatures close to the boiling point and reaching the glass transition temperature T_g , where the liquid becomes an amorphous solid.^{1–7} In particular, light scattering, dielectric, and NMR spectroscopy have provided a wealth of information. In contrast, binary glass formers are less studied, and no broadly accepted picture of the rather complex dynamics has established so far. Of special interest are so-called asymmetric glass formers, which are characterized by a large difference of the T_g values of the components. They are most conveniently prepared by blending a polymer with a low-molecular mass additive,^{8–13} yet also purely low-molecular weight mixtures have been studied.^{14–18} It is well established that such systems exhibit two glass transition temperatures albeit they are fully miscible.^{19–25} In other words, such binary liquids display pronounced dynamic heterogeneities,^{5,26,27} which are in particular well documented by NMR.^{28–30} For example, intrinsic confinement effects are expected when the mobile (low- T_g) component still relaxes in a matrix of an arrested (high- T_g) component. Indeed, the NMR phenomenology is similar to that of neat glass formers embedded in porous systems.^{31–34}

Binary systems consisting of soft or hard spheres have also been investigated by simulations^{35–37} as well as by mode

coupling theory (MCT).^{38–41} In contrast to neat systems, for which a type-B glass transition scenario is expected by MCT, which is triggered by cage formation and characterized by a discontinuous change of the non-ergodicity parameter f from zero to $f > 0$ at a critical temperature T_c , the mobile molecules in binary liquids are expected to exhibit a type-A transition, and f should increase continuously from zero upon cooling below T_c . Here, the mobile (small) particles undergo a localization transition, while the less mobile (large) ones are still arrested due to the cage effect. In a recent paper by Blochowicz *et al.*¹³ experimental hints have been given that indeed such type-A transitions might be observed in mixed molecular liquids. We note that such dynamic heterogeneities have also been explained either by concentration fluctuations^{42,43} or so-called self-concentration effects.⁴⁴ It is the aim of the present contribution to dwell on this issue by applying several experimental methods to study selectively the dynamics of each component on a (short-chain) polymer-additive system.

The binary glass tripropyl phosphate (TPP)/(deuterated) polystyrene (PS/PS- d_3 , $M_w \approx 2 \times 10^3$ g/mol) is characterized by means of dielectric spectroscopy (DS), ^2H and ^{31}P NMR as well as by dynamic depolarized light scattering (DLS) and differential scanning calorimetry (DSC). Thirteen concentrations equally spread over the full concentration range are investigated. The system is characterized by a large T_g contrast of the pure components ($\Delta T_g \cong 200$ K).^{45,46} Due to the choice of this system the application of ^{31}P and ^2H NMR allows for probing selectively the dynamics of TPP

^{a)}Author to whom correspondence should be addressed. Electronic mail: ernst.roessler@uni-bayreuth.de.

TABLE I. TPP mass concentrations c_{TPP} of mixtures studied by the different methods, including the assumed errors (see text). NMR data of 80% will be discussed in Paper II.⁴⁷

c_{TPP} [%] nom.	0	10	20	30	36	45	50	60	70	80	90	95	100
DS	0	8 ± 3	18 ± 3	29 ± 2	...	45 ± 1	...	60 ± 1	...	80 ± 1	90 ± 1	95 ± 1	100
DSC	0	10 ± 1	20 ± 1	...	36 ± 1	45 ± 1	...	60 ± 1	70 ± 1	83 ± 1	90 ± 1	...	100
DLS	80 ± 1	90 ± 1	...	100
² H NMR	0	10 ± 1	20 ± 1	50 ± 1	80 ± 1 (Paper II) ⁴⁷	90 ± 1
³¹ P NMR	...	10 ± 1	20 ± 1	50 ± 1	80 ± 1 (Paper II) ⁴⁷	90 ± 1	...	100

and PS-d₃, while dielectric spectroscopy provides essentially information on the dynamics of the mobile component TPP, since its molecular dipole moment is significantly higher than that of PS. Regarding the pronounced β -process present in the mixed system, it has been studied thoroughly by our group.⁴⁵ Its time constant shows the typical Arrhenius behavior with an activation energy $\langle E \rangle/k \cong 24 T_g$, which virtually does not vary due to mixing, and which is associated with a spatially highly hindered dynamics as found in other glasses. Actually, throughout this work, only a spatially highly restricted process shall be understood as a β -process. Although introduced by TPP, in the mixture both components participate in the β -process. This has been taken as an indication of its cooperative nature.

In the present contribution we focus on the dynamics of both components above T_g , more precisely above T_{g2} of the mobile component. By performing DSC experiments we can identify two glass transition temperatures. We will demonstrate that the high- T_g component PS shows liquid dynamics similar to that of neat systems while TPP displays rather complex heterogeneous dynamics. For example, the temperature dependence of the correlation time changes from super-Arrhenius at high c_{TPP} to Arrhenius behavior at low concentrations. Thus, the additive process may be confused with a β -process, and it is up to NMR to proof whether the process is still liquid-like (isotropic) or β -process-like.

This contribution consists of two parts, the present one essentially deals with the results collected by dielectric spectroscopy, complemented by time constants provided by NMR and DLS as well as DSC. In Paper II⁴⁷ continuative NMR experiments are reported and analyzed in accordance with the dielectric results.

II. EXPERIMENTAL DETAILS AND DATA ANALYSIS

A. Systems

A polystyrene sample with the molecular mass $M_w = 2250$ g/mol (PS), and another polystyrene sample, partially deuterated at the backbone, with very similar mass $M_w = 2440$ g/mol (PS-d₃) were purchased from Polymer Standards Service (Mainz, Germany) and used without further treatment. For the DS experiments PS was used for the preparation of the mixtures, while PS-d₃ was used for the NMR measurements. Tripropyl phosphate (TPP, 99%) was bought from Sigma Aldrich and used as received, too. We do not find any indication that phase separation or crystallization occurs in the mixtures. Among other tests, light scattering

experiments show a homogeneous sample. NMR and DLS samples were prepared in the measurement tubes and cells, while the DSC and DS samples had to be prepared in separate test tubes (exact concentrations valid for different methods are listed in Table I). Generally a concentration error of $\pm 1\%$ is assumed for the sample preparation. After the preparation all sample vessels were left at elevated temperatures for one or two days in order to guarantee a maximum possible spatial homogeneity. In the case of DSC and DS the sample had to be transferred afterwards from the preparation vessel to the measurement cell. In the case of DS the samples of low concentrations had to be heated carefully during the transfer, because they are highly viscous at room temperature. Since some fraction of the TPP content may have evaporated during this process, the assumed actual error for the $c_{TPP} = 10\%$ – 30% samples is somewhat higher (Table I). In contrast, the DSC samples could be transferred to the measurement cells without heating. For the sake of clarity the nominal (nom.) concentrations are discussed throughout the paper.

B. Dielectric spectroscopy

Dielectric measurements were carried out with the Alpha-A Analyzer by Novocontrol while temperature was kept constant within ± 0.2 K by using the Quatro-H temperature controller by Novocontrol. The absolute accuracy is assumed to be better than ± 1 K. The sample cell has the design described by Wagner and Richert and assures a constant sample volume.⁴⁸ In order to extract time constants from the dielectric susceptibility data, unless described differently in the text a Kohlrausch stretched exponential was used to fit the α_1 -relaxation peaks (on the timescale of PS dynamics), and the mean relaxation time $\tau = \Gamma(1/\beta_K) \tau_0/\beta_K$ is discussed. For the α_2 -peaks (reflecting faster TPP dynamics) a Havriliak-Negami (HN) function had to be used due to stretching parameters significantly less than unity on the low-frequency side of the peak. In these cases the maximum correlation times given by $\tau_{max} = 1/(2\pi\nu_{max})$ are discussed.

C. Depolarized light scattering

Depolarized dynamic light scattering measurements were performed with a vertically polarized Coherent Verdi-V2 laser at a wavelength of 532 nm and 200 mW optical power in combination with a tandem Fabry-Pérot interferometer (TFPI; JRS Scientific, triple-pass-tandem Etalon) working parallel with a double monochromator (DM; Jobin Yvon, U1000). The TFPI was operated at horizontal polarization in almost

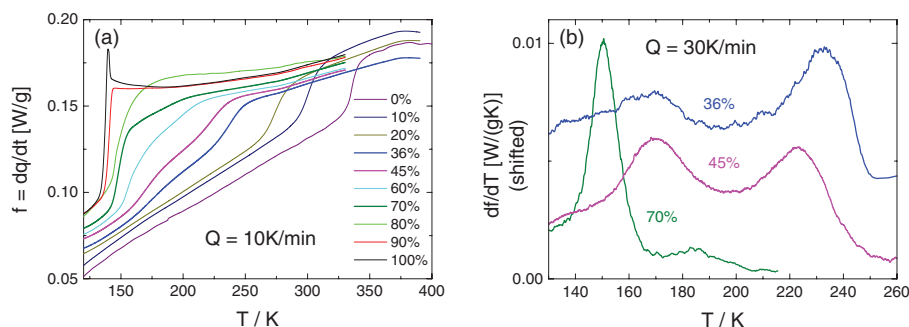


FIG. 1. (a) DSC traces (heat flow per sample mass $f = dq/dt$) for mixtures and neat systems ($c_{TPP} = 0\%$ – 100%) at the heating rate $Q = 10$ K/min. (b) Temperature derivative of DSC traces df/dT at heating rate $Q = 30$ K/min for indicated concentrations.

backscattering geometry, whereas the DM was operated at orthogonal geometry (for details, see Refs. 49 and 50). The TFPI measurements were done with three different free spectral ranges, and the DM measurements with two combinations of slits and frequency intervals. The spectral parts are then adjusted in amplitude to match together and form a smooth spectrum.

D. DSC

DSC experiments were performed with a Q1000 analyzer by TA Instruments. By using a liquid nitrogen cooling system the temperature range $T = 120$ – 400 K was covered. Experiments presented were run at heating rates $Q = 10$ – 40 K/min. Figure 1(a) displays DSC traces of neat PS and TPP as well as mixtures with $c_{TPP} = 10\%$ – 90% TPP in PS (nominal concentrations, see Table I), recorded with a heating rate of $Q = 10$ K/min. For both of the neat samples a distinct glass step is found. For the mixtures a comparably broad glass transition temperature range is observed, consisting of two individual, more or less separated steps. This is best seen in Fig. 1(a) for intermediate concentrations. In order to achieve a better resolution of both contributions the temperature derivative of the DSC traces¹³ are considered (Fig. 1(b)). The best results were obtained here by choosing a heating rate of $Q = 30$ K/min for all samples. Glass temperatures as yielded by DSC experiments were defined as the peak temperatures of the temperature derivatives just described (cf. Fig. 10).

In order to calculate calorimetric time constants the formula,

$$\tau_{cal} \approx \frac{RT_g^2}{\Delta H_{eff}} \cdot \frac{1}{Q}, \quad (1)$$

was used.^{17,51} It turns out that for all systems a constant prefactor $\frac{RT_g^2}{\Delta H_{eff}} \approx 1.7$ could be used in good approximation, leading to an error in τ_{DSC} smaller than a factor of two. The extracted time constants are included in Fig. 9.

E. NMR

Regarding the NMR analysis we refer to Paper II.⁴⁷ In the present paper we only report some of the NMR results concerning correlation times.

III. RESULTS

A. Neat components – dielectric spectra

The susceptibility spectra of PS ($T_g = 335$ K) are shown in Fig. 2 and fit well into the collection of dielectric data on polystyrene samples of different molecular weights given in Ref. 52. Above T_g a pronounced peak is visible, which is identified as structural or α -relaxation shifting to high frequencies with increasing temperature. The low amplitude reflects the rather non-polar nature of the PS monomer. Close to T_g , the high-frequency side of the α -peak is made up of a crossover from one power-law behavior to another one, the latter often being called excess wing.^{1,7,53} When the sample is cooled below T_g the α -peak moves out of the frequency window and the signal, now consisting only of the excess wing contribution, drops close to the resolution limit of the spectrometer. No indications for a secondary (β) relaxation peak are observed for PS (cf. Ref. 45).

The dielectric spectra of neat TPP ($T_g = 135$ K) are also displayed in Fig. 2. As in the case of PS, above T_g an α -relaxation peak can be identified, the amplitude of which exceeds the one of PS by a factor of 1000, i.e., the TPP molecule carries a high dipole moment. At frequencies several decades above the maximum position of the α -peak a secondary relaxation is well resolved (type-B glass former). This secondary (β -) peak survives at temperatures below T_g when the α -peak has already left the frequency window. When temperature is increased above, say, $T = 150$ K, both peaks approach each

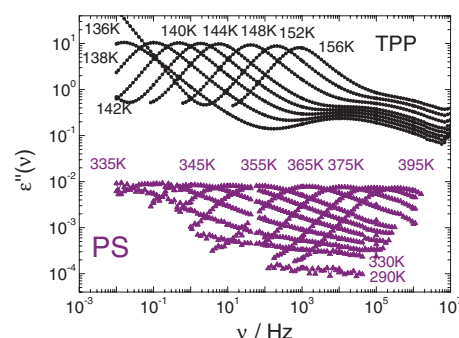


FIG. 2. Susceptibility spectra of neat TPP (top, circles; temperatures indicated). Dielectric spectra of neat PS; $T = 290$ K and $T = 330$ – 355 K in 5 K steps, $T = 365$ – 395 K in 10 K steps (bottom, triangles; some temperatures indicated).

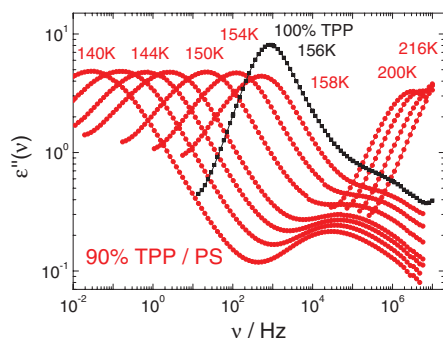


FIG. 3. Susceptibility of the mixture 90% TPP in PS (circles, some temperatures indicated). Data of neat TPP at $T = 156$ K for comparison (squares). Temperature gap is due to crystallization.

other until above $T = 156$ K the measurement of the supercooled liquid cannot be continued due to the crystallization of the sample. Spectra of the β -process have been analyzed in Refs. 45 and 54, and are not considered further here. At the low-frequency side of the α -peak a contribution of ionic conductivity is found which, for the sake of clarity, is only shown for the 152 K data of TPP.

Time constants of TPP and PS, as well as of some mixtures, are shown in Fig. 5. A collection of the time constants of all analyzed systems is given in Fig. 9. Good agreement with NMR measurements on neat PS⁵⁵ is observed. We further note that FTS applies for the spectra of the neat systems, i.e., all spectra can be collapsed to a single master curve (cf. Fig. 11). This feature is well known for being characteristic of cooperative dynamics.^{2,7}

B. Mixtures

In order to develop a conclusive picture of the relaxation processes over the full concentration range it is useful to start with the dielectric results of the very high and the very low concentrated mixtures, i.e., the limiting cases of the investigated concentration series. Figure 3 shows the susceptibility of 90% TPP/PS, i.e., some small amount of polystyrene has been added to TPP. For comparison one spectrum of neat TPP (not scaled) is included in Fig. 3. Note that due to the low dipole moment of PS exclusively TPP dynamics is monitored. Clearly, the α -peak of the 90% sample is significantly broader,

and the maximum value of the peaks is lower than in the case of 100% TPP. In particular, the low-frequency side of the α -peaks follows obviously a power-law with a lower exponent than in the case of neat TPP. In contrast, the high-frequency flanks of the relaxation peaks found for both samples are almost parallel. The peak position of the 158 K data set of the 90% mixture is situated at a lower frequency than the one of the 156 K data set of neat TPP. This slowing down of the TPP dynamics is due to the anti-plasticizer effect caused by the presence of PS. TPP time constants $\tau_{max} = 1/(2\pi\nu_{max})$ provided by DS (full red circles) as well as ³¹P-NMR (open red circles, cf. Paper II⁴⁷) and DLS (red pentagons) are included in Fig. 5 (nominal concentrations given there, see Table I). Good agreement between all three methods is found.

Figure 4 shows dielectric data of the (a) 10% and (b) 20% TPP/PS mixture. In contrast to the 90% mixture now two relaxation phenomena (grey and black data points) are observed. In Figure 4(b) the onset of the β -relaxation is recognized at high frequencies for the spectra at 169 K and 190 K. Note that for the mixtures the spectra of the β -process below T_g (more precisely below T_{g2} , cf. below) are always omitted (for an analysis of the β -process see Ref. 45). Regarding high temperatures (triangles), the $c_{TPP} = 10\%$ mixture shows relaxation peaks with a low-frequency flank following a Debye behavior, i.e., $\epsilon'' \sim \nu^1$, and FTS holds in good approximation. At lower temperatures ($c_{TPP} = 10\%$: $T = 163$ – 281 K; $c_{TPP} = 20\%$: $T = 169$ – 270 K), when the peaks just discussed have left the accessible frequency range, another relaxation peak (circles) dominates the susceptibility, which exhibits a strong flattening on the low-frequency flank qualitatively similar to what is also observed for TPP in the 90% mixture. Moreover, FTS does not apply. This relaxation is best resolved in the 20% data (Fig. 4(b)).

For the $c_{TPP} = 20\%$ sample time constants of both relaxation peaks are shown in Fig. 5, the time constants for all mixtures are collected in Fig. 9 and will be discussed later. As mentioned in Sec. II B a Kohlrausch function was fitted to the high-temperature peaks (later called α_1 -relaxation), and a HN function was fitted to the peak found at lower temperatures (α_2 -relaxation, see below). While the high-temperature relaxation shows a strongly non-Arrhenian temperature dependence, which is similar to that of neat PS, yet shifted to somewhat lower temperature, the low-temperature relaxation

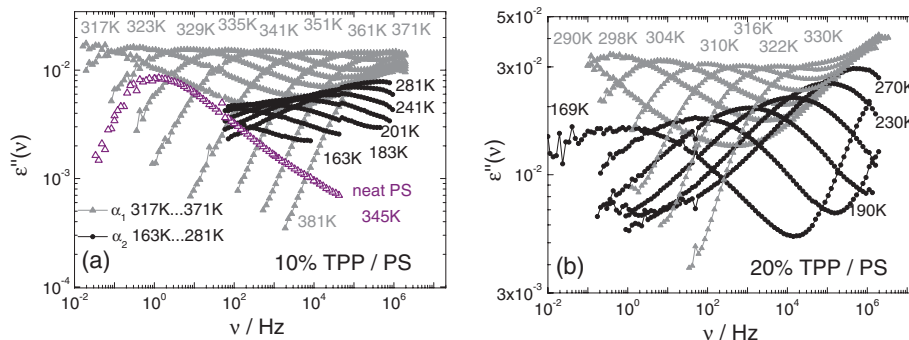


FIG. 4. Dielectric susceptibility of TPP/PS mixtures with low TPP concentration. Triangles, higher temperatures: α_1 -relaxation; full circles, lower temperatures: α_2 -relaxation. (a) 10% TPP in PS; open triangles: pure PS at 345 K. (b) 20% TPP in PS.

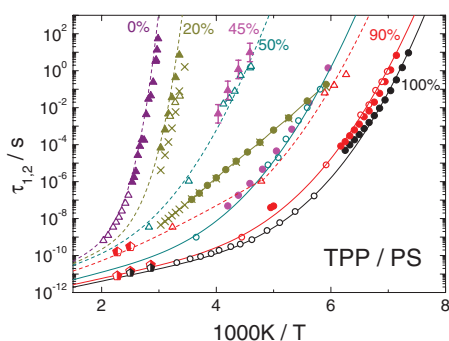


FIG. 5. Time constants for selected mixtures with (nominal) $c_{TPP} = 0\%$, 20%, 45%, 50%, 90%, 100% TPP in PS as obtained by DS (full symbols) and ^2H or ^{31}P NMR (open symbols). See Table I for exact concentration values. For $c_{TPP} = 0\%$ NMR data by He *et al.*⁵⁵ are included, and for TPP we included ^{31}P NMR results.⁴⁶ Triangles: time constants of the α_1 -process, circles: α_2 -process; Crosses (x): results obtained by the scaling analysis of dielectric data discussed in Appendix A. Pentagons (●): light scattering data of α_1 -process. Pentagons (⦿): DLS data of α_2 -process. Lines are guides for the eye; solid lines concern the α_2 -relaxation, dashed lines represent the α_1 -process. Except the case of $\tau_1(T)$ for $c_{TPP} = 45\%$ error bars are estimated to be smaller than the size of the symbols.

follows an Arrhenius law with a rather low activation energy ($E_A(20\%) = 6058 \text{ K} \approx 21T_{g1}$; $E_A(10\%) = 5241 \text{ K} \approx 17T_{g1}$). ^2H -NMR experiments probing again the PS dynamics yield correlation times in good agreement with the time constants of the dielectric high-temperature peak (cf. Fig. 5). Comparing the spectral shapes of the relaxations, the high-temperature peak in the 10% mixture is broader and by a factor of about two higher than the α -relaxation of neat PS, in the case of $c_{TPP} = 20\%$ by a factor of four. In other words, the high-temperature peaks are dominated by the TPP signal. Thus we conclude that a fraction of TPP molecules is associated with PS, and therefore part of its α -relaxation. In the following, this relaxation shall be called α_1 -process, and the faster relaxation α_2 -process. The nature of the latter remains still to be clarified (see below), though, given the two T_g reported in the mixtures, it is natural to assume that it belongs to a second population of TPP molecules reorienting highly decoupled from the PS component. The process may be a liquid-like (isotropic) motion or, given its Arrhenius temperature dependence with rather low-activation energy at low concentrations, a kind of secondary β -process. Clearly, at high TPP concentrations also the α_2 -process displays a super-Arrhenius temperature dependence, and for $c_{TPP} \rightarrow 1$ it develops continuously into the primary process of neat TPP.

Another phenomenon can be recognized for both data sets in Fig. 4. While the amplitude of the α_1 -process decreases, the amplitude of the α_2 -process increases with temperature. It appears that, when temperature rises, more and more TPP molecules are freed from being associated with the polymer dynamics. This phenomenon is quantified in Fig. 6, where the relaxation strengths $\Delta\epsilon_{1,2}(T)$ of both processes are displayed for the case of the 20% mixture. The corresponding fitting strategy is explained in Appendix A. At low temperatures $\Delta\epsilon_2(T)$ increases only weakly with T while at high temperatures a stronger increase is observed. A complementary decrease is revealed for the relaxation strength $\Delta\epsilon_1(T)$ of the α_1 -relaxation. The rise of $\Delta\epsilon_2(T)$ around T_g

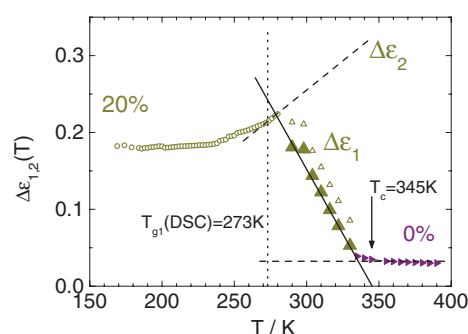


FIG. 6. Relaxation strengths $\Delta\epsilon_{1,2}(T)$ of the 20% mixture as a function of temperature: $\Delta\epsilon_2$ of the α_2 -process (open circles); obtained from fitting procedure described in Appendix A (cf. Fig. 13). Linear extrapolation of the α_2 -relaxation strength indicated as dashed line. Open triangles: $\Delta\epsilon_1$ of the α_1 process; full triangles (▲): $\Delta\epsilon_1(T)$ after subtraction of PS contribution. Full triangles (▶): α -process of neat PS. Dashed line: extrapolation of $\Delta\epsilon(T)$ of neat PS, approximated as constant. Solid line: guide for the eye. Dotted line: Glass temperature T_{g1} (associated with the α_1 -process) as obtained by DSC measurements.

may again remind of the universal behavior of β -processes found in structural as well as orientational glasses.^{54,56} In the present case, interpreting the α_2 -relaxation again as a population of fast molecules (TPP) in a matrix of slow molecules (PS and TPP), a redistribution of TPP molecules among the two populations takes place, which finally leads to the disappearance of the slowly moving TPP fraction at high temperatures. In other words, when temperature is lowered, more TPP molecules will contribute to the α_1 -dynamics dictated by the PS segments instead of performing the α_2 -relaxation. After subtraction of the contribution of neat PS (weighted with $c_{PS} = 1 - c_{TPP}$), which is approximated as a constant (dashed line), from the $\Delta\epsilon_1(T)$ the full triangles in Fig. 6 are obtained. Accepting a linear extrapolation, one finds a temperature $T_c = 345 \text{ K}$, at which the TPP molecules attached to the slow reorienting PS molecules disappear. Above T_c only fast TPP and slow PS molecules exist.

In Fig. 7 the relaxation strengths $\Delta\epsilon_1(c_{TPP})$ and $\Delta\epsilon_2(c_{TPP})$ for the α_1 - and α_2 -processes of different mixtures are compared. Since at $c_{TPP} > 45\%$ the α_1 -relaxation is not discernible in the DS spectra, and at low c_{TPP} both processes are never situated in the accessible frequency range

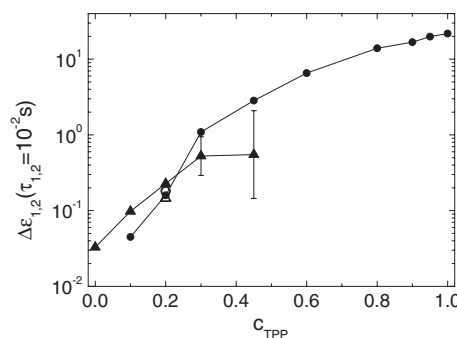


FIG. 7. Relaxation strengths $\Delta\epsilon_{1,2}$ of α_1 -relaxation (▲) and α_2 -relaxation (●), respectively, probed at $\tau_{1,2} = 10^{-2} \text{ s}$ for different concentrations. Results of the fitting procedure explained in Appendix A are included for $c_{TPP} = 20\%$ ($\Delta\epsilon_1$: Δ, $\Delta\epsilon_2$: ○). Lines: guides for the eye.

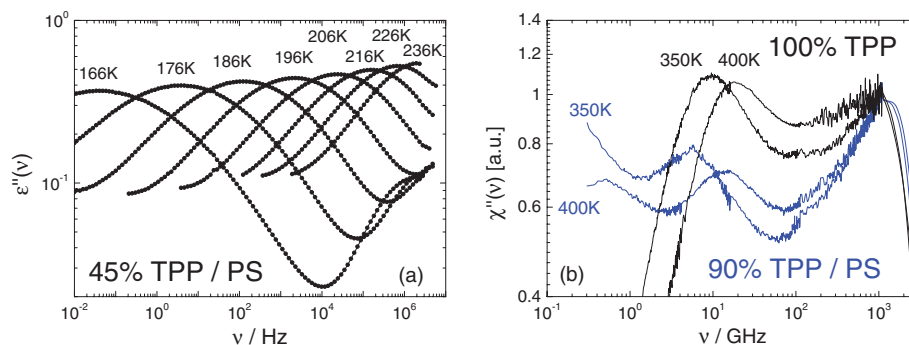


FIG. 8. (a) Dielectric susceptibility of the 45% mixture. (b) Depolarized light scattering spectra of 90% mixture (blue) and neat TPP (black).

simultaneously (at the same temperature), relaxation strengths at identical time constants ($\tau_1 = \tau_2 = 10^{-2}$ s) are used. In spite of the consequence, that spectra of different temperatures are compared, this analysis yields a qualitative estimate of the relative relaxation strengths of the α_1 - and α_2 -processes at different TPP concentrations. The $\Delta\epsilon_{1,2}$ were obtained by fitting a Kohlrausch function to the α_1 -peak and the HN function to the α_2 -peak. The relaxation strengths $\Delta\epsilon_{1,2}$ of α_1 - and α_2 -relaxation as yielded by the alternative fitting procedure for $c_{TPP} = 20\%$ described in Appendix A are also included in Fig. 7 as open symbols; similar results are found. For $c_{TPP} = 30\%$ and 45% the α_1 -peak had to be revealed by the procedure described in Appendix B. Starting at lowest c_{TPP} , the $\Delta\epsilon_{1,2}$ of α_1 - and α_2 -relaxation show similar concentration dependences. At $c_{TPP} \approx 25\%$ both curves intersect. Beyond $c_{TPP} = 30\%$ $\Delta\epsilon_1(c_{TPP})$ shows indications of a saturation behavior, while $\Delta\epsilon_2(c_{TPP})$ continues its distinct increase. Note that the data in Fig. 7 are presented on logarithmic scale; in the range

of $c_{TPP} = 30\%–100\%$ $\Delta\epsilon_2(c_{TPP})$ increases monotonically by a factor of 20.

Figure 8(a) displays the dielectric spectra for $c_{TPP} = 45\%$ TPP in PS (β -relaxation and ionic conductivity omitted). As already pointed out above, only one dielectric relaxation peak is observable as is the case for all mixtures at $c_{TPP} \geq 30\%$. At $c_{TPP} = 30\%$ still clear traces of the α_1 -relaxation are observed, yet obscured by the α_2 -relaxation peak and the ionic conductivity contribution (cf. Fig. 14(a) in Appendix B). In Appendix B we show how time constant and relaxation strength of the hidden α_1 -relaxation can be estimated. The resulting $\tau_1(T)$ are included in Figs. 5 and 9 and fit well into the overall scenario. Dielectric data of further concentrations ($c_{TPP} = 60\%, 80\%, 95\%$) are collected in Appendix C.

In Fig. 8(b) we show the results from our depolarized light scattering (DLS) experiments, which clearly reveal two separated relaxation peaks up to highest TPP concentrations,

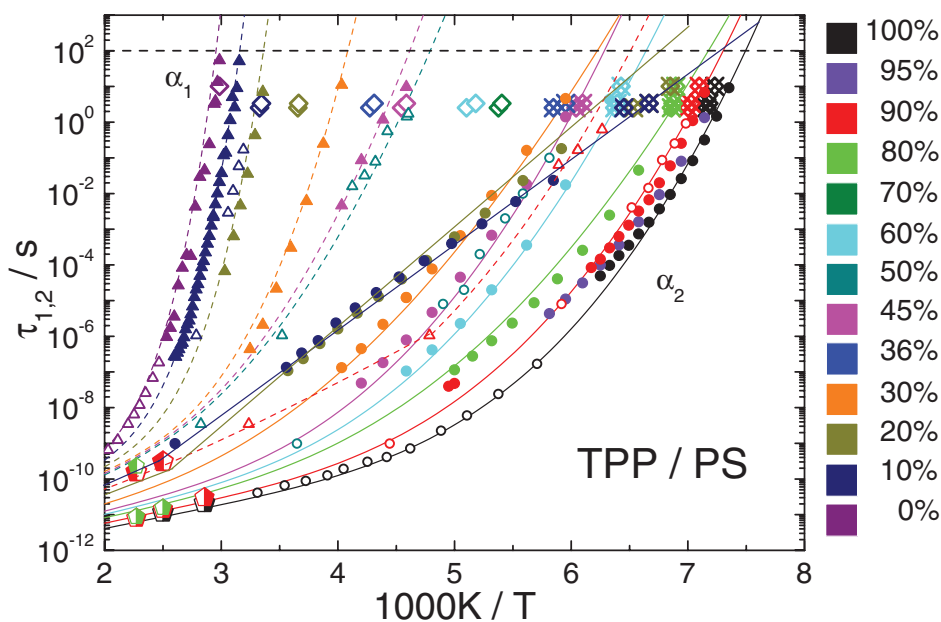


FIG. 9. Time constants from DS (\blacktriangle : α_1 ; \bullet : α_2), NMR (Δ : α_1 ; \circ : α_2), DSC (\diamond : α_1 ; \boxtimes : α_2) and DLS (\circ : α_1 ; \bullet : α_2) for all investigated concentrations (cf. color code). For $c_{TPP} = 0\%$ NMR data by He *et al.*⁵⁵ are included, and for TPP we included ^{31}P NMR results.⁴⁶ Exact concentrations are given in Table I. Lines are guides for the eye (dashed: α_1 -relaxation; solid: α_2 -relaxation). Horizontal dashed line marks $\tau_{1,2} = 100$ s (indication of T_g). Error bars in the case of $c_{TPP} = 45\%$ omitted for the sake of clarity; for other concentrations estimated to be smaller than the symbols.

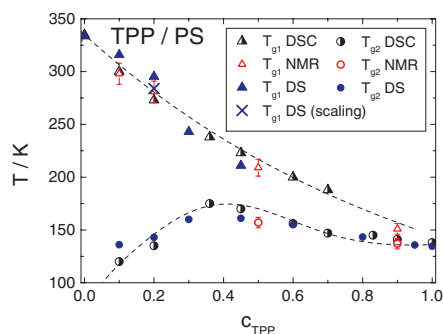


FIG. 10. Glass transition temperatures T_g as a function of TPP concentration as yielded by DSC, NMR, and DS for all investigated mixtures. Dashed lines: guides for the eye.

as demonstrated for $c_{TPP} = 90\%$ in comparison to $c_{TPP} = 100\%$ TPP. The two peaks refer to TPP and PS molecules; TPP molecules attached to PS are probably not present since very high temperatures are investigated. In any case, two time constants can be extracted, which are shown in Figs. 5 and 9. Comparing different concentrations, some weak anti-plasticizer effect is observable in Fig. 8(b) for the high-frequency relaxation reflecting the dynamics of TPP.

In Fig. 9 we collect all the time constants obtained with the help of DS, NMR, DSC, and DLS experiments. Admittedly, the figure is quite “crowded,” but it reflects the rather complex dynamics in an asymmetric binary mixture. Again, for the sake of clarity the nominal concentrations are discussed (Table I); the color code defines the concentration, triangles and circles distinguish between α_1 - and α_2 -process, respectively. Clearly, for the α_2 -relaxation one can observe a

continuous crossover from super-Arrhenius to thermally activated behavior of the $\tau_2(T)$ when c_{TPP} is reduced.

Given the definition of T_g via $\tau_{1,2}(T_g) = 100$ s we derive two glass transition temperatures T_{g1} (associated with α_1 -relaxation) and T_{g2} (associated with α_2 -relaxation). The results are displayed in Fig. 10 (triangles: T_{g1} , circles: T_{g2} , cross: T_{g1} as obtained by the scaling procedure presented in Appendix A). While $T_{g1}(c_{TPP})$ decreases steadily from neat PS down to highly diluted PS due to the plasticizer effect, $T_{g2}(c_{TPP})$ is significantly lower and exhibits a maximum around $c_{TPP} = 35\%$. Up to our knowledge such relative maximum in $T_{g2}(c_{TPP})$ has not been reported before; actually it is a natural consequence of the ever-decreasing activation energy displayed by the Arrhenius straight lines in Fig. 9 at low concentrations. In contrast to previous reports^{14,17} we do not find any indications that there exists a concentration range in which only a single T_g is observed. The results at $c_{TPP} = 70\%$ still allow to extract two T_g . Moreover, the DLS spectra at $c_{TPP} = 90\%$ show two separate relaxation peaks (Fig. 8(b)). It appears that T_{g2} and T_{g1} approach each other at highest TPP concentrations, but can still be distinguished.

After having discussed the temperature dependence of the two relaxation processes (α_1 and α_2), we inspect in more detail the evolution of the spectral shapes of α_1 - and α_2 -process at different concentrations. As already mentioned, the spectra of α_1 -relaxation of the 10% and 20% mixtures, as well as the spectra of the α -relaxation of neat PS can be collapsed to provide a master curve when scaled to their maximum (Fig. 11(a), solid lines). Clearly, FTS is fulfilled, and each master curve can be interpolated with a Kohlrausch function (dashed lines). Obviously the α_1 -peak of the 10% data is more broadened ($\beta_K = 0.27$) than the α -peak of pure PS

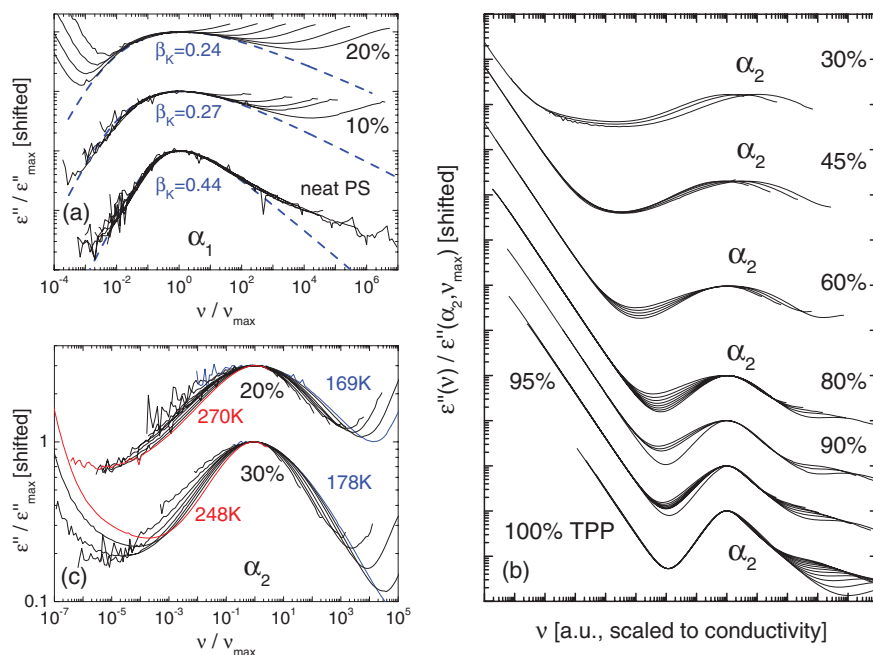


FIG. 11. (a) Master curves for the α_1 -relaxation peaks at different temperatures for 20% and 10% TPP in PS, and α -relaxation of neat PS (solid lines). For each system the susceptibility curves are scaled to the maximum; dashed lines: Kohlrausch interpolations with indicated stretching parameters. (b) Susceptibility data representing the α_2 -relaxation for mixtures with $c_{TPP} = 30\%$ – 95% and for neat TPP, scaled to maximum height and conductivity position. (c) α_2 -relaxation data of the 20% and 30% TPP/PS mixtures scaled to peak maximum. All panels: Sets of curves representing different concentrations are separated from each other by applying an arbitrary shift factor.

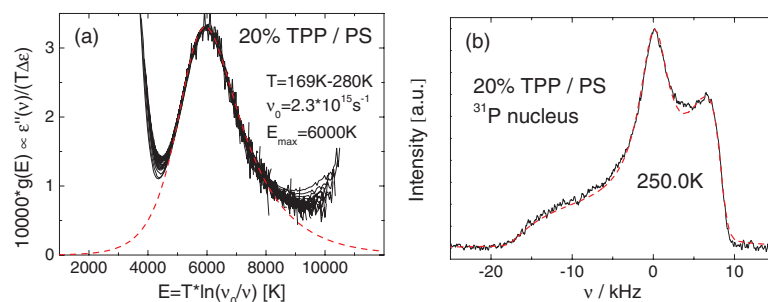


FIG. 12. (a) Results of the $g(E)$ -scaling of the α_2 -relaxation data for $T = 169$ – 280 K (solid lines, cf. text). Dashed line: fit to $g(E)$, function given in Ref. 65. (b) Solid line: ^{31}P NMR spectrum of the 20% sample at $T = 250$ K. Dashed line: weighted sum of a powder spectrum and a Lorentzian line, the latter representing isotropic molecular reorientation, fitted to the data.

($\beta_K = 0.44$). The α_1 -peak of the 20% data looks similar to the 10% peak, however, the stretching parameter is slightly more reduced ($\beta_K = 0.24$).

The situation is more complicated for the α_2 -relaxation. Figure 11(b) displays attempts to get master curves for $c_{\text{TPP}} = 30\%$ – 100% . Here, as a first step, the spectra are scaled vertically to their α_2 -maximum values. In a second step the resulting curves are shifted horizontally in order to match best in the region of the conductivity contribution. In the case of neat TPP one sees clearly that this procedure leads, in good approximation, also to a scaling of the complete α -relaxation, which is interfered only by the β -relaxation approaching the high-frequency side of the α -peak. From that we conclude, firstly, that the rotational correlation time is coupled to the time scale of the diffusive process causing ionic conductivity. Secondly, the relaxation peak of neat TPP obeys FTS in good approximation. For concentrations down to 60% a strong broadening of the master curve is observed, in accord with Fig. 3 and Fig. 16 in Appendix C. Additionally, a failure of FTS is recognized, yet at the high-frequency flank the curves still appear to scale. The broadening on the low-frequency side of the main relaxation peak reminds of super-cooled liquids in confinement.^{57,58} For $c_{\text{TPP}} \leq 60\%$ the peak position is fully decoupled from the conductivity time scale. In addition, FTS is hurt at low- as well as high-frequency flank (demonstrated for $c_{\text{TPP}} = 30\%$ in more detail in Fig. 11(c)), which is a signature well-known for a β -process.^{45,53,54} This is also reflected in the HN parameter $a(T)$ displayed in Fig. 17, Appendix D.

In accord with these findings the temperature dependence of the time constants $\tau_2(T)$ of the α_2 -processes show super-Arrhenius behavior at high concentrations and Arrhenius behavior at low concentrations (Figs. 5 and 9), i.e., strong failure of FTS and Arrhenius behavior of the time constants go together. This suggests to apply a scaling procedure, developed in the context of thermally activated dynamics as observed for β -relaxations,^{45,54,60–63} to the α_2 -relaxation at low concentrations. If thermally activated dynamics are determined by a broad (temperature independent) distribution of activation energies $g(E)$ (see also Ref. 64), the scaling law yields

$$g(E) = g(T \ln(\nu_0/\nu)) = \frac{2}{\pi} \frac{\epsilon''(\nu)}{T \Delta \epsilon}. \quad (2)$$

Since a possible distribution of attempt frequencies ν_0 has no strong influence as logarithmic scales are considered, a single ν_0 value (as fit parameter) allows for collapsing all spectra. In Fig. 12(a) the results of the scaling procedure applied to the α_2 -relaxation of the 20% TPP/PS mixture are shown. All datasets collapse onto a single master curve, which directly provides the activation energy distribution $g(E)$ of the thermally activated α_2 -process. The rescaled peaks can be interpolated by an asymmetric function introduced in Ref. 65 (dashed line in Fig. 12(a)), which finally yields the relaxation strength $\Delta \epsilon_2(T)$ displayed in Fig. 6.

It appears that the α_2 -process at low concentrations shows many features of a β -process which would imply that the reorientational process is not isotropic (as typical of a glass), but rather involves a spatially hindered motion as has been proven for a typical β -process.⁶⁶ However, as shown in Figure 12(b), the ^{31}P NMR spectrum of the $c_{\text{TPP}} = 20\%$ mixture recorded at $T = 250$ K ($< T_{g1} = 283$ K) shows, besides a solid-state spectrum, a Lorentzian central line originating from TPP molecules reorienting isotropically on a time scale shorter than, say $100 \mu\text{s}$. At the same time the PS molecules are immobilized since a temperature below T_{g1} is considered. Thus, the solid-state fraction in the NMR spectrum in Fig. 12(b) contains both slowly but isotropically reorienting TPP molecules involved in the broadly distributed α_2 -process, as well as a fraction of immobilized TPP molecules associated with the α_1 -process of PS. With the help of two-dimensional ^{31}P NMR it can be shown that essentially all TPP molecules involved in the α_2 -process reorient isotropically. Moreover, exchange between fast and slow α_2 -molecules is observed as will be discussed in Paper II.⁴⁷

IV. DISCUSSION AND CONCLUSIONS

By combining the results of different methods and covering the full concentration range we reveal the dynamics of both components in an asymmetric binary mixture, which actually discloses a rather complex scenario not fully clarified before. Two glass transition temperatures T_{g1} and T_{g2} are found for all concentrations, a behavior now well established for binary liquids.^{20–25} There are no indications that the mixture becomes dynamically homogeneous in the sense that only a single T_g is observed beyond some concentration, a

scenario suggested previously.^{17,28} As demonstrated by light scattering experiments even at 90% TPP in PS two separate relaxation peaks are observed (Fig. 8(b)).

As already reported by Blochowicz and co-workers^{13,17} and overlooked in previous reports, in such asymmetric mixtures there exist two relaxation processes of the low- T_g component (α_1 and α_2). They are attributed, in the present case, to two different sub-ensembles of TPP molecules. One is involved in the (slow) dynamics of the high- T_g component PS (α_1 -process), another performs faster, highly decoupled dynamics in the more or less immobilized PS matrix (including the α_1 fraction of TPP). ³¹P NMR demonstrates that the α_2 -process involves isotropic reorientations of at least most TPP molecules within a broad distribution $G(\ln\tau)$. At low concentrations $G(\ln\tau)$ of the α_2 -process can be mapped to a temperature independent distribution of activation energies $g(E)$, which corresponds to a strong failure of FTS; then its mean correlation time $\tau_2(T)$ displays an Arrhenius temperature dependence. In spite of the isotropic liquid-like nature of the motion, the dynamics shows features which can easily be confused with those of a secondary (β -) process. In particular, its mean activation energy ($E_A(10\%) = 5241 \text{ K} \approx 17T_{g1}$) is typical for β -processes. When concentration is increased, $\tau_2(T)$ of the isotropic motion of the α_2 -sub-ensemble displays a monotonic transition from a strong to a fragile temperature dependence.

In accordance with Blochowicz *et al.*^{13,17} we take the low-concentration behavior of the TPP molecules contributing to the α_2 -process as a signature of intrinsic confinement effects exerted by the rigid PS matrix. NMR^{28,30} spectra reported for binary glass formers as well as dielectric^{13,17} spectra of their α_2 -process resemble those found in neat glass formers confined in porous systems.^{33,34,57,59} For example, “lubricated” pores lead to a flattening of the low-frequency part of the α -relaxation,^{57,58} similar to what is found for the α_2 -relaxation at high TPP concentrations in Fig. 11(b). The spectra typical for confined systems have been explained in accordance with simulation work^{58,67} by assuming a spatial gradient of dynamics, i.e., a distribution of T_g or, more precisely, a distribution $G(\ln\tau)$ induced by an interaction of the pore walls with the contained liquid up to a certain penetration length. For many liquids under confinement molecular slowing down is observed at the pore walls, and simulations suggest that the penetration length increases with lowering temperature.⁶⁸ In that sense PS could provide a confinement for the TPP molecules which becomes “hard” below T_{g1} . The higher the concentration, the more TPP molecules are beyond the influence of the confinement effect of the PS matrix, and the dynamics becomes similar to that of neat glass formers. In contrast, at low concentrations most TPP molecules are controlled by an immobilized polymer, which causes a broad distribution of activation energies of liquid-like (isotropic) motion. It shall be noted at this point that dynamical exchange is observed within the (broadly distributed) α_2 -dynamics. This will be discussed in detail in Paper II.⁴⁷

Regarding the fraction of TPP molecules involved in the dynamics of PS (α_1 -process), they become isotropic only when the primary process of the PS matrix sets in. Their relaxation characteristics are similar to those of PS itself, e.g., FTS

applies. The α_1 -fraction of TPP molecules increases when the overall TPP concentration is reduced. If only few TPP molecules are added to the PS sample ($c_{TPP} \rightarrow 0$), it appears that the molecules preferably become associated to the matrix. Figure 7 suggests that beyond a certain threshold the matrix sites appear to “saturate,” i.e., no more additive molecules are incorporated in the α_1 -process. One consequence of this interpretation is that the TPP molecules still may act as a probe for the matrix dynamics, but only in the case of low TPP concentrations. When the TPP content is increased beyond a certain level, the overall TPP dynamics become bimodal and highly heterogeneous, and the α_1 -relaxation is difficult to identify in the dielectric spectra. The situation is improved when the T_g contrast is high.¹⁷ We note that the existence of two different sub-ensembles of additive molecules may also be related to phenomena observed for gas transport in polymers, for which a dual mode sorption model has been proposed.⁶⁹ Above T_{g1} the fraction of the TPP molecules associated with PS decreases with increasing temperature until at some temperature T_c all α_1 -TPP molecules have disappeared. Such behavior has been interpreted in the frameworks of MCT.¹³ While the high- T_g component undergoes a normal glass transition (type-B scenario), a localization transition (type-A scenario) appears for the low- T_g component at lower temperatures. In the present case, the temperature dependent fraction of TPP molecules associated with the slow dynamics of PS may be taken as a measure of the non-ergodicity parameter, which decreases continuously and finally becomes zero at a critical temperature T_c . It remains an experimental challenge to show that the translational diffusion involved in the α_2 -process indeed is sub-diffusive as suggested by simulations^{35–37} and MCT.^{38–40}

ACKNOWLEDGMENTS

Financial support by Deutsche Forschungsgemeinschaft (DFG) through Project Nos. RO 907/10 and RO 907/11 is acknowledged. The authors thank Ute Kuhn, Lehrstuhl für Polymere Werkstoffe, Universität Bayreuth, for her assistance in performing the DSC measurements.

APPENDIX A: ESTIMATION OF RELAXATION STRENGTHS FOR THE 20% SAMPLE

In the case of the 20% mixture both relaxations (α_1 and α_2) are well resolved and an unusual temperature dependence is observed, which is important to be estimated appropriately. Figure 13 shows again the data of the 20% mixture already displayed in Fig. 4(b), now on linear scale. By using the activation energy scaling results (Fig. 12(a)), i.e., $\Delta\epsilon_2(T)$ and its extrapolation to higher temperatures (dashed line in Fig. 6), susceptibility curves are calculated from $g(E)$ along Eq. (2) for the α_2 -peaks (dashed lines in Fig. 13). Good correspondence with the measured α_2 -data is found for $T = 169$ – 280 K. In the temperature range $T = 290$ – 330 K the α_1 -process is well recognized in the accessible frequency window; still a strong influence of the α_2 -contribution is anticipated at high

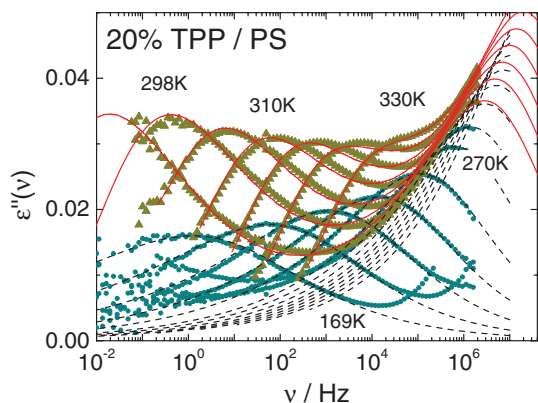


FIG. 13. Data from Fig. 4(b); triangles: α_1 -relaxation for $T = 290$ – 330 K, circles: α_2 -relaxation for $T = 169$ – 280 K. Dashed lines: α_2 -contributions calculated from the $g(E)$ scaling result shown in Fig. 12(a) along Eq. (2). Solid lines: fits (cf. text).

frequencies. In this temperature range, each spectrum was fitted with the sum of a Kohlrausch function with $\beta_K(T) = 0.28$ – 0.38 and the corresponding (fixed) α_2 -contribution calculated from the temperature independent $g(E)$. The results (solid red lines in Fig. 13) agree with the data. Resulting time constants τ_1 , as well as $\tau_{2,calc} = (1/2\pi\nu_0)\exp(E_{max}/T)$ calculated with $E_{max} = 6000$ K and $\nu_0 = 2.3 \times 10^{15} \text{ s}^{-1}$ (Fig. 12(a)), are included in Fig. 5 (crosses). Good correspondence with the experimental τ_2 as well as, respectively, the τ_1 yielded by the direct fitting analysis of the α_1 -peak (Secs. II B and III B), is observed. The resulting relaxation strengths $\Delta\epsilon_1(T)$ are included in Fig. 6 (open triangles).

APPENDIX B: REVEALING THE α_1 -PROCESS AT INTERMEDIATE CONCENTRATIONS

Figure 14 shows dielectric data for the (a) 30% and (b) 45% TPP/PS mixtures. In contrast to the 10% and 20% data (Fig. 4) only one relaxation peak is explicitly observable. Note that between 30% and 100% TPP only a single peak is observed in the susceptibility (besides the β -process; cf. Appendix C), and with higher concentrations this peak increases further in amplitude and develops continuously into the α -process of neat TPP. In the case of the 30% and 45% mixtures still traces of the α_1 -relaxations can be identified.

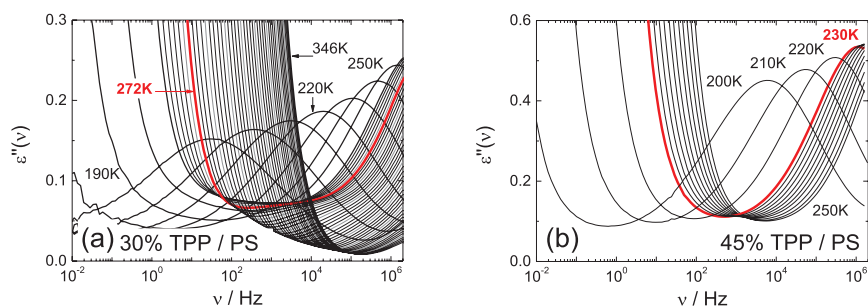


FIG. 14. Dynamic susceptibility data of TPP/PS mixtures. (a) 30% TPP in PS, $T = 190$ – 260 K in 10 K steps and $T = 262$ – 346 K in 2 K steps. (b) 45% TPP in PS, $T = 200$ – 230 K in 10 K steps and $T = 232$ – 250 K in 2 K steps.

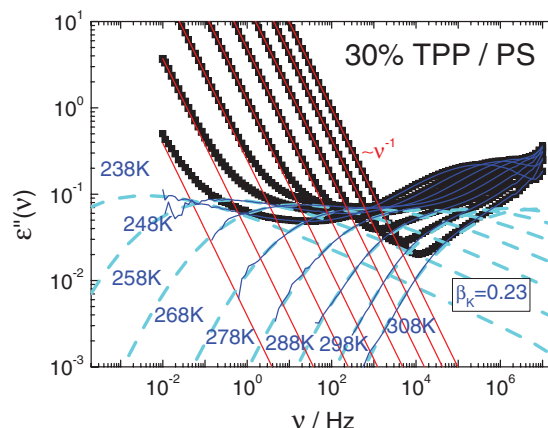


FIG. 15. Susceptibility of the $c_{TPP} = 30\%$ sample (squares). Red lines: conductivity contribution. Blue lines: susceptibility after subtracting conductivity contribution. Dashed lines: Kohlrausch functions with $\beta_K = 0.23$.

By plotting the data on linear scale, one can infer from Fig. 14(a) that a very broad minimum is located between conductivity and α_2 -peak. When temperature is increased beyond about 272 K up to 346 K the initially broad minimum becomes narrower and decreases its amplitude. A similar, yet weaker effect is observed for $c_{TPP} = 45\%$ between $T = 230$ K and 250 K (Fig. 14(b)). Since in the case of the 10% and 20% mixtures a decrease of $\Delta\epsilon_1(T)$ with increasing T is observed, we speculate that the decreasing minimum reflects a hidden α_1 -relaxation peak.

In order to reveal the α_1 -relaxation peak, the conductivity contribution has to be subtracted. This allows for estimating relaxation time and strength. In Fig. 15 this is demonstrated exemplarily for the susceptibility data of the 30% sample; for the 45% data a similar procedure was applied. The resulting $\tau_1(T)$ correspond well with the NMR findings (Fig. 5).

APPENDIX C: FURTHER SUSCEPTIBILITY DATA

Fig. 16 shows further spectra for the mixtures with the TPP concentrations $c_{TPP} = 60\%$, 80% , 95% . At these high concentrations no reasonable estimation of the dielectric time constant τ_1 of the α_1 -relaxation is possible any more.

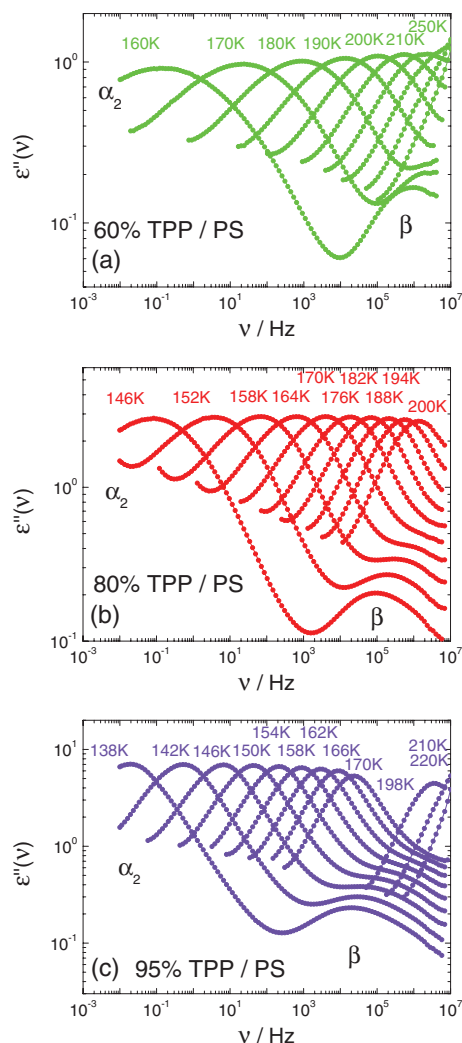


FIG. 16. Susceptibility spectra of mixtures with a TPP concentration of (a) $c_{\text{TPP}} = 60\%$, (b) $c_{\text{TPP}} = 80\%$, and (c) $c_{\text{TPP}} = 95\%$.

APPENDIX D: LINE SHAPE PARAMETERS OF THE α_2 -PROCESS AT HIGH CONCENTRATIONS

As is demonstrated in Fig. 11(b), at high TPP concentrations the main temperature effect regarding the shape of the spectra is a broadening on the low-frequency flank of the α_2 -

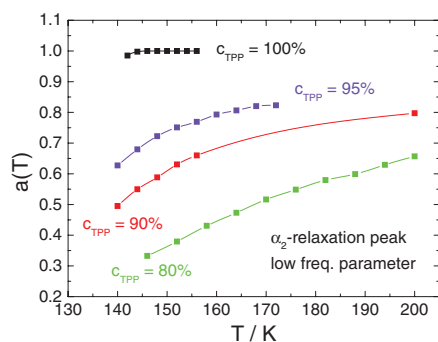


FIG. 17. Havriliak-Negami fit parameter $a(T)$, representing the low frequency exponent of the α_2 -relaxation peak, for several concentrations. Lines: guides for the eye.

relaxation upon cooling. This is also reflected in the shape parameters of the α_2 -peak as obtained by fits with the Havriliak-Negami function. In Fig. 17 the temperature dependence of the HN parameter a is displayed for several concentrations. In all cases the strong temperature dependence observed at low temperatures seems to disappear at high temperatures, although a Cole-Davidson behavior with low-frequency exponent 1 cannot be inferred. Yet, one may speculate that the spectral shape does not change any longer at high temperatures, i.e., here FTS applies also for the α_2 -process.

- ¹P. Lunkenheimer, U. Schneider, R. Brand, and A. Loidl, *Contemp. Phys.* **41**, 15 (2000).
- ²K. Binder and W. Kob, *Glassy Materials and Disordered Solids* (World Scientific, New Jersey, 2005).
- ³A. Brodin, C. Gainaru, V. Porokhonsky, and E. A. Rössler, *J. Phys.: Condens. Matter* **19**, 205104 (2007).
- ⁴L. Berthier and G. Biroli, *Rev. Mod. Phys.* **83**, 587 (2011).
- ⁵M. D. Ediger and P. Harrowell, *J. Chem. Phys.* **137**, 080901 (2012).
- ⁶R. Richert, in *Structural Glasses and Supercooled Liquids*, edited by P. G. Wolynes and V. Lubchenko (Wiley, Hoboken, 2012), p. 1.
- ⁷N. Petzold, B. Schmidtke, R. Kahlau, D. Bock, R. Meier, B. Micko, D. Kruk, and E. A. Rössler, *J. Chem. Phys.* **138**, 12A510 (2013).
- ⁸P. J. Hains and G. Williams, *Polymer* **16**, 725 (1975).
- ⁹M. A. Desando, S. Walker, and W. H. Baarschers, *J. Chem. Phys.* **73**, 3460 (1980).
- ¹⁰M. Scandola, G. Ceccorulli, and M. Pizzoli, *Polymer* **28**, 2081 (1987).
- ¹¹M. Nakazawa, O. Urakawa, and K. Adachi, *Macromolecules* **33**, 7898 (2000).
- ¹²D. Cangialosi, A. Alegría, and J. Colmenero, *J. Chem. Phys.* **126**, 204904 (2007).
- ¹³T. Blochowicz, S. Schramm, S. Lusceac, M. Vogel, B. Stühn, P. Gutfreund, and B. Frick, *Phys. Rev. Lett.* **109**, 035702 (2012).
- ¹⁴T. Blochowicz and E. A. Rössler, *Phys. Rev. Lett.* **92**, 225701 (2004).
- ¹⁵K. Kessairi, S. Capaccioli, D. Prevosto, M. Lucchesi, and P. Rolla, *J. Chem. Phys.* **127**, 174502 (2007).
- ¹⁶S. Capaccioli, K. Kessairi, M. Shahin, D. Prevosto, and M. Lucchesi, *J. Non-Cryst. Solids* **357**, 251 (2011).
- ¹⁷T. Blochowicz, S. A. Lusceac, P. Gutfreund, S. Schramm, and B. Stühn, *J. Phys. Chem. B* **115**, 1623 (2011).
- ¹⁸D. Cangialosi, A. Alegría, and J. Colmenero, *J. Chem. Phys.* **128**, 224508 (2008).
- ¹⁹T. P. Lodge, E. R. Wood, and J. C. Haley, *J. Polym. Sci., Part B: Polym. Phys.* **44**, 756 (2006).
- ²⁰K. Adachi and Y. Ishida, *Polym. J.* **11**, 233 (1979).
- ²¹D. A. Savin, A. M. Larson, and T. P. Lodge, *J. Polym. Sci., Part B: Polym. Phys.* **42**, 1155 (2004).
- ²²Y. Miwa, K. Usami, K. Yamamoto, M. Sakaguchi, M. Sakai, and S. Shimada, *Macromolecules* **38**, 2355 (2005).
- ²³J. E. G. Lipson and S. T. Milner, *J. Polym. Sci., Part B: Polym. Phys.* **44**, 3528 (2006).
- ²⁴A. N. Gaikwad, E. R. Wood, T. Ngai, and T. P. Lodge, *Macromolecules* **41**, 2502 (2008).
- ²⁵S. Schramm, T. Blochowicz, E. Gouirand, R. Wipf, B. Stühn, and Y. Chushkin, *J. Chem. Phys.* **132**, 224505 (2010).
- ²⁶H. Sillescu, *J. Non-Cryst. Solids* **243**, 81 (1999).
- ²⁷M. D. Ediger, *Annu. Rev. Phys. Chem.* **51**, 99 (2000).
- ²⁸T. Blochowicz, C. Karle, A. Kudlik, P. Medick, I. Roggatz, M. Vogel, C. Tschirwitz, J. Wolber, J. Senker, and E. Rössler, *J. Phys. Chem. B* **103**, 4032 (1999).
- ²⁹M. Vogel and E. Rössler, *J. Phys. Chem. A* **102**, 2102 (1998).
- ³⁰D. Bingemann, N. Wirth, J. Gmeiner, and E. A. Rössler, *Macromolecules* **40**, 5379 (2007).
- ³¹S. A. Lusceac, C. Koplin, P. Medick, M. Vogel, N. Brodie-Linder, C. LeQuellec, C. Alba-Simionesco, and E. A. Rössler, *J. Phys. Chem. B* **108**, 16601 (2004).
- ³²M. Vogel, P. Medick, and E. A. Rössler, *Annu. Rep. NMR Spectrosc.* **56**, 231 (2005).
- ³³S. Grädmann, P. Medick, and E. A. Rössler, *J. Phys. Chem. B* **113**, 8443 (2009).
- ³⁴M. Vogel, *Eur. Phys. J.: Spec. Top.* **189**, 47 (2010).

- ³⁵T. Voigtmann and J. Horbach, *Phys. Rev. Lett.* **103**, 205901 (2009).
- ³⁶K. Kim, K. Miyazaki, and S. Saito, *Eur. Phys. J.: Spec. Top.* **189**, 135 (2010).
- ³⁷J. Kurzidim, D. Coslovich, and G. Kahl, *J. Phys.: Condens. Matter* **23**, 234122 (2011).
- ³⁸J. Bosse and Y. Kaneko, *Phys. Rev. Lett.* **74**, 4023 (1995).
- ³⁹V. Krakoviack, *Phys. Rev. E* **79**, 061501 (2009).
- ⁴⁰S. Lang, R. Schilling, V. Krakoviack, and T. Franosch, *Phys. Rev. E* **86**, 021502 (2012).
- ⁴¹T. Voigtmann, *Euro. Phys. Lett.* **96**, 36006 (2011).
- ⁴²R. Kant, S. K. Kumar, and R. H. Colby, *Macromolecules* **36**, 10087 (2003).
- ⁴³J. Colmenero and A. Arbe, *Soft Matter* **3**, 1474 (2007).
- ⁴⁴T. P. Lodge and T. C. B. McLeish, *Macromolecules* **33**, 5278 (2000).
- ⁴⁵D. Bock, R. Kahlau, B. Micko, B. Pötzschner, G. J. Schneider, and E. A. Rössler, *J. Chem. Phys.* **139**, 064508 (2013).
- ⁴⁶S. Adishchev, D. Bock, C. Gainaru, R. Kahlau, B. Micko, N. Petzold, B. Pötzschner, and E. A. Rössler, *Z. Phys. Chem.* **226**, 1149 (2012).
- ⁴⁷D. Bock, R. Kahlau, B. Pötzschner, T. Körber, E. Wagner, and E. A. Rössler, "Dynamics of asymmetric binary glass formers. II. Results from nuclear magnetic resonance spectroscopy," *J. Chem. Phys.* (submitted).
- ⁴⁸H. Wagner and R. Richert, *J. Phys. Chem. B* **103**, 4071 (1999).
- ⁴⁹J. Wiedersich, N. V. Surovtsev, V. N. Novikov, and E. Rössler, *Phys. Rev. B* **64**, 064207 (2001).
- ⁵⁰N. Petzold and E. A. Rössler, *J. Chem. Phys.* **133**, 124512 (2010).
- ⁵¹I. M. Hodge, *J. Non-Cryst. Solids* **169**, 211 (1994).
- ⁵²J. Hintermeyer, A. Herrmann, R. Kahlau, C. Goiceanu, and E. A. Rössler, *Macromolecules* **41**, 9335 (2008).
- ⁵³A. Kudlik, S. Benkhof, T. Blochowicz, C. Tschirwitz, and E. Rössler, *J. Mol. Struct.* **479**, 201 (1999).
- ⁵⁴R. Kahlau, T. Dörfler, and E. A. Rössler, *J. Chem. Phys.* **139**, 134504 (2013).
- ⁵⁵Y. He, T. R. Lutz, M. D. Ediger, C. Ayyagari, D. Bedrov, and G. D. Smith, *Macromolecules* **37**, 5032 (2004).
- ⁵⁶C. Tschirwitz, S. Benkhof, T. Blochowicz, and E. Rössler, *J. Chem. Phys.* **117**, 6281 (2002).
- ⁵⁷M. Arndt, R. Stannarius, H. Groothues, E. Hempel, and F. Kremer, *Phys. Rev. Lett.* **79**, 2077 (1997).
- ⁵⁸P. Scheidler, W. Kob, and K. Binder, *Europhys. Lett.* **59**, 701 (2002).
- ⁵⁹G. Dosseh, C. Le Quellec, N. Brodie-Linder, C. Alba-Simionesco, W. Haeussler, and P. Levitz, *J. Non-Cryst. Solids* **352**, 4964 (2006).
- ⁶⁰K. S. Gilroy and W. A. Phillips, *Philos. Mag. B* **43**, 735 (1981).
- ⁶¹J. Wiedersich, S. V. Adichtchev, and E. Rössler, *Phys. Rev. Lett.* **84**, 2718 (2000).
- ⁶²L. Wu and S. R. Nagel, *Phys. Rev. B* **46**, 11198 (1992).
- ⁶³C. Gainaru, R. Böhmer, R. Kahlau, and E. Rössler, *Phys. Rev. B* **82**, 104205 (2010).
- ⁶⁴C. J. F. Böttcher and P. Bordewijk, *Theory of Electric Polarization: Dielectrics in Time-Dependent Fields* (Elsevier, Amsterdam, 1978), Vol. 2.
- ⁶⁵T. Blochowicz, C. Tschirwitz, S. Benkhof, and E. A. Rössler, *J. Chem. Phys.* **118**, 7544 (2003).
- ⁶⁶M. Vogel, C. Tschirwitz, G. Schneider, C. Koplin, P. Medick, and E. Rössler, *J. Non-Cryst. Solids* **307–310**, 326 (2002).
- ⁶⁷P. Scheidler, W. Kob, and K. Binder, *Europhys. Lett.* **52**, 277 (2000).
- ⁶⁸P. Scheidler, W. Kob, and K. Binder, *J. Phys. Chem. B* **108**, 6673 (2004).
- ⁶⁹J. H. Petropoulos, "Mechanisms and theories for sorption and diffusion of gases in polymers," in *Polymeric Gas Separation Membranes*, edited by D. R. Paul and Y. P. Yampol'skii (CRC Press, Boca Raton, FL, 1994).

Bibliography

- [1] K. ADACHI, H. SUGA, S. SEKI, S. KUBOTA, S. YAMAGUCHI, O. YANO, and Y. WADA, *Molecular Crystals and Liquid Crystals* **18**, 345 (1972).
- [2] J. P. AMOUREUX, G. NOYEL, M. FOULON, M. BÉE, and L. JORAT, *Molecular Physics* **52**, 161 (1984).
- [3] R. BRAND, P. LUNKENHEIMER, and A. LOIDL, *Physical Review B* **56**, R5713 (1997).
- [4] S. BENKHOF, A. KUDLIK, T. BLOCHOWICZ, and E. RÖSSLER, *Journal of Physics: Condensed Matter* **10**, 8155 (1998).
- [5] R. BRAND, P. LUNKENHEIMER, U. SCHNEIDER, and A. LOIDL, *Physical Review Letters* **82**, 1951 (1999).
- [6] P. LUNKENHEIMER, R. BRAND, U. SCHNEIDER, and A. LOIDL, *Philosophical Magazine Part B* **79**, 1945 (1999).
- [7] S. BENKHOF, T. BLOCHOWICZ, A. KUDLIK, C. TSCHIRWITZ, and E. RÖSSLER, *Ferroelectrics* **236**, 193 (2000).
- [8] R. BRAND, P. LUNKENHEIMER, and A. LOIDL, *The Journal of Chemical Physics* **116**, 10386 (2002).
- [9] M. DESCAMPS, N. T. CORREIA, P. DEROLLEZ, F. DANEDE, and F. CAPET, *The Journal of Physical Chemistry B* **109**, 16092 (2005).
- [10] M. KLIMAKOW, J. LEITERER, J. KNEIPP, E. RÖSSLER, U. PANNE, K. RADEMAN, and F. EMMERLING, *Langmuir* **26**, 11233 (2010).
- [11] W. GÖTZE, *Complex Dynamics of Glass-Forming Liquids - A Mode-Coupling Theory*, Oxford University Press, New York, 2009.
- [12] H. Z. CUMMINS, G. LI, W. M. DU, and J. HERNANDEZ, *Physica A: Statistical Mechanics and its Applications* **204**, 169 (1994).
- [13] A. KUDLIK, *Dielektrische Spektroskopie an organischen Glasbildnern – ein Beitrag zur Linienform der dynamischen Suszeptibilität*, PhD thesis, Universität Bayreuth, 1997.

- [14] D. KRUK, A. HERRMANN, and E. A. RÖSSLER, *Progress in Nuclear Magnetic Resonance Spectroscopy* **63**, 33 (2012).
- [15] P. LUNKENHEIMER, U. SCHNEIDER, R. BRAND, and A. LOIDL, *Contemporary Physics* **41**, 15 (2000).
- [16] J. L. YARNELL, M. J. KATZ, R. G. WENZEL, and S. H. KOENIG, *Physical Review A* **7**, 2130 (1973).
- [17] E. DONT, *The Glass Transition - Relaxation Dynamics in Liquids and Disordered Materials*, Springer, Berlin, Heidelberg, 2001.
- [18] C. A. ANGELL, K. L. NGAI, G. B. MCKENNA, P. F. McMILLAN, and S. W. MARTIN, *Journal of Applied Physics* **88**, 3113 (2000).
- [19] P. LUNKENHEIMER and A. LOIDL, *Chemical Physics* **284**, 205 (2002).
- [20] H. WAGNER and R. RICHERT, *The Journal of Physical Chemistry B* **103**, 4071 (1999).
- [21] D. BINGEMANN, N. WIRTH, J. GMEINER, and E. A. RÖSSLER, *Macromolecules* **40**, 5379 (2007).
- [22] I. GUTZOW and J. SCHMELZER, *The Vitreous State*, Springer, Berlin, 1995.
- [23] W. KAUZMANN, *Chemical Reviews* **43**, 219 (1948).
- [24] C. A. ANGELL and J. C. TUCKER, *The Journal of Physical Chemistry* **78**, 278 (1974).
- [25] K. BINDER and W. KOB, *Glassy Materials and Disordered Solids – An Introduction to Their Statistical Mechanics*, World Scientific Publishing Co. Pte. Ltd., Singapore, 2005.
- [26] M. D. EDIGER and P. HARROWELL, *The Journal of Chemical Physics* **137**, 080901 (2012).
- [27] E. RÖSSLER, M. TAUPITZ, and H. M. VIETH, *Journal of Physical Chemistry* **94**, 6879 (1990).
- [28] P. N. PUSEY and W. VAN MEGEN, *Nature* **320**, 340 (1986).
- [29] P. N. PUSEY and W. VAN MEGEN, *Physical Review Letters* **59**, 2083 (1987).
- [30] W. KOB and H. C. ANDERSEN, *Physical Review E* **51**, 4626 (1995).
- [31] W. KOB and H. C. ANDERSEN, *Physical Review E* **52**, 4134 (1995).

- [32] A. ARBE, D. RICHTER, J. COLMENERO, and B. FARAGO, *Physical Review E* **54**, 3853 (1996).
- [33] F. MEZEI, W. KNAAK, and B. FARAGO, *Physical Review Letters* **58**, 571 (1987).
- [34] J. WUTTKE, I. CHANG, O. RANDL, F. FUJARA, and W. PETRY, *Physical Review E* **54**, 5364 (1996).
- [35] T. BLOCHOWICZ, S. SCHRAMM, S. LUSCEAC, M. VOGEL, B. STÜHN, P. GUTFREUND, and B. FRICK, *Physical Review Letters* **109**, 035702 (2012).
- [36] N. PETZOLD, B. SCHMIDTKE, R. KAHLAU, D. BOCK, R. MEIER, B. MICKO, D. KRUK, and E. A. RÖSSLER, *The Journal of Chemical Physics* **138**, 12A510 (2013).
- [37] H. CUMMINS, G. LI, W. DU, R. PICK, and C. DREYFUS, *Physical Review E* **53**, 896 (1996).
- [38] M. D. EDIGER, *Annual Review of Physical Chemistry* **51**, 99 (2000).
- [39] R. RICHERT, *Journal of Physics: Condensed Matter* **14**, R703 (2002).
- [40] L. BERTHIER, *Physics* **4** (2011).
- [41] L. BERTHIER and G. BIROLI, *Reviews of Modern Physics* **83**, 587 (2011).
- [42] E. RUSSELL, N. ISRAELOFF, L. WALTHER, and H. ALVAREZ GOMARIZ, *Physical Review Letters* **81**, 1461 (1998).
- [43] E. V. RUSSELL and N. ISRAELOFF, *Nature* **408**, 695 (2000).
- [44] T. BLOCHOWICZ, *Broadband Dielectric Spectroscopy in Neat and Binary Molecular Glass Formers – Frequency and Time Domain Spectroscopy, Non-Resonant Spectral Hole Burning*, PhD thesis, Universität Bayreuth, 2003.
- [45] T. BLOCHOWICZ and E. A. RÖSSLER, *The Journal of Chemical Physics* **122**, 224511 (2005).
- [46] E. RÖSSLER, *Physical Review Letters* **65**, 1595 (1990).
- [47] M. D. EDIGER, P. HARROWELL, and L. YU, *The Journal of Chemical Physics* **128**, 034709 (2008).
- [48] M. K. MAPES, S. F. SWALLEN, and M. D. EDIGER, *The Journal of Physical Chemistry B* **110**, 507 (2006).
- [49] D. EHLICH and H. SILLESCU, *Macromolecules* **23**, 1600 (1990).

- [50] F. STICKEL, F. KREMER, and E. FISCHER, *Physica A: Statistical Mechanics and its Applications* **201**, 318 (1993).
- [51] F. STICKEL, E. W. FISCHER, and R. RICHERT, *The Journal of Chemical Physics* **104**, 2043 (1996).
- [52] C. J. F. BOETTCHER and P. BORDEWIJK, *Theory of Electric Polarization - Dielectrics in Time-Dependent Fields*, volume II, Elsevier Scientific Publishing Company, Amsterdam; Oxford; New York, 1978.
- [53] C. P. GAINARU, *Dielectric Properties of Molecular Glass Formers; from the Liquid State to the Tunneling Regime*, PhD thesis, Universität Bayreuth, 2008.
- [54] G. WILLIAMS, M. COOK, and P. J. HAINS, *Journal of the Chemical Society, Faraday Transactions II* **68**, 1045 (1972).
- [55] F. SCHWABL, *Statistische Mechanik*, Springer, Berlin, Heidelberg, New York, 2006.
- [56] N. WIENER, *Acta Mathematica* **55**, 117 (1930).
- [57] A. KHINTCHINE, *Mathematische Annalen* **109**, 604 (1934).
- [58] T. BLOCHOWICZ, A. KUDLIK, S. BENKHOF, J. SENKER, E. RÖSSLER, and G. HINZE, *The Journal of Chemical Physics* **110**, 12011 (1999).
- [59] N. E. ISRAELOFF, *Physical Review B* **53**, 11913 (1996).
- [60] N. E. ISRAELOFF and X. WANG, *Review of Scientific Instruments* **68**, 1543 (1997).
- [61] H. FRÖHLICH, *Theory of dielectrics - Dielectric constant and dielectric loss*, Clarendon Pr., Oxford, 1958.
- [62] F. KREMER and A. SCHÖNALS, *Broadband Dielectric Spectroscopy*, Springer, Berlin, Heidelberg, New York, 2003.
- [63] L. ONSAGER, *Journal of the American Chemical Society* **58**, 1486 (1936).
- [64] C. GAINARU, O. LIPS, A. TROSHAGINA, R. KAHLAU, A. BRODIN, F. FUJARA, and E. A. RÖSSLER, *The Journal of Chemical Physics* **128**, 174505 (2008).
- [65] T. BLOCHOWICZ, C. TSCHIRWITZ, S. BENKHOF, and E. A. RÖSSLER, *The Journal of Chemical Physics* **118**, 7544 (2003).
- [66] P. DEBYE, *Verhandlungen der Deutschen Physikalischen Gesellschaft* **15**, 777 (1913).

- [67] P. DEBYE, *Polare Molekeln*, S. Hirzel, Leipzig, 1929.
- [68] C. GAINARU, R. MEIER, S. SCHILDMANN, C. LEDERLE, W. HILLER, E. A. RÖSSLER, and R. BÖHMER, *Physical Review Letters* **105** (2010).
- [69] C. GAINARU, S. KASTNER, F. MAYR, P. LUNKENHEIMER, S. SCHILDMANN, H. J. WEBER, W. HILLER, A. LOIDL, and R. BÖHMER, *Physical Review Letters* **107** (2011).
- [70] U. KAATZE, R. BEHRENDTS, and R. POTTEL, *Journal of Non-Crystalline Solids* **305**, 19 (2002).
- [71] C. GAINARU, A. RIVERA, S. PUTSELYK, G. ESKA, and E. RÖSSLER, *Physical Review B* **72**, 174203 (2005).
- [72] U. SCHNEIDER, P. LUNKENHEIMER, R. BRAND, and A. LOIDL, *Journal of Non-Crystalline Solids* **235-237**, 173 (1998).
- [73] S. ADICHTCHEV, T. BLOCHOWICZ, C. GAINARU, V. N. NOVIKOV, E. A. RÖSSLER, and C. TSCHIRWITZ, *Journal of Physics: Condensed Matter* **15**, S835 (2003).
- [74] K. NGAI, *Journal of Non-Crystalline Solids* **275**, 7 (2000).
- [75] A. KUDLIK, S. BENKHOF, T. BLOCHOWICZ, C. TSCHIRWITZ, and E. RÖSSLER, *Journal of Molecular Structure* **479**, 201 (1999).
- [76] C. GAINARU, A. BRODIN, V. N. NOVIKOV, and E. A. RÖSSLER, *arXiv:condmat/0604597* (2006).
- [77] C. TSCHIRWITZ, S. BENKHOF, T. BLOCHOWICZ, and E. RÖSSLER, *The Journal of Chemical Physics* **117**, 6281 (2002).
- [78] A. KUDLIK, C. TSCHIRWITZ, T. BLOCHOWICZ, S. BENKHOF, and E. RÖSSLER, *Journal of Non-Crystalline Solids* **235-237**, 406 (1998).
- [79] T. BLOCHOWICZ, C. GAINARU, P. MEDICK, C. TSCHIRWITZ, and E. A. RÖSSLER, *The Journal of Chemical Physics* **124**, 134503 (2006).
- [80] P. DIXON, L. WU, S. NAGEL, B. WILLIAMS, and J. CARINI, *Physical Review Letters* **65**, 1108 (1990).
- [81] N. MENON, K. P. O'BRIEN, P. K. DIXON, L. WU, S. R. NAGEL, B. D. WILLIAMS, and J. P. CARINI, *Journal of Non-Crystalline Solids* **141**, 61 (1992).
- [82] L. WU, P. K. DIXON, S. R. NAGEL, B. D. WILLIAMS, and J. P. CARINI, *Journal of Non-Crystalline Solids* **131**, 32 (1991).

- [83] A. KUDLIK, S. BENKHOF, R. LENK, and E. RÖSSLER, *Europhysics Letters* **32**, 511 (1995).
- [84] A. KUDLIK, T. BLOCHOWICZ, S. BENKHOF, and E. RÖSSLER, *Europhysics Letters* **36**, 475 (1996).
- [85] N. OLSEN, T. CHRISTENSEN, and J. DYRE, *Physical Review Letters* **86**, 1271 (2001).
- [86] A. BRODIN, C. GAINARU, V. POROKHONSKYY, and E. A. RÖSSLER, *Journal of Physics: Condensed Matter* **19**, 205104 (2007).
- [87] S. CAPACCIOLI, M. SHAHIN THAYYIL, and K. L. NGAI, *The Journal of Physical Chemistry B* **112**, 16035 (2008).
- [88] T. GNUTZMANN, R. KAHLAU, S. SCHEIFLER, F. FRIEDRICHS, E. A. RÖSSLER, K. RADEMANN, and F. EMMERLING, *CrystEngComm* **15**, 4062 (2013).
- [89] G. P. JOHARI and M. GOLDSTEIN, *The Journal of Chemical Physics* **53**, 2372 (1970).
- [90] M. VOGEL and E. RÖSSLER, *The Journal of Chemical Physics* **114**, 5802 (2001).
- [91] M. VOGEL and E. RÖSSLER, *The Journal of Chemical Physics* **115**, 10883 (2001).
- [92] M. VOGEL, C. TSCHIRWITZ, G. SCHNEIDER, C. KOPLIN, P. MEDICK, and E. RÖSSLER, *Journal of Non-Crystalline Solids* **307-310**, 326 (2002).
- [93] M. VOGEL and E. RÖSSLER, *The Journal of Physical Chemistry B* **104**, 4285 (2000).
- [94] B. MICKO, S. A. LUSCEAC, H. ZIMMERMANN, and E. A. RÖSSLER, *The Journal of Chemical Physics* **138**, 074503 (2013).
- [95] B. MICKO, D. KRUK, and E. A. RÖSSLER, *The Journal of Chemical Physics* **138**, 074504 (2013).
- [96] B. MICKO, C. TSCHIRWITZ, and E. A. RÖSSLER, *The Journal of Chemical Physics* **138**, 154501 (2013).
- [97] H. WAGNER and R. RICHERT, *Journal of Non-Crystalline Solids* **242**, 19 (1998).
- [98] G. P. JOHARI, *Annals of the New York Academy of Sciences* **279**, 117 (1976).

- [99] S. HENSEL-BIELOWKA, M. PALUCH, J. ZIOLO, and C. M. ROLAND, *The Journal of Physical Chemistry B* **106**, 12459 (2002).
- [100] S. HENSEL-BIELOWKA and M. PALUCH, *Physical Review Letters* **89** (2002).
- [101] M. PALUCH, S. PAWLUS, S. HENSEL-BIELOWKA, E. KAMINSKA, D. PREVOSTO, S. CAPACCIOLI, P. A. ROLLA, and K. L. NGAI, *The Journal of Chemical Physics* **122**, 234506 (2005).
- [102] M. MIERZWA, S. PAWLUS, M. PALUCH, E. KAMINSKA, and K. L. NGAI, *The Journal of Chemical Physics* **128**, 044512 (2008).
- [103] K. NGAI, *Relaxation and Diffusion in Complex Systems (Partially Ordered Systems)*, Springer, New York, 2011.
- [104] S. ADISHCHEV, D. BOCK, C. GAINARU, R. KAHLAU, B. MICKO, N. PETZOLD, B. PÖTZSCHNER, and E. A. RÖSSLER, *Zeitschrift für Physikalische Chemie* **226**, 1149 (2012).
- [105] A. CUISSET, G. MOURET, O. PIRALI, P. ROY, F. CAZIER, H. NOUALI, and J. DEMAISON, *The Journal of Physical Chemistry B* **112**, 12516 (2008).
- [106] I. N. SMIRNOVA, A. CUISSET, F. HINDLE, G. MOURET, R. BOCQUET, O. PIRALI, and P. ROY, *The Journal of Physical Chemistry B* **114**, 16936 (2010).
- [107] R. L. LEHENY and S. R. NAGEL, *Europhysics Letters* **39**, 447 (1997).
- [108] L. COMEZ, D. FIORETTO, L. PALMIERI, L. VERDINI, P. ROLLA, J. GAPINSKI, T. PAKULA, A. PATKOWSKI, W. STEFFEN, and E. FISCHER, *Physical Review E* **60**, 3086 (1999).
- [109] A. BRODIN, R. BERGMAN, J. MATTSSON, and E. A. RÖSSLER, *The European Physical Journal B - Condensed Matter* **36**, 349 (2003).
- [110] C. GAINARU, R. BÖHMER, R. KAHLAU, and E. RÖSSLER, *Physical Review B* **82**, 104205 (2010).
- [111] U. SCHNEIDER, R. BRAND, P. LUNKENHEIMER, and A. LOIDL, *Physical Review Letters* **84**, 5560 (2000).
- [112] R. CASALINI and C. ROLAND, *Physical Review Letters* **91** (2003).
- [113] M. VOGEL, P. MEDICK, and E. A. RÖSSLER, *Annual Reports on NMR Spectroscopy* **56**, 231 (2005).
- [114] P. J. HAINS and G. WILLIAMS, *Polymer* **16**, 725 (1975).

- [115] M. A. DESANDO, S. WALKER, and W. H. BAARSCHERS, *The Journal of Chemical Physics* **73**, 3460 (1980).
- [116] M. SCANDOLA, G. CECCORULLI, and M. PIZZOLI, *Polymer* **28**, 2081 (1987).
- [117] M. NAKAZAWA, O. URAKAWA, and K. ADACHI, *Macromolecules* **33**, 7898 (2000).
- [118] D. CANGIALOSI, A. ALEGRÍA, and J. COLMENERO, *The Journal of Chemical Physics* **126**, 204904 (2007).
- [119] T. BLOCHOWICZ and E. RÖSSLER, *Physical Review Letters* **92**, 225701 (2004).
- [120] K. KESSAIRI, S. CAPACCIOLI, D. PREVOSTO, M. LUCCHESI, and P. ROLLA, *The Journal of Chemical Physics* **127**, 174502 (2007).
- [121] S. CAPACCIOLI, K. KESSAIRI, M. S. THAYYIL, D. PREVOSTO, and M. LUCCHESI, *Journal of Non-Crystalline Solids* **357**, 251 (2011).
- [122] T. BLOCHOWICZ, S. A. LUSCEAC, P. GUTFREUND, S. SCHRAMM, and B. STÜHN, *The Journal of Physical Chemistry B* **115**, 1623 (2011).
- [123] K. ADACHI and Y. ISHIDA, *Polymer Journal* **11**, 233 (1979).
- [124] D. A. SAVIN, A. M. LARSON, and T. P. LODGE, *Journal of Polymer Science Part B: Polymer Physics* **42**, 1155 (2004).
- [125] Y. MIWA, K. USAMI, K. YAMAMOTO, M. SAKAGUCHI, M. SAKAI, and S. SHIMADA, *Macromolecules* **38**, 2355 (2005).
- [126] J. E. G. LIPSON and S. T. MILNER, *Journal of Polymer Science Part B: Polymer Physics* **44**, 3528 (2006).
- [127] A. N. GAIKWAD, E. R. WOOD, T. NGAI, and T. P. LODGE, *Macromolecules* **41**, 2502 (2008).
- [128] S. SCHRAMM, T. BLOCHOWICZ, E. GOUIRAND, R. WIPF, B. STÜHN, and Y. CHUSHKIN, *The Journal of Chemical Physics* **132**, 224505 (2010).
- [129] D. CANGIALOSI, A. ALEGRÍA, and J. COLMENERO, *The Journal of Chemical Physics* **128**, 224508 (2008).

Danksagung

Ich möchte mich an erster Stelle bei Herrn Prof. Dr. Ernst Rößler bedanken. Er hat mir ermöglicht, als Teil seiner Arbeitsgruppe über mehrere Jahre auf hohem Niveau wissenschaftlich tätig zu sein und abschließend diese Dissertation zu verfassen. In erster Linie halfen hierbei vom ersten Tage an seine präzise fachliche Anleitung und sein stetes, motivierendes Interesse an den Ergebnissen der dielektrischen Spektroskopie. Darüber hinaus haben Herrn Rößlers Aufrichtigkeit und sein empathisches Handeln allezeit ein angenehmes zwischenmenschliches Klima am Lehrstuhl erzeugt.

Besonderer Dank und große Wertschätzung gebühren Dr. Catalin Gainaru, der mir in der Anfangsphase meiner Arbeit die essentiellen Grundlagen zum Glasübergang und zur dielektrischen Spektroskopie vermittelt hat. Viele angenehme Tage, Abende und Nächte haben wir während unserer gemeinsamen Zeit in Bayreuth messend, diskutierend und lachend verbracht. Auch bei jeder späteren Kooperation und bei jedem Treffen habe ich viel von ihm lernen können.

Gerne erinnere ich mich an die Zusammenarbeit mit den wenigen weiteren Mitarbeitern in der dielektrischen Abteilung, Julia Hintermeyer, Dr. Azza Moharram Hassan Abou Elfadl und Tobias Dörfler, die zum Teil in ferner Vergangenheit liegt. Große Zufriedenheit bereitet mir die Gewissheit, das dielektrische Labor nun in die Hände von Fathia Mamdouh El Shahat Mohamed geben zu dürfen, die sich in der nächsten Zeit zusammen mit Stefan Kachel um den Fortbestand der dielektrischen Spektroskopie und die Erweiterung des durch die Methode berührten Forschungshorizonts innerhalb der Arbeitsgruppe kümmern wird. Ich bin sehr glücklich darüber, sie kennengelernt und mein Wissen an sie weitergegeben haben zu dürfen.

Natürlich möchte ich auch allen anderen Mitgliedern der Arbeitsgruppe für die schöne gemeinsame Zeit danken. Stellvertretend seien hier die Doktoranden „meiner Generation“ aus dem Bereich der NMR und der Lichtstreuung Nikolaus Petzold, Bernd Schmidtke, Dr. Björn Micko, Dr. Axel Herrmann, Roman Meier, Marius Hofmann und Björn Pötzschner erwähnt, sowie Dr. Alexander Brodin. Besonderer Dank gilt jedoch Daniel Bock, mit dem sich in den letzten Jahren eine besonders intensive und ertragreiche Zusammenarbeit entwickelt hat. Ihre Früchte sind ein wesentlicher inhaltlicher Bestandteil dieser Arbeit.

Ich danke auch allen nichtwissenschaftlichen Mitarbeitern des Lehrstuhls, die mir die Zeit durch ihre freundliche Gesellschaft verschönert und durch manche kleineren und größeren Hilfestellungen jenseits ihrer dienstlichen Verpflichtungen erleichtert haben. Stellvertretend seien an dieser Stelle Gabriele Thiel, Irene Bauer, Michaela Fischer und Frank Schirmer genannt. Für seine jederzeit spontane und

wertvolle Hilfsbereitschaft möchte ich in diesem Zusammenhang ebenfalls Herrn Dr. Thomas Vogtmann danken.

Gesonderter Hervorhebung in der Dankeshymne bedürfen die obergärigen Beiträge des Herrn Jürgen Gmeiner.

Mein Dank gilt ebenso den bisher noch unerwähnten Kooperationspartnern Prof. Dr. Roland Böhmer, Prof. Dr. Danuta Kruk sowie Dr. Thomas Blochowicz und Prof. Dr. Vladimir Novikov. Als besonders angenehm und spannend bleibt mir die mehrjährige Zusammenarbeit mit Tanja Gnutzmann, Dr. Franziska Emmerling und Prof. Dr. Klaus Rademann in Erinnerung, die von interessanten Mess- und Tagungsreisen begleitet war und zu wesentlichen inhaltlichen Bestandteilen dieser Arbeit geführt hat.